كلية العلوم و التقنيات فاس
ⵜⴰⵙⴷⴰⵡⵉⵜ ⵏ ⵜⵎⴰⵙⵙⴰⵏⵉⵏ ⴷ ⵜⵉⵜⵉⵇⵏⵉⵢⵉⵏ
Faculté des Sciences et Techniques de Fès

جامعة سيدي محمد بن عبد الله
ⵜⴰⵙⴷⴰⵡⵉⵜ ⵙⵉⴷⵉ ⵎⵓⵃⵎⵎⴰⴷ ⴱⵏ ⵄⴱⴷⵍⵍⴰⵀ
Université Sidi Mohamed Ben Abdellah

Centre d'Etudes Doctorales : Sciences et Techniques de l'Ingénieur

N° d'ordre   04 /2020

THESE DE DOCTORAT

Présentée par

Melle/Mme/Mr : Lhoussaine TENGHIRI

- Spécialité : - Energies Renouvelables

Sujet de la thèse : Study of integrated design and manufacture of a small wind turbine in the Moroccan context within certification type IEC 61400.

Thèse présentée et soutenue le--- 04 /01 /2020--------------devant le jury composé de :

Nom Prénom	Titre	Etablissement	
Pr TajDine LAMCHARFI	PES	FST Fès	Président
Pr David Wood	PES	University of Calgary, Canada	Rapporteur
Pr Fouad Mohammed ABBOU	PES	Al Akhawayn University	Rapporteur
Pr Abdellah EL BERKANY	PH	FST Fès	Rapporteur
Pr El Ghzizal Abdelaziz	PES	EST Fès	Examinateur
Pr Anas Bentamy	PH	Al Akhawayn University	Directeurs de thèse
Pr Farid ABDI	PES		

Laboratoire d'accueil : -*Signaux, Systèmes et Composants*-

Etablissement : Faculté des Sciences et Techniques de Fès

Centre d'Etudes Doctorales Sciences et Techniques de l'Ingénieur
Faculté des Sciences et Techniques - Fès ; Route d'Immouzer, B.P.2202 Fès-, Maroc –
Tél. : (212) 5 35 60 80 14 ; Tél. : (212) 5 35 60 29 53 ;   Fax : (212) 5 35 60 82 14 ;   Site web : www.fst-usmba.ac.ma

ABSTRACT

The design process of a small wind turbine (rated power less than 50 kW or rotor swept area less than 200 m²) consists in defining optimum rotor blade geometry and a reliable mechanical power transmission system that will be able to extract maximum energy from the wind. The objective of the present work is to conduct an integrated design and analysis of a small wind turbine system under normal and extreme wind conditions. These design conditions are defined by the International Electrotechnical Commission (IEC) standard for small wind turbines; IEC 61400-2 which was adopted as a reference during the selection process and the analysis of the turbine components.

The IEC 61400-2 standard recommends Simple Load Model (SLM) as a starting point for the design of a small wind turbine system. This model combines straightforward, and possibly simplistic, equations for the main loads with high safety factors. As its name implies, it is the simplest design methodology. However, the high safety factors associated with this model increases conservatism and leads to overdesigned structures.

Due to the fact that the rotor blades of small wind turbines experience high numbers of fatigue cycles compared to large wind turbines, fatigue analysis was also included as a part of the design process in this study.

The results of stress and fatigue analysis based on SLM showed that the main shaft of the wind turbine passes successfully all the load scenarios. However, the rotor blades failed fatigue analysis. This failure is due mainly to three reasons. The first reason is related to the rough approximation used by SLM and which consists in using one single "bin" to compute the number of fatigue cycles. This approach leads to an overestimation of the number of the fatigue cycles with a difference of 3.1E+9 cycles compared to the results obtained from other advanced tools such as FAST-Mlife codes and nCode DesignLife composites. The second reason concerns the forces and moments on the blade during normal operation (load case A). The associated stress level, that is used to calculate the fatigue damage factor, was determined based on the assumption that the wind speed during normal operation has a constant value of 10.5 m/s. The use of such a relatively high wind speed leads to an overestimate of the centrifugal loads and the bending moments on the blade during normal conditions. The third reason concerns the high safety factors that are imposed by IEC 61400-2 when full material

characterization cannot be achieved, especially during early stages of the design process. This usually leads to heavy structure and affects the cost of the final blade design.

Throughout this research project, we succeeded to build a prototype of an 11 kW small wind turbine by following the guidance of the IEC 61400-2 standard. Also, we concluded by suggesting revisions of both the design parameters and the partial safety factors that are used during the design process of the wind turbine components using SLM.

RÉSUMÉ

L'objectif du present travail c'est la conception d'une petite éolienne d'une puissance nominale de 11 kW suivant les directives de la norme internationale IEC-64100-2 (Commission électrotechnique internationale) relative aux petites éoliennes. L'analyse de structure de la nacelle de l'éolienne a été réalisée en se basant sur le Modèle de Charge Simplifié (Simple Load Model (SLM)).

Vu que les pâles de petites éoliennes peuvent être sujet d'un nombre élevé de cycles de fatigue en comparaison avec les grandes éoliennes, l'analyse de la fatigue a également été incluse comme partie intégrante dans le processus de conception dans cette étude.

Les résultats de l'analyse de structure basée sur SLM ont montré que l'arbre principal de la turbine passe avec succès tous les scénarios de charge imposés par le standard IEC 61400-2. Cependant, les pâles ont échoué l'analyse de la fatigue. Cet échec est principalement dû à trois raisons. La première raison est liée à l'approximation grossière utilisée par SLM et qui consiste à utiliser un seul scenario pour calculer le nombre de cycles de fatigue. Cette approche conduit à une surestimation du nombre des cycles de fatigue avec une différence de 3.1E+9 cycles par rapport aux résultats obtenus à partir d'autres outils tels que les codes FAST-Mlife et le module nCode DesignLife. La deuxième raison concerne les forces et les moments sur les pâles pendant le fonctionnement normal (cas de charge A). Le niveau de stress associé, qui est utilisé pour calculer le paramètre d'endommagement critique, a été déterminée sur la base de l'hypothèse que la vitesse du vent pendant le fonctionnement normal a une valeur constante de 10,5 m/s. L'utilisation d'une telle valeur elevée conduit à une surestimation des forces centrifuges ainsi que les moments fléchissant sur les pâles dans des conditions normales de fonctionnement. La troisième raison concerne les facteurs de sécurité élevés qui sont imposées par la norme CEI 61400-2 lorsqu'une caractérisation complète des matériaux ne peut être atteinte, en particulier au cours des premières phases du processus de conception. Cela conduit généralement à une structure lourde et onéreuse.

A la fin de ce projet de recherche, un prototype d'une éolienne domestique d'une puissance de 11 kW a été mis en place. Les résultats obtenus à partir de ce travail démontrent que certains paramètres de design ainsi que les facteurs de sécurité imposés par le standard IEC 61400-2 nécessitent une révision puisqu'ils conduisent à des structures lourdes et surdimensionnées

Mots clés: Éolienne domestique; Pâles; Performances aérodynamiques; Analyse des structures; SLM; Analyse de la fatigue.

CONTENT

LISTE OF TABLES

LISTE OF FIGURES

ABBREVIATONS

AC: Alternating Current

AFM: Axial Flux Machines

AGMA: American Gear Manufacturers Association

ANRT: National Telecommunications Regulatory Agency

ASCE: American Society of Civil Engineering

BEM: Blade Element Momentum

CAD: Computer-aided Design

CAE: Computer-Aided Engineering

CCM: Continuous Conduction Mode

CFD: Computational Fluid Dynamics

CLA: Classical Laminate Analysis

DEL: Damage Equivalent Load

DLC: Design Load Cases

NCDC: National Climatic Data Center

NOAA: National Oceanic and Atmospheric Administration

DC: Direct Current

DCM : Discontinuous Conduction Mode

DU: Delft University

E-Glass: Electrical Glass

EWM: Extreme Wind Speed Model

FAST: Fatigue, Aerodynamics, Structure and Turbulence

FEA: Finite Element Analysis

FPVS: Fixed Pitch Variable Speed

FRP: Fiber reinforced Plastics

FVF: Fiber Volume Fraction

GA: Genetic Algorithm

GFRP: Glass Fiber Reinforced Plastics

GRG: Generalized Reduced Gradient

HAWT: Horizontal-axis Wind Turbine

IEC: International Electrotechnical Commission

IGBT: Insulated Gate Bipolar Transistor

IPMSG: Internal Permanent Magnet Synchronous Generator

LRTM: Light Resin Transfer Molding

MDE: Maximum Distortion Energy Theory

MSST: Maximum Shear Stress Theory

NACA: National Advisory Committee for Aeronautics

NREL: National Renewable Energy Laboratory

ONEE: National Electricity and Water Utility Company

PI: Proportional Integral

PBL: Planetary Boundary Layer

PERG: Global Rural Electrification Program

PMSG: Permanent Magnet Synchronous Generator

PPT: Pick Power Tracker

PWM: Pulse Width Modulation

Re: Reynolds Number

RFM: Radial Flux Machines
ROM: Rule of Mixture
RPM: Revolution per Minute
RTM: Resin Transfer Molding
SLM: Simple Load Model
SMR: Switch Mode Rectifier
SWRDC: Small Wind Rotor Design Code
SWT: Small Wind Turbine
TDH: Total Dynamic Head
TFM: Transversal Flux Machines
TSR: Tip Speed Ratio
UBEC: Universal Battery Elimination Circuit
UD: Unidirectional Direction
UPS: Uninterrupted Power Supply
VI: Vacuum Infusion

SYMBOLS

α : Apparent angle of attack as seen from the tail vane (degree)

α_L : Frequency dependent sound absorption coefficient

α_{design} : Design angle of attack (degree)

β : Furling tilt angle (degree)

β_s : Inclination of the load on the foundation (degree)

γ_l : Required kinematic viscosity of the fluid

γ_f : Load partial safety factor

γ_m : Partial safety factor for material

Δ_θ : Yaw error (degree)

ε : Convergence criteria for the iterative process

ξ : Fiber reinforcement factor of the composite material

η : Drive train efficiency

$\eta_{airfoil}$: Airfoil losses

η_c : Factor for contamination level for bearings

η_d : Diameter distribution factor

η_{lE} , η_{lS} : Reinforcement length efficiency factor for stiffness and strength

η_0 : Reinforcement orientation distribution factor

$\Gamma()$: Gamma function

θ_a : Angular position (degree)

θ : Blade section twist angle (degree)

λ : Tip speed ratio

$\lambda_{0.5}$: Tip speed ratio of the middle section of the rotor blade

λ_{design}: Design tip speed ratio

λ_{e50} : Tip speed ratio for 3s-50year extreme wind speed

λ_{opt}: Optimum tip speed ratio

λ_{ri} : Blade section tip speed ratio

λ_{10} : Middle blade section tip speed ratio

μ : Kinematic viscosity of the air (m^2/s)

V : Furling lateral inclination angle (Degree)

V_s : Soil unit weight (KN/m^3)

$V_s{'}$: Effective unit weight above the base level of the foundation

V_f, V_m : Poisson's ratio of fibers and matrix (KN/m^3)

ρ : Air density (Kg/m^3)

ρ_f , ρ_m : Fiber and matrix density (Kg/m^3)

ρ_t : Tower material density (Kg/m^3)

σ_a : Allowable stress (MPa)

σ_c : Blade composite tensile strength (MPa)

σ_{dr} : Composite tensile strength at the blade root (MPa)

σ_{eq} : Equivalent stress (MPa)

σ_f , σ_m: Fiber and matrix tensile strength (MPa)

σ_{fc} , σ_{mc}: Fiber and matrix compressive strength (MPa)

σ_{root} : Stress on the blade root (MPa)

σ_{11} : Blade composite tensile strength from generalized rule of mixture (MPa)

ϕ_i : Blade section angle of relative wind (degree)

ϕ_s : Soil friction angle (degree)

$\boldsymbol{\psi}$: Maximum packing factor of the fibers

$\boldsymbol{\omega}$: Rotor's angular velocity (rad/s)

$\boldsymbol{\omega_s}$: Pulse voltage (rad/s)

$\boldsymbol{\omega_{yaw,max}}$: Maximum yaw rate

$\boldsymbol{\Omega}$: Rotor rotational speed (RPM)

$\boldsymbol{\Omega_{design}}$: Design rotational speed (RPM)

$\boldsymbol{\Omega_{max}}$: Maximum rotational speed (RPM)

$\boldsymbol{A}$: Rotor swept area (m^2)

$\boldsymbol{A'}$: Meyerhof's effective area of the turbine foundation (m^2)

$\boldsymbol{A_f}$: Area of the wind turbine foundation (m^2)

$\boldsymbol{A_h}$: Tower top cross section area (m^2)

$\boldsymbol{A_{proj,B}}$: Projected area of the blade (m^2)

$\boldsymbol{A_{proj,N}}$: Projected area of the nacelle side (m^2)

$\boldsymbol{A_{tail}}$: Projected area of the furling tail (m^2)

$\boldsymbol{AR}$: Aspect ratio

$\boldsymbol{a}$: Axial induction factor

$\boldsymbol{a'}$: Angular induction factor

$\boldsymbol{B}$: Blade number

$\boldsymbol{B'}$: Meyerhof's effective width of the turbine foundation (m)

$\boldsymbol{B_f}$: Wind turbine foundation's width (m)

$\boldsymbol{b}$: Fatigue coefficient

$\boldsymbol{c}$: Weibull distribution scale parameter (m/s)

$\boldsymbol{c_a}$: Weibull distribution scale parameter at the anemometer height (m/s)

$\boldsymbol{c'}$: Soil cohesion (KN/m^2)

$\boldsymbol{C}$: Airfoil chord length (m)

$\boldsymbol{CF}$: Capacity factor

$\boldsymbol{CR}$: Crossover factor

$\boldsymbol{C_D}$: Drag coefficient

$\boldsymbol{C_H}$: Hydraulic constant ($\frac{\text{kg.s.h}}{\text{m}^2}$)

$\boldsymbol{C_{L\ design}}$: Design lift coefficient

$\boldsymbol{C_L}$: Lift coefficient

$\boldsymbol{C_{ST}}$: Nacelle side-on force coefficient

$\boldsymbol{C_T}$: Torque coefficient

$\boldsymbol{C_i}$: Blade section chord length (m)

$\boldsymbol{C_{lmax}}$: Maximum lift coefficient

$\boldsymbol{C_p}$: Power coefficient

$\boldsymbol{C_{pSchmitz}}$: Schmitz power coefficient

$\boldsymbol{C_{pmax}}$: Maximum power coefficient

$\boldsymbol{C_{th}}$: Thrust coefficient

$\boldsymbol{C_0}$: Basic static loading (N)

$\boldsymbol{CME_f}$, $\boldsymbol{CME_m}$: Moisture expansion of the fibers and matrix (m/m)

$\boldsymbol{CTE_f}$, $\boldsymbol{CTE_m}$: Thermal expansion of the fibers matrix (m/m)

$\boldsymbol{D}$: Rotor diameter (m)

$\boldsymbol{D_{b0}}$: Tower base diameter (m)

$\boldsymbol{D_d}$: Wind turbine foundation depth (m)

$\boldsymbol{D_f}$: Deflection (m)

D_{h0} : Minimum tower top diameter (mm)

D_i : Inner diameter (mm)

D_m : Accumulated damage over the wind turbine lifetime

$D_{outer,min}$: Minimum outer diameter (m)

D_s : Shaft diameter (mm)

D_{solid} : Diameter of solid cross section (m)

D_t : Tower diameter (mm)

D_u : Duty ratio

D_0 : Outer diameter (mm)

d_L : Distance from the noise source (m)

d_f : Fiber diameter (mm)

d_m : Mean raceway diameter on the bearing (mm)

e: Eccentricity of applied loading on the wind turbine foundation (m)

E : Material young's modulus (GPa)

E_c : Blade composite young's modulus (GPa)

E_{elec} : Equivalent electric energy needed per day (Kwh)

E_f , E_m : Fiber and matrix young's modulus (GPa)

E_{11} : Blade composite young's modulus from generalized rule of mixture (GPa)

F_A : Material minimum yield stress (Mpa)

F_L : Tip losses

F_S : Safety factor for soil bearing capacity

F_{So}: Safety factor for foundation overturning

F_a : Rotor axial loading (N)

F_k : Material ultimate tensile strength (Mpa)

F_{rm} : Minimal radial loading (N)

F_{thrust} : Wind thrust force (N)

F_{sc} : Application service factor for coupling selection

F_y : Material maximum yield stress (Mpa)

f : Voltage frequency (HZ)

$f(V)$: Weibull probability density function of the wind speed v

f_b : Blade passing frequency (HZ)

f_r : Turbine rotor frequency (HZ)

f_0 : Tower natural frequency (HZ)

G : Short circuit torque factor

G_b : Bolt thread diameter (mm)

G_f : Shear modulus of E-glass fibers (GPa)

G_m : Shear modulus of Epoxy resin (GPa)

g : Acceleration due to the gravity (m/s^2)

H_{Hub} : Wind turbine hub height (m)

h_{opt} : Optimum tower height (m)

I : Area moment of inertia (M^4)

I_{15} : Turbulence intensity

I_r: Output current from the rectifier (A)

I_{max} : Maximum current (A)

I_{opt}: Reference direct current (A)

I_{root} : Area moment of inertia of the blade root section (m^4)

I_{solid} : Area moment of inertia for solid cross section (m^4)

J : Rotor inertia (Kg.m^2)

J_B : Blade inertia (Kg.m^2)

J_g : Generator inertia (Kg.m^2)

J_{total} : Turbine total inertia (Kg.m^2)

J_0 : Shaft and other component inertia (Kg.m^2)

K_f, K_m : Thermal conduction of the fibers and matrix (Watt/m/Kelvin)

K_p : Constant of proportionality in potential flow lift equation

K_v : Constant of proportionality in vortex lift equation

k : Weibull distribution shape parameter (-)

k_a : Weibull distribution shape parameter at the anemometer height (-)

k_r: Viscosity ratio

k_f : Fiber area correction factor

L: Side length of the tower octagonal section (mm)

L': Meyerhof's effective length of the turbine foundation (m)

L_{dc} : Input inductor (H)

L_k : Minimum clamp length of the bolt (mm)

L_f : Wind turbine foundation length (m)

L_p : Sound pressure level (dB (A))

L_{rb} : Distance from rotor center to the first bearing (m)

L_{rt} : Distance from the rotor center to the yaw axis (m)

L^{MF} : Fixed mean of the fatigue load (KN)

L^{ult}: Ultimate design load of the component (KN)

L_w : Sound power level (dB (A))

L_{10h} : Basic rating life of bearings (hour)

L_{90} : Sound level present at least 90% of time (dB (A))

m_t : Tower mass (Kg)

M : Component bending moment (N.m)

M_b : Tail boom mass (Kg)

M_h : Tower base overturning moment (KNm)

M_R : Resisting moment to overturning of the turbine foundation (KNm)

M_{root} : Blade root bending moment (N.m)

M_s : Bending moment on the shaft (N.m)

M_T : Aerodynamic moment applied on the furling tail (N.m)

M_{tilt} : Tilting moment (N.m)

M_v : Tail vane mass (Kg)

M_0 : Bending moment on the tower top region (N.m)

m : Power law exponent

m_B : Blade mass (Kg)

m_f : Wind turbine foundation weight (Kg)

m_{rotor} : Rotor mass (Kg)

m_{tail} : Mass of the tail assembly (Kg)

m_{tt} : Wind turbine tower top mass (Kg)

N_{cycle} : Number of cycles to failure

N_p : Number of control points

N_{se} : Number of tower sections

N_c, N_q, N_V : Meyerhof's bearing capacity factors

N_{cs}, N_{qs}, N_{Vs} : Meyerhof's shape factors;

N_{cd}, N_{qd}, N_{Vd} : Meyerhof's depth factors;

N_{ci}, N_{qi}, N_{Vi} : Meyerhof's inclination factors;

n : Safety factor of the shaft material

n_i : Number of fatigue cycles

P : Power production (W)

PR_{total} : Total price of the wind turbine (USD)

P_d : Equivalent static loading (N)

P_{design} : Design power output (W)

P_{input} : Input power from the turbine rotor (W)

P_{opt}: Optimum power output (W)

R_P: Water pumping system efficiency

P_{pole} : Number of peer poles

$q_u{}'$: Meyerhof's general ultimate bearing capacity (KN/m^2)

q_{min} : Minimal pressure on the soil (KN/m^2)

q_{max} : Maximal pressure on the soil (KN/m^2)

Q : Maximum pressure on the soil (KN/m^2)

Q_{design} : Design rotor torque (N.m)

Q_f : Required water flow per day (m^3/day)

Q_{ult} : Allowable bearing capacity of the foundation (KN/m^2)

R: Rotor radius (m)

R_S: Stress ratio

R_b : Reaction force (N)

R_{cog} : Distance from the rotor center to the blade center of gravity (m)

R_e : Reynolds number

R_t : Capital cost of the turbine (USD)

R_{tu} : Capital cost of the tower per unit meter (USD)

r: Radial co-ordinate along blade (m)

r_{root} : Root section radius (m)

S : Wall thickness of the flange (mm)

S_i : Stress level of the fatigue cycles (Mpa)

S_0 : Permissible static loading (N)

S_f , S_m : Shear strength of fibers and matrix (MPa)

$T_{B,total}$: Total brake torque (N.m)

T_{aero} : Aerodynamic torque (N.m)

T_{cl} : Tip clearance (mm)

T_{cnom} : Nominal torque for the coupling (Nm)

$T_{cdesign}$: Design torque of the shaft coupling (Nm)

T_d : Wind turbine life (second)

T_{ds} : Dynamic torque of the shaft (N.m)

$T_{electric}$: Generator torque (N.m)

$T_{friction}$: Torque due to the friction (N.m)

T^{fail}: Time until failure (s)

T_{hmax} : Maximum wind thrust (N)

$T_{inertia}$: Torque generated from inertia of moving parts (N.m)

T_{opt} : Optimum torque (N.m)

T_{rotor} : Rotor torque (N.m)

T_s : Switching time (second)

T_{st} **:** Blade starting time (Second)

T_{total} : Total torque (N.m)

t : Tower section wall thickness (mm)

t_{p0} **:** 0° ply total thickness (mm)

t_l : Laminate total thickness (mm)

U_{e50} : 3s-50 year extreme wind speed (m/s)

U_{rel} : Relative wind speed (m/s)

U_0 : Offset wind speed (m/s)

U_{10} : Wind speed at a reference height of 10 m (m/s)

V : Wind speed (m/s)

V_{AMWS} : Annual mean wind speed (m/s)

V_{ave} : Average wind speed (m/s)

$V_{control}$: Control signal voltage (V)

V_{cout} : Wind turbine cut-out wind speed (m/s)

V_d : Voids percentage

V_{dc}: Generator rectification voltage (V)

V_{design} : Design wind speed (m/s)

V_f : Fiber volume fraction

V_{furl} : Furling wind speed (m/s)

V_m : Matrix volume fraction

V_{out} : Output voltage (V)

V_{rated} : Rated wind speed (m/s)

V_{ref} : Reference wind speed (m/s)

V_{tan} : Tangential velocity (m/s)

V_{wake} : Wind speed in the rear wake region (m/s)

V_y : Wind speed viewed from the yaw angle (m/s)

ACKNOWLEDGEMENTS

CHAPTER 1: INTRODUCTION

Small wind turbine design is the process of defining the form and the specifications of a wind power system able to extract energy from the wind. This design process involves selection and conceptual assembling of a number of mechanical and electrical components into a single system which is able convert the varying power contained in the wind into a useful form of energy (electricity) that can be directly exploited by the users. Any design process is usually subject to a number of technical and economic constraints that mainly contribute to the decision-making, and hence to the final design topology. For the present design study, three fundamental constraints are considered to be the key requirements that must be satisfied by the final prototype of the small wind turbine. These are the potential economic viability of the system, the reliability of the assembly and the efficiency of the overall wind energy conversion system.

The ultimate objective of the present study is to develop a conceptual design of an efficient, reliable and economically attractive small wind turbine for an electrical power generation of 11 kW. This small wind turbine system will ideally be designed to be implemented in remote communities to cover typical individual household's electricity requirements (supplying household appliances) including water pumping systems for irrigation in rural areas.

In designing a wind turbine system, the wind energy community adopts different systematic approaches. Manuell JF et al. [1] give an example of a generalized approach that can be used in wind turbine design and analysis. For the present study, the design procedure will be based on an iterative method. This design process is composed of three main steps. The first step consists in defining different energy requirements. The design requirements usually act as design constraints for which a product should be designed. The second step consists in generating and developing solutions and concepts that can satisfy the already defined requirements. In this step, all design solutions have the same weight. The third and final step consists in evaluating design solutions. This last step is the most important phase in the design process as it decides on the technical feasibility of the selected solutions. An iterative process is generally based on a cyclic process of prototyping, analyzing and refining of the wind turbine design. That is, based on the obtained results from the most recent design iteration, changes and refinements can be made. The chosen design process is intended to ultimately improve both the quality and functionality of the final prototype.

The key steps that will be taken towards the final small wind turbine design are given in figure 1. The analysis undertaken in this document will focus on steps one through four.
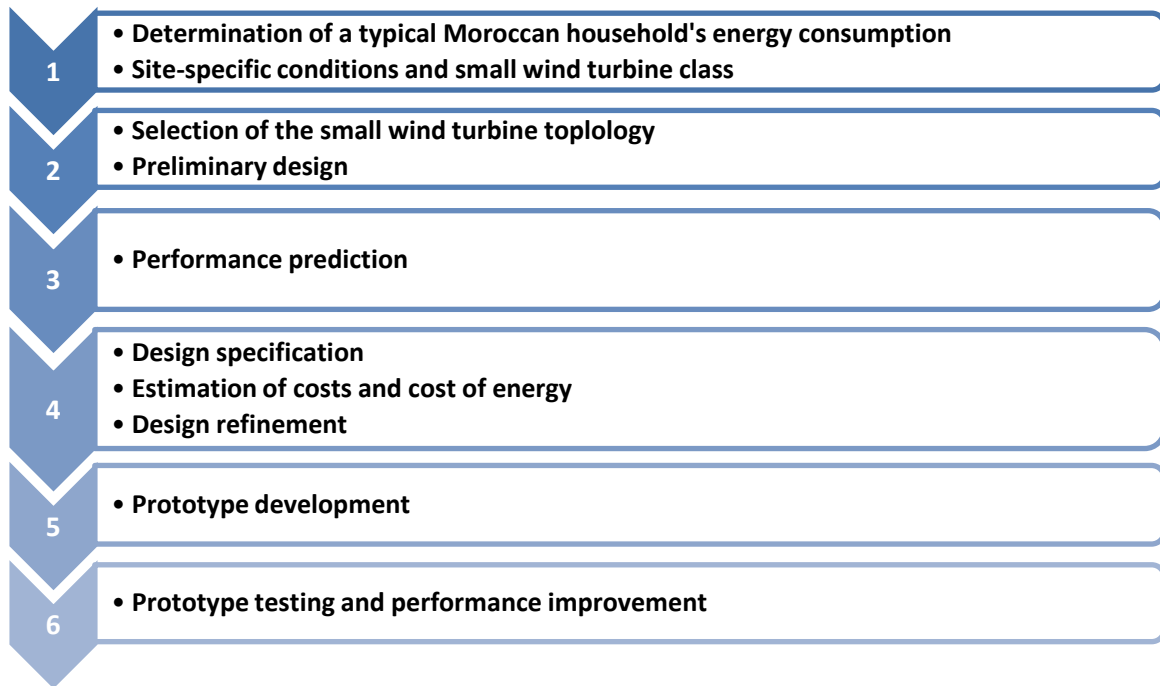
Figure 1: Design procedure of the small wind turbine

The work within this document is divided into several sections which are given as follows:

In the first section of this document, an overview of technological trends in the design of small wind turbines will be presented. This review section provides a comparative study of present technologies widely used in the wind energy industry. This study will be based on both an exhaustive review of the state of the art and an effective comparison of different topologies adopted for the design and manufacture of commercially available small wind turbines having rated power between 10 kW and 11 kW. Then, the needs of the users will be defined. The user's energy requirements are expressed in terms of daily electricity consumption of a typical Moroccan household. Identifying the users' needs allows determining the required power output of the wind turbine system that will be able to ensure a stable power supply for the overall household appliances. Secondly, the site-specific wind conditions will be discussed. The ultimate objective of this wind site assessment is to define an appropriate wind turbine class for which the small wind turbine will be designed. This is one of the factors which need to be considered during the complex process of designing a wind power system.

The second section of this design report will discuss different design parameters upon which the whole design process will be built. Wind classes are used to determine which design of the wind turbine is suitable for normal and extreme wind conditions in a specific area. The wind conditions are mainly defined by the average annual wind speed (measured at the turbine's hub height), the speed of extreme gusts that could occur over 50 years and by the turbulence there is at the wind site. As a final part of this section, other design parameters will be

determined. These include the design and the rated wind speed, the wind turbine rotor diameter, the rotor blades number and, finally, the wind turbine drive train topology.

The third section of this report will be devoted to the analysis of the wind turbine blades. The purpose of this section is to determine the blade aerodynamic shape with the chord length and the twist angle distribution, at a certain design tip speed ratio, λ_{design}, at which the blade has a maximum power coefficient. To achieve this goal, the following steps will be completed:

The first step will be concerned with the selection of an appropriate airfoil section. The section view of a wind turbine blade is basically defined by an airfoil shape (one or more airfoils), which is expected to generate high lift to drag ratio. The shape of the blade is vital as it determines the energy captured and the loads experienced. Consequently, the airfoil selection is a particularly critical aspect of the blade design process of small horizontal axis small wind turbines. The second step will mainly discuss some blade design parameters such as the design tip speed ratio, the turbine rotational speed, and the design angle of attack. The blade tip speed ratio (often known as the TSR) is of vital importance in the design of wind turbine generators. Normally, when the rotor of the wind turbine turns too slowly, most of the wind will pass undisturbed through the gap between the rotor blades. Alternatively if the rotor turns too quickly, the blurring blades will appear like a solid wall to the wind. Wind turbines are usually designed with optimal tip speed ratios to attain a maximum power coefficient (C_{pmax}), and hence a maximum power production. Therefore, identifying an appropriate design tip speed ratio is essential. Other design parameters like the wind turbine rotational speed and the design angle of attack must also be considered carefully.

Determination of the blade aerodynamic shape with the chord length distribution and twist angle distribution, at a certain design tip speed ratio, is the main task of the third step. Once the fundamental design parameters have been identified, the aerodynamic shape is determined using both the optimum rotor theory and the Blade Element Momentum theory (**BEM**). BEM theory is considered as the oldest and the most widely used method for wind turbine blade design and analysis [2]. The values given in this step are just an initial design values and iterations are followed normally [3].

The fourth step presents some results of a simulation approach which enables the annual average energy production of the wind turbine to be increased by automatically optimizing its airfoil twist and chord distribution. For simulation purposes, Small Wind turbine Rotor Design Code (**SWRDC**) and Q-blade software will be used [4, 5].

The fifth step in the small wind turbine blade design will be concerned with selection process of an appropriate composite blade material. The mechanical properties of the selected fiber composite materials will be also discussed. Finally, the wind turbine blade design will be

completed by a preliminary tentative design of the blade internal structure (shear web and spar caps), the blade tip transition and the blade root connection.

For safe operation, the final subsection of the wind turbine blade design will discuss the blade tip deflection and the required minimum tip clearance. In wind turbines operation, many failure cases are mainly caused by the event that blade tip hits the tower [6]. Thus, one of the most important indicators in a wind turbine design is the tip deflection estimation. Usually, the maximum tip deflection possibly occurs in some extreme conditions during wind turbine operation; therefore, study of the tip displacement must be conducted for the worst wind conditions (generally at three-second gust with a recurrence period of 50 years).

Once the overall structure of the rotor blade is determined, a tentative design of the rotor and the nacelle components will be developed. This will be covered in the fourth section. In this section, the wind turbine system will be considered to consist of different subsystems. The following subsystems, together with some of their principal components, will be designed:

- Rotor components (rotor hub and front nose cone);
- Nacelle structure (main frame and nacelle cover) ;
- Drive train components (main shaft, shaft coupling, and main shaft bearings);
- Generator and safety system (Generator and brake system);
- Yaw system (yaw bearings);
- Furling system (tail fin and tail boom);

The conceptual design of the nacelle components will be based on trade-off between technical and economic considerations. Some considerations that have been taken into account are the cost-effectiveness of the turbine components, structural stability of the system, strength and rigidity of the components, visual aesthetics of the turbine's nacelle, efficient manufacturing methods and aerodynamic considerations for the design of some nacelle components (nacelle cover design for example). The final part of this section will also discuss two major aspects of the wind turbine operation which are the wind turbine operation mode and the wind turbine control strategy for maximum power extraction. A particular attention must be paid to this subsection since the major goal of a wind turbine control strategy is to optimize the power production: below the rated wind speed, the goal is to maximize energy production, and above rated wind speed the goal is to limit the power production. This optimal control strategy can be achieved by using a combination of different methods such as variable/constant rotor speed and passive stall regulation.

In order to obtain a cost-effective wind turbine, an optimum tower design must be included in the design process. In a wind turbine design, it is necessary to find an optimum design for the tower by mainly taking into consideration different external conditions (loads from the wind

and dead loads applied by the nacelle components). Nowadays, computer tools based on reliable optimization algorithms can be used to design small wind turbine towers. These simulation tools help understanding the effects of design parameters such as the hub height, the tower diameters and the wall thickness of the tower sections. The fifth section of this document will be devoted to design and analysis of the small wind turbine tower. Throughout this section, three main aspects will be discussed: tower type selection (circular or octagonal cross sections), optimum design of the tower (top and base diameter as well as optimal wall thickness of the tower sections) and finally the structural analysis of the tower by studding the different involved loads.

The sixth section of the present engineering design process will present the wind turbine foundation design. The main objective of this section is to determine an optimal foundation geometry that will be able to support the tower and nacelle structures and withstand heavy loads and moments due to extreme wind conditions. As a first step of this section, the foundation type will be selected based on literature review and previous experiences. Afterwards, soil characteristics will be determined. As the small wind turbine machine is mainly designed to be installed in remote area and agricultural sites, typical agricultural soil will be selected for the design process. Once the foundation type and the geotechnical characteristics of the supporting soil are identified, the foundation geometry can be determined using the ultimate bearing capacity calculation. Finally, given the design loads and the soil properties, design checks of bearing capacity, overturning and rotational stiffness will be performed.

Small wind turbines could eventually be origin of some disorders in nearby inhabitants. This is due to the fact that these small wind energy systems are generally located close to residential areas and farmers' households. Therefore, it is necessary to develop expectations regarding noise production before the turbines are actually installed. This will be covered in the seventh section of this report. Throughout this section, the sound power level of the wind turbine system and the noise level at a given distance from the source will be determined using a prediction model based on simple equations that involve the main wind turbine parameters (rated power, rotor diameter, blade area, tip speed, etc.).

The loading regime to which small wind turbines are subject to is extremely complex and requiring special attention in their design. An understanding of the loads and their origin as well as the wind turbine ability to withstand them, during normal and extreme conditions, is crucial to avoid catastrophic failure of the entire system. For this reason, the eighth section of this report will cover the wind turbine loads assessment. In order to evaluate the functional response of the wind turbine to different applied loads, the structural integrity of the system

will be analyzed using Simple Load Model (SLM). This is one the most widely used models in small wind turbines structural analysis. This model is highly recommended by the international standard of small wind turbines; IEC-64100-2-Design requirements for small wind turbines [7]. Given the fact that functional behavior of a wind turbine is made up of complex interactions of subsystems, the use of SLM model is just a first attempt to create a preliminary tentative load analysis. Analyzing such a complex behaviour actually requires a multidisciplinary team working with a range of different skills in multiple areas such as meteorology, rotor aerodynamic, control and electrical engineering, structural and civil engineering. To be able to analyze such a complex system, it is necessary to use computational design codes capable of performing complete simulations of the behavior of wind turbines over a wide range of different operational conditions (ANSYS, FAST, etc.)

A wind turbine blade when manufactured to a certain set of standards and specifications has to demonstrate its reliability during its lifetime. Indeed, the wind turbine blades are considered to be the most delicate parts in the wind turbine and that is due to the repetitive load or cyclic load applied by the wind. Hence, a fatigue analysis needs to be conducted in order to know whether the designed blades will withstand the wind loads over a lifetime of over 20 years. Blade fatigue analysis will be discussed in the last section of the present document. The process of fatigue analysis consists of three main parts. The first part will cover the blade mechanical characterization which includes computation of cross-coupled stiffness properties, inertia properties, and offsets of the blade shear center, tension center, and center of mass with respect to the blade pitch axis. The second part of the process consists of generating the time-series using FAST (Fatigue, Aerodynamics, Structures, and Turbulence) code. This is a powerful tool developed by the National Renewable Energy Laboratory (NREL) and used to predict fatigue loads of two- and three-bladed horizontal-axis wind turbines (HAWTs). The final step of the process consists in calculating of the fatigue accumulated damage using MLife code which is a Matlab- based program developed by NREL.

CHAPTER II: LITERATURE REVIEW AND RESEARCH METHODOLOGY

After several years of continuous growth, small wind industry continues to provide the market with small wind turbines of different features and topologies. The generated power ranges from few hundred Watts to tens of kilowatts. According to the world wind energy association [8], the average size of small wind turbines continues to grow: In 2010, the average installed size was 0.66 kW, in 2011 0.77 kW, in 2012 0.84 kW and in 2013 it has already reached 0.85 kW. In regards to their structure, small wind turbines topology varies from one manufacturer to another. Actually, worldwide manufacturers maintain almost the same conversion chain from the kinetic energy of the wind to the output power from the inverter. The difference lies in the nature of the rotor blades, the type of electrical generator as well as the control and protection system.

2.1 Small wind turbine market and forecasts

According to the small wind world report [8], five countries account for over 50 % of the small wind manufacturers. These are: Canada, China, Germany, United Kingdom, and United states. By the end of 2011, over 330 other small wind manufacturers have been identified in the world offering complete one-piece commercialized generation systems, and an estimate of over 300 additional firms supplying parts, technology, consulting and sales services.

Regarding the worldwide distribution of the wind turbine manufacturers, the production of small wind turbines remains concentrated in few world regions such as China, in North America, and in some European countries. Developing countries continue to play a minor role in small wind manufacturing. It is obvious that the considerable wind resources of Africa, Southeast Asia and Latin America, where many regions are ideally suited for small wind application, have not yet lead to the establishment of domestic small wind industries.

Concerning the technology and applications, the early horizontal axis wind turbine (HAWT) type has dominated the market for over 30 years. Despite a market trend that leans towards a grid-tied system with larger capacity, off-grid applications continue to play an important role in remote areas of developing countries. Over 80 % of the manufacturers produce stand alone applications. Nowadays, small wind turbines are used in many different applications. These include: residential, commercial and industrial, fishery and recreational boats, decentralized hybrid systems, pumping systems, desalination and purification, remote monitoring and finally telecom base stations.

Regarding the future of this technology, the increasing demand for clean energy all over the world will lead to an increasing demand for small wind turbines. In particular in the developing countries, small wind turbines can easily and fast contribute to electrify millions of people in rural areas. Also several industrialized countries have ambitious small wind targets and corresponding policies in place. In general, political support can be expected to increase the installed capacity of small wind in the upcoming years further. Accordingly, small wind industry can be expected to follow similar growth patterns of the large wind and solar industry until 2020. Based on a conservative assumption, the market could subsequently see a steady compound growth rate of 20 % from 2015 to 2020. The industry is forecasted to reach approximately 480 MW of newly installed capacity added annually in 2020 and achieves a cumulative installed capacity of close to 3 GW by 2020 [8]. Increasing fossil fuel prices, global warming and the ever-growing electricity demand will continue to be the three long-term drivers of the small wind industry. In order for the small wind technology to mature, however, the industry must be driven by supportive policies and standards. Figure 2 gives the total cumulative installed capacity and its projection over the next four years.
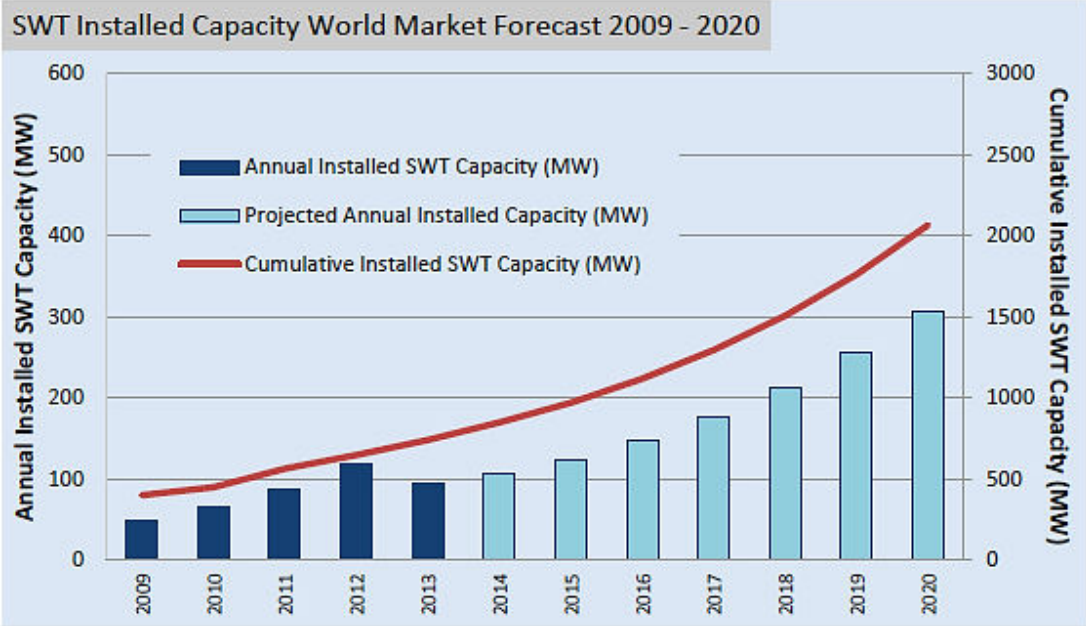
Figure 2: Small wind turbine installed capacity world market forecast, [8]

2.2 Review of commercially available small wind turbines

In order to have a clear understanding of the commonly used topologies in commercial small scale wind turbines, a comparison study of twenty different small wind turbines with rated power outputs ranging from 10 kW to 11 kW, has been conducted. Table 1 summarizes the criteria upon which this comparison is based.

Turbine component	Characteristics
Turbine	Rated power output (kW)
	Maximum power (kW)
	Cut-in wind speed (m/s)
	Rated wind speed (m/s)
	Cut-out wind speed (m/s)
	Survival wind speed (m/s)
	Turbine mass (Kg)
Rotor blades	Rotor swept area (m²)
	Rotor rotational speed (RPM)
	Blade material
Drive train	Drive train topology
Generator	Generator technology
	Generator voltage (V)
	Generator efficiency (%)
Control system	Wind turbine control system
Regulation system	Yaw system
	Wind turbine protection system
Tower	Tower type
	Tower height (m)

Table 1: Criteria of the comparison of small wind turbines

Results of the comparison showed similarities regarding certain mechanisms and differences in others. It should be noted that the value describing each design parameter of the whole studied wind turbine systems is given as average value. Table 2 summarizes all the obtained results.

Wind turbine parameter	Representative value
Rated power output (kW)	**10.8**
Maximum power (kW)	**13.5**
Cut-in wind speed (m/s)	**2.98**
Rated wind speed (m/s)	**10.91**
Cut-out wind speed (m/s)	**24.6**
Survival wind speed (m/s)	**52.97**
Turbine mass (Kg)	**414**
Rotor diameter (m)	**7.8**
Rotor swept area (m²)	**48.16**
Rotational speed (RPM)	**230**
Blade material	**Fiber-reinforced composites**
Generator type	**Permanant Magnet Generator**
Drive Train topology	**Direct drive system**

Regulation system	**Passive/Active**
Protection system	**Autofurl/Braking**
Tower type	**Stand-alone tower**
Tower height (m)	**12 m to 30 m**

Table 2: Typical design parameters used by small wind turbines manufacturers

Some mechanisms are the same for all the listed wind turbines. For instance, synchronous permanent magnet generators and direct drivetrain topology are typical solutions that have been adopted by the majority of small wind turbine manufacturers. These particular choices are not surprising since they offer a good techno-economic compromise. Some other mechanisms present a variety of choices. The use of a particular solution depends on the manufacturer's technological expertise and his target market segment. Wind turbine control and safety systems present an example of these mechanisms.

2.3 Electricity consumption of a typical Moroccan household

2.3.1 Approaches to assess typical household's power consumption

The global energy context in Morocco is marked by a significant increase of electricity demand over the years. This increase is specifically obvious in residential sector where the households' electricity consumption continues to rise as the population's standard of living is improving. Despite all the efforts that have been deployed, the problem of energy demand is becoming more complex that it is not easy to meet the ever-growing needs while continuing to exploit fossil fuel resources whose reserves are limited. Within such context, the kingdom of Morocco is facing an immediate challenge to anticipate possible energy crises by creating alternative renewable energy projects (including wind energy conversion systems) which will be able to ensure reliable electricity supply through decentralized power generation.

Demographic increase and economic growth are the main factors that have greatly contributed to the increase of the national average household electricity consumption. Additionally, improvements seen in the population's standard of living is also considered as an important factor leading to the increase of the household's average electricity consumption. For a developing country like Morocco, the electricity demand per capita increases very rapidly and the provision of enough electricity remains a key factor for any successful development in the country. Figure 3 gives the main regions in Morocco where the evolution of the electricity consumption per capita is becoming higher than the national average electricity consumption per capita [9].
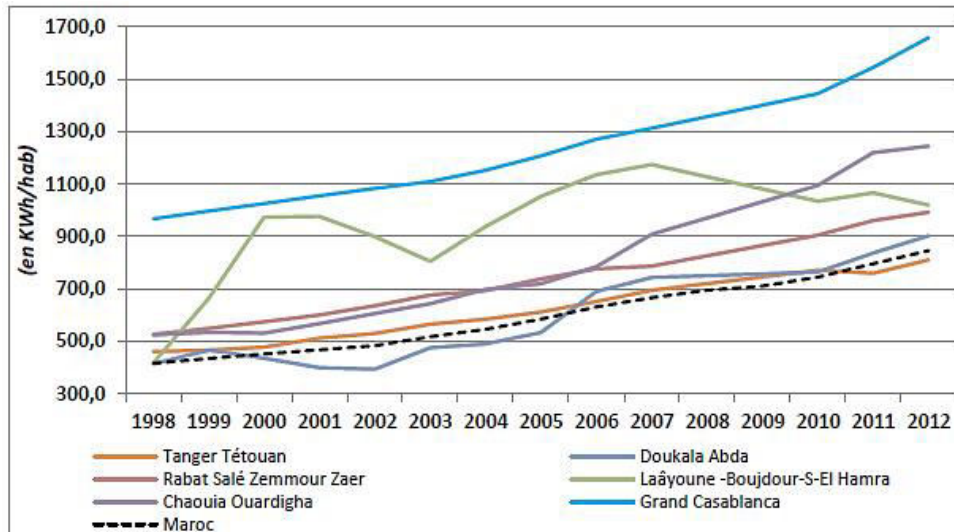
Figure 3: Electricity consumption per capita in some Moroccan regions [9]

Typical household's electricity consumption is normally defined as the required electricity to feed all the devices acquired by a household and having a primary objective to satisfy the daily needs of its occupants. The power consumption includes specifically all the most popular appliances that use electricity as a power source and which are indispensable for a daily domestic comfort. These include cookers and kitchen appliances, cooling appliances, heating and air conditioning as well as audio-visual and entertainment devices. The main purpose of the present design project is to meet the household's needs of typical farmers in rural areas including water pumping systems for irrigation. Nowadays, the majority of farmers rely on fossil fuels (butane and diesel) to irrigate their farmlands. For this reason, any kind of optimisation or modernization of water irrigation systems in rural areas will increase their efficiency and hence the annual households' income.

According to latest studies, several approaches have been used to determine a typical electricity consumption of households in urban and rural areas. Some of these are based on simplistic assumptions, while others give an estimation based on complex approaches describing the possible relationship that may exist between the occupants' habits and the household appliances use. To select an appropriate approach for the current design process, a comparative study of previously used methods is conducted. The approaches involved in this comparison are given as follows:

- **Estimating average typical electricity consumption using annual power consumption per household**: this is a straightforward method as it assumes that the regional/national average household electricity consumption can be used to determine the necessary power output of the wind energy conversion system. According to the report on assessment of regional potential development of photovoltaic in regions of Meknes-Tafilalet, Oriental and

Souss Massa Draa [10], the national average electricity requirements is **904 kWh/household. Year**. According to this approach, this annual consumption can be used as a typical households' annual electricity requirement in order to determine of the wind turbine size. The main drawback of this approach is that the values extracted draw a blurry picture regarding the type of household appliances that are represented by this consumption. Besides, the corresponding social classes that are represented by this consumption are not clearly defined. Subsequently, the aforementioned approach may cloud the vision upon which we are sizing the wind power system. Table 3 gives the electricity consumption per household in three main regions in Morocco as well as the national average value.

	Region of Meknès-Tafilalet	Eastern Region	Region of Souss-Massa-Draa	National average requirement
Average annual consumption [kWh/(household. Year)]	857	1100	992	904

Table 3: Average annual electricity consumption per household by region

- **Estimating average typical electricity consumption using minimum household electricity requirements:** based on this approach, the wind energy conversion system must produce the necessary power to supply a limited number of devices for short periods of times. This approach was used in the Global Rural Electrification Program (PERG) which was launched in 1996 by the national electricity and water utility company (ONEE). According to this approach, each household has a basic daily lighting, two hours of black and white television and an electrical outlet for mobile phone charger [10]. Users who want to use other appliances (example of refrigerators) should use other systems with higher power output. Table 4 summarizes the appliances involved in this approach for rural household [11].

Application	Power (W)	Number	Operating hours (hour/day)	Required energy (Wh/day)
Lamps	10	4	3	120
TV + satellite dish	15	1	3	45
Radio	10	1	4	40
Mobile phone	5	1	1	5
			Total daily consumption	210
			Total annual consumption	**76.650 Kwh/year**

Table 4: Average household electricity consumption per day

The size of the decentralized energy systems under the PERG program was taken to be 75W (75Wc represents the installed capacity of each system). The average power consumption per

household in remote areas was determined on the basis of this installed power. Therefore, the restriction on the power generation requires a limited number of household appliances. Limitations in terms of household appliances involved in this estimation make this approach unsuitable for this project.

• **Estimating average typical electricity consumption based on the users' standard of living:** according to this approach, the power produced from a stand-alone system, must ensure a satisfactory standard of living for the occupants of the household, and this for long periods of time. The power consumption of a household is assessed on the basis of a full coverage of necessary electrical needs. Table 5 summarizes all the appliances used in this approach and their power consumption.

Application	Power (W)	Number	Operating hours (hour/day)	Required energy (Wh/day)
Lamps	10	4	6	240
TV	50	1	5	250
Refrigerator	80	1	10	800
			Total daily consumption	1290
			Total annual consumption	**470.850 Kwh/year**

Table 5: Average electricity consumption for a satisfactory standard of living

In order to estimate the average power consumption of a typical household, it is assumed that the appliances considered here are sufficient to ensure basic domestic needs for its occupants. The determination of electricity requirements (the list of appliances) within this approach is based on a stand-alone system with an installed power of 260 W_p. Again, limitations in power installation impose a limited number of appliances. The impact of the improvement in standard of living on the households electricity needs is a key factor when this methodology is used. However, this parameter is difficult to quantify.

• **Estimating average typical electricity consumption using monitoring and measures:** this method consists in determining the power consumption of a household using technical instrument installed on the supply line of the household. For instance, a Datalogger can record the average power consumed over a period of 5 minutes and for a representative period of 2 years. An annual average value of 200,000 measurements can be collected for each household [12]. According to this method, the appliances in a household can be divided into four categories:

• Appliances continuously switched ON with constant power consumption (Continuous appliances);

- Appliances actively switched ON by householders. When they are not in use, their power consumption may be non-zero (Standby appliances);
- Appliances continuously switched ON with a power consumption cycles between zero and a set power level (Cold appliances);
- Appliances actively switched ON by householders. When they are not in use, their power consumption is zero (Active appliances);

The calculation of the average appliances power consumption is based on the combination of the results of the data analysis and the consumption profile of each appliances category. Analyzing the results of the collected data and combining them with the rhythm of the daily use of each appliance category, the daily power consumption of each category can be easily deduced. Table 6 gives the appliances categories and their power consumption (in-use and standby power consumption).

Appliance category	Category Description	Example of Appliance	typical in-use power(W)	Typical standby power (W)
Continuos	Continuously switched on and constant power consumption	- Clocks - Burglar Alarms - Broadband modems	2.5 4 5	- - -
standby	Actively switched on by householders. When not in use, power consumption may be non-zero.	- CRT TV - LCD TV - Plasma TV - Set-top boxes - Hi-fi - Mobile phone charger - Desktop	84 130 253 17 14 4 100	3.5 2 2.7 8 8.2 2.8 7.1
Cold	Continuously switched on and power consumption cycles between zero and a set power level	- Fridge / freezer	80-250	8.8
Active	Actively switched on by householders. When not in use, power consumption is zero.	- Kettle - Electric plate - Washer - Electric shower - Lighting—CFL - Lighting—incandescent	2000-3000 2500 2000 4000-9000 9-13 60-100	- - - - - -

Table 6: Household appliances categories and their in-use power consumption [12]

This evaluation model presents an accurate methodology in terms of the power consumption. However it requires considerable resources and sophisticated measuring instruments.

- **Estimating average household power consumption using statistical data:** the household electricity requirements are evaluated on the basis of the results of surveys on electricity consumption of households for a representative section of population. Power consumption is

strongly dependents on the people' standard of living, their financial ability to provide a variety of appliances and their daily habits. A set of useful information can be derived from these surveys including:

- Number of persons per household;

- Electrical energy consumption for lighting;

- Household appliances and the frequency of their use;

- Use of air conditioning or heating;

- Habits of the occupants of the household and their influence on power consumption;

Based on the data collected, the average annual electricity consumption per household can be determined by multiplying the unit power of each appliance by the number of operating hours, taking into account a load factors. This latter is generally useful to assess the consumption of an appliance that can undergo a number of ON/OFF cycles or when the appliance operate at different modes where the power consumption can vary from one operating mode to another (example of the normal operating mode and standby mode). Akinobu Murata et al. [13] give an estimation of urban residential electricity demand in China by using household survey data and by applying load factors. The advantage of this method is the simplicity of its use and the accuracy of its results as it is based on real data. Table 7 gives the load factors that have been used by the author to estimate the annual electricity consumption per urban household in China.

Household appliance	Load factors
TV	0.8
Refrigerator	0.36
washing machine	1
laptop computer	0.6
Lighting-CFL	1
Microwave	1

Table 7: Load factors for some household appliances [13]

Jung-Hyun Y et al. [14] present another approach using statistical survey data. Their method consists in determining the current and future electricity consumption in the residential sector on the basis of the daily habits of the occupants and their interactions with appliances inside the house. According to this approach, the electricity consumption of the household can be significantly affected by changes in the lifestyle of the occupants. Through their study, the authors found that refrigerators, lights, rice cookers and televisions account for over 70% of

the total electricity consumption in households. Therefore, any method of assessing power requirements must pay particular attention to this category of appliances.

This approach has more advantages than the previous ones as it incorporates the behavior and habits of the occupants of the household in the evaluation of the appliances load profile. However, it requires the more sophisticated surveys targeting people's habits and lifestyles within the home in order to conclude on the power consumption. A comparison between the above mentioned approaches reveals that the approach using residential power consumption survey data is the most adequate solution for the present project. This choice can be justified by the fact that this method has a simple and straightforward procedure. Additionally, the results derived from this approach are relatively significant. The approach based on statistical surveys has the following advantages:

- Availability of statistical data (e.g. national surveys on households consumption);
- simplicity of the used procedure;
- Accuracy of the results in comparison with the other approaches;
- Possibility of improving this approach by including other parameters derived from previous approaches such as the use of the appliances' load factors and their power consumption during standby mode;

2.3.2 Estimating power consumption of household appliances

Assessment of typical household electricity consumption consists in listing all the most used appliances. This step will be based on the results of the national survey of households' standard of living [15]. First, the power consumption of each appliance in normal operation is determined, and the household daily electricity use is calculated by multiplying the power of each appliance by an average number of daily operating hours. An estimation of the power consumption of a typical Moroccan household is done using the following steps:

❖ **Determination of typical household appliances in urban and rural areas**: this first step aims to evaluate the acquisition rate of household appliances. The acquisition rate is defined as the ratio of the number of households owning the appliance at the total number of households. The acquisition rate allows identifying the most common end-household appliances in urban and rural areas. The acquisition of a typical household appliance is strongly related to different parameters such as the location of the household (urban or rural area), the annual income of the household, the age of the head of household and his education level, the household size and finally the activity of the head of household's spouse. Based on the high planning commission report [15], table 8 summarizes the acquisition rate of appliances in a typical Moroccan household.

No.	Durable Appliance	Place of residence		
		Urban (%)	Rural (%)	All (%)
1	**Cookers, ovens and small kitchen appliances**			
2	Electric cooker	7.9	0.9	5.3
3	Electric stove with oven	2.3	0.4	1.6
4	Electric stove without oven	6.1	0.6	4.0
5	Electric oven	6.2	1.9	4.6
6	Microwave	4.5	0.3	2.9
7	Hood	1.9	0.0	1.2
8	Appliance Robot	55.0	23.7	43.2
9	**Refrigeration Equipment**			
10	Refrigerator	82.6	34.5	64.5
11	Freezer	5.4	0.5	3.6
12	**Large Appliances**			
13	Dishwasher	1.3	0.2	0.9
14	Washing machine	35.4	2.5	23.1
15	Electric dryer	1.7	0.1	1.1
16	Electric vacuum cleaner	6.7	0.5	4.4
17	Fan	11.4	6.1	9.4
18	**Other Appliances**			
19	Electric sewing machine	4.2	1.2	3.1
20	Electric machine knitting	5.2	2.5	4.2
21	**Heaters**			
22	Immersion heater	2.9	0.2	1.9
23	Electric heating device	3.2	0.5	2.2
24	**Audio-visual and Leisure Appliances**			
25	Radio	57.9	63.6	60.0
26	Radio only	17.7	26.3	20.9
27	Radiocassette	50.1	47.3	49.1
28	Color TV	89.8	52.9	75.9
29	Satellite Dish	60.6	27.2	48.0
30	Stereo	2.3	0.6	1.6
31	CD player	29.2	23.7	27.1
32	Printer	4.2	0.5	2.8

Table 8: Acquisition rate of appliances in a Moroccan Households

Determining the number of lighting points in a given household requires knowing its size. According to the High Planning Commission [16], the national average household size in 2014 was 4.6 people per household. This average is 4.2 people in urban areas and 5.3 people in rural areas. In order to determine the number of lighting points in a household with five

occupants, it is assumed that each household member has his own room. By adding the lighting point of a living room, kitchen, and bathroom, 8 light bulbs are sufficient to ensure an adequate lighting level inside the house. Table 9 gives the acquisition rate of the lighting points in rural and urban areas. Since lighting bulbs are the primary electric devices of an electrified household, the acquisition rate of lighting in rural areas is taken the same as the rural electrification rate which is given as 98% in 2011 [10].

		Urban (%)	Rural (%)
33	Lighting	100	98

Table 9: Acquisition rate of lighting points in a Moroccan household

The acquisition rate of household appliances, upon which this study is based, dates back to 2006/2007. Therefore, the estimation of power consumption of a typical household should take into account an eventual change in acquisition rate of some appliances. For instance, the use of the information and communications technology has experienced a rapid increase in recent years. Their acquisition rate is given by the National Telecommunications Regulatory Agency (ANRT) [17]. Table 10 gives the acquisition rate of the main information and communications technologies.

No.	Durable Appliance	Place of residence	
		Urban (%)	Rural (%)
34	Mobile Phones	97	88
35	Landline	34	11
36	Laptop computer	59	23

Table 10: Acquisition rate of information and communications technology

The appliances involved in the calculation of the power consumption in rural areas must include water pumping systems. This is because pumping systems in these geographic areas play a vital role in providing optimized solutions for energy and water supply, especially for agricultural activities which are the main source of the households' income. According to the national report on animal genetic sources [18], 77.7% of rural households (from a total number of 1,921,958) are farm households. The major part of water sources in these regions are underground and their use is mainly based on diesel or butane pumping systems.

Table 11 shows the acquisition rate of water pumps for irrigation in rural areas.

No.	Durable Appliance	Acquisition Rate (%)
37	Pumping system for irrigation	77.7

Table 11: Acquisition rate of water pumping systems for irrigation

Figures 4 and 5 summarize the acquisition rates of the household appliances in urban and rural areas.
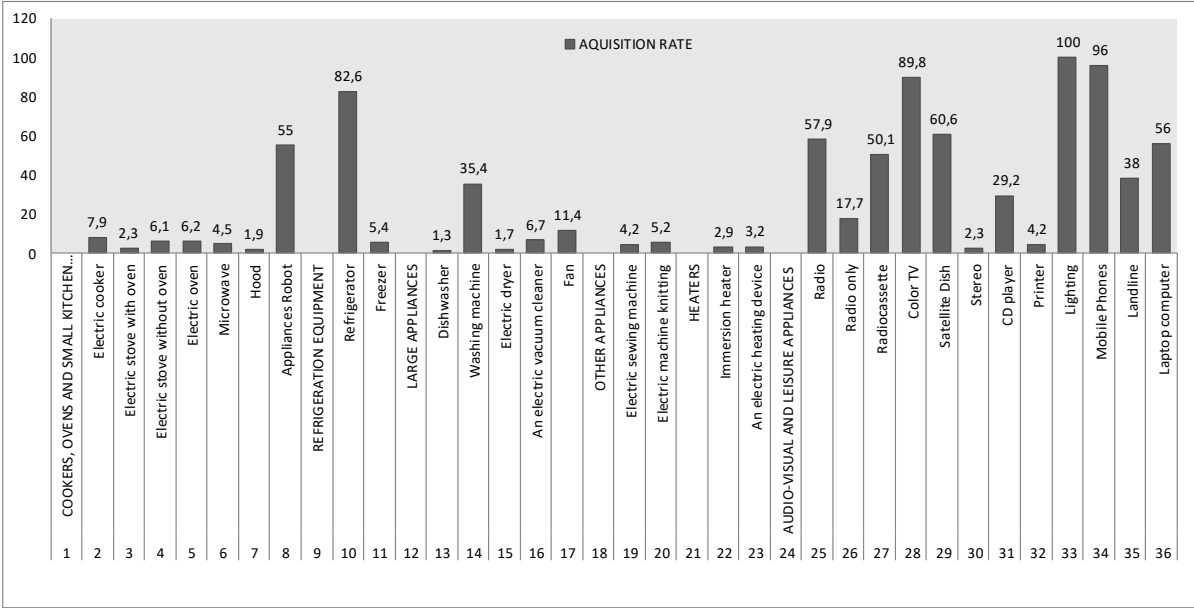
Figure 4: Acquisition rate of household appliances in urban areas
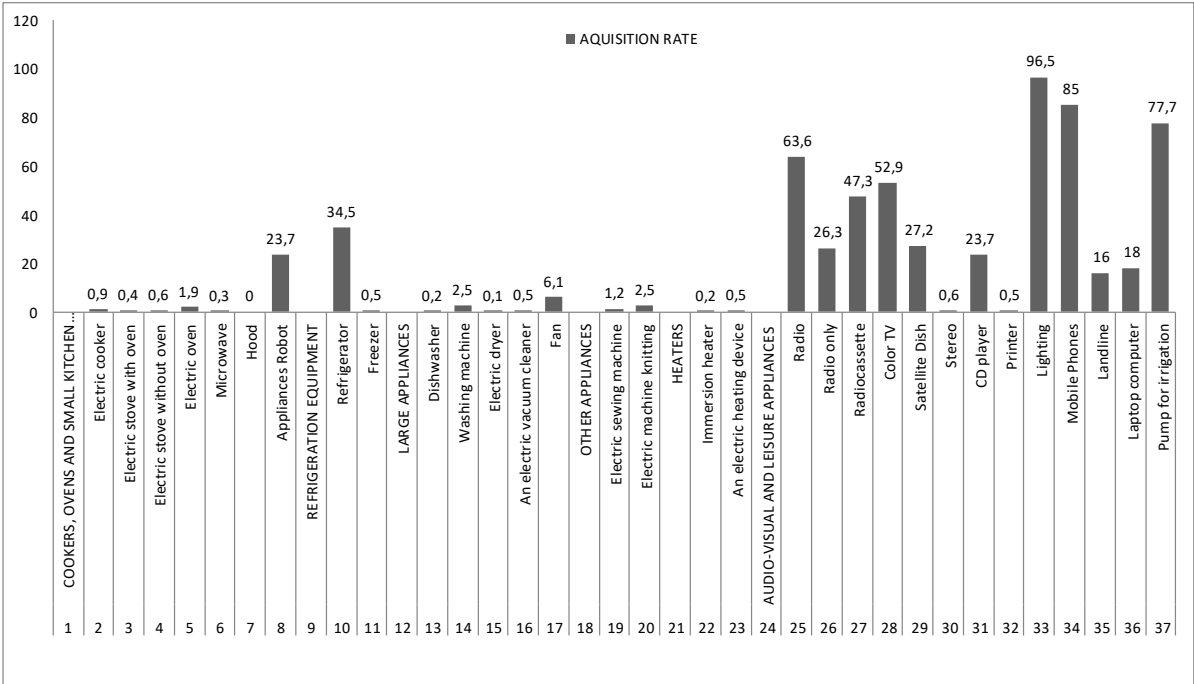
Figure 5: Acquisition rate of household appliances in rural areas

To ensure that the estimated electricity consumption is as representative as possible, only appliances with an acquisition rate exceeding 10% are considered. This percentage will cover all household appliances most affected by the improvement in the people's standard of living during the past decade. Actually, the improvement in population's standards of living combined with a significant increase in the annual expenditure per household make a set of

durable appliances accessible to different social classes **[19]**. Figure 6 illustrates the increase in acquisition rate of some household appliances.
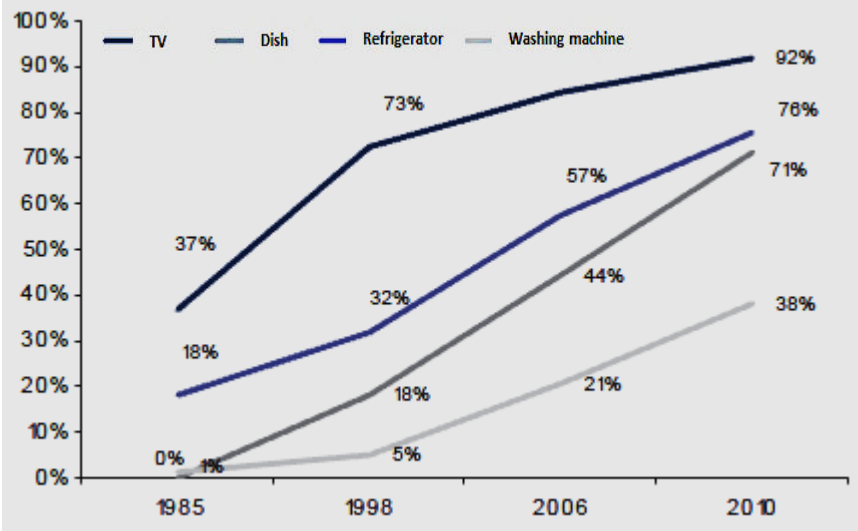
Figure 6: Acquisition rate of household appliances in rural areas, **[19]**

Balancing all the considerations mentioned previously, Table 12 shows the most accessible appliances upon which the calculation of typical household electricity consumption will be based.

Durable appliances in urban area	Durable appliances in rural area
Appliances Robot	Appliances Robot
Refrigerator	Refrigerator
Washing machine	Radio
Fan	Color TV
Radio	Landline
Color TV	Satellite Dish
Satellite Dish	Lighting
Lighting	Mobile Phones
Mobile Phones	Laptop computer
Laptop computer	CD player
CD player	Pumping system for irrigation
Landline	

Table 12: Typical household appliances in urban and rural areas

• **Determination of the daily electricity consumption of a typical household**: the size of the wind turbine system is strongly dependent on the overall daily energy consumption of the already selected appliances. In order to determine this required electricity, first the combined rated power of the household appliances must be determined. Then, the required electric energy is determined by multiplying the rated power of each appliance by the number of

operating hours per day. Table 13 summarizes the electricity requirements of typical urban households.

Appliance type	power unit (w)	period of use	frequency of use	Daily Consumption
Laundry C (60 ° C Cotton)	From 2500 to 3000	48 weeks	4 cycles/week	1.35 kWh /cycle 259 kWh/year
Refrigerator	200 to 350	365 days	Continuous	1370
Vaccum cleaner	450	240 days	30min/jour	225
Fan	Between 55-90	90 days	4h/day	360
Radio	5 to 10	365 days	5h/day	50
Color TV	From 80 to 100	365 days	5h/day	360
Satellite Dish	22	365 days	5h/day	110
Mobile Phones	5	335 days	2h/day	10
Laptop computer	From 50 to 100	365 days	5h/day	500
CD player	15-25	365 days	4h/day	100
Landline	5-13	365 days	Continuous	312
Lighting	15 to 25W (8 bulbs)	365 days	5h/day	600
Total Daily Electricity Consumption				5347 Wh/day
Total Annual Electricity Consumption				1952 kWh/year

Table 13: Daily electricity consumption of household appliances in urban areas

These consumptions represent an average values assessed on the basis of average real power, not the power measured in reality. For the fridge, the power used varies during the day. The data given for the evaluation of energy consumption are those contained in the data sheet of similar devices. For washing machine, power varies during the cycle. The data given for the evaluation of energy consumption are those contained in the data sheet of similar devices device.

Given that the significant amount of electricity attributed to water pumping systems in rural areas, it is essential to detail the methodology of calculating their daily energy requirements. The assessment of water requirements in rural areas is difficult to estimate. This is due to the fact that the water needs vary continuously and depend on several parameters such as the vegetation type, the weather conditions of geographical areas (temperature, humidity, wind speed, evapotranspiration), the season of the year and the type of the used irrigation system. The estimated water flow (m³/day) per household is based on data gathered from the report on the state of plant genetic resources for food and agriculture [20], wherein about 70% of farms have less than 5 hectares. To irrigate one hectare of crops, the necessary water flow rate

should be at least 60 m³/(hectare.day). This value represents an average of what is required to irrigate a range of vegetable crops. Table 14 gives the water flow requirement per day per hectare of crops.

Crops	Water flow (m³/ha.day)
Rice	100
Seeds	45
Sugar cane	65
Cotton	55
Celery	84
Chili pepper	50
Broccoli	54
Onion	34
Carrot	42
Lettuce	58
Average	**58.7**

Table 14: Required water flow for some vegetable crops

Groundwater availability is an essential element in assessing the needed power for pumping applications. Water availability is generally determined by the static and dynamic levels, which are directly related to the geographical conditions of the site. These two fundamental parameters are combined to define the Total Dynamic Head (TDH) of a water pumping systems. TDH is defined as the total equivalent height that water to be pumped, taking into account friction losses in the pipe. In Morocco, groundwater resources represent 20% of the overall water resources in the country, with a total number of 103 groundwater tables. Among the listed groundwater tables, 20 of them are considered deep. According to Lahmouri A. [21], the groundwater level in Morocco varies mostly between 10 and 30 m. Among the main groundwater tables, which are subjected to a regular piezometric monitoring program, 50% of them had levels below 10 m, 25% between 10 and 30 m and 25% have deeper levels. Taking into account an annual average decrease of groundwater piezometric level of 2 m/year, the majority of the groundwater tables throughout the country must currently have an average depth of 60 to 80 m.

The needed power to supply a water pumping system is calculated using the fluid power formula [22]:

$$E_{elec} = \frac{C_H \cdot Q_f \cdot TDH}{R_P} \qquad (1)$$

Where E_{elec} is the equivalent electric energy needed per day, Q_f is the required water flow per day, C_H is the hydraulic constant which is taken as 2.725 $\frac{kg.s.h}{m^2}$, and R_P is the water pump efficiency, depends on the type of pump and motor (this is assumed to be 0.65).

Using equation 1, the electricity required to cover daily water needs of five hectares of vegetables is estimated at **100 Kwh/day**. In order to validate the obtained result, existing experimental findings are used. Luc JP et al. **[23]** have conducted a set of experiments on 115 water pumps (from three different manufacturers) to determine the unit energy consumption required to raise 1 m³ of water to 1 m, and the actual absorbed energy density required to raise 1m of water in a particular pumping installation. For an irrigation system with a daily water flow of 300 m³/day and a TDH of 80 m, the required unit energy and the actual absorbed energy are given in Table 15.

Specification	Unit Energy (kWh/m³/m)	Actual absorbed energy density (kWh/m³)
- Nominal flow rate: 37.5 m³/h - TDH: 80 m	0.0049	0.32
Total energy required (kWh/day)	**117.6**	**96**

Table 15: Unit energy and actual absorbed energy density of a water pumping system

The comparison has revealed significant similarity between the results obtained from the present analysis and the experimental findings. The small differences in the results can be justified by the difference between the pump and motor efficiencies used in the calculation.

To sum up, table 16 gives the electricity requirements of a typical rural household.

Appliance type	Power unit (w)	Period of use	Frequency of use	Daily Consumption
Refrigerator	200 to 350	365 days	Continuous	1370
Appliances Robot	450	240 days	30min/jour	225
Radio	5 to 10	365 days	5h/day	50
Color TV	From 80 to 100	365 days	5h/day	360
Satellite Dish	22	365 days	5h/day	110
Mobile Phones	5	335 days	2h/day	10
Laptop computer	From 50 to 100	365 days	5h/day	500
CD player	15-25	365 days	4h/day	100
Landline	5-13	365 days	Continuous	312
Lighting	15 to 25W (8 bulbs)	365 days	5h/day	600
Pumping system for irrigation	From 15,000 to 30,000	365 days	8h/day	100000

Total Daily Electricity Consumption	103 637 Wh/day
Total Annual Electricity Consumption	37.8 MWh/year

Table 16: Daily electricity consumption of household appliances in rural areas

2.4 Research methodology

The present research work is concerned with the design process of a small wind turbine within Moroccan context and following the guidance of the international standard IEC 61400-2 for the design requirement of small wind turbines. The work in the present document is based on: the previous research work, calculations and/or simulation and on the best engineering practice. Figure 7 gives some details on the research methodlogy that was adopted for every step of the design process.
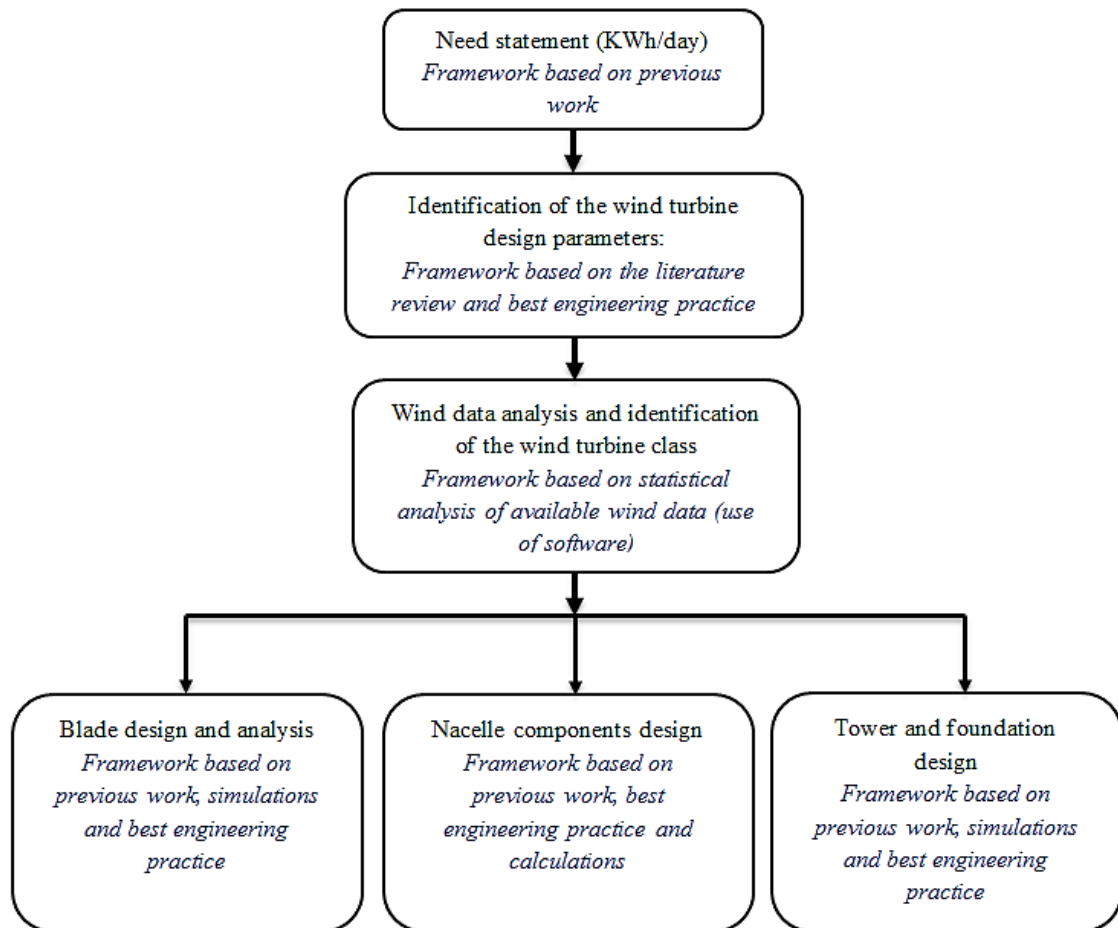
Figure 7: Research methodology for the design steps

2.5 Conclusion

The first part of the second chapter gives an overview of technological trends in the design of small wind turbines around the world. Based on the small wind world report, five countries account for over 50% of the small wind manufacturers. However, developing countries continue to play a minor role in small wind manufacturing. According to the same report, over

80% of the manufacturers of small wind turbines produce systems for stand-alone applications that include: residential, commercial and industrial, fishery and recreational boats, decentralized hybrid systems, pumping systems, desalination and purification, remote monitoring and finally telecom base stations. Regarding the future of this technology, the political support can be expected to increase the installed capacity of small wind in the upcoming years further. Accordingly, small wind industry can be expected to follow similar growth patterns of the large wind and solar industry until 2020. Based on a conservative assumption, the market could subsequently see a steady compound growth rate of 20 % from 2015 to 2020. The industry is forecasted to reach approximately 480 MW of newly installed capacity added annually in 2020 and achieves a cumulative installed capacity of close to 3 GW by 2020. Finally, this review section provides a comparative study of present technologies widely used in the wind energy industry. This study will be based on both an exhaustive review of the state of the art and an effective comparison of different topologies adopted for the design and manufacture of commercially available small wind turbines having rated power between 10 kW and 11 kW.

The second part of this chapter gives a detailed assessment of the need in terms of kWh/day for a typical household in Morocco. Based on the results of the national survey on electricity consumption of households, an electricity consumption of 103 637 Wh/day was found. This electricity consumption will be used to determine the power of the wind power system.

CHAPTER 3: WIND TURBINE DESIGN FRAMEWORK

Small wind turbines are subject to different external conditions that may affect the efficiency and the durability of the entire system. To ensure an appropriate level of safety and reliability, environmental conditions must be considered in the design process of the wind turbine.

Based on the external conditions, the wind class of the turbine machine can be determined. The environmental conditions can be divided into two categories: wind conditions and other external conditions (temperature, humidity, lightning, sunlight, etc.). Each type of these conditions can be further subdivided into normal and extreme conditions. Normal conditions are generally related to the situations in which the turbine machine is operating at its rated wind speed, while the extreme conditions are rare to happen but potentially critical as they may affect the security and stability of the whole turbine machine. Each wind turbine model is usually designed according to whether it is intended to be installed in areas with low wind speeds or in very windy areas. To avoid over-designing wind turbines (that can operate reliably on all sites), manufacturers design their wind turbines for a specific wind class. Therefore, each commercially available wind turbine is associated to a particular wind regime which is expressed in terms of a wind class.

The aim of this chapter is to determine the behavior of the wind in different regions across Morocco and specify the design parameters of the wind turbine. Wind data analysis will be done using statistical analysis of wind data provided by the Climatic Data Center (NCDC) of the National Oceanic and Atmospheric Administration (NOAA). The structure of this chapter is given as follows: first, an overview of wind turbine classes will be given. After, a description the commonly used methods for statistical analysis of wind data will be presented. Finally, the results the statistical analysis of wind data, for different locations across Morocco, will be discussed. Determination of an appropriate wind class is based on the recommendations of the international standard **IEC-64100-2** (International Electrotechnical Commission). This standard, specifically addressed to small wind turbine designers, presents different requirements that are intended to ensure that any small wind turbine design will appropriately be engineered against damage from different operating scenarios within its planned lifetime.

3.1 Small wind turbine class

In designing a small wind turbine, the external conditions are mainly defined by the wind conditions of the site where the system will be implemented. These conditions are specifically

defined by different wind speeds and by the turbulence intensity. Wind turbine classes are mainly defined by an average annual wind speed, V_{ave}, (measured at the hub height), a reference speed, **V_{ref}**, which is defined as the extreme 10-min average wind speed with a recurrence period of 50 years at the turbine hub height and by the turbulence intensity on the site. The term turbulence in this case, indicates the variation of the wind speed from the average wind speed over a typical period of 10 minutes. Generally, the turbulence intensity, I_{15}, is measured for a wind speed of 15 m/s [7]. In order to classify the wind turbines according to extreme wind conditions, the modern wind power industry is mainly oriented to the international standards including those of the International Electrotechnical Commission (IEC). The classification given by this standard is used to define different types of wind turbines according to their behavior in different wind conditions (normal and extreme). Five different classes are defined and Table 17 summarizes the main characteristics of each class. The parameter **a** is the slope parameter for turbulence standard deviation model.

SWT Class		I	II	III	IV	S
V_{ref}	(m/s)	50	42.5	**37.5**	30	Values specified by the designer
V_{ave}	(m/s)	10	8.5	**7.5**	6	
I_{15}	(-)	0.18	0.18	**0.18**	0.18	
a	(-)	2	2	**2**	2	

Table 17: Basic parameters of wind turbine classes

To select an appropriate wind turbine for a typical site, all the wind conditions of that site (average speed, gust, and turbulence) must be covered by the wind class of the chosen wind turbine. For instance, a small wind turbine designed for lower wind speeds, the design loads are going to be smaller; therefore its blades can be chosen to be larger and the hub height must be taller. As a result, bigger rotors of class **III** capture more wind energy and yield higher capacity factors compared to class **I** or **II** rotors. In the case of a special design (the case of special wind conditions or other external conditions), a new class of small wind turbines, class S, is defined. The design values for the small wind turbine class S shall be chosen by the designer and specified in the design documentation. For this type of wind turbines, the values chosen for the wind conditions must reflect more severe environment than anticipated for the use of small wind turbines.

According to the **IEC-64100-2**, external conditions defined for classes **I, II, III** and **IV** are not intended to cover conditions at sea or wind conditions encountered in tropical conditions such as hurricanes, cyclones and typhoons. These conditions require very specific turbine design according to the class S criteria [7].

3.1.1 Site-specific wind characterization

To characterize the wind on a given site, it is necessary to determine its behavior by specifying different wind parameters. These include the wind directional profile which is defined as the probabilistic trends in wind direction, the wind speed distribution in these directions, the distribution of energy in these directions, the wind profile (which is the probabilistic wind speed trends, the law of probability distribution of these speeds, the wind speed most often encountered, the extreme wind speed, and the wind gusts, etc.) and the annual/daily variations. Typically, the wind data in a well-determined site is often collected either by using physical measurement or by calculation and modelization.

The acquisition of physical measurement of wind data consists in using measurement towers, which are equipped with a set of instruments (vanes, anemometers, thermometers and/or barometer and/or hygrometer etc.) and placed on specific points of the site. With these devices, a set of data can be recorded and transmitted to the Datalogger of the tower.

Measurements are recorded within an interval of time, typically 10 minutes. The choice of this interval is justified by the fact that the data recorded will be least disturbed by random and non-effective variations [24]. Figure 8 shows an example of fluctuations in wind data during different intervals of time.
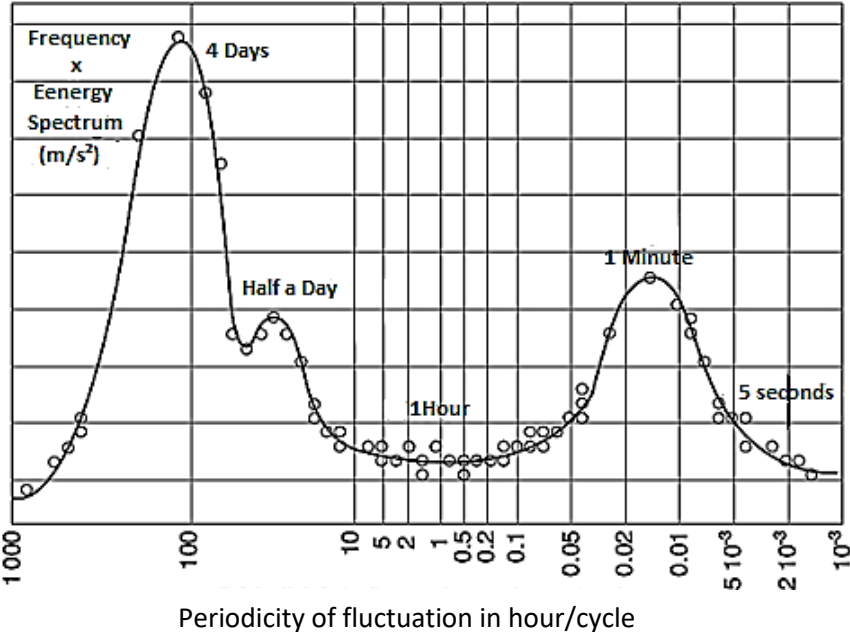
Figure 8: Example of turbulent fluctuations in wind data [24]

For periods of 10 min and the 5 hours, it can be seen that the energy content of the wind is not affected by turbulent fluctuations. Therefore, if an average rate of 10 min is chosen, while getting a good sampling rate of time along the 24 hours, data will be less random. Therefore, the measurements will be more reliable as they reflect physical properties of the wind on the

site. In general, wind data measurements over a period of 12 months at several heights are sufficient to understand the behavior of the wind at a given site. During this period, three different parameters must be recorded every 10 minutes. These are the average and the maximum wind speeds, the wind directions, and the standard deviation of the 10 minutes wind speeds. These measurements should be taken at three different heights in order to fully understand their vertical profile.

3.1.2 Statistical analysis of wind speed distribution

The wind speed at a given location is continuously varying in a random and unpredictable manner. The annual mean wind speed is subject to changes from year to year, from one season to another, with passing weather systems, on a daily basis and from second to second [25]. For this reason, statistical analysis of wind speeds is of paramount importance as it allows determining the frequency of occurrence of each wind speed.

The most important characteristics of the long-term variations of wind speed can be described by a frequency or probability distribution. Various mathematical tools have been used for the analysis of wind speed data. A convenient mathematical distribution function that has been found to fit well with data is the Weibull probability density function, whose probability density match in most of the times the actual wind speed measurements [26,27]. This function is mainly described using two parameters: the shape parameter **k** and the scale parameter **c**. The general form of the Weibull distribution, for a specific wind speed,V, is given by [28]:

$$f(v) = \frac{k}{c} \cdot \left(\frac{V}{c}\right)^{k-1} \cdot e^{-\left(\frac{V}{c}\right)^k} \tag{2}$$

This formula is valid for k>1, V≥0, and c>0. The value of the shape parameter varies usually between 1.5 and 3 [29]. At an average wind speed, a low shape parameter indicates a relatively wide distribution of wind speeds around the average and a high shape parameter indicates a relatively tight distribution of wind speed around the average. If the value of these parameters, at the anemometer height, z_a, are c_a and k_a, then their corresponding values, at a higher level $z \neq z_a$, can be determined using equations 3, 4, and 5 [30].

$$C_z = c_a \cdot \left(\frac{z}{z_a}\right)^n \tag{3}$$

$$k_z = \frac{k_a \cdot \left[1 - 0.088 \ln\left(\frac{z_a}{10}\right)\right]}{\left[1 - 0.088 \ln\left(\frac{z}{10}\right)\right]} \tag{4}$$

The exponent n is expressed as:

$$n = \frac{[0.37 - 0.088 \ln c_a]}{\left[1 - 0.088 \ln \left(\frac{Z_a}{10}\right)\right]} \tag{5}$$

Various methods have been developed to estimate the Weibull distribution parameters [31]. The most widely used are the method of moments [30, 32], the Maximum Likelihood method [33], the least square method [30, 34], and the Chi-square method [34]. The method of moments has been selected for wind data analysis in this study. This method presents a very simple and straightforward procedure as it enables determining the Weibull parameters by just using the main wind speed, V_{ave}, and the standard deviation, σ. This technique is commonly used in the field of parameter estimation [35]. Once the mean wind speed and the standard deviation of the wind data are known, the following equations can be used to calculate the Weibull parameters:

$$k = \left(\frac{0.9874}{\frac{\sigma}{V_{ave}}}\right)^{1.0983} \tag{6}$$

$$c = \frac{V_{ave}}{\Gamma\left(1 + \frac{1}{k}\right)} \tag{7}$$

Where $\Gamma()$ is the gamma function, which is given by:

$$\Gamma(x) = \int_0^\infty t^{x-1} e^{-t} dt \tag{8}$$

A special case of Weibull distribution function is Rayleigh probability density function. This single parameter density function is recommended by the **IEC-64100-2** standard, especially when the wind data analysis is mainly based on rough estimates without measurements. The Rayleigh distribution is a special case of the Weibull distribution, in which the shape parameter is taken as 2. The Rayleigh distribution function is given by [36]:

$$f(v) = \left(\frac{2V}{c^2}\right) \cdot e^{-\left(\frac{V}{c}\right)^2} \tag{9}$$

The vertical wind profile is another important factor that must be taken into account when estimating wind speeds for different heights. In general, wind speed measurements are made at a standard height which is usually taken to be 10 m. For projects involving wind conversion system, it is crucial to estimate wind speeds at various elevation.

The common power law that can be used to obtain the extrapolated values of wind speed at different heights is given by [37]:

$$V(z_2) = V_{z1} \left(\frac{z_2}{z_1}\right)^m \tag{10}$$

Where

V_{z1}: Wind speed at the measurements height, usually taken as 10m;
z_2: Height at which a wind speed estimation is required;
m: Power law exponent of wind speed;

Power law exponent, called also roughness coefficient, varies according to the roughness of the terrain. The value of roughness coefficient ranges between 0.10 (smooth terrain) to 0.40 (very rough terrain) [24]. If there is no specific information, the **IEC 61400-2** standard recommends using a roughness coefficient of 0.2. This value corresponds to a roughness length of approximately 0.10 m (agricultural land with some houses and 8 m high hedges with spacing of approximately 1250 m) [3]. The normal wind profile model, in the present study, will be used with a roughness coefficient of 0.2.

Another important parameter that can be used in wind data analysis is the wind power density function. This parameter gives the distribution of wind energy at different wind speeds. It is well known that the power of the wind that flows at speed V through a blade sweep area A increases as the cube of its velocity and is given by [38, 39]:

$$P(V) = \frac{1}{2}.\rho.A.V^3 \tag{11}$$

Where

ρ : Air density, taken as 1.225 Kg/m^3
A : Wind turbine rotor swept area (m²)

Wind power density per unit area for a specific region, based on the Weibull probability density function, can be expressed as follows [28, 29, 35]:

$$P = \int_0^\infty P(V)\, f(v)\, dv = \frac{1}{2}.\rho.c^3.\Gamma\left(1+\frac{3}{k}\right) \tag{12}$$

3.1.3 Wind data analysis and wind class selection

The present analysis is carried out using annual mean wind speed data of different locations across Morocco. A time series of daily measured wind speeds, recorded over a period of 20 years, were used for the statistical analysis of the wind speed and the wind power density. The used wind data are provided by the Climatic Data Center (NCDC) of the National Oceanic and Atmospheric Administration (NOAA) [40]. NCDC center, which is based in Asheville, North Carolina, United States, maintains the largest archive of climate data in the world and

provides climate services to different worldwide users. The first mission of this center is to preserve climate data and make them available to the general public, businesses, industry and researchers. Climate data provided by NCDC were used in a wide variety of applications, including agriculture, construction, education, energy, and engineering. Besides, it represents a reliable source for wind energy community, especially for pre-feasibility study of wind farm projects development. Statistical methods applying Weibull distribution was used to evaluate the wind speed characteristics and the wind potential at a height of 10 m above the ground level using annual average data. Annual mean wind speed is derived for three hub heights of 18 m, 24 m, and 40m. These tower heights are presented here because they are commonly used in small wind turbine installations. The number of locations that have been analyzed is 45. Among them, 16 windiest locations are selected for the statistical analysis. The analysis includes calculation of shape and scale parameters, annual mean wind speed, and mean power density. The results obtained give a global picture of the distribution of the wind potential in Morocco, especially for small wind turbine applications. Table 18 summarizes the main results of the statistical analysis.

Location	Vave (m/s) 10 m	c (m/s)	k	Vave (m/s) 18 m	Vave (m/s) 24 m	Vave (m/s) 40 m	Power density (W/m²)-10 m
k.Elbaida (**TETOUAN**)	8,38	9,46	2,26	9,43	9,99	11,06	615,15
SENDOUK (**TANGER**)	6,91	7,8	2,07	7,77	8,23	9,12	373,09
FARDIWA (**KSAR SGHIR**)	7,58	8,57	2,39	8,52	9,03	10	438,11
MY BOUSSALHAM (**KENITRA**)	3,35	3,74	1,66	3,77	3,99	4,42	54,05
BOUZNIKA (**BENSLIMANE**)	3,42	3,86	2,28	3,84	4,07	4,51	41,49
EL GAADA (**TIZNIT**)	4,06	4,57	1,9	4,57	4,84	5,36	82,27
TAMAGROUT-ZAGORA (**OUARZAZATE**)	3,43	3,75	1,4	3,85	4,08	4,52	73,99
TAN-TAN PORT	4,32	4,88	2,12	4,86	5,15	5,7	89,30
TINIGHIR (**DAKHLA**)	6,75	7,59	2,72	7,59	8,04	8,91	280,66
Tarfaya	6,32	7,03	3,39	7,11	7,53	8,34	203,59
FOUM EL OUAD (**LAAYOUNE**)	8,26	9,12	3,68	9,29	9,84	10,9	434,65
CAP SIM (**ESSAOUIRA**)	7,32	8,25	1,92	8,23	8,72	9,66	478,19
COL DE TOUAHAR (**TAZA**)	6,40	7,21	1,9	7,20	7,63	8,45	323,08
SELOUANE (**NADOR**)	2,96	3,32	1,72	3,33	3,53	3,91	35,88
TALIOUINE (**TAROUDANT**)	4,73	5,2	1,42	5,32	5,63	6,24	191,59
HAD HRARA (**SAFI**)	5,24	5,88	1,77	5,89	6,24	6,91	191,57
National average wind speed	**5,6**	**6,3**	**2,2**	**6,3**	**6,7**	**7,4**	**244,2**

Table 18: Wind data for different locations in Morocco

As it can be seen, a mean annual wind speed of 7.4 m/s is to be expected when installing a small wind turbine at a hub height of 40 m. This particular wind speed is almost the same as

that required by the wind class three of the **IEC 61400-2**. In order to ensure an appropriate level of safety and reliability of the turbine design, wind loadings at the most likely used hub heights (18 m, 24 m and 40 m) must be considered. Therefore, a **wind turbine class three-III** is selected for the current design process. Based on wind data provided by this wind class and through a proper load analysis, it is possible to check the ability of the turbine system to withstand the most extreme wind conditions that may experience during its life cycle. Additionally to the annual mean wind speed, determining the modal wind speed is an important task to carry out in order to know the speed at which the wind most frequently blows in a given site. This can be easily done by plotting the probability density function for each wind speed against the corresponding wind speed, as shown in Figure 9.
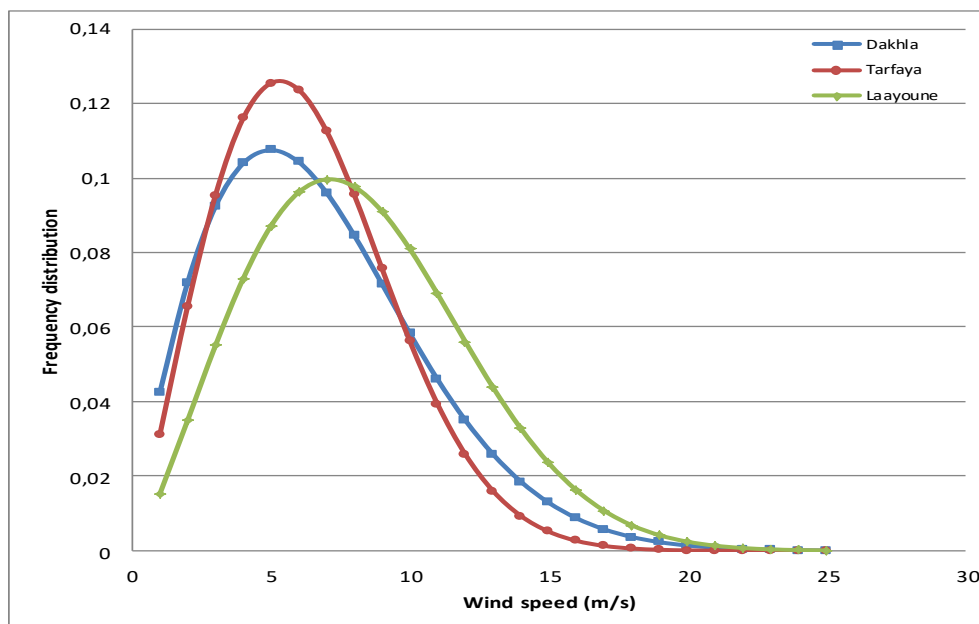
Figure 9: Weibull distribution for fifteen windiest locations in Morocco

From the figure above, it is clear that the most probable wind speed, at a reference height of 10 m, ranges between 2 and 5 m/s. As a wind class three was selected for the present design process, the corresponding annual mean wind speed, V_{AMWS}, is set to 7.5 m/s.

3.2 Small wind turbine design power output

The small wind turbine has a rated power output of 11.000 W. The selected generation power was determined by considering the use of electrical appliances to meet the needs of a typical household in remote areas. Based on a daily electricity consumption of 103.637 kWh, which is taken as the average consumption of a typical Moroccan household in a rural area, equation 13 gives the design electrical power of the small wind turbine **[41]**.

$$P_{design} = \frac{103.637}{C_{ptot} \cdot 24h/j} = 10.795 \text{ kW} \tag{13}$$

Where C_{ptot} is the total efficiency of the wind turbine conversion system. Including the efficiency of the drive train, the generator (assuming an overall transmission efficiency of 90%), and aerodynamic losses through the action of viscosity, it is reasonable to assume that the power converted into electricity is about 40% [41]. For the next steps of the design process, an electrical power generation of 11 kW will be taken as the design power output of the small wind turbine.

3.3 Design wind speed and rated wind speed

The rated wind speed is the wind speed at which the rotor is spinning at its maximum conversion efficiency. For a good blade design, the turbine should produce its rated power which usually corresponds to the generator rated power output considering the overall transmission efficiency (mechanical and electrical efficiencies) [42]. The design wind speed is defined as the wind speed at which the wind turbine rotor spines with a maximum power coefficient [43]. For a fixed pitch variable speed wind turbines, there is no simple way to express power output exactly in a mathematical expression for the rotor for wind speeds above rated wind speed. But for an optimum control strategy, between the cut-in wind speed (3 m/s in the case of this project) and the rated wind speed, the rotor should work at its maximum efficiency, and between the rated wind speed and the cut-out wind speed, the rotor is expected to produce a constant rated power [42]. According to the IEC61400-2 standard, the design wind speed, V_{design}, of a small wind turbine should be 1.4 times of the annual mean wind speed, V_{AMWS}. For the present study, as the mean annual wind speed is set to 7.5 m/s, the design wind speed can be calculated using equation 14 [7]:

$$V_{design} = 1.4\ V_{AMWS} = 10.5\ \text{m/s} \tag{14}$$

Given that the wind turbine will be designed to operate at its maximum power coefficient (Cp), from cut-in speed to the rated wind speed, **the design wind speed is chosen to be the same as the rated wind speed.**

3.4 Wind turbine rotor diameter

The rotor diameter, D, is calculated using equation (15) which describes the turbine power output, P_{design}, as a function of the design wind speed, V_{design}.

It can be seen that the power output from the turbine is a cubic function of the design wind speed. Therefore, slight deffirence in wind speed will significantly affect the power output of the wind turbine.

$$P = C_{ptot} \cdot \frac{1}{2} \cdot \rho \cdot \left(\frac{\pi}{4} \cdot D^2\right) \cdot V_{design}^3 \tag{15}$$

ρ: The air density ($\rho= 1.225 \text{ kg/m}^3$);

V$_\text{design}$: Design wind speed ($V_\text{design}=10.5\text{m/s}$);

By considering various components efficiencies, and fixing a target power output of 11 kW, the required rotor diameter is 7 m. Therefore, the new blade design will be planned for a length of 3.5 m from the center of the hub to the blade tip, to maintain a 7 m rotor diameter.

3.5 Wind turbine blades number

Blade number selection is also an important parameter in the small wind turbine design. This is due to the fact that this parameter will eventually affect solidity (which is defined as the ratio of the planform area of the blades to the swept area) of the turbine. Additionally, the blade number is related to the balance of gyroscopic loads (because yawing of the turbine while the rotor is spinning may result in significant gyroscopic loads) [44]. Most modern wind turbines used for generating electricity have three blades, although some have two or even one. Three blades have the particular advantage that the polar moment of inertia with respect to yawing is constant, and is independent of the azimuth position of the rotor. This characteristic contributes to relatively smooth operation even while yawing. Using more than three blades could also result in a rotor with a moment of inertia independent of blades position, but more than three blades are seldom used. This is primarily because of the higher costs that would be associated with the additional blades [45]. The only disadvantage of a three-bladed wind turbine is its relatively high price which is about twice the price of a two-bladed wind turbine [41]. Two blades are significantly cheaper, require a physically smaller and hence cheaper generator for the same power and have a lower brake torque. For the present design process, the three bladded option was selected.

3.6 Wind turbine drive train topology

Different wind turbine concepts have been developed and built to maximize the energy production, to minimize the cost and to improve the power quality. Such turbine concepts can be classified on the basis of the rotational speed, power regulation, and drive train topology.

One of the key components in a wind turbine system is its drive train system. This mechanical system is used to link the aerodynamic rotor and the electrical output terminals. Optimization of wind turbine generators cannot be realized without considering mechanical and structural performance of the drive train.

When considering the power transmission concepts, the wind turbine systems can be classified into the direct-drive and the geared concepts:

- **Conventional: gearbox and high speed generator with few pole pairs**: in a geared wind turbine, the generator speed is increased by transferring the mechanical energy from low to high speed. The geared generator system has the advantages in terms of the size and weight (small generators). However, the Implementation of a gearbox has its own disadvantages such as maintenance problem, installation complication and cost of equipment. The gearbox is one of the reasons for audible noise in wind energy systems. The losses in the gearbox are comparable to the losses in the electric machine [46].

- **Direct drive: any drive train without a gearbox and low speed generator with many pole pairs.** Direct drive topology is a solution where the wind turbine rotor is directly, through a shaft, connected to the generator rotor. By using a direct drive generator, the gearbox is excluded from the system. When excluding a gearbox, the overall system becomes simple easier to install, quite in operation. Moreover, the direct-drive generator system is better in terms of the energy yield, reliability, and maintenance [47].

According to a review of previous studies, it can be concluded that the direct-drive systems are the most suitable solution for small scale wind turbine machines [48, 49, 50, 51, 52]. With a focus on designing a wind turbine which is both efficient and reliable, it was easily recognized that the gearbox must be eliminated. Gearboxes, commonly found in many turbines, create mechanical losses and places more stress on the generator. The gearbox is also prone to failure. Each time the gearbox needs to be replaced, a costly repair is necessary involving a crane and significant downtime. Due to the possibility of employing power electronics converters, gearless, or in other words, direct driven systems can suite for variable speed applications. Therefore, **this particular solution is selected for the present project.**

3.7 Flow regime

Wind turbine systems always operate at relatively low hub height above the sea level where the lowest portion of planetary boundary layer (PBL) is found. Within this atmospheric boundary layer, the laminar air flow is made turbulent and slowed down by obstacles and topology, and as a result, the turbine's startup behavior is affected together with its performance [53]. Therefore, it is necessary for small wind turbines to achieve good start up response and low wind speed performances. These parameters are mainly defined by the Reynolds number at which the wind turbine operates. The Reynolds number is defined as the ratio of the inertial force to the viscous forces of the air, and can be determined using equation 16.

$$R_e = \frac{U_{rel} \cdot C}{\mu} \tag{16}$$

Where μ is the kinematic viscosity of the air, U_{rel} is the relative wind velocity to the airfoil, and C is the chord length of the airfoil. By using a chord length of 0.25 m (an average value from literature), at the middle section of an 11 kW wind turbine blade, the range of Reynolds number can be obtained from the relative wind velocity, U_{rel}, which in turn, can be calculated from the velocity triangle at the middle section of the blade [43, 54, 55]. According to Wood H. [41], for sufficiently high tip speed ratios, λ, the relative wind speed can be approximated using the following formula:

$$U_{rel} = \lambda_{0.5} \cdot V_{design} \tag{17}$$

Where, $\lambda_{0.5}$ is the tip speed ratio of the middle blade section,

As the majority of small wind turbines are usually designed to achieve maximum efficiency at the tip speed ratio of 6 to 8 [56], the corresponding Reynolds numbers for this operating rang are shown in table 19:

Tip speed ratio	Chord length (m)	Relative wind speed (m/s)	Reynolds number
6	0.25	31.5	525 000
7	0.25	36.75	612 500
8	0.25	42	700 000

Table 19: Estimated Reynolds number for a typical small wind turbine blade

3.8 Rotor blade airfoil selection

3.8.1 Low Reynolds number airfoils

Generally, the rotor blades of small horizontal-axis wind turbines operate at low Reynolds numbers, R_e, along their entire span. The low Reynolds number regime can be defined as that for which laminar separation dominates the drag. Therefore, the Reynolds number range that defines this subcritical flow regime is airfoil dependent. Actually, there is no fixed Reynolds number range that bounds the low Reynolds number regime. Most research work states that the term low Reynolds number has come to mean the flow regime where the chord Reynolds numbers below 500.000 [57, 58, 59, 60]. This is why small HAWTs are said to usually operate at low Reynolds numbers independently of the airfoil(s) used on the blades. Some other research work states that the low Reynolds numbers regime is fixed below 1.000.000 [61].

At low Reynolds numbers, turbulent reattachment usually follows laminar separation, thereby forming the so-called laminar separation bubble. Most of the unusual aerodynamic characteristics at low Reynolds numbers can be justified by the presence of a laminar separation bubble on the airfoil. The length and behavior of the laminar separation bubble is

airfoil, Reynolds number, and angle of attack dependent, typically moving toward the leading edge with increasing angle of attack.

Airfoils at low Reynolds numbers do not behave like aerofoils at high Reynolds numbers. For example, thick airfoils and those designed for higher Reynolds numbers usually have an undesirably wider Reynolds number range for which the flow is subcritical as compared with thin and low Reynolds number airfoils. Generally, traditional airfoils exhibit poor performance at low Reynolds numbers because of laminar separation effects. Therefore, optimum aerodynamic performance of small HAWTs is found through the use of airfoils designed for this subcritical flow regime. From the large variety of airfoils, only a few low Reynolds number airfoils have been designed specifically for small HAWTs [57].

3.8.2 Aerofoils for horizontal-axis small wind turbines

Blade airfoils are the most important elements in a wind turbine rotor structure. Airfoil characteristics will determine the performance of the wind turbine, expressed in terms of lift coefficient, C_L, and drag coefficient, C_D. Lift and drag coefficients of an airfoil are the central parameters for designing a wind turbine rotor and are the foremost parameters to be considered.

There are many different airfoils including the general aviation airfoil NACA (National Advisory Committee for Aeronautics) series, which have been widely employed in wind turbine applications. With the rapid growth of wind power industry, dedicated airfoils have been developed. For example, the S series airfoils, which were designed by National Renewable Energy Laboratory (NREL) in the USA, are popular in stall-regulated wind turbine blades due to their gentle stall behaviors; the FFA-W series airfoils originate from Sweden and Risø series from Denmark, which were designed for lower Reynolds number wind turbine blades; and the DU series airfoils, which were designed in the Netherlands, are popular in middle and high Reynolds wind turbine blades [62]. The section below gives an overview on the most used low Reynolds number airfoils.

❖ **S8XX Airfoils:**

Aerofoils that are of interest here are the S823 and the S822 (used for root and tip regions, respectively) which were designed for small stall-regulated wind turbines ranging from 2 to 20 Kw [63]. The tip and root regions are only considered because of their contribution in power extraction (outer part of the blade) and starting torque (part near the hub). Their design Reynolds numbers are 400,000 and 600,000 for root and tip sections, respectively. To comply with the stall-regulated type, they were designed to produce restrained lift to limit excessive torque. Their thicknesses are 0.21% and 0.16%. They were experimentally investigated by

Selig and McGranahan over a Reynolds number range from 100,000 to 500,000 up to the stall angle [64]. Seven airfoil families consisting of 23 airfoils have been designed for various size rotors since 1984.The appropriate blade length and generator size for the first three airfoils along with the corresponding airfoils type are shown in Table 20. Greater thickness is desired for the blade-root airfoils to accommodate structural and dynamic considerations. The blade-root airfoil thickness falls in the range of 18% to 24%. Thicknesses greater than 26% were found to result in unacceptable performance characteristics [63].

Blade length (m)	Generator size (KW)	Thickness category	Airfoil Family (root----------------Tip)			
1-5	2-20	Thick		S823		S822
5-10	20-150	Thin		S804		S803
5-10	20-150	Thin	S808	S807	S805A	S806A

Table 20: National Renewable Energy Laboratory (NREL) Airfoil Families [63]

From the literature, it appears that the S822 and S823 airfoils are the only two airfoils that have been specially designed for small blades [65]. These two airfoils are principally intended for stall regulated HAWTs and form one of the nine advanced NREL airfoil families [66].

❖ **SG604X Airfoils:** this aerofoil series was developed specifically for small variable-speed wind turbines sized from 1 to 5kW [66]. For this type of operation, the turbine blade is controlled to operate within a smaller angle of attack range than that of stall-regulated type. The design, therefore, focused primarily on a narrower incidence range than those of stall-regulated types. The series consists of four aerofoils: SG6040, SG6041, SG6042, and SG6043 with a design Reynolds number of 300,000 [67].

❖ **DU 93-W-210 Airfoil:**

The 21% thick wind turbine airfoil DU 93-W-210 was designed by Timmer and tested in a same low speed wind tunnel at Delft University of Technology. The DU 93-W-210 airfoil is the only high Reynolds number airfoil that is considered in this analysis. The design Reynolds number is in the range of this airfoil family range from 2.10^6 to 4.10^6. The DU 93-W-210 airfoil the airfoil exhibits a maximum lift-to-drag ratio of 143 at $R_e=3.10^6$. DU airfoils are being used by various wind turbine manufacturers worldwide in over 10 different rotor blades for turbines with rotor diameters ranging from 29 m to over 100 m corresponding to machines with maximum power ranging from 350 kW to 3.5 MW [68].

❖ **SD7062 Airfoil:**

Another aerofoil that is of interest here is the SD7062 which started its life as an aerofoil for model gliders [67]. It has a thickness ratio and a camber of 14 % and 4 %, respectively. The airfoils discussed above are summarized in table 21.

Airfoil	Thickness (%)	Camber (%)	Design Re
S822	16	1.89	600,000
DU 93-W-210	21	2.86	$2.10^6 - 4.10^6$ (High Reynolds number airfoil)
SG6043	10	5.5	300,000
SD7062	14	4	-

Table 21: Design parameters of small wind turbine airfoils

According to the literature review, It is shown that the aerofoils performing best during start-up are 'the SG6043' and 'the SD7062' [67].

3.8.3 Blade airfoil selection

For horizontal-axis small wind turbines, the rotor blades usually operate at low Reynolds numbers along the entire span. The unusual aerodynamic characteristics associated with low Reynolds number airfoil aerodynamics can severely degrade the performance of the blade if the selected airfoils are not suitable for low Reynolds number applications. Consequently, the airfoil selection is a particularly critical aspect of the blade design process of HAWTs [57]. Blade aerofoils are often designed to be used at low attack angle, where the drag coefficient is usually much lower than the lift coefficient. It has been found in some applications that more than one aerofoil shape can be used for the wind turbine blade design, but there will be bending between these aerofoils which may add to design and structural uncertainties in the design process. For a stall-regulated wind turbine, it is better to choose an aerofoil shape to make sure that stall occurs gently after the maximum lift-to-drag point [42].

From the review of small wind turbine airfoils, it is now possible to establish general and specific guidelines for the selection of appropriate airfoil for the design of small wind turbine.

The first step in the airfoil selection process is to estimate the Reynolds number range over which the blades will operate. This step can be applied to any size of HAWT but this is particularly important for small wind turbines because of the wide variation in drag at low Reynolds numbers [57].

The mechanical power of the wind turbine can be expressed as a function of the tip speed ratio using the following equations:

$$P = T_{rotor}.\Omega \qquad (18)$$

$$\Omega = \frac{V_{design} * 60 * \lambda_{design}}{\pi * D} \qquad (19)$$

Then

$$P = T_{rotor}.\frac{V_{design} * 30 * \lambda_{design}}{\pi * R} \qquad (20)$$

According to Wood H., the most of a turbine's power is produced near the tip, so the value of R_e most often quoted is the tip Reynolds number [41]. As mentioned before, if λ is sufficiently high, the relative wind speed at the tip should be taken as $U_{rel} \approx \lambda \times V_{design}$, but for everywhere along a stationary or slowly rotating blade, the relative wind speed can be written as: $U_{rel} \approx V_{design}$ [41]. Based on this, the operating Reynolds number of the wind turbine blades can be calculated using equation 21 [69]:

$$Re = \frac{V_{design}.\lambda_r.C}{1.5x10^{-5}} \qquad (21)$$

Assuming that the blade spanwise location at 0.72R (72% of the blade radius) is the effective radius for which the aerodynamic performance approaches significantly those of the whole blade, and by taking an average chord length of 0.2 m, at this specific location, **equation 22 gives an operating Reynolds number of 604,800**. This value corresponds to a blade tip speed ratio of 6. This value represents the minimum of the range (usually taken between 6 and 8) used in small wind turbine blade design.

Once the operating Reynolds number range is known for a particular rotor blade, the shape of the drag polar at the Reynolds numbers of interest is a key element for the selection of airfoils for a small wind turbine design. Drag polar characteristics, such as the maximum lift-to-drag ratio are important features in evaluating the potential of an airfoil for wind turbine applications under design and off-design conditions. For wind turbines that operate up to and beyond stall, the maximum lift coefficient is another important parameter to consider [57].

Generally, thick airfoil sections do not have good performance at low R_e. Thin airfoils with high camber would be expected to produce more power with low thrust load [44]. The key requirement was that blade airfoils should exhibit a high lift-to-drag ratio at low Reynolds number. Aerodynamic lift is the force that enhances the power generated by the turbine and it is necessary to maximize this specific force using an appropriate blade design. A resistant drag force does not contribute to the power generation and must be minimised. Therefore, in order to obtain high efficiency, it is essential to use airfoil shaped rotor blades with a very

high lift to drag ratio. This is particularly necessary in the section of the blade near the tip, where the speed relative to the air is much higher than close to the centre of the rotor. Keeping this in mind, four promising different airfoils emerged: the S822, SD7062, SG6043 and DU 93-W-210 [67].

Unfortunately, there was not a single consistent database or airfoil selection method in the literature. To minimize the risk and to take maximum advantage from previous experiences, candidate airfoils for the new blade design were evaluated on three main points: First, an appropriate airfoil will be selected based on an evaluation of the aerodynamic performance of real wind turbine that have been produced and tested. The size of the wind turbine blades, chosen for the evaluation, should be close to that used for the present study; 3.5 meter diameter or around 11 kW rated power. Secondly, application of the airfoil would not infringe patents or be expected to have to intellectual property issues. Finally, the airfoil should be thick enough to provide a good reserve of strength in bending when operating, while still maintaining good lift and drag characteristics.

With these considerations in mind, the range of candidate airfoils was minimized to S822, DU 93-W-210 and SD7062. The SD 7062 has very high ratio of C_L over C_D at low Re number and excellent aerodynamic performance for small wind turbine blades. However, this is a thin airfoil, which would be expected to increase the difficulty of blade manufacture [44].

The S822 airfoil has a thick section which would help to strengthen the blade structure against loading. Usually, it is important for structural reasons to use a thick aerofoil section near the hub of the blades, but this, also, would lead to poor aerodynamic performance [57]. Generally, this aerofoil is used only in the tip region within a mixed blade (usually with the S823 in the root region) to enhance a maximum power extraction, which may result in additional structural constraints during the process of design and manufacture.

The DU 93-W-210 airfoil has good comprehensive performance: a thickness of 21% provides more options for strengthening and manufacturing, and the airfoil has good lift and drag characteristics at typical design Reynolds numbers at which most small wind turbines operate. **Balancing these considerations, DU 93-W-210 airfoil was selected for the new blade design.** Figure 10 gives the shape of the selected airfoil.
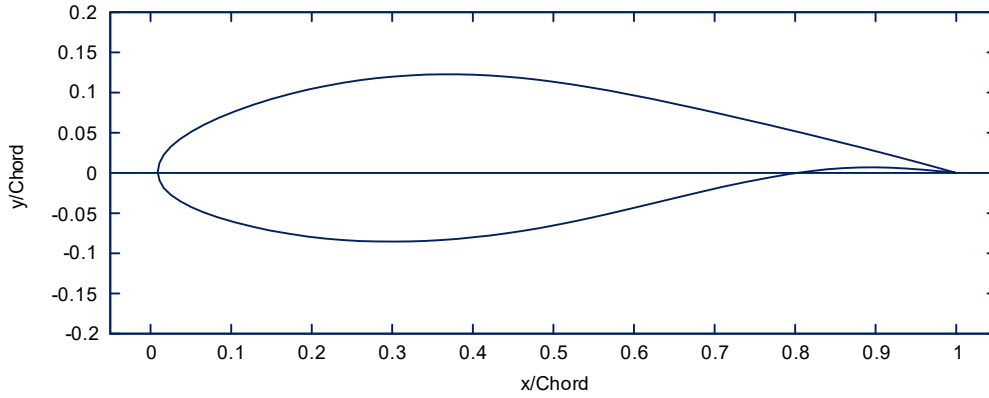
Figure 10: DU93-W-210 aerofoil shape

3.9 Design tip speed ratio

Blade tip speed ratio is the first parameter to be considered in a blade design procedure. This parameter is generally taken as 6 to 8 in modern wind turbines, but the optimum value remains uncertain for different aerofoil shapes and blade numbers. As a higher lift coefficient means a larger lift force, a higher drag coefficient means a larger drag force, a turbine with an airfoil of a higher lift coefficient and a lower drag coefficient is expected to produce more power with better load conditions. The maximum lift-to-drag ratio should be used in the optimal design, and the attack angle at which the maximum lift-to-drag ratio occurs should be considered to be the optimal attack angle. This optimal attack angle, which is equal to the angle of relative wind minus twist angle at all sections, should be used in the design to calculate ideal power coefficient.

For initial selection of the design tip speed ratio, the empirical relation between the power coefficient and the tip speed ratio is used. Wilson et al. **[1, 70, 71]** give an equation describing the maximum power coefficient of a wind turbine rotor with a finite number of blades.

$$C_{pmax} = \left(\frac{16}{27}\right).\lambda.\left[\lambda + \frac{1.32 + \left(\frac{\lambda - 8}{20}\right)^2}{B^{\frac{2}{3}}}\right]^{-1} - \frac{0.57.\lambda^2}{\frac{C_l}{C_d}.\left(\lambda + \frac{1}{2B}\right)} \tag{22}$$

Wilson has discovered that this multivariable relationship can be summarized to a high degree of accuracy, 0.5%, for tip speed ratios from 4 to 20, lift to drag ratios $\left(\frac{C_l}{C_d}\right)$ from 25 to infinity, and from one to three blades (B).

Yurdusev MA et al. **[72]** presented a similar procedure to assess optimum tip speed ratio for different airfoils with different blade numbers. According to authors, the real wind turbine

productivity is less than the theoretical one because of the losses that are not considered in theory. These losses are: airfoil losses, tip losses whirlpool losses, and blade number losses. Having considered all these losses, the power coefficient is a function of TSR, blade number and maximum lift/drag ratio [72]:

$$C_p = C_{Pschmitz} \cdot \eta_{airfoil} \cdot F_L \tag{23}$$

Where $C_{Pschmitz}$ is the Schmitz power coefficient which is function of λ. The parameter $\eta_{airfoil}$ is the profile losses which is used to take into account the effect of drag force (resistance force) in the calculation of the power coefficient [72];

$$\eta_{airfoil} = 1 - \frac{\lambda}{C_l/C_d}: \tag{24}$$

F_L is the blade tip losses which can be considered as the whirlpool losses. In the end of a blade, airflow from the lower side of the profile to the upper side takes place. Coupling with the airflow coming towards the blade, this airflow widens gradually ($F_L = 1 - \frac{1.84}{B.\lambda}$). B is the blade number which taken as 3, and the ratio $\frac{C_l}{C_D}$ is the maximum lift to drag coefficient;

In the idealized derivation of the Betz equation, the wind does not change its direction after it encounters the turbine rotor blades. In fact, it does change its direction after the encounter. This is accounted for by a modified form of the power coefficient known as the Schmitz power coefficient $C_{pSchmitz}$ [72].

From the above mentioned approaches, it can be seen that there is a relationship between the power coefficient of the turbine and the rotor blade tip speed. Using a maximum lift-to-drag ratio, the ideal power coefficients can be expressed as a function of the tip speed ratio. Based on XFOIL software, the maximum lift to drag coefficients for the selected DU93-W-210 airfoil is found to be **93.76**. This maximum value occurs at an attack angle of **5°**. Based on the methods given by Wilson and Yurdusev, the plot of the power coefficients against different tip speed ratios is given in figure 11. Table 22 summarizes the values of the power coefficient versus different tip speed ratios.
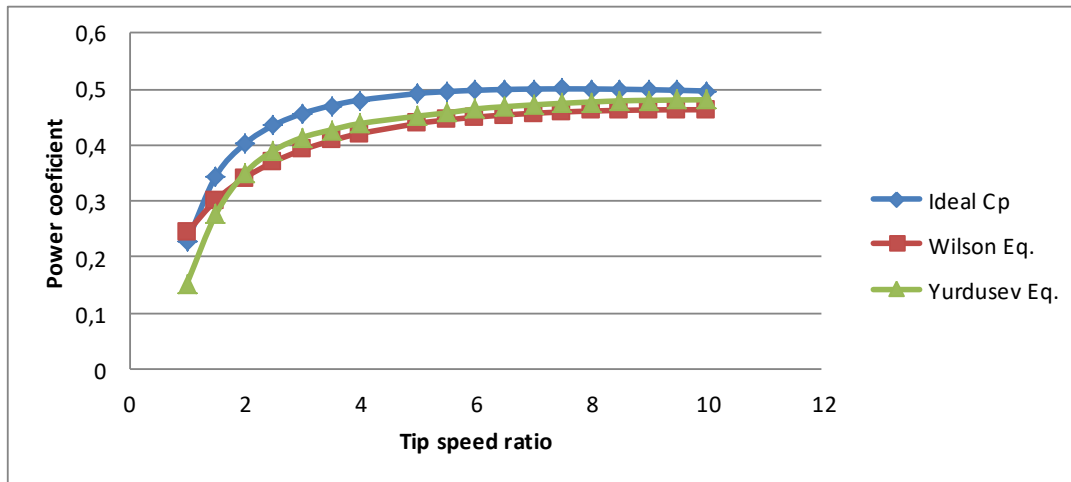
Figure 11: Ideal power coefficient curve of DU93-W-210 airfoil

TSR	CL/CD	Cp schmitz	BITZ LIMIT	Ideal Cp	Wilson Eq.	Çetin Cp
1	93,76	0,4	0,5926	0,226694782	0,243893596	0,153017065
1,5	93,76	0,475	0,5926	0,344688363	0,301426193	0,276285812
2	93,76	0,515	0,5926	0,402105056	0,341167579	0,349450057
2,5	93,76	0,531	0,5926	0,435290993	0,369917611	0,39004306
3	93,76	0,537	0,5926	0,456361552	0,391401987	0,413543965
3,5	93,76	0,538	0,5926	0,470509038	0,407833407	0,427158054
4	93,76	0,541	0,5926	0,480329604	0,420608889	0,438505427
5	93,76	0,544	0,5926	0,492182278	0,438606002	0,451817684
5,5	93,76	0,547	0,5926	0,49563047	0,444918454	0,457492182
6	**93,76**	**0,553**	**0,5926**	**0,497977264**	**0,449922564**	**0,464700349**
6,5	93,76	0,556	0,5926	0,499476828	0,453866011	0,468628276
7	93,76	0,559	0,5926	0,500310712	0,456937688	0,47194345
7,5	93,76	0,562	0,5926	0,500612053	0,459284162	0,474762021
8	93,76	0,565	0,5926	0,500480701	0,461020905	0,477171104
8,5	93,76	0,568	0,5926	0,499993014	0,46224012	0,479237314
9	93,76	0,57	0,5926	0,499208382	0,463016325	0,480170061
9,5	93,76	0,572	0,5926	0,498173691	0,463410399	0,480856145
10	93,76	0,574	0,5926	0,496926449	0,463472562	0,481329365

Table 22: Power coefficients for different tip speed ratios at R_e: 600.000

The optimal design tip speed ratio for the DU93-W-210 airfoil corresponds to high tip speed ratios. However, using a high tip speed ratio for the design of small wind turbine presents many drawbacks. These include:

- Noise generation in the audible and non-audible ranges;

- Excessive rotation would lead to a runway turbine, leading to a catastrophic failure;

- Problems of vibration;

- Rotor blade tip rotating at high speeds will be subject to erosion of leading edge which is caused by dust and sand particles in the air;

As the maximum efficiency at the tip speed ratio between 6 and 10 does not vary sharply, **the tip speed ratio λ=6 is selected as the design tip speed ratio for the design process.**

3.10 Design rotational speed

The design rotational speed of the wind turbine can be determined using equation 25:

$$\Omega_{design} = \frac{V_{design} * 60 * \lambda_{design}}{\pi * D} = 172 \text{ rpm} \tag{25}$$

Where:

D: Rotor diameter;

λ_{design} : Design tip speed ratio; taken as 6

For a direct drivetrain topology, the maximum rotational speed of the wind turbine rotor is set by the maximum generator speed because the latter is directly connected to the hub. This is the reason why the maximum rotational speed operation occurs when the generator rotational speed reaches its maximum limit.

During the turbine design process, the maximum rotor power generation must not exceed the generator maximum overloading, which is generally set to 120% of the rated power [43, 73, 74]. As we are designing an 11 kW wind turbine, the maximum rotor power output must not exceed 11 kW*120% = 13,200 W. The maximum overloading to the generator is 120%, and we should rule out any case with maximum rotor power output over 13,2 kW. Otherwise, we are not talking about 11 kW wind turbine. In other words, the generator should tolerate up to 20% of its maximum output power (which is equal to 13.2 kW in the case of this project) before the stall regime takes place, particularly when the wind speed is above the rated speed (rated wind speed is taken as V_{design}=10.5 m/s, in this case).

3.11 Reynolds number verification

Once the design tip speed ratio and the corresponding rotational speed are known, it is easy to check the operating Reynolds number by using the actual relative wind velocity, U_{rel}, which can calculated from the velocity triangle, at a location of 0.72R of the blade length.

The operating Reynolds number can be calculated using following equations [43]:

$$Re = \frac{U_{rel}.C}{1.5x10^{-5}} \tag{26}$$

The relative wind speed, which represents the actual wind speed involved in the aerodynamic operation of the rotor blades, can be determined using equation 27.

$$U_{rel} = \sqrt{((1 + a').\Omega.r)^2 + (1 - a)^2 V_{design}^2} \tag{27}$$

If we assume that the wind turbine is operating at its maximum efficiency where a=1/3 and a' is negligible. Then the equation 17 becomes:

$$U_{rel} = \sqrt{V_{tan}^2 + \frac{2^2}{3} V_{design}^2} \quad , \quad V_{tan} = \Omega \text{ x } r_{0.72 \text{ section}} \tag{28}$$

Where:

$r_{0.72\ section}$: Blade radius at 72% on the blade span; $r_{0.72\ section} = 2.52$ m
a: Axial induction factor;
a': Rotational induction factor;
V_{design}: Design wind speed; $V_{design} = 10.5$ m/s
C: Chord length (m); C= 0.2 m
Ω: Rotor rotational speed; $\Omega = 18.01$ rad/s for an estimated tip speed ratio of λ=6
U_{rel} : Relative wind velocity (m/s); $U_{rel} = 45.92$ m/s

By using equations 22 and 26, table 23 summarizes the Reynolds number values over which the small turbine blades is supposed to operate.

	Representative chord length (m)	Estimated Reynolds number
Equation (22)	0.2	604 800
Equation (26)	0.2	612 266

Table 23: Estimated Reynolds number for the small wind turbine rotor design

As can be seen from the table, both equations give almost the same value of Reynolds number. Therefore, it seems reasonable to use an operating Reynolds number of 600 000 for the present blade design process.

3.12 Design angle of attack

The design angle of attack is often selected at the critical angle of attack where the lift to drag ratio is maximum. However, a good practice in wind energy engineering states that the design angle of attack should be selected to be slightly lower than the optimum angle of attack (which gives the maximum lift to drag coefficient). This practice allows the blade to operate at good angles of attack, near the optimum value while avoiding the blade airfoil to come rapidly into the stall regime when the angle of attack goes beyond the optimum value. For the selected DU 93-W-210 airfoil, the plot of the lift and drag coefficients against different angles of attack is shown in figure 12.
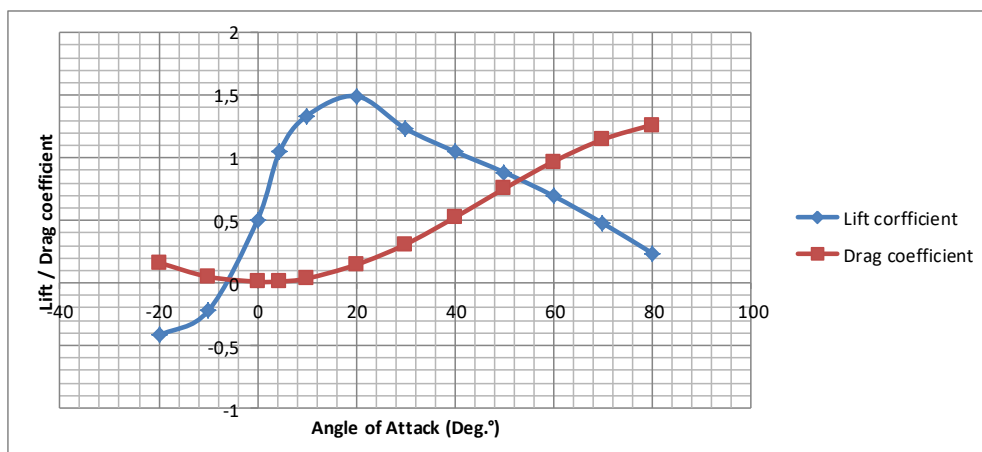
Figure 12: Lift and drag coefficients of DU 93-W-210 airfoil for Re=600,000

As can be seen from the figure above, the drag coefficient increases after an attack angle of 5°, and the maximum lift-to-drag ratio occurs at **5**. As wind speed increases, the angle of attack increases, and the outer region of the blade first comes into stall development regime causing decreased lift force, increased drag force, therefore decreased power coefficient. As the wind speed increases to high wind speed, the whole blade comes into deep stall regime when the blade speed stays constant and does not change. Therefore, a constant power can be achieved with a well-designed blade aerofoil. **For the current design process, the design angle of attack, α_{design}, is chosen to be the critical angle 4.5°.** The polar data were extrapolated to a range of 360° by using viterna method which has been widely used to predict different airfoils post-stall performance [43, 75].

3.13   XFOIL solver

Values of the lift and the drag coefficients, for different angles of attack, are necessary to characterize a wind turbine blade airfoil. Ideally, researchers test the airfoil in a wind tunnel over a range of Reynolds numbers and surface conditions to get data for accurate design and assessment. The alternative methods consist in using one of several software applications that rely on potential flow techniques or Computational Fluid Dynamics (CFD) to predict airfoil performance under wind conditions. XFOIL program is an example of the applications that are widely used in airfoil flow simulations. XFOIL is an interactive program used for the design and analysis of subsonic isolated airfoils. It consists of a collection of menu-driven routines which perform various useful functions such as viscous (or inviscid) analysis of an existing airfoil. This tool represents a potential flow based solver available free of charge and has proven to be a powerful tool for subcritical airfoil design, particularly for low Reynolds number airfoils [76].

3.14   Blade airfoil characteristics

For wind turbine blade design and analysis, it is essential to have the aerodynamic data of the selected airfoil, and this for the operating flow conditions (expressed in terms of Reynolds numbers). For the DU 93 airfoil series, no wind tunnel results of the wind turbine airfoils at Reynolds numbers below $1x10^6$ are available. The only data available were performed in the low-speed low-turbulence wind tunnel of the Faculty of Aerospace Engineering of Delft University at a Reynolds numbers of $1x10^6$ [68]. For an initial blade design, the aerodynamic data were evaluated using XFOIL solver at a design Reynolds number of 600,000. Figure 13 gives a screen shot of the data given XFOIL solver.

Figure 13: Aerodynamic data of DU-93-W-210 from XFOIL (Re=600,000)

XFOIL program is particularly useful when no wind tunnel data are available in literature. However, it worth mentioning that the results of the aerodynamic performance from XFOIL are usually not accurate for low Reynolds numbers. To validate the aerodynamic data given by XFOIL, a comparison has been made with the data obtained from computational fluid dynamics using ANSYS. The geometry of the airfoil was first imported into the design modeler in Ansys-Fluent. Then, the flow domain (C-Mesh type) around the airfoil is created (as shown in figure 1). The flow domain should have high dimensions (the chord length of the airfoil multiplied by 25). A Boolean function is created in order to subtract the airfoil from its domain. Finaly, the geometry obtained (by the Boolean function) was meshed (as shown in figure 2). The quality of the mesh should be respected by having low skewness and high orthogonal quality. the mesh was also refined near of the airfoil. After meshing the flow domain, the boundary conditions are defined. The circular arc represents the inlet, in which the inlet velocity should be defined (10.5 m/s). The straight line behind the airfoil represents the outlet, and the edges of the airfoil represent a wall for the flow. As output, the lift and drag

coefficients are demanded at each angle of attack. Actually, the results are accurate for small values of angles. To have the overall distribution from -180 to 180 degrees, an extrapolation is done using Viterna method.
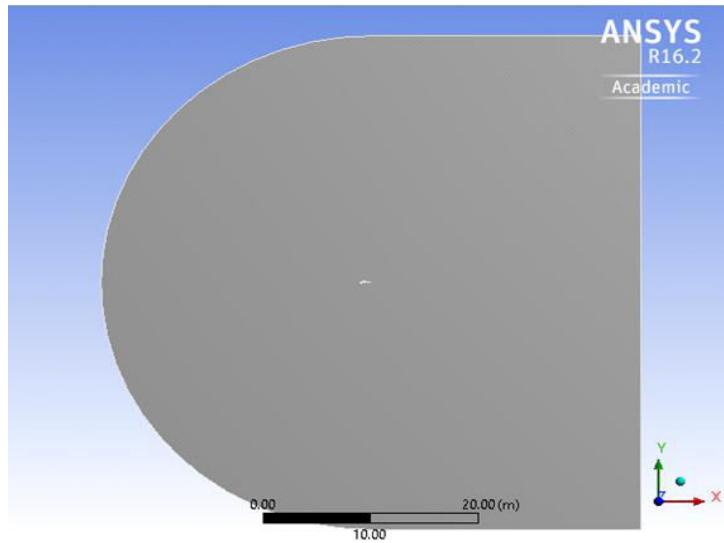
Figure 14: DU 93-W-210 airfoil and its flow domain
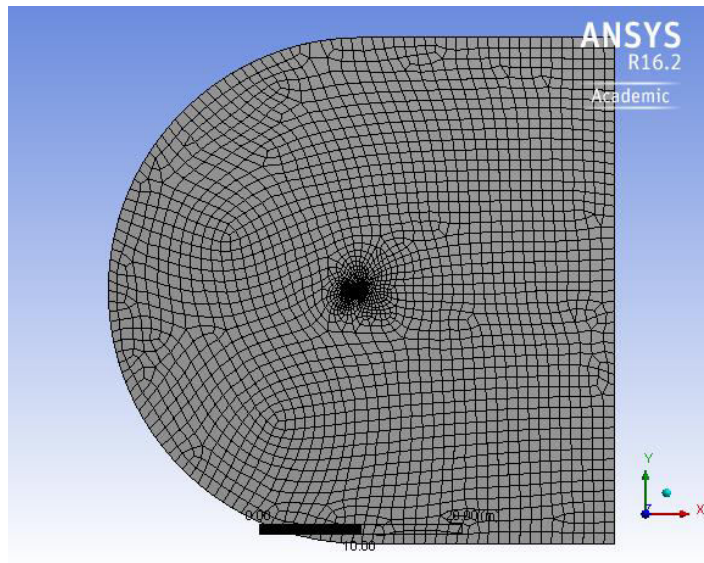
Figure 15: Mesh of the flow domain around the airfoil

Based on the results of CFD analysis, a maximum lift to drag ratio of 95 can be reached. The fundamental parameters that will be used for the small wind turbine design are summarized in Table 24.

Design Parameter	Value	Unit
Wind turbine generator rated power	**11.000**	W
Design wind speed (rated wind speed)	**10.5**	m/s
Assumed rotor aerodynamic power coefficient	**0.449 [Equation 23]**	-
Assumed total power coefficient	**0.4 [Equation 15]**	-
Number of blades	**3**	-

Design tip speed ratio	6	-
Design angle of attack	4.5	Deg.°
Air density	1.225	Kg/m^3
Rotor radius	3.5	m
Design rotational speed	172	RPM
Design Reynolds number	600 000	-
Airfoil type	DU 93-W-210	-

Table 24: Fundamental design parameters for the small wind turbine design

3.15 Conclusion

The first part of this chapter covers the statistical analysis of wind data of 45 sites around Morocco. The ultimate objective of the wind site assessment is to define an appropriate wind turbine class for which the small wind turbine will be designed. This is one of the factors which need to be considered during the complex process of designing a wind power system. Wind classes are used to determine which design of the wind turbine is suitable for normal and extreme wind conditions in a specific area. Based on the results obtained, an average wind speed of 6.65 m/s was found at a hub height of 24 m which is considered as an average of tower heights of small wind turbine. For this typical wind speed value and based on the IEC standard 61400-2, a wind turbine class III is to be considered for the design process. This corresponds to an annual mean wind speed of 7.5 m/s and a design wind speed of 10.5 m/s. The second part of this chapter discussed the design parameters that must be considered during the design procedure. These include the design and the rated wind speed, the wind turbine rotor diameter, the rotor blades number and, finally, the wind turbine drive train topology. A design wind speed of 10.5 m/s was considered. This corresponds to a rotor diameter of 7 m and a power output of 11 kW. For the design tip speed ratio, literature review shows that when the rotor of the wind turbine turns too slowly, most of the wind will pass undisturbed through the gap between the rotor blades. Alternatively when the rotor turns too quickly, the blurring blades will appear like a solid wall to the wind. Therefore, an optimum tip speed ratio of 6 was selected. The third part of the present chapter was concerned with the selection of an appropriate airfoil section. Among many law Reynolds number airfoil, the optimized airfoil DU 93-W-210 was selected as it presents the highest lift to drag ratio at the design Reynolds number of around 600000.

CHAPTER 4: BLADE DESIGN AND MANUFACTURE

The rotor is the most important component in a wind turbine system which is designed to capture wind energy and convert it into rotating mechanical energy. Turbine blades should be strong enough to stand steady, periodic and randomly changing loads. The rotor assembly consists of several blades joined to a common hub, a nose cone and fasteners.

The blades are the critical components of the rotor, and consist of the airfoils which interact with the wind and convert the power in the wind to mechanical power. The geometry and dimensions of the blades are determined by the performance requirements of the wind turbine. Two fundamental issues must be considered simultaneously in the turbine blade design process: aerodynamic performance and structural design. For example, after the overall shape of the blade is optimized aerodynamically, it is common that the root of the blade must be redesigned to meet structural requirements. Aerodynamically advantageous features such as nonlinear distribution of the chord length and twist angle are often difficult to build. For this reasons, some compromises must be considered so that the blade design can be manufactured with minimum expenses (low cost).

4.1 Blade chord and twist angle distribution

4.1.1 Initial blade design

The sectional shape of a horizontal-axis wind turbine blade consists of the two dimensional airfoils, which result in the lift and drag forces by virtue of pressure differences across the 2D airfoil. For the aerodynamic design of the turbine blades, Blade Element Momentum (BEM) theory (for performance prediction) and optimum rotor theory (for blade shape design) are widely used [1, 43]. The optimum distribution of the chord length and the twist angle in each section is strongly dependent on several design parameters such as the design wind speed, the number of the rotor blades, the design tip speed ratio, the design angle of attack and the design lift coefficient, $C_{ldesign}$ (which is set here to 1.07). Once these input parameters have been determined, the optimum rotor theory can be used to determine the blade shape, and then the turbine performance can be predicted using BEM. The BEM theory divides the blade into **30 sections** from root to the tip and the total power coefficient is calculated by integrating the power coefficients at these sections, as described by J.F. Manwell et al. [1]:

$$C_p = \left(\frac{8}{\lambda^2}\right) . \int_{\lambda_h}^{\lambda} F_t . \sin^2 \phi . (\cos \phi - \lambda_r \sin \phi) . (\sin \phi + \lambda_r \cos \phi) . \left[1 - \left(\frac{C_d}{C_l}\right) . \cot \phi\right] . \lambda_r^2 d_{\lambda r} \quad (29)$$

Where F_t is the blade tip losses factor. The most straightforward approach to calculate the blade tip losses is the one developed by Prandtl. The Prandtl tip loss factor is an approved

procedure for the correction of profile data to get a better agreement between measured and computed data. Prandtl modeled the helicoidal vortex sheet wake behind the rotor as a succession of solid disks moving with the wake.

If the main part of the equation 29 is at its maximum, the total power coefficient is maximized.

$$F_t. \sin^2 \phi. (\cos \phi - \lambda_r \sin \phi). (\sin \phi + \lambda_r \cos \phi). [1 - \left(\frac{C_d}{C_l}\right). \cot \phi]. \lambda_r{}^2 d_{\lambda r} \longrightarrow \textbf{Max} \qquad (30)$$

Ignoring the drag-to-lift coefficient ratio and setting the partial derivative of the main part to zero, the chord, C_i, and twist angle, θ_i, can be obtained by the following equations:

$$\lambda_{ri} = \lambda_{design}. \left(\frac{r_i}{R}\right) \qquad (31)$$

$$\phi_i = \left(\frac{2}{3}\right). \tan^{-1}(\frac{1}{\lambda_{ri}}) \qquad (32)$$

$$C_i = \frac{8. \pi. r_i}{B. C_{ldesign}} (1 - \cos \phi_i) \qquad (33)$$

$$\theta_i = \phi_i - \alpha_{design} \qquad (34)$$

Where i indicates the i_{th} blade section, λ_{ri} is the speed ratio of the i_{th} blade section, r_i is the distance from the i_{th} blade section to the rotor center, ϕ_i is the angle of relative wind at the i_{th} blade section. $C_{ldesign}$ and α_{design} are the design lift coefficient and the design angle of attack at the i_{th} blade section respectively. Figures 16 and 17 give the chord and twist angle distributions based on equations 31-34.
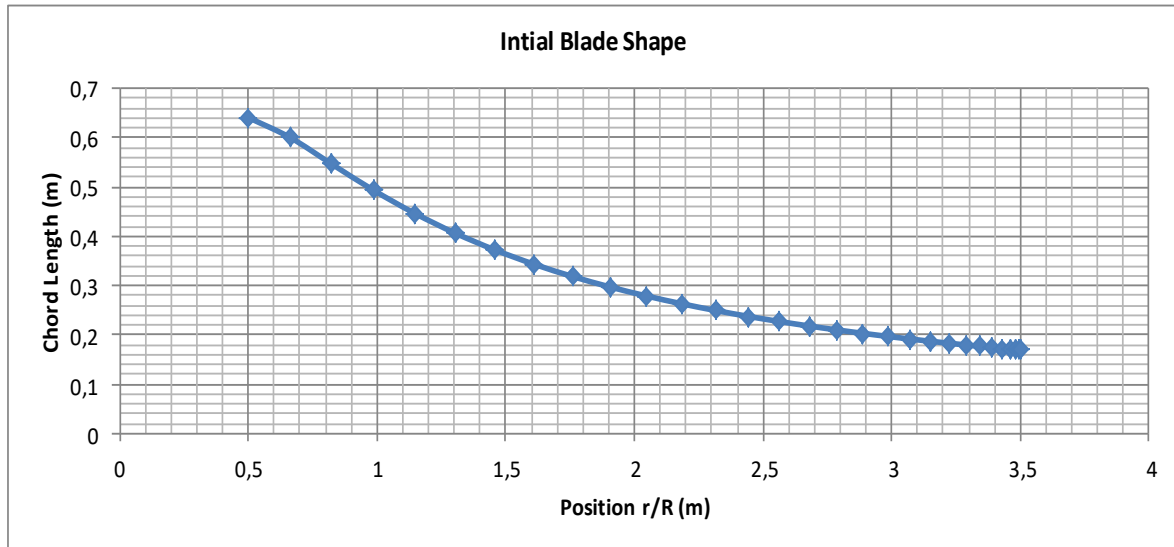
Figure 16: Chord distribution of an initial blade design
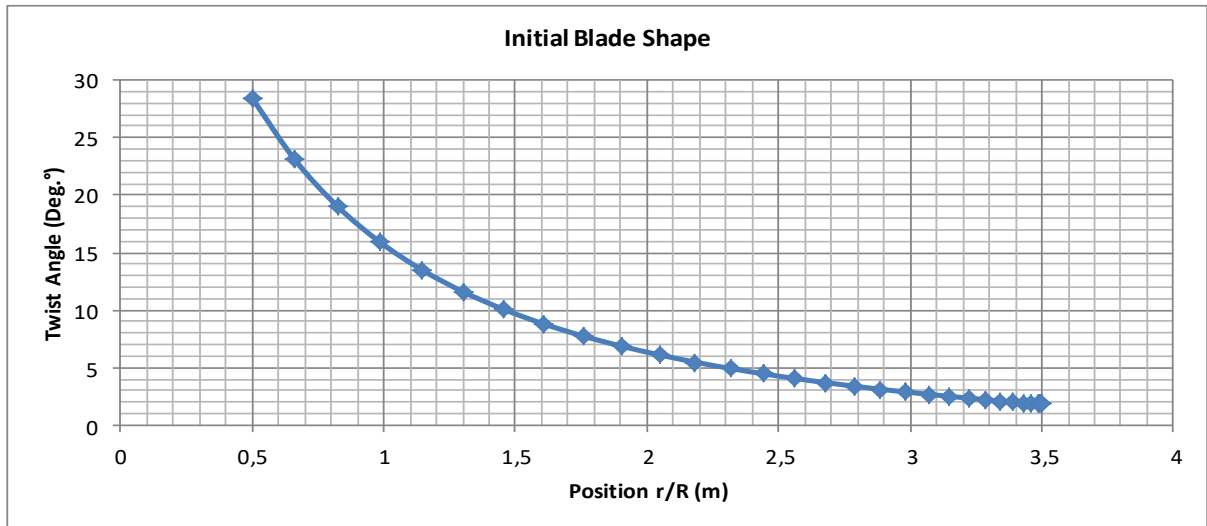
Figure 17: Twist distribution of an initial blade design

These two distributions demonstrate that the chord length is larger at the inner sections of the blade (closer to the root) and smaller at the outer sections of the blade. The twists of the sections close to the root are larger than those close to the tip. The chord at the blade root section (0.14 R) is around 0.62 m, and the twist angle varies from 28.43° at the blade root to 1.8° at the blade tip. Generally, wind turbine blade design optimization based on the optimum rotor theory is carried out using an iterative approach [1]. Once the blade has been designed for optimum operation, at a specific design tip speed ratio, the performance of the rotor needs to be determined. From the starting optimum blade design, the tip loss factor can be calculated using equation 35.

$$F_t = \left(\frac{2}{\pi}\right). \cos^{-1}\left[\exp\left(-\left\{\frac{\frac{B}{2}.\left(1-\frac{r}{R}\right)}{\frac{r}{R}.\sin\phi}\right\}\right)\right] \tag{35}$$

Having solved the equations for the performance at each blade element, the power coefficient is determined using a sum approximating the integral in Equation 29.

$$C_p = \sum_{i=1}^{N}\left(\frac{8\Delta\lambda_r}{\lambda^2}\right) F_{ti}. \sin^2\phi i. (\cos\phi i - \lambda_{ri}\sin\phi i).(\sin\phi i + \lambda_{ri}\sin\phi i).\left[1 - \left(\frac{C_d}{C_l}\right).\cot\phi i\right].\lambda_{ri}^2 \tag{36}$$

If the total length of the hub and blade is assumed to be divided into N equal length blade elements, then:

$$\Delta\lambda_r = \lambda_{ri} - \lambda_{r(i-1)} = \frac{\lambda}{N} \tag{37}$$

$$C_p = \frac{8}{\lambda.N}\sum_{i=1}^{N} F_{ti}.\sin^2\phi i.(\cos\phi i - \lambda_{ri}\sin\phi i).(\sin\phi i + \lambda_{ri}\cos\phi i).\left[1 - \left(\frac{C_d}{C_l}\right).\cot\phi i\right].\lambda_{ri}^2 \tag{38}$$

The power coefficient given here represents the aerodynamic performance of an ideal rotor which includes wake rotation, drag effects, and tip losses. The chord and twist distributions

obtained from the above equations are just initial design values, and an iterative process should be followed normally. The most used iterative procedure is summarized in the following five steps [1, 43]:

1) Estimate initial values of the axial induction factor, a, and angular induction factor, a'. The first values can be taken from the initial design blade:

$$\phi_{i,1} = \left(\frac{2}{3}\right) \tan^{-1}\left(\frac{1}{\lambda_{r,i}}\right) \tag{39}$$

$$a_{i,1} = \frac{1}{\left[1 + \frac{4\sin^2\phi_{i,1}}{\sigma'_{i,1}\, C_{L\,design}\cos\phi_{i,1}}\right]} \tag{40}$$

$$a'_{i,1} = \frac{1 - 3a_{i,1}}{4a_{i,1} - 1} \tag{41}$$

Where $\sigma'_{i,1}$ is the local solidity of the ith blade section expressed as:

$$\sigma'_{i,1} = \frac{BC_i}{2\pi r_i} \tag{42}$$

2) Start the iterative process for the jth. For the first iteration $j = 1$, the following equations are used:

$$\tan\phi_{i,j} = \frac{U(1 - a_{i,j})}{\Omega r(1 + a'_{i,j})} = \frac{1 - a_{i,j}}{(1 + a'_{i,j})\lambda_{ri}} \tag{43}$$

$$F_{ti,j} = \left(\frac{2}{\pi}\right) . \cos^{-1}\left[\exp\left(-\left\{\frac{\frac{B}{2}.\left(1 - \frac{r_i}{R}\right)}{\frac{r_i}{R}.\sin\phi_{i,j}}\right\}\right)\right] \tag{44}$$

3) Calculate the new angle of attack, $\alpha_{i,j}$, and determine the corresponding lift coefficient, $C_{Li,j}$, and the drag coefficient, $C_{Di,j}$ from the polar data of the used airfoil.

$$\alpha_{i,j} = \phi_{i,j} - \theta_{i,j} \tag{45}$$

Where $\theta_{i,j}$, is the twist angle of the blade the ith blade section.

4) Calculate the local thrust coefficient by using the following equation:

$$C_{Thi,j} = \frac{\sigma'_i (1 - a_{i,1})^2 \left(C_{Li,j}\cos\phi_{i,j} + C_{Di,j}\sin\phi_{i,j}\right)}{\sin^2\phi_{i,j}} \tag{46}$$

5) Update the values of a and a' for the next iteration. If $C_{Thi,j} < 0.96$, then:

$$a_{i,j+1} = \frac{1}{\left[1 + \frac{4F_{ti,j}\sin^2\phi_{i,1}}{\sigma'_i\, C_{Li,j}\cos\phi_{i,j}}\right]} \tag{47}$$

If $C_{Thi,j} > 0.96$, then the axial induction factor is computed using the following equation:

$$a_{i,j+1} = \left(\frac{1}{F_{ti,j}}\right)\left[0.143 + \sqrt{0.0203 - 0.6427(0.889 - C_{Thi,j})}\right] \tag{48}$$

$$a'_{i,j+1} = \frac{1}{\dfrac{4F_{ti,j}\cos\phi_{i,j}}{\sigma'_i\, C_{Li,j}} - 1} \tag{49}$$

If the difference between the j^{i+1} and j^i iteration is within the acceptable convergence criteria, then the process converges, and the power performance can be computed. The convergence criterion, ε, defines when an iteration has converged. The maximum of the difference of axial and angular induction factor between the last and the current iteration has to be below ε. A typical value that can be used is given by [5]:

$$\max\left(|a_{i,j+1} - a_{i,j}|, |a'_{i,j+1} - a'_{i,j}|\right) < 10^{-5} \tag{50}$$

In the present study, the iterative process for the blade design was conducted using **Q-blade** software. This design project tool is realized being a part of the wind energy group at the Berlin Technical University Department of Experimental Fluid Mechanics. Q-blade is a free-of-charge wind turbine calculation software that enables the user to rapidly design his wind turbine blades by determining the chord and the twist distribution, as well as the corresponding aerodynamic performance (C_p and the torque coefficients, C_T). Determination of an optimum chord length and the twist angle in Q-blade is based on BEM and Double-Multiple Streamtube (DMS) model which are integrated into an XFOIL graphical user interface. The integration of the XFOIL allows evaluating the aerodynamic lift and drag coefficients of the airfoils, and directly integrating them into the blade simulation. The Q-Blade software consists of four different parts:

❖ **The aerofoil design:** in this submodule, the airfoil data (coordinates) can be imported to the software.

❖ **Direct analysis using XFOIL**: this submodule is used to determine the lift and the drag coefficients, as well as the lift to drag ratio of the selected airfoils;

❖ **Extrapolation of polar data to the full 360°**: this submodule allows extrapolating the data given by XFOIL in order to generate the polar coordinates over a number of attack angles ranging between -180 and 180. This extrapolation submodule uses either Montgomery or Viterna method.

❖ **Rotor design**: When the fundamental design parameters of the blade are defined, the optimization process of the rotor blade can be performed by using the rotor design submodule. Figure 18 shows the final blade geometry given by Q-blade after optimization:
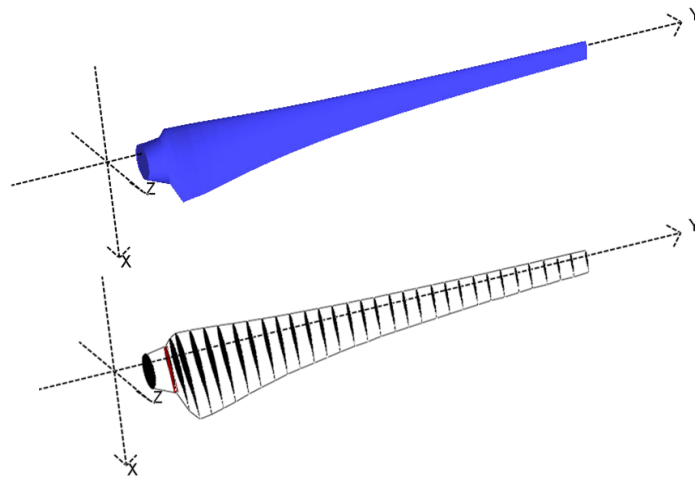
Figure 18: Blade geometry after blade optimization

Figures 19 and 20 give the chord length twist angle distributions along the blade span using Q-blade software:
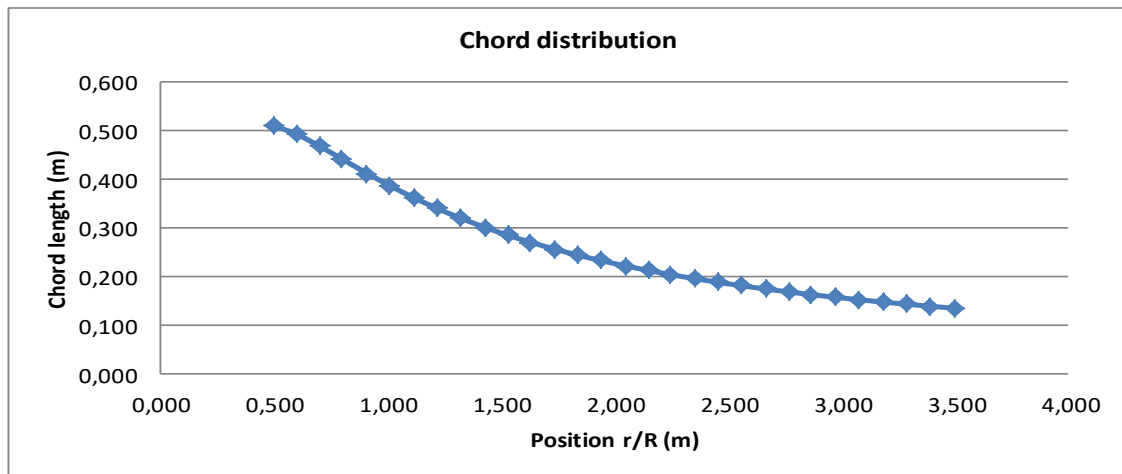
Figure 19: Chord length distribution from Q-blade software
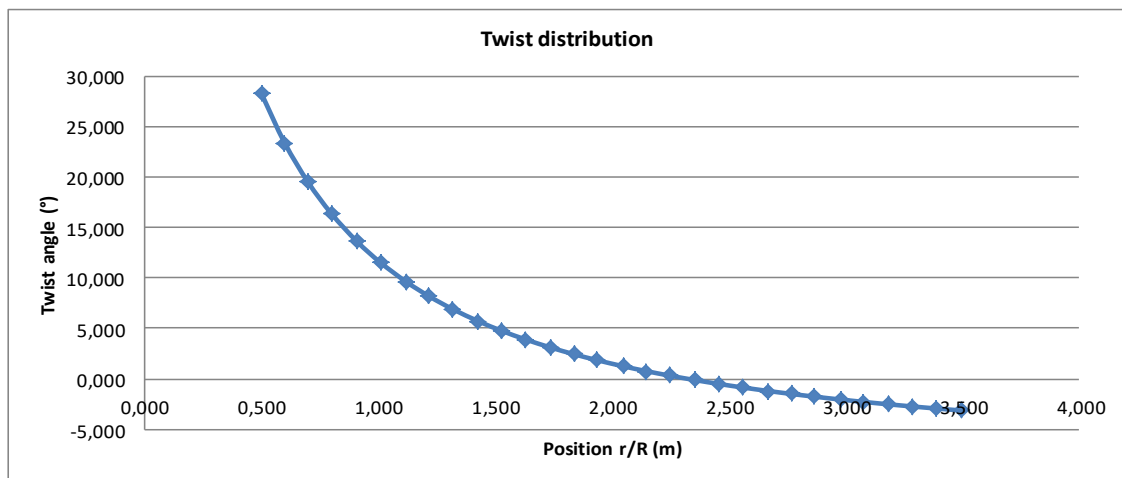
Figure 20: Twist angle distribution from Q-blade software

Similarly, the blade geometry shows that the chord length is larger at the inner sections of the blade (closer to the root) and smaller at the outer sections of the blade. The optimum chord

distribution was optimized according to Schmitz method (equation 33) whereas the twist angle distribution was chosen to keep the ratio of the lift to drag ratio at its maximum along the blade span (at the design tip speed ratio).

The evolution of the power coefficient as a function of the blade tip speed ratio is given in figure 21.
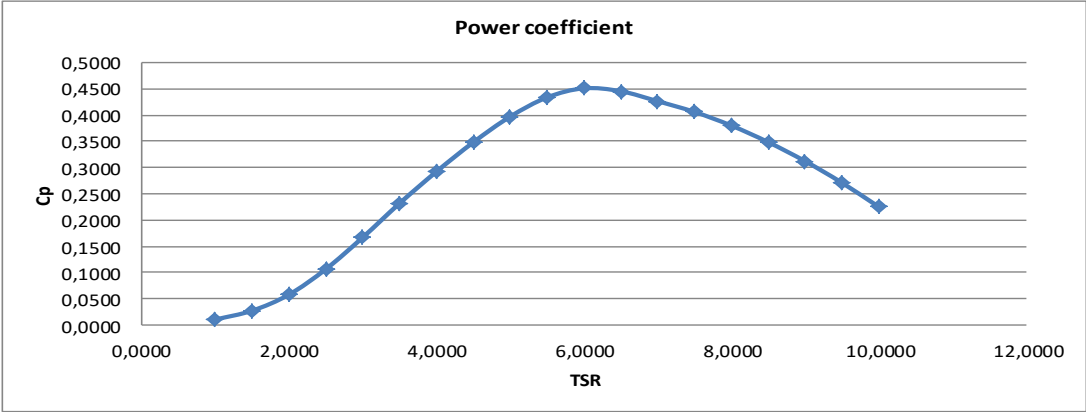
Figure 21: Power coefficient as a function of λ from Q-blade

The maximum achievable power coefficient is 0.45, which corresponds to a tip speed ratio of 6. The value given by Q-blade is the same as the value obtained from the Wilson's approximation (equation 23). The value of C_p was computed for an ideal rotor by taking into consideration wake rotation, drag effects and tip losses (Prandtl correction factor).

Figure 22 shows the power curve of the wind turbine with the optimized rotor blades.
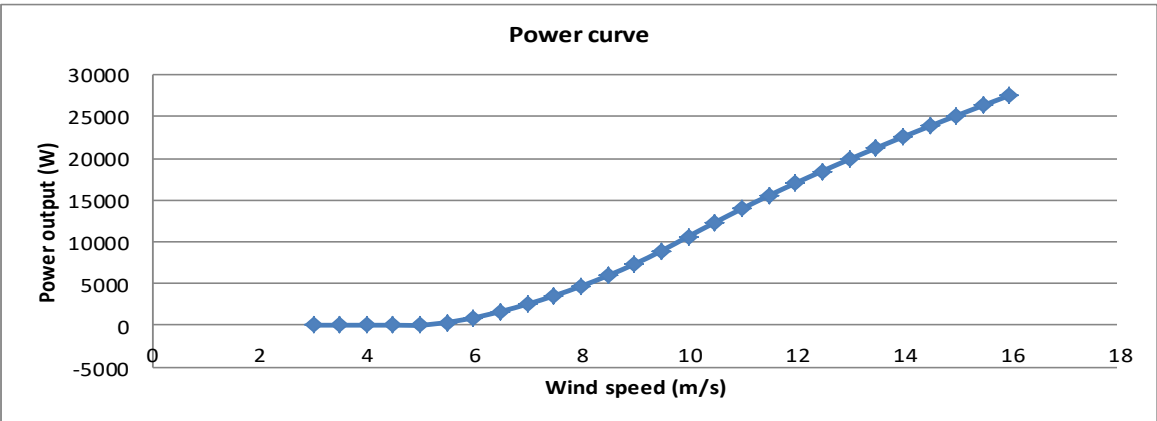
Figure 22: Power curve of the small wind turbine with an optimized rotor

From the figure 22, three main conclusions can be drawn:

1) The rotor power output increases with the wind speed. At the design wind speed of 10.5 m/s, the rotor power generation was found to be 12.3 kW. This high power generation can be justified by the fact that the turbine simulation was performed for a rotor blades having a maximum achievable aerodynamic efficiency (C_p=0.45).

2) The starting time of the rotor is relatively high (5 m/s). This makes the wind turbine design not suitable for geographical areas with low wind speeds (the design cut-in wind speed was originally set to 3 m/). Therefore, multi-variable optimization is required.

3) The rotor power increases and exceeds the maximum overloading to the generator which was set to 120 %. This can be fixed using an appropriate control strategy of the wind turbine: below the rated wind speed, the wind turbine system maximizes energy production, and above the rated wind speed, the control system will limit the power production by using passive control system (stall regulation) combined with another active control algorithm (electronic regulation system for example).

4.1.2 Blade design optimisation

The chord and twist angle distributions given by the initial design (maximization of C_p only) correspond to an ideal rotor that includes the effects of wake rotation, drag effects and tip losses. However, in the design process of a real rotor blade, additional design criteria such as blade mass, m_B, and rotor starting time, T_{st}, must be taken into consideration. For such nonlinear exercises, multi-variable optimisation is required. For the present study, the design optimization of the blades will be performed using Small Wind-Turbine Rotor Design Code (SWRDC).

SWRDC is an aerodynamic design and optimization tool that uses genetic algorithm, blade element momentum (BEM) theory, simple Euler-Bernoulli beam theory, a model for starting from Wood [41] and a noise model of Zhu [77] to design small-scale, fixed-pitch variable-speed horizontal-axis wind-turbine rotors. This code is based on the work of a M.Sc. project done at the University of Calgary, designed for large-scale wind-turbines and which has been recorded for the purpose of designing small-scale wind-turbine rotors [78].

The SWRDC program is designed for variable-speed turbines that can operate at a single tip-speed ratio between the wind speed at starting and the wind speed at which the maximum generator rotational speed can be reached. The genetic algorithm used in SWRDC is a search heuristic that mimics the process of natural selection. This heuristic (also called meta-heuristic) can be used to solve optimization problems such as the design of wind-turbine rotors. SWRDC can optimize rotors based on a single or multiple criteria. Each criterion is called an objective and is optimized by either minimizing or maximizing its objective function. The rotor design optimization is formulated as a weighted min-max problem:

$$\text{Minimize } \max_{i=1}^{q} W_i \cdot \left[\frac{f_i(x) - Z_i^{min}}{Z_i^{max} - Z_i^{min}} \right] \tag{51}$$

$$\text{Subject to } x \in S$$

Where q is the number of objectives, W_i are weights that satisfy $W_i \geq 0$ and $\sum_{i=1}^{q} W_i = 1$, $f_i(x)$ are the objective functions, Z_i^{max} and Z_i^{min} are the maximum and the minimum objective values of the population in the current iteration, and S is the feasible region (region where the constraints are satisfied). The objective functions of the present small scale rotor optimization are the power coefficient, C_p, the blade mass, m_B, and the rotor starting time, T_{st}. SWRDC attempts to minimize the maximum value of the following vector:

$$\left[W_1 \frac{C_p(i) - C_P^{min}}{C_P^{max} - C_P^{min}}, W_2 \frac{T_{st}(i) - T_{st}^{min}}{T_{st}^{max} - T_{st}^{min}}, (1 - W_1 - W_2) \frac{m_B(i) - m_B^{min}}{m_B^{max} - m_B^{min}} \right] \tag{52}$$

For each blade iteration, the maximum value of C_p and the minimum values of T_{st} and m_B are taken from the current generation. Figure 23 gives a screen shot of the SWRDC program interface with the following multi-objective optimization: AEP (W_1=0.85), starting time (W_2=0.05), mass (W_3=0.1), and noise (W_4=0). In this example, noise constraints will not be considered in the optimization process.
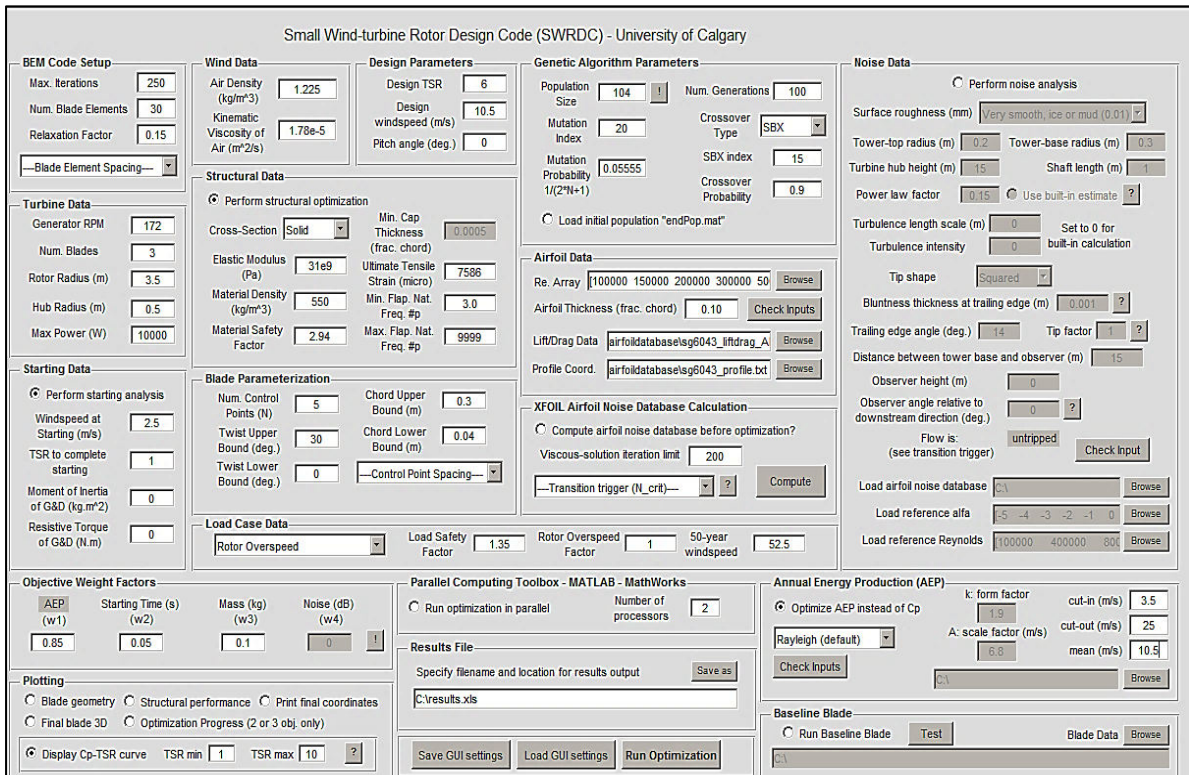
Figure 23: Graphical user interface (GUI) of the SWRDC tool
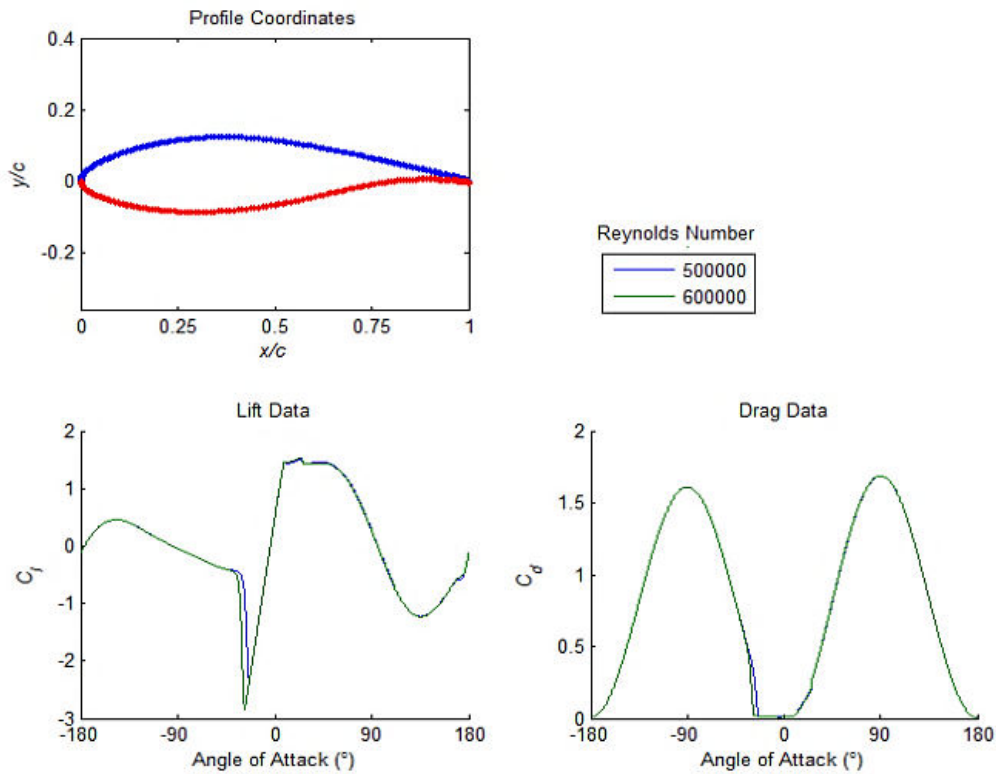
Figure 24: Aerodynamic date for SWRDC inputs

Figure 24 shows a screen shot of the main input data for the SWRDC code which includes airfoil coordinates, aerodynamic lift and drag coefficients, and the Reynolds numbers range. For all the runs in this study, table 25 summarizes the genetic algorithm parameter values that have been used:

Parameter	Value
Population size	104
Number of generations	100
Mutation index	20
Crossover type	simulated binary crossover (SBX)
Mutation probability	0.0555
Crossover probability	0.9

Table 25: Genetic algorithm parameters used for the blade design

It is suggested that genetic algorithm may work well with large crossover probability and with a small mutation probability as the use of high mutation probability may destroy already found good information [79]. Through multiple iterations, the chord length and the twist angles are calculated and presented in figures 25 and 26:
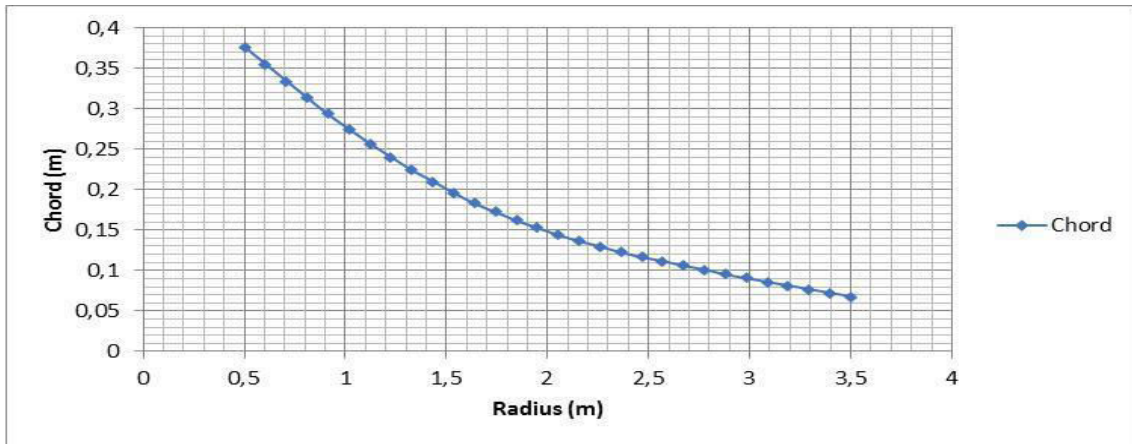
Figure 25: Optimized chord distribution
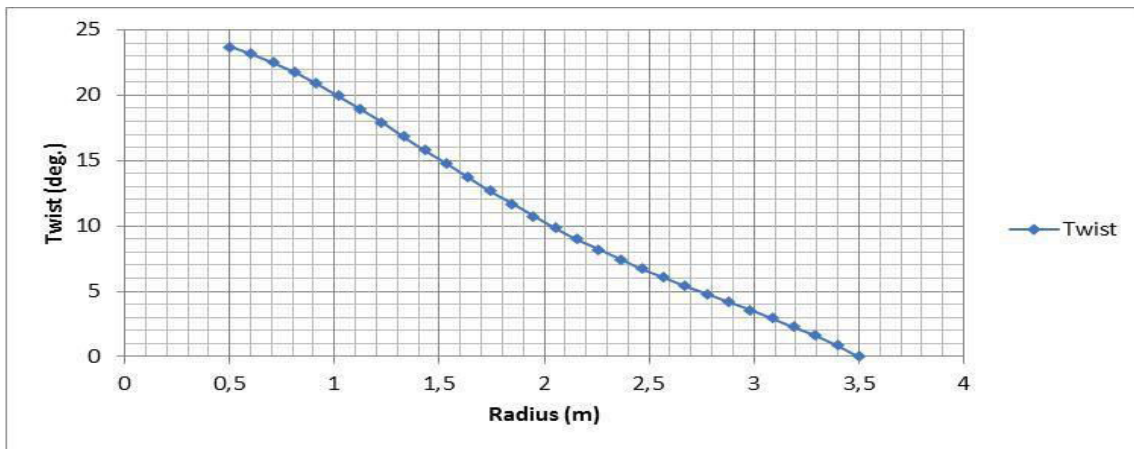
Figure 26: Optimized twist distribution

The results show a noticeable difference in the twist distribution at the tip region between the optimized blade and the initial distribution. This difference is due to the fact that the SWRDC program was set such that the twist distribution at the tip becomes zero. The evolution of the power and torque coefficients (C_p and C_T) as a function of the blade tip speed ratio is shown in figures 27 and 28.
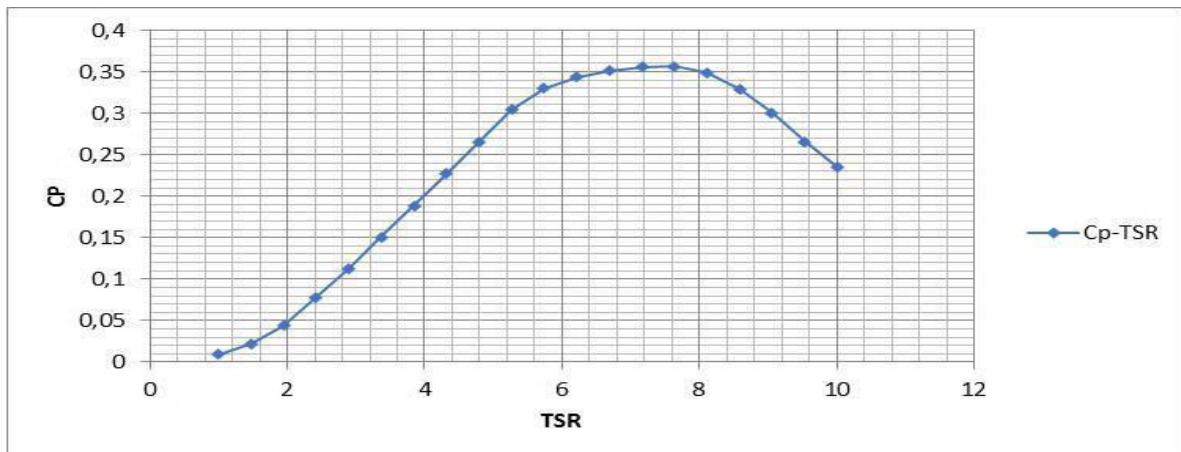
Figure 27: Variation of the power coefficient as a function of the tip speed ratio λ

Although the optimization has been performed for a design blade tip speed ratio of 6, the optimization results give a maximum power coefficient of 0.35 which corresponds to an optimum tip speed ratio of $\lambda= 6.21$. As it can be noticed, the value of the power coefficient given by the SWRDC code is lower than both the maximum rotor aerodynamic power coefficient ($C_p = 0.45$ for $\lambda=6$) given by the equation 23 (from Wilson et al.) and the power coefficient computed by Q-blade. The apparent disparity between the obtained results seems logical since the Wilson's approximation and the BEM theory are theoretical approaches that describe the maximum theoretically possible power coefficient for an optimum blade shape. These approaches compute the aerodynamic power coefficient by using the main wind turbine rotor parameters (number of blades, tip speed ratio, and the maximum lift/drag). However, an optimum blade shape is a hard target when multivariable optimization is used. Therefore, the use of optimization software would lead to an interaction between the design aspects that are defined by the variables of the objective function (e.g. starting time, blade mass, and optimal power coefficient). For this reason, the design process tends to achieve a compromise between the different design aspects by optimizing some variables in detriment of others.
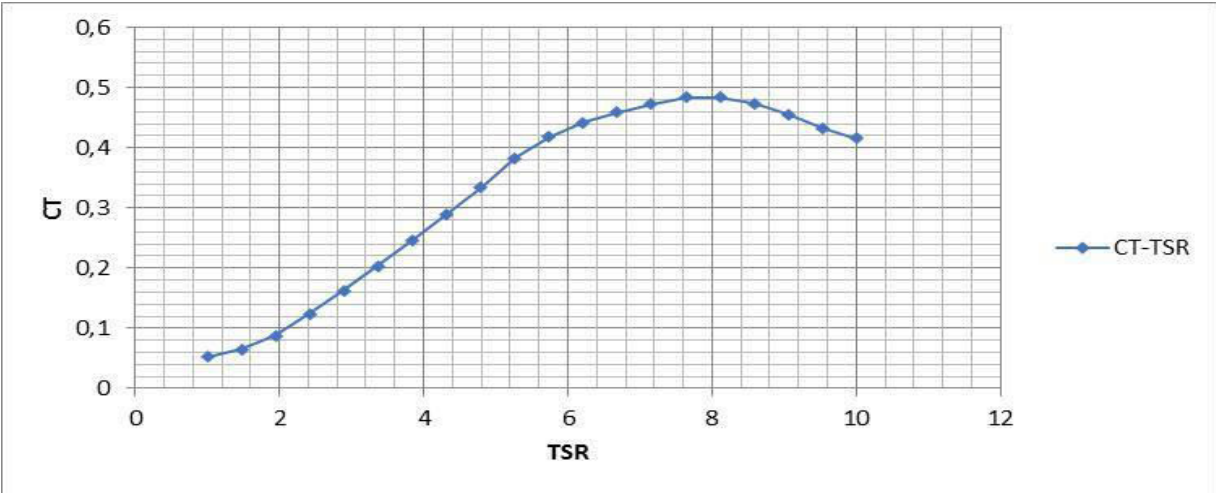
Figure 28: Variation of the torque coefficient as a function of the tip speed ratio λ

The variation of the power and the torque coefficients show that the tip speed ratio has a major effect on wind turbine performances. This is because it controls the angle of attack of the blades. As the value of C_p determines how much power is extracted at a given wind speed, the results imply that a constant rotational speed turbine cannot operate at maximum efficiency over a large range of wind speed. Thus, to obtain a maximum power coefficient before the rated wind speed, the rotor rotational speed should be variable according to the maximum power coefficient curve. Figure 29 shows the blade shape given by the SWRDC software.
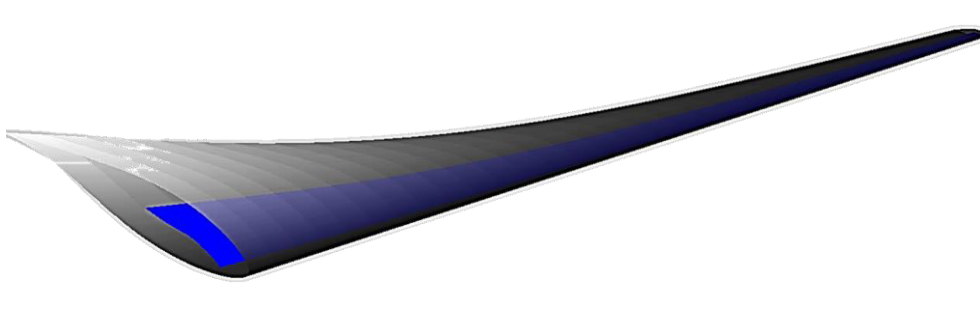
Figure 29: Small wind turbine blade shape

The optimal distribution of the chord and the twist angle with and without optimization process are plotted in figures 30 and 31:
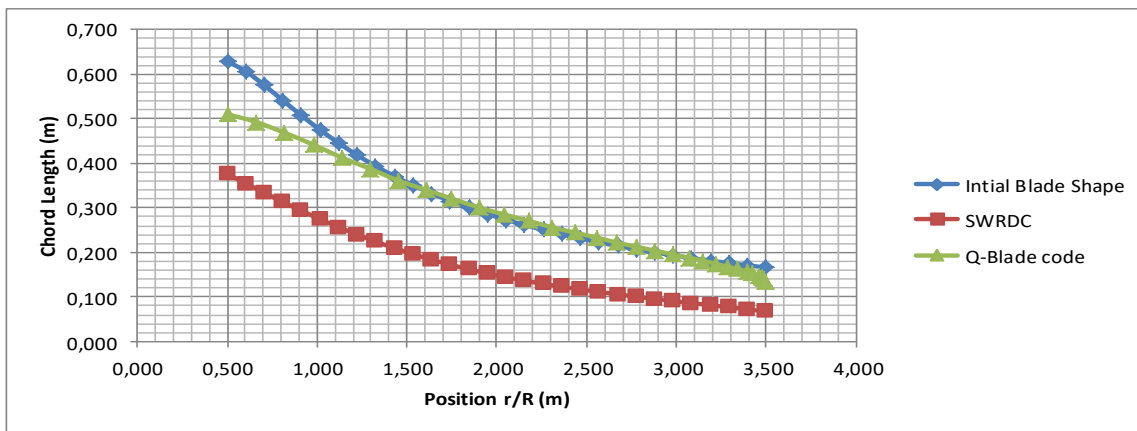
Figure 30: Chord length distribution
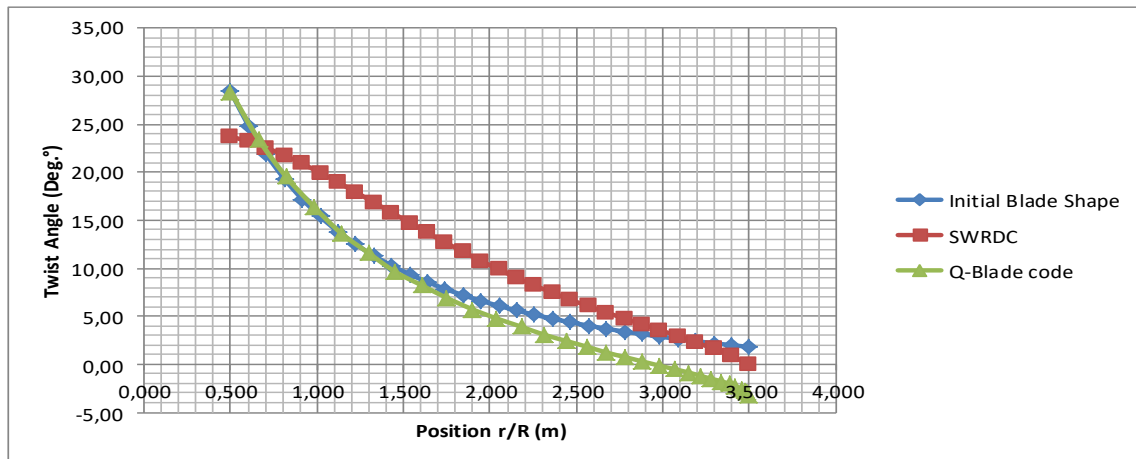
Figure 31: Twist angle distribution

The optimization results obtained from the **SWRDC** program shows that the distribution of the chord length follows the same shape as the two previous methods but shifted to lower values. This reveals that we could achieve better aerodynamic performance by optimizing the geometry of the designed blade. The decrease of the obtained chord length (fig.29) can be justified by the fact that the SWRDC program integrates the blade mass as one of its objective

function parameters. Thus, if this parameter is enabled in the graphical user interface of the program, the program will minimize the blade mass while attempting to meet maximum allowable strain.

Figure 30 shows a nonlinear distribution of the twist angle given by the first two approaches (initial blade design and Q-blade software). In practice, these distributions present a set of manufacturing difficulties. However, the outcomes of the SWRDC program gives a linearized twist distribution which could offers a good opportunity for the designed small wind turbine blade design to achieve a better power performance and low manufacturing cost.

Some modifications of the twist angle and chord length distributions may also be conducted to decrease the drag and thrust forces to the rotor at high winds. However they should be close to the theoretical distributions so as to make sure the maximum power coefficient and low start up characteristics can be achieved. Any modification should make the real attack angle to approximate the optimum attack angle and make sure the lift force is not decreased sharply.

4.2 Wind turbine blade material

Due to the relatively high costs of repair and maintenance of a remotely located small wind turbine, its reliability (especially the rotor blades as the most important part of the wind turbine) should be increased to ensure efficient operation during its lifetime (20 years or more).The reliability and the high lifetime performance can be ensured if the wind blades have high stiffness, high strength to withstand extreme winds, high resistance to fatigue damage and environmental loading (to ensure a proper functioning for more than 10^8 cycles) as well as low weight to reduce the load on the tower and the effects of gravitational forces [80]. The design of the wind turbine blade is driven by compromises between aerodynamic and structural considerations. The structural considerations are strongly dependent on the blade material choices. Therefore, selecting an appropriate composite material for the blade has an important role in gathering the design and manufacturing in order to produce the optimum solution in terms of performance and cost. Generally, lightweight material is used for blade manufacture because of their advantages:

- Less material cost;

- High natural frequency (which means the tower passing frequency will not be a problem);

- Less fatigue loading;

- Reduced edgewise bending moment (which is caused by the weight of the blade flexing it one way then the other as it rotates);

The advancement of fiber composite materials has provided the best solutions to overcome inefficiencies caused by traditional materials used in wind turbine construction. Nowadays,

the majority of wind turbine blades are constructed with glass fiber reinforced plastic (GFRP) [81].

4.2.1 Fiber material selection

Modern small wind turbine blades are made from fiber-reinforced plastics (FRP) owing to the materials' superior strength-to-weight ratio compared to other materials [82]. Currently, Glass Fiber Reinforced Plastics (GFRPs) and carbon fiber are the most widely used material for the rotor blade manufacture. Carbon fibers are about twice as strong as glass and three times stiffer. Their extra stiffness also allows the surrounding resin to withstand fatigue better by reducing the strain in the resin. However, carbon fibers are much more expensive, so they tend to be used only where their properties are essential for the performance of the blade. In general this means carbon is used only on some of the largest turbines, and even then only on the spar caps [83]. Glass fiber is manufactured by pushing melted glass produced from a specially designed furnace which holds small holes at the base. A wide range of fibers material stretching from glass to carbon are used in the composite to make wind turbine blades. E-Glass and S+R Glass types are mainly used [84]. E-glass ("Electrical" grade glass) is by far the most used fiber in reinforced plastic composites. In many industries it represents over 90% of the reinforcements used [85]. The E in E-glass fiber represents electrical, as it has good electrical properties [3]. The E-glass performs well in tension and compression and has reasonable stiffness. The cost of the fiber is the lowest and is commonly used fiber in wind blade manufacturing industry. **Therefore, the E-Glass fibers are the selected solution for the design of the small wind turbine blades.** Table 26 gives the mechanical characteristics of the selected E-glass fibers.

E-glass fiber	
Long. Modulus, E1$_f$ (GPa)	74,00
Tran. Modulus, E2$_f$ (Gpa)	74,00
Shear Modulus, G12$_f$ (Gpa)	30,00
Poission ratio, v12$_f$	0,22
Therm. Exp, CTE$_{1f}$ (m/m/c)	$5,3 \cdot 10^{-6}$
Therm. Exp, CTE$_{2f}$ (m/m/c)	$5,3 \cdot 10^{-6}$
Mois. Exp, CME$_{1f}$ (m/m)	0,00
Mois. Exp, CME$_{2f}$ (m/m)	0,00
Tens. Strength, σf (Mpa)	1800
Comp. Strength, σcf (Mpa)	1500
Shear Strength, S$_f$ (Mpa)	60
Density, ρ_f (Kg/m^3)	2500
Therm. Cond., K$_{f1}$ (W/m/K)	1,28
Therm. Cond., K$_{f2}$ (W/m/K)	1,28

Table 26: Typical characteristics of E-glass fibers

4.2.2 Polymer matrix selection

Blade composites can be divided into a matrix whose function is to distribute the load throughout the blade and a fiber whose function is to carry the loads. The main function of a matrix is to support the fibers and bond them together in the composite material. This element transfers the applied loads to the fibers, keeps the fibers in their position and chosen orientation, gives the composite environmental resistance and determines the maximum service temperature of a composite. Taking into account the requirements related to the wind turbine blade weight, polymers are the main choice for the matrix material for wind blade composites. Typically, thermosets (epoxies, polyesters, and vinylesthers) are the mostly used resins in wind blade composites. The advantages of thermosets are the possibility of low temperature cure, and lower viscosity (thus, allowing better impregnation and adhesion) **[3, 86]**. Another load that must be taken into account when selecting a typical resin for blade manufacturing is fatigue; the blade matrix must be able to withstand the cyclic loading applied by the fluctuating winds along the entire lifespan of the turbine machine. According to the literature, epoxy resin is the most commonly used matrix in the composite industry. This is mostly because of their good properties in terms load carrying ability and their resistance to environmental damage and degradation. Epoxy has a tensile strength of around 75 MPa and an average Young's modulus of 3.3 GPa. It is known by low viscosity which is essential in different blade manufacturing methods. Epoxy also has lesser shrinkage compared to its other counterpart thus maintaining good dimensional tolerance during curing **[87]**. **To optimally**

trade off technical and economic considerations, Epoxy resin is selected for the current project. Table 27 summarizes the mechanical characteristics of the selected resin.

Epoxy resin	
Modulus, E_m (Gpa)	3,35
Shear Modulus, G_m (Gpa)	1,30
Poisson ratio, v_m	0,35
Therm. Exp, CTE_m (um/m/°C)	45 10^{-6}
Mois. Exp, CME_m	0,0033
Tens. Strength, σm (Mpa)	75,00
Comp. Strength, σcm (Mpa)	90,00
Shear strength, S_m (Mpa)	55,00
Density, ρ_m (Kg/m^3)	1200,00
Therm.Cond., K_m (W/m/K)	0,20

Table 27: Typical characteristics of epoxy resin

4.2.3 Laminate orientation and stitching pattern

A fiber is the most important load carrying element of the composite material. The fabrics orientation gives the material strength and stiffness. Normally, the composite material is only strong and stiff in the direction of the fibers. In a wind turbine blade structure, the blade shells have two major functions. First, they provide the required aerodynamic shape to the blade. Secondly, they play a structural role in stiffening and strengthening the spar caps, particularly to resist torsion (twisting) loads. Normally, structures loaded in torsion experience pure shear loading, so just like the blade's shear webs, the shells must have high proportions of fibers running diagonally to resist shear (±45° orientations). The blade shells must also have fibers running along the length of the blade (0° orientation). This assists the spar caps in flapwise bending and gives the blade more strength in edgewise bending as structural beams work best with the load-carrying material separated as far apart as possible [83]. In order to minimize the blade tip deflection and ensure structural stability for the blade under wind loading, the blade root and shells will be manufactured with E-glass fabrics diagonally oriented along with some unidirectional plies to assist spar caps in flapwise bending. Layup thickness of the blade sections will be modeled according to the layup schedule presented in Table 28.

Component	Radius %	Location (m)	Layup schedule	Airfoil	Thickness (m)
Root	7.14 to 11.4	0.250 to 0.400	$[(\pm45)_3/0_{12}/(\pm45)_3/0_{12}/(\pm45)_3]_s$	Circle	0.033
Root Transition	11.4 to 12.8	0.400 to 0.450	$[(\pm45)_3/0_8/(\pm45)_3/0_8/(\pm45)_3]_s$	DU 97-W-300	0.025
	12.8 to 14.2	0.450 to 0.500	$[(\pm45)_3/0_6/(\pm45)_3/0_6/(\pm45)_3]_s$	DU 91-W2-250	0.021
Spar caps	14.2 to 32	0.500 to 1.121	$[(\pm45)_2/0_4/(\pm45)_2/0_4/(\pm45)_2]_s$	DU 93-W-210	0.014
	32 to 40.8	1.121 to 1.431	$[(\pm45)_2/0_3/(\pm45)_2/0_3/(\pm45)_2]_s$	DU 93-W-210	0.012
	40.8 to 49.7	1.431 to 1.741	$[(\pm45)_2/0_2/(\pm45)_2/0_2/(\pm45)_2]_s$	DU 93-W-210	0.01
	49.7 to 70.4	1.741 to 2.466	$[(\pm45)/0_2/(\pm45)/0_2/(\pm45)]_s$	DU 93-W-210	0.007
	70.4 to 100	2.466 to 3.500	$[(\pm45)/0_2/(\pm45)]_s$	DU 93-W-210	0.004
Leading Edge	11.4 to 12.8	0.400 to 0.450	$[(\pm45)_2/0_7/(\pm45)_2]_s$	DU 97-W-300	0.011
	12.8 to 14.2	0.450 to 0.500	$[(\pm45)_2/0_5/(\pm45)_2]_s$	DU 91-W2-250	0.009
	14.2 to 49.7	0.500 to 1.741	$[(\pm45)_2/0_3/(\pm45)_2]_s$	DU 93-W-210	0.007
	49.7 to 70.4	1.741 to 2.466	$[(\pm45)/0_2/(\pm45)]_s$	DU 93-W-210	0.004
	70.4 to 100	2.466 to 3.500	$[(\pm45)/0/(\pm45)]_s$	DU 93-W-210	0.003
Trailing Edge	11.4 to 12.8	0.400 to 0.450	$[(\pm45)_2/0_7/(\pm45)_2]_s$	DU 93-W-210	0.011
	12.8 to 14.2	0.450 to 0.500	$[(\pm45)_2/0_5/(\pm45)_2]_s$	DU 93-W-210	0.009
	14.2 to 49.7	0.500 to 1.741	$[(\pm45)_2/0_3/(\pm45)_2]_s$	DU 93-W-210	0.007
	49.7 to 70.4	1.741 to 2.466	$[(\pm45)/0_2/(\pm45)]_s$	DU 93-W-210	0.004
	70.4 to 100	2.466 to 3.500	$[(\pm45)/0/(\pm45)]_s$	DU 93-W-210	0.003
Shear Web	14.2 to 73.4	0.500 to 2.569	$[(\pm45)/0_6/(\pm45)]$	_	0.004

Table 28: Lay-up schedule of the wind turbine blade

As it can be seen from the table 29, stitching pattern varies in a way that will make the material stronger and more resistant indifferent directions. This makes the blade able to support different types of loads (e.g. gravitational, centrifugal and aerodynamic loads) along the whole blade span. In the present project, four main parts of the blade were defined with different stitching patterns. These are the circular region of the blade root (as the biggest edgewise bending moment occurs at the blade root, some extra reinforcement is needed near the root), the blade root transition, the leading and trailing edges as well as the blade spar caps. Because boundary conditions influence buckling, it was necessary to develop a root design for the reference blade. It was assumed that bolts with a 11 mm diameter would be used for the connection and that the thickness of the composite layup at the root section be at least 3 times the bolt diameter. The other part of the turbine blade consists of two faces, joined together and stiffened by one integral (shear) web linking the upper and lower parts of the blade shell. The fibers in the spar caps were oriented diagonally and along the blade span in order to reinforce the strcture against flapwise bending and gianst shear. The number of laminates was reduced towards the tip in order to reduce the weight. The flapwise load is caused by the wind pressure, and the edgewise load is caused by gravitational forces and torque load. The flapwise bending is resisted by the spar, internal webs or spar inside the blade, while the edges of the profile carry the edgewise bending. From the point of loads on

materials, one of the main laminates in the main spar is subjected to cyclic tension-tension loads (pressure side) while the other (suction side) is subjected to cyclic compression-compression loads. The laminates at the leading and trailing edges that carry the bending moments associated with the gravitation loads are subjected to tension-compression loads. The aeroshells, which are made of the same oriented fibers (0° and 45°), are intended to resist elastic buckling. The different cyclic loading at the various locations at the blades suggest that it could be advantageous to use different materials for different lay-up schedules along the blade.

4.3 Blade manufacturing process

Small wind energy industry is using several manufacturing techniques to produce turbine blades. It is important to note that the manufacturing process may strongly affect the quality and repeatability of the turbine blades. Thus, it is crucial to select an appropriate process which produces blades with better mechanical properties. Generally, the blade manufacturing techniques can be divided into two categories: open molding and closed molding processes. An open mold is open at the atmosphere at the top; whereas a closed mold is either two-sided or has a vacuum film at the top. An example of open mold processes would be Hand Lay-up. Resin Transfer Molding (RTM), Prepreg and Vacuum Infusion are closed mold processes. There are advantages and drawbacks associated with each method, this is why; a comparative analysis weighing benefits and risks would aid in the deciding which process is best to use. Here is a brief description of the most widely used manufacturing processes in the wind energy industry:

- **Hand lay-up method**:

Hand lay-up, also called wet lay-up is the oldest and simplest technique for manufacturing composite components. Basically, hand lay-up is an open mold technique, performed by manually placing dry fabric mats in the mold and subsequently applying resin. Then resin is forced through the reinforcements using hand rollers to ensure its uniform distribution and removal of air entrapped inside the laminate. This process is to be repeated as many times as necessary, until the desired thickness is reached. When the fabric is fully saturated, excess resin is removed with squeegees. The layered structure is then allowed to cure and finally, the hardened part is extracted from the mold [85]. Hand lay-up technique is performed in four basic steps. The first step consists of applying a thin layer of release agent to the mold surface in order to facilitate the extraction of the finished part. After a proper mold preparation, a gel coat is applied to produce a high-quality finish of the laminate. Actually, the gel surface becomes the outer surface of the finished part, and thus protects fiber reinforcement. When

gel coat has partially set, layers of fabrics and resin are applied. Each layer is rolled to impregnate fibers with resin and remove air. Curing is usually accomplished under standard atmospheric conditions. Once the part has fully cured, it is removed from the mold.

Because hand lay-up only requires simple tools and one mold surface, it is not expensive to handle. However, it requires a large amount of labor and high cycle times to produce parts. In addition, the quality of parts manufactured from hand lay-up tends to be inferior to parts produced by other processing methods. The fiber placement and impregnation process results in a considerable amount of fabric handling which may displace fibers. Part thickness depends on the amount of resin added and is highly variable. High fiber volume fractions are not possible since there is not another mold face to compress the part. In addition, molds with steep sides may pose difficulty if the resin viscosity is too low, and hollow parts are difficult to produce with good dimensional tolerance. Another limitation is that parts are only finished on the mold side. Finally, since hand lay-up is an open mold process, a considerable amount of 27 volatiles are released from the resin during processing. The shortcomings of hand lay-up result in unnecessary blade weight as well as extra time processing and assembling blade parts, and exposure of workers to volatile resin components. Therefore, this technique is ruled out in this project.

- **Prepreg technology:**

Prepreg is an abbreviation for 'pre impregnation'. It refers to a semi-raw product consisting of fiber fabrics pre-impregnated with resin to form a homogeneous stack that will be used to produce composite structures. An inherent feature of resins used for prepregs manufacturing is high viscosity. These resins are semi-solid at ambient temperature and thus enable easy handling, cutting and application into the mold without any contamination from the resin. Once prepregs are properly positioned in the mold, they are allowed to cure under vacuum at high temperatures typically ranging from 80 to 140 °C [88]. Prepregs are generally processed using either a standard vacuum bag or by autoclave. The autoclave is a pressured oven operating at 6 atmospheres, used generally in the aerospace industry [89]. It is an extremely expensive approach due to the equipment it requires, especially when it comes to large components. For the majority of industry applications, Prepreg is rather processed using the standard vacuum bag technique. As previously mentioned, it is necessary to use a combination of pressure and heat in order for the laminate to cure. Pressure is actually achieved using vacuum bagging; an oven is used to apply the necessary heat [89].

Prepreg is a cost prohibitive technology mainly because of the necessity of chilled storage, shipping and curing at elevated temperatures. Actually, one kilogram of prepregs turns out to be more expensive than the equivalent resin and reinforcement in an infusion process [90].

For a 35 meters long blade, the total cost for prepregged fabrics is approximately 31600 USD, the equivalent resin and reinforcement in vacuum infusion is roughly 28000 USD. Thus, Vacuum infusion saves around 3600 USD. Therefore, Prepreg technology must be ruled out.

- **Resin Transfer Molding-RTM :**

The basic Resin Transfer Molding (RTM) process involves injection of a resin through reinforcement into a two-sided, closed mold. The process begins with gel coat application; gel coat may be brushed or sprayed on the top and bottom mold surfaces. Fabrics are then laid up as a dry stack of materials. The mold is closed and clamped using toggle clamps to hold halves of tool together. Once the mold is completely closed, the resin pump pumps simultaneously both catalyst and resin to the mix head, where they are mixed together as a single component, and injected into the mold cavity at a pressure of around 6 bars. Resin is injected from a central point into the cavity between the molds, pushing air out to the edges. It would be expected that a small amount of resin leaks around the perimeter and out of the bottom mold's vents; this indicates that the part has reached full saturation. The injection head is removed and the resin inlet is closed. Once the resin has cured at ambient temperature, the mold is opened and lifted to allow de-molding.

A variant of the RTM is Light Resin Transfer Molding (LRTM). Light RTM is also known as Vacuum Assisted Resin Injection (VARI) because, as its name suggests, it uses a combination of vacuum and pressure during injection: Resin is injected at low pressure through a peripheral channel (Max. 1 bar); vacuum is used both to clamp molds and to assist in drawing resin into the fabrics within the mold cavity. LRTM is developed as a cheap alternative to current resin infusion methods like resin transfer molding (RTM) and Vacuum infusion (VI). In comparison to the conventional resin infusion methods (RTM and Vacuum Infusion) LRTM demonstrates a possible cost saving, improvement in dimensional stability, a reductions in resin wastage and infusion time and a decrease in internal void formation resulted in an increase in mechanical performance [91]. LRTM mold sets are composed of a rigid base mold and a semi-rigid, transparent, upper mold. This small amount of flexibility allows the upper mold to match perfectly the bottom mold, which is critical for achieving the required vacuum pressure and finished parts' accuracy. It is important to note that LRTM requires the laminate to cure under vacuum, generally at ambient temperature.

RTM process presents several limitations. The first limiting factor to Resin Transfer Molding is start-up cost. Typical equipment capital cost is in the order of 65000 USD. This includes the injection machine, the tooling frame and the control system for mold temperature control. Another concern associated with RTM is the difficulty of predicting resin flow because of the closed mold feature: In case the laminate is not completely impregnated with resin. As a

result, dry spots or voids may appear, leading ultimately to part reject. Defects in RTM components can also be introduced if the resin injection pressure or flow rate are too high. This may result in distorted fibers, which reduces the mechanical strength of the blade parts [92].

- **Vacuum Infusion process -VI :**

Vacuum Infusion (VI) is a process which uses vacuum pressure to drive resin into a reinforcement package. Dry materials are positioned into the mold and vacuum is applied before resin is injected. Once complete vacuum is achieved, resin is literally aspirated into the laminate via carefully placed tubing. This process is assisted by a variety of supplies and consumables [93]. Vacuum Infusion Process results in a product with roughly 60% fiber volume content with minimal to no voids in the finished laminates [94]. Vacuum is applied while the fibers are still dry. From that point, resin is infused using vacuum pressure. Ideally, any excess resin that is introduced will eventually be sucked out into the resin trap via the vacuum line. Consequently, only the amount of resin required is driven into the laminate. **This reduces weight, increases strength and stiffness and generates a finished part with better mechanical properties**. Besides, resin content is remarkably consistent with vacuum infusion. Actually, upon repeated attempts, resin usage will be predictably similar which yields to less wasted resin, and therefore; less wasted money. Furthermore, vacuum infusion requires much lower tooling cost compared to RTM because one half of the tool is a vacuum film, although vacuum infusion remains a slower process compared to RTM due to the long time needed for preparing a vacuum-tight mold and further curing resin at room temperature.

Vacuum Infusion is a clean process as it requires neither brushes nor rollers, and therefore there is no spattering. Also, no one will be required to hover over an open mold, applying resin by hand trying not to drip on his/her clothes. Furthermore, fumes are only released from the resin reservoir and thus are relatively containable. To wrap up, Vacuum Infusion is a safe and environmental-friendly process. Yet, it is necessary to work in a well-ventilated space and wear appropriate protective equipment. However, vacuum infusion set-up quite complex as it requires different devices that must be positioned with care in order to make good parts.

4.3.1 Applicable criteria for the blade manufacturing process selection

Selecting an appropriate blade manufacturing process needs to be done on the basis of specific criteria, most importantly **cost-effectiveness (first criterion)** which is a determining factor in the decision making. Given the little experience we have in the small wind energy industry, it would be more appropriate to practice with inexpensive materials in order to minimize loss in case of failure. This is to say that the manufacturing technique that will be

selected has to be economically viable (the tooling it requires needs to be relatively cheap). Also, the feasibility of a manufacturing technique is determined by its **applicability in the Moroccan context (second criterion)**. The ultimate objective of the project is to contribute, even if only modestly, to the national development effort. For this reason, the qualifications need to be exclusively Moroccan to create job opportunities locally. Hence, the manufacturing process to be selected shall not require a high-level expertise in order for any operator, even with little experience in the manufacturing industry, to be able to perform it. What is more, availability of raw material in Morocco needs to be investigated; to determine whether there are suppliers who can provide the necessary material of the required quality. Last but not least, **mechanical performance (third criterion)** of the finished part has to be considered while selecting the most suitable blade manufacturing process. These three criteria will be the basis of the analysis that will lead to one manufacturing process that will be adopted.

1) Cost-Effectiveness: taking into account the cost limitation, Prepreg and RTM would definitely be ruled out. Prepreg involves an initial 'prepregging' step; which drastically increases the cost of raw material. Furthermore, it requires refrigerated shipping and storage to prevent reducing the out-life plus curing at elevated temperatures (Oven to apply heat). For the RTM process, a resin injection machine is required, plus matched tooling is heavy to withstand high pressures; the technique is therefore very expensive. It remains to us to evaluate both Vacuum Infusion and Hand Lay-up in order to determine the most appropriate technology. Regarding cost-effectiveness, Hand Lay-up is definitely cheaper than Vacuum Infusion in terms of tooling as it uses basic equipment. Vacuum Infusion uses a number of consumables such as peel plies, infusion meshes, tacky tape and vacuum films which results in high disposables' costs. However, Vacuum Infusion is a less labor intensive process compared to Hand Lay-up and thus generates important savings on labor costs.

2) Mechanical Performance of the Finished Part: RTM and Prepreg technologies generate blades with high fiber volume fraction, which increases strength of the finished structure. In addition, both processes are consistent and repeatable, which enhances dimensional stability and decreases variability between blades. Yet, as stated previously, because of the relatively cheap tooling they do require, Vacuum Infusion or eventually Hand Lay-up seems to be more economically viable. In terms of mechanical performance, Vacuum Infusion generates samples with higher fiber-to-resin ratio compared to Hand lay-up. Furthermore, Vacuum Infusion reduces weight, increases strength and stiffness and generates components with better mechanical properties [95]. Actually, Hand Lay-up results in relatively weak, heavy laminates with excessive quantities of voids; which reduce the mechanical strength of the part.

3) Applicability in the Moroccan Context: Hand Lay-up requires the operator to have the necessary skills to make constant adjustments in order to optimize resin content, make the laminate more uniform, and control part thickness. The closed molding feature of Vacuum Infusion eliminates the need for operators to make adjustments during the process. Eliminating the human variable increases the finished part consistency and decreases defects in the component. Yet, the injection equipment set-up needs to be executed properly to minimize the risk of failure. Another advantage of closed molding processes; including Vacuum Infusion is that they offer a working environment which is healthier and safer for operators. Consequently; they feel more comfortable and therefore become much more productive. It is important to note that closed molding processes in general are associated with lower employee turnover.

Balancing all the consideration mentioned above, the Vacuum Infusion process seems to be the most appropriate for the present project. Therefore, it will be adopted for the small wind turbine blade manufacturing. An alternative to commonly used consumables for Vacuum Infusion is the use of reusable vacuum bags. Reusable vacuum bagging is often described as a hybrid process that borrows desirable features from both LRTM and VI. This type of vacuum bags is custom made. It already includes resin inlets, vacuum inlets and distribution channels. Also, it conforms exactly to the mold surface and contours which significantly reduces lay-up time. The production life of the bag is determined by a number of factors such as the type of resin used and the length of time the bag surface is exposed to the resin as well as external factors like temperature and whether the part is to be cured inside of a heated autoclave. Epoxy and Vinylester can be harsh on bag surface; the volume of parts may be limited with some resin combinations to less than 20 with direct resin contact to the bag but is more commonly around 30 parts. This results in reduced labor and material costs while improving parts' consistency.

Typically, cost savings are 40% or greater per part, depending on the size of the production run [96]. A customized vacuum bag offers a number of advantages such as:

- **Short manufacturing time**: silicone vacuum bags are ready for use right after full cure. Approximately 4 hours from bag manufacture to part production.

- **Reusability:** this reduces or eliminates traditional consumables such as peel-ply and flow media.

- **Self-Sealing** : this eliminates bagging tape traditionally used for sealing the vacuum bag to the mold surface

- **Chemical Resistance**: this gives better performance against chemically harsh resins, Heat Resistance – up to 260°C.

Silicone Vacuum Bags are environment-friendly because they minimize the use of traditional vacuum bagging consumables resulting in low environmental impact. Plus, since all channels are already incorporated in the bag, a step-by-step operating guide would be enough in order for the newest operator in the plant to perform a successful Vacuum Infusion.

4.3.2 Vacuum Infusion step-by-step process

As the Vacuum Infusion process was adopted for the present blade manufacturing, here are the steps that must be followed:

Step 1:

The first step consists in preparing the mold. This step includes four additional sub-steps which are:

- Gel coating the Mold: For resin infusion technology, the mold needs to be rigid and have a shiny finished surface. The mold is usually a concave female mold so the finished smooth surface, in the case of wind turbine manufacture, is the outer surface of the blade. After a proper treatment of the molding tool (Cleaning, and Waxing to allow for the parts to be released), a gel coat is applied. The function of the gel coat is to protect fiberglass surfaces and produce a high-quality finish.

- Applying the Fabric Layers: Once the gel coat is fully cured, the fabric laminates are laid out onto the mold. It is recommended to cut the fiberglass in between strands in order to reduce chances of separation and therefore obtain a final part with cleaner edges. During fabrics lay-up, it is necessary to avoid the bridging effect which may cause an uncontrolled flow of resin after applying vacuum. Bridging is typically characterized by areas of high permeability that represent an easy path where resin can move past the laminate.

- Position the peel-ply: Cut a piece of peel-ply so that it is large enough to cover the core materials and have some extra centimeters on the periphery. Peel-ply prevents the rest of the bagging stack to stick into the part. Once the part is cured, it allows the excess resin and flow media to be peeled off the finished part.

- Flow Media: Generally, the resin is slow; it follows the path of least resistance. Since many fabrics provide great resistance that may hinder resin flow, a flow media is added in order to facilitate resin flow. The flow media is typically an infusion mesh, laid as a single layer on top of the peel-ply to help the resin flow through the part.

Step 2:

This step consists in installing the Resin and vacuum lines. Bagging tape is applied around the tool flange approximately 3 centimeters from the edge. It will anchor the seal for the vacuum bag to the tool surface. On the inlet side of the mold, spiral tubing wrapped in peel ply is used

to feed the resin into the mesh; small pieces of masking tape are used to hold the tubing in place. Spiral wrap has to stay in contact with the infusion mesh to create a natural path for the flow. A silicone connector is positioned on the infusion spiral at approximately the mid-point of the tube as shown in figure 32. This will serve as a resin connector. A length of spiral tubing wrapped in peel-ply is extended along the outlet side of the mold, and vacuum line silicone connector is placed on top of it at approximately the mid-point of the tube; facing the first silicone connector. It is worth mentioning that any element that will be removed after the part has fully cured (Flow media or spiral tubing for example) needs to be placed on peel-ply. Otherwise, it will be soaked into the part.

Figure 32: Example of a resin connector

Step 3:

During this step, the vacuum bag should be positioned on the mold and the resin line must be connected. The bagging film must be (which serves as the vacuum bag) oversized with around 20 centimeters wider and longer than the taped area on the mold in order to allow pleating. These pleats will enable the bag to drop down following the contours of the mold without bridging. The bag is then sealed down onto the tape. Once the bag is positioned, the tubes should be attached for resin and vacuum lines. Actually, two tubes will be needed: a first length of tube from the first silicone connector to the resin pot. This represents the resin line. For this purpose, a length of bagging tape should be wrapped around the end of the tube leaving about 2 centimeters gap. The bag must be pierced above the connector using a utility knife. Then, the hose is taken with the sealing tape and pushed through the silicone connector. The tape will seal the hose to the connector. Particular attention must be paid when piercing the bag for these tubes; it is often these connections which introduce air into the part.

Step 4:

During this step, the vacuum of the bag is performed. To do that, a vacuum line must be installed; a second tube goes from the second silicone connector to the vacuum pump via the catch pot (resin trap). This represents the vacuum line. A resin trap is an airtight container

sitting between the laminate and the vacuum pump to catch any excess resin before it enters the pump, preventing its damage or total destruction. For a proper set-up, a length of tube is cut and firmly connected to the second silicone connector. The connection is done through one tube end. The other end is connected to the catch pot. A separate tube will then leave the resin trap and connect to the vacuum pump.

A clamp is used to close the resin feed line to stop any air from being drawn into the bag. The vacuum pump is then switched on. It will allow drawing air out of the bag. A vacuum is pulled until the vacuum gauge levels off at maximum value. This is the opportunity to ensure that the bag is firmly positioned against the surface. It is critical for the vacuum bag not to have any leaks. Actually, air may penetrate into the laminate even through the smallest leaks and because of the pressure gradient in the infused laminate, air will propagate across the laminate very quickly. The most widespread technique for checking the integrity of the vacuum system and tooling is the Vacuum Drop Test. This test consists of tracking the amount of vacuum being drawn out of a part through leaks, as it is probably the most crucial factor in the success of the infusion process.

Once leaks and obvious air paths are tightly closed, a Vacuum Drop Test is performed to check whether or not the system is completely air tight. The bag is isolated from the vacuum pump using a line clamp. The bag is left for 5 minutes during which the vacuum level is recorded every minute to determine the loss of vacuum. According to the literature, a successful infusion requires that the loss shall not exceed 5mbar in 5 minutes starting when the vacuum was shut off. It is not recommended to carry out an infusion with a loss any greater than 50 mBar in five minutes; because it is a rather significant drop that may lead to reduced quality laminates.

Step 5:

This step consists in injecting resin into the mold. First, the required amount of resin must be measured. Vacuum hose is attached to insert port. This line will initiate the vacuum process for resin infusion. Resin and hardener are mixed together and the resin pot is gently shaken to allow air bubbles to rise to the surface. Then, the mixture is left to sit for 2 minutes to further remove any air bubbles. If any bubbles are trapped in the resin, they will be drawn into the part during infusion creating porosity in the laminate. Resin feed line is attached to the resin pot using a spare line clamp. This feed line will introduce resin into the vacuum bag. Vacuum pump is turned on to start the infusion process. Before the pump is turned on, it is mandatory to clamp the resin line. Vacuum Infusion Process consists of drawing vacuum into the package before introducing resin; this is why, the resin tube represents a 'temporary' leak that

has to be sealed. For this purpose, resin tube is clamped using a spare line clamp to hold it in place.

Once full vacuum has been achieved (25-29 in Hg), the blade is ready to be infused. Normally, full vacuum is achieved in five to eight minutes. It is necessary to make sure that the resin pot assembly is firmly in place in order for the tube not to leave the pot. The resin feed line's clamp must be removed to initiate resin flow. Resin is quickly sucked through the tube and into the bag under vacuum. Resin thoroughly and uniformly saturates the glass fiber stack under vacuum. When the fiberglass laminates are fully saturated (Glass fiber sandwich turns darker and resin reaches the catch pot), feed line is clamped to stop flow of resin. Resin is left to fully cure, overnight, under vacuum at room temperature (Around 23°C).

Step 6:

The last step consists in removing the blade part from the mold. After the blade half has fully cured, the peel-ply, green flow media, and vacuum bag is removed from the mold. It is important to handle the blade with care to avoid damaging either the mold or blade during the de-molding process. After removing the blade half from the mold, it is recommended to conduct a visual inspection in order to ensure there are no dry spots or large air bubbles on the blade's back and front sides. The root section needs to be very carefully examined because it is a very critical area for structural integrity.

4.4   Fiber volume fraction

In a wind turbine machine, the structure of the blade material combines the properties of the composite components (fibers and matrix). Many of the composite mechanical properties such as strength, stiffness and toughness depend on the fiber volume fraction (V_f) which is defined as the amount of the fibers in the composite. The amount of fiber in the composite is largely governed by the used manufacturing process [88]. Therefore, determination of a proper fiber volume fraction is crucial as it improves the mechanical properties of the wind turbine blades. Experimental results show that the mechanical properties were improved when V_f is increased. However, when the fiber volume fraction was sufficiently large, some other characteristics of the composite (ultimate strength for example) start to degrade [97]. The reason of this degradation is due to the lack of sufficient resin to hold the fibers together properly. Normal hand layup technique achieves fiber volume fraction of around 30-35 %, while sophisticated techniques like and vacuum infusion using prepregs can achieve up to 70% [98]. Actually, the composite manufacturing technique is interrelated with three key composite parameters which are the fiber volume fraction in the composite, the reinforcement form and the matrix type. As vacuum infusion was selected as the blade manufacturing

technique, a theoretical maximum achievable fiber volume fraction (FVF) of 60 % can be achieved (for unidirectional reinforcement). **The nominal fiber volume fraction employed in the present blade design is 50 %. According to the blade design experts, optimum mechanical properties can be achieved at this volume content**. This value is too much above the estimated critical fiber content. Normally, the reinforcement action of the fibers is only observed once the fiber volume fraction exceeds the critical volume fraction ($\approx$10 %) **[99]**.

4.5 Composite mechanical properties

Composite mechanical properties are affected by various parameters such as fiber properties, volumetric composition (where the sum of the volume fraction of the fibers V_f, matrix V_m, and voids V_d is unity ($V_f + V_m + V_d = 1$)), geometry of the fibers and fiber/matrix interface properties, packing arrangement (which includes orientation and stacking sequence of the fiber reinforcements) and matrix properties **[99]**. The effect of all these parameters can be demonstrated by the fundamental equations used in several analytical methods that are widely used for mechanical characterization of composite blades. In this project, five analytical models are used to characterize E-glass/Epoxy composite. These models are based on mathematical formulas to calculate the longitudinal, transverse and shear properties of the fiber reinforced composite. The models presented here are the Rule of Mixtures and modified Rule of Mixture, the ten percent rule (or the Hart-smith's model), the Halpin-Tsai Model, Chamis Model, Nielsen Elastic Model and netting method.

4.5.1 Unidirectional glass fiber composite

The following models are used for composite with unidirectional glass fibers:

• **Rule of Mixture (ROM)**: this is one of the simplest methods to determine the mechanical properties of a composite material **[100,101]**. Using this method, longitudinal, transverse and shear properties of unidirectional fibers can be computed using the equations given in Table 29:

Longitudinal Properties	
Young's Modulus (E_1)	$E_1 = V_f . E_f + (1 - V_f). E_m$
Poisson's Ratio (ν_{12})	$\nu_{12} = V_f . \nu_f + (1 - V_f). \nu_m$
Transverse Properties	
Young's Modulus (E_2)	$E_2 = \dfrac{E_f . E_m}{E_m . V_f + E_f . (1 - V_f)}$

Poisson's Ratio (ν_{21})	$\nu_{21} = \dfrac{\nu_{12}}{E_1} \cdot E_2$
Shear Properties	
Longitudinal Shear Modulus (G_{12})	$G_{12} = \dfrac{G_f \cdot G_m}{G_m \cdot V_f + G_f \cdot (1 - V_f)}$

Table 29: Mechanical properties of the unidirectional fiber composite

- **Halpin-Tsai model:** this is a semi-empirical model that uses an empirical factor, which measures fiber reinforcement of the composite material to estimate the values of transverse Young's modulus and longitudinal shear modulus **[102]**. The blade composite properties are calculated using the following equations:

(53)

$$E_2 = E_m \cdot \left(\frac{1 + \xi \cdot \eta \cdot V_f}{1 - \eta \cdot V_f} \right)$$

Where ξ is an empirical factor which measures fiber reinforcement of the composite material that depends on the loading and boundary condition of the fiber geometry. The factor ξ is used to describe the influence of geometry of the reinforcing phase on a particular property. This factor is different for different properties in the same composite. For aligned continuous and shorter fibers, this factor is given by:

$$\xi = 1 + 40 \cdot V_f^{10} \tag{54}$$

For a volume fraction of 50%, a value of 1.03 will be used.

$$G_{12} = G_m \cdot \left(\frac{1 + \xi \cdot \eta \cdot V_f}{1 - \eta \cdot V_f} \right) \tag{55}$$

For this model, the longitudinal properties can be calculated using ROM model:

$$E_1 = V_f \cdot E_{1,f} + V_m \cdot E_m \tag{56}$$

$$\nu_{12} = V_f \cdot \nu_f + V_m \cdot \nu_m \tag{57}$$

The parameter η, in the both equations, is computed using the following equation :

$$\eta = \frac{\left({}^{P_f}/_{P_m} \right) - 1}{\left({}^{P_f}/_{P_m} \right) + \xi} \tag{58}$$

Where P_f is the composite fiber material modulus E_f, G_f and ν_f. P_m is the Composite matrix material modulus E_m, G_m and ν_m.

- **Nielsen Elastic Model:** this model is similar to the Halpin-Tsai's model but includes maximum packing fraction, φ_{max} **[103]**. The maximum packing factor depends on geometry

of the model. Based on this model, the mechanical characteristics are calculated using the following equations:

$$E_2 = E_m \cdot \left(\frac{1 + \xi.\eta.V_f}{1 - \eta.\psi.V_f} \right) \tag{59}$$

Where the parameter ψ is given by:

$$\psi = 1 + \frac{1 - \phi_{max}}{\phi_{max}^2}.V_f \tag{60}$$

$$G_{12} = G_m \cdot \left(\frac{1 + \xi.\eta.V_f}{1 - \eta.\psi.V_f} \right) \tag{61}$$

For a square array of fibers, φ_{max} is equal to 0.785. For hexagonal arrangement of fibers, it is equal to 0.907 and for near random arrangements, it is equal to 0.820. The parameter ξ is the empirical factor that measures the fiber reinforcement with respect to the loading boundary condition of the fiber's geometry. For the case of this study, the array square of fibers' factor will be used in the calculation of the mechanical properties.

● **Chamis Model:** this is a modified model from the rule of mixture method by replacing the fiber volume fraction by its square root [104]. This is the most used method to evaluate the blade elastic properties. The mechanical properties of the blade are given in table 30.

Longitudinal Properties	
Young's Modulus (E_1)	$E_1 = V_f.E_f + V_m.E_m$
Poisson's Ratio (ν_{12})	$\nu_{12} = V_f.\nu_f + V_m.\nu_m$
Transverse Properties	
Young's Modulus (E_2)	$E_2 = \dfrac{E_m}{1 - \sqrt{V_f}.\left(1 - \dfrac{E_m}{E_f}\right)}$
Poisson's Ratio (ν_{21})	$\nu_{21} = \dfrac{\nu_{12}}{E_1}.E_2$
Shear Properties	
Longitudinal Shear Modulus (G_{12})	$G_{12} = \dfrac{G_m}{1 - \sqrt{V_f}.\left(1 - \dfrac{G_m}{G_f}\right)}$

Table 30: Mechanical properties of the fibers based on Chamis Model

For a volume fraction of 50%, Table 31 gives the mechanical characteristics of unidirectional E-glass/Epoxy composite.

Model	E_1(GPa)	E_2 (GPa)	ν_{12}	ν_{21}	G_{12} (GPa)
ROM	38.67	6.4	0.28	0.046	2.49
Halpin-Tsai	38.67	9	0.28	0.065	3.5

Nielsen Elastic	38.67	10.5	0.28	0.076	4.08
Chamis	38.67	10.31	0.28	0.074	4.01

Table 31: Mechanical properties of unidirectional fibers

As can be seen from the tables above, the models for unidirectional fibers give same results for the longitudinal stiffness and the longitudinal Poisson's ratio **[103]**. The value of the transverse stiffness and the shear modulus are quite different.

To validate the results of unidirectional E-glass material, the **Laminator software** was used. This software is designed to compute and analyse laminated composites properties. After defining both the mechanical properties of the matrix and the fiber, the program outputs each of the longitudinal and transverse Young's moduli, the longitudinal and transverse shear moduli, Poisson's ratio, shear and compressive strengths along both longitudinal and transverse directions, density of the composite and thermal and moisture expansion of the material. The laminator software, which is based on the classical laminated plate theory, generates the properties of the composites and the load factors for ply failure based on Maximum Stress, Maximum Strain, Tsai-Hill, Hoffman and Tsai-Wu failure theories. These are the most common theories for the determination the failure criteria of composite materials. Using the Laminator, Table 32 gives the mechanical characteristics of a unidirectional E-glass/epoxy.

E-glass/Epoxy (FVF:50%)	
Long. Modulus, E11 (GPa)	**38,67**
Tran. Modulus, E22 (Gpa)	**11,10**
Shear Modulus, G12 (Gpa)	**3,50**
Poission ratio, v12	**0,28**
Therm. Exp, CTE (m/m/c)	**7×10^{-6}**
Therm. Exp, CTE (m/m/c)	**$3,16 \times 10^{-6}$**
Mois. Exp, CME (m/m)	**0,00010**
Mois. Exp, CME (m/m)	**0,00022**
Longitudinal Tensile Strength, σ (Mpa)	**900**
Longitudinal Compressive Strength, σc (Mpa)	**784**
Shear Strength, S (Mpa)	**44,1**
Density, ρ (Kg/m^3)	**1850**
Therm. Cond., K_1 (W/m/K)	**0,74**
Therm. Cond., K_2 (W/m/K)	**0,48**

Table 32: Mechanical properties of the E-glass/Epoxy from the Laminator software

4.5.2 Multi-axial glass fiber composite

For tri-axial glass fiber composite, the following models can be used:

- **Ten percent rule (Hart smith's model)**: an approach for predicting the strength and stiffness of fibrous composite laminates is given by Hart-Smith's model, which is known as the Ten-percent Rule [105]. According to this method, the primary fibers for each uniaxial load condition are considered to develop 100 percent of the reference strength of the composite material for each environment, while the secondary (transverse) fibers are credited with only 10 percent of this strength and stiffness, whether they are inclined at 90 degree to the primary fibers or at 45 degree. This simple and reliable method could be applied to uniaxial loads, to biaxial loads of the same sign and to biaxial loads of opposite signs (which is equivalent to in-plane shear with respect to rotated axes). When first proposed, this approach was specifically used to predict the strength of well-designed laminates with fiber patterns of $0°/\pm45°/90°$. Later supplementary efforts have been deployed to expend its capability to predict composites strength for other fiber patterns [106].

$$E_c = E_{11}.\,(0.1 + 0.9 * \% \text{ Plies at } 0°) \tag{62}$$

$$\sigma_c = \sigma_{11}.\,(0.1 + 0.9 * \% \text{ Plies at } 0°) \tag{63}$$

Where E_{11} and σ_{11} are the composite young's modulus and the composite tensile strength, calculated from general ROM method. In order to accurately assess the wind turbine blades' mechanical properties, more accurate methods have been developed. These include the widely used Classical Laminate Analysis (CLA) method. In fact, the two above mentioned approaches (ROM and the ten-percent rule) present some limitations as they ignore the effect of coupling between shear and extension within laminate stacking sequences. The Classical Laminate Analysis takes full account of this effect as it enables analytical stress-strain analysis of the arbitrary laminated structures, which are subjected to combined shear and axial forces and bending and twisting moments. This process is too long and complex for hand calculations. Therefore, spreadsheets and software should be used in this case. David Richardson [107] has conducted a comparison between four different approaches that are widely used in composite material stiffness prediction. As can be seen in figure 32, the general ROM method gives optimistic predictions, while the ten-percent rule of mixture seems to be reasonably accurate when it is compared to the classical laminate analysis.
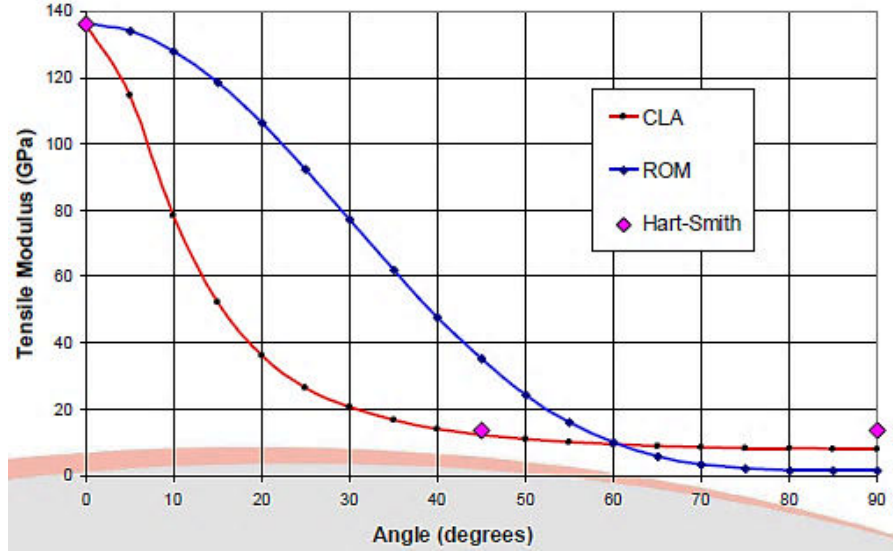
Figure 33: Tensile modulus glass fibers for different orientation angles **[107]**

- **Rule of mixture with efficiency factor:** for blade composite materials with different orientations, the mechanical characteristics can be computed using the following equations:

$$E_c = E_f . V_f . \eta_{lE} . \eta_0 + V_m . E_m \tag{64}$$

$$\sigma_c = \sigma_f . V_f . \eta_{ls} . \eta_0 + V_m . \sigma_m \tag{65}$$

$$\rho = \rho_f . V_f + \rho_m . V_m \tag{66}$$

$$\rho = (\rho_f - \rho_m) . V_f + \rho_m \tag{67}$$

Where E_f and σ_f are the young's modulus and the ultimate strength of the fiber. V_f and V_m are the fiber and the matrix volume fractions. η_{lE} and η_{lS} are the reinforcement length efficiency factors for stiffness and strength (incorporating the effect of fiber geometry and interfacial properties). η_0 is the reinforcement orientation distribution factor (incorporating the effect of packing arrangement and orientation of the fiber reinforcements). E_m and σ_m are the young's modulus and the tensile strength of the matrix. ρ_f and ρ_m are the fiber and matrix densities.

Regarding the reinforcement geometry and orientation, for a blade composite with balanced triaxial reinforcements in 0° and ±45° stacking sequence $[(\pm 45)°/0_2/(\pm 45)°]_s$, it can be shown that the orientation factor is **$\eta_0 = 0.5$** (by using the rule of mixture). Moreover, the calculated fiber length efficiency factor for stiffness and strength is very close to unity for the most used composites in wind turbine manufacture **[99]**. According to literature review, the E-Glass fibers with high length efficiency factor enable good transferring capabilities. Therefore, fiber length factors $\eta_{lE} = \eta_{lS} = 1$ is used for analysis in this project. The assumptions upon which the ROM model is based are:

- All fibers have identical geometry and properties;

- Homogenous and uniform distribution of fibers in the matrix;

- Iso-strain within the composite;

- Ideal fiber/matrix interface;

- Elastic deformation of the fiber and matrix;

- No transverse deformation;

- Zero and maximum tensile stress at the fiber ends and center respectively;

- No effect of porosity content on composite properties;

As fiber composites require very specific considerations, recent work has led to a modified ROM that has been shown to be more adequate for GFRPs. The modified ROM, presented by equations 57 and 58, includes some additional factors:

- A factor to simulate the negative effects of porosity on the tensile properties of GFRPs ($1 - v_p$);

- A fiber diameter distribution factor (η_d) to incorporate the effect of approximately linear decline in fiber tensile modulus with increasing fiber diameter d_f;

- A fiber area correction factor (k_f) to describe the discrepancy between the true cross-sectional area of the fiber and the apparent circular cross-sectional area calculated by the measurement of the apparent fiber diameter;

The above mentioned modifications have been validated with experimental results only for limited data sets. Therefore, the applicability of the modified ROM to GFRPs should be investigated further. The modified ROM model is generally difficult to use at this design stage as it requires a deeper knowledge of the composite characteristics.

$$E_c = (E_f. V_f. \eta_{lE}. \eta_0. \eta_d. k + V_m. E_m). (1 - v_p)^2 \qquad (68)$$

$$\sigma_c = (\sigma_f. V_f. \eta_{ls}. \eta_0. k + V_m. \sigma_m). (1 - v_p)^2 \qquad (69)$$

In spite of these simplifications and assumptions, the ROM model has proven to be adequate for the prediction of the properties of the fiber composites. The simplicity of this generalized model implies that it has become a widely used model for Fiber Reinforced Plastics (FRPs) [108]. ROM method gives accurate estimations in terms of the main stiffness directions (longitudinal, transverse and shear modulus). However, with respect to the strength properties (tensile strength for example), ROM method over-estimates the parameters.

• **Netting model**: Netting method is an empirical composite laminate analysis method. It assumes that only lamina fiber direction provides stiffness or strength. Off axis plies have no

contribution no contribution to the laminate mechanical properties. The composite laminate tensile mechanical properties can be computed using the following equations [109]:

$$\sigma_c = \sigma_{11} . \frac{t_{po}}{t_l} \tag{70}$$

$$E_c = E_{11} . \frac{t_{po}}{t_l} \tag{71}$$

Where t_{po} is the 0° ply total thickness and t_l is the laminate total thickness. It has been found that netting analysis was the best overall method for estimating the cross-ply laminate tensile properties [109]. Table 33 summarizes the mechanical properties of E-glass/Epoxy composite laminate with a specific lay-up of $[(\pm 45)°/0_2/(\pm 45)°]_s$.

Model	Ultimate tensile strength (MPa)	Longitudinal stiffness (GPa)	Composite density (Kg/m³)
Hart smith's	**375**	**15.46**	**1850**
ROM with efficiency factor	487	20.17	1850
Netting analysis	468	19.33	1850

Table 33: Mechanical properties of the material with a lay-up $[(\pm 45)°/0_2/(\pm 45)°]_s$

Regarding the models for glass fibers with a specific lay-up schedule, the ROM model with efficiency factor (η) over-estimates the ultimate tensile strength of the composite. Hart smith's model presents reasonable values when compared to the Classical Laminate Analysis, especially for 0°, ±45° and 90° orientations. Chandler HD et al. [110] have conducted a comparative study between experimental results, obtained from tensile tests on carbon-fibre-reinforced epoxy laminates having different constructions, and simulation results from more established maximum stress, Tsai-Hill criteria and 10 % rule of mixture. They found that the hart smith's model presents reasonable values when conventional ply angle are used (0°, ±45° and 90°). **For the present design and analysis, an ultimate tensile strength of 375 MPa will be used for structural analysis of the blade composite.** This typical value will be considered as the failure criteria of the blade composite beyond which the structure will not be able to carry the external loads. Such a low value allows establishing a conservative analysis of the blade composite.

4.6 Wind turbine blade root design

4.6.1 Blade root and hub attachment

Wind turbine blade root is the heaviest and the thickest part of the blade because it carries the blade structure and it is the junction point between the blade body and the hub. The root has to resist the maximum moments and torques transmitted by the aerodynamic forces through the

blade to the rotor shaft, and therefore, the stresses and strains are concentrated in the root sectional area [111]. Blade root attachment is a critical design region of any blade, which typically represents 20% of the blade cost [112]. The Connection between the root and the hub has often proven to be difficult. This is largely due to dissimilarities in material properties and stiffness between the blades, the hub and the fasteners. The connection is usually made by steel bolts, which can either be embedded in the blade material in the axial direction or aligned radially to pass through the blade skin, but in either case stress concentrations are inevitable. Different connections types are used to connect the blade root to the hub. Here are some common methods that have been used in wind energy industry:

- **T-bolt attachment:** In a T-bolt connection, bolts passes through axial holes in the blade root and are tightened into pins passing transversely through the blade skins as shown in figure 34. The faces of the metal studs bear directly on the blade composite, and attached to the hub using metal nuts. Over the last decade, T-bolt designs have become more popular in blade designs due to their low manufacturing costs as compared to threaded inserts. Also, a T-bolt connection does not rely on adhesives, and more importantly, damaged studs or barrel nuts can be removed and replaced. However, T-bolt connections create a highly stressed region on the composite blade around the cross bolt. T-bolts also need high drilling accuracy to prevent bending of root stud. For larger blades, multiple rows of T-bolts may be used to better distribute stresses through the composite and over a greater number of bolts. When T-bolts are used in a root connection, laminates that have been used for blade stiffness should be reinforced to accommodate the local bearing pressure of the connection. This can be achieved by increasing the percentage of off-axis fibers in the root region ($\pm 45°$ and $90°$ orientations), which result in a reduced laminate modulus in the load bearing axis [113].
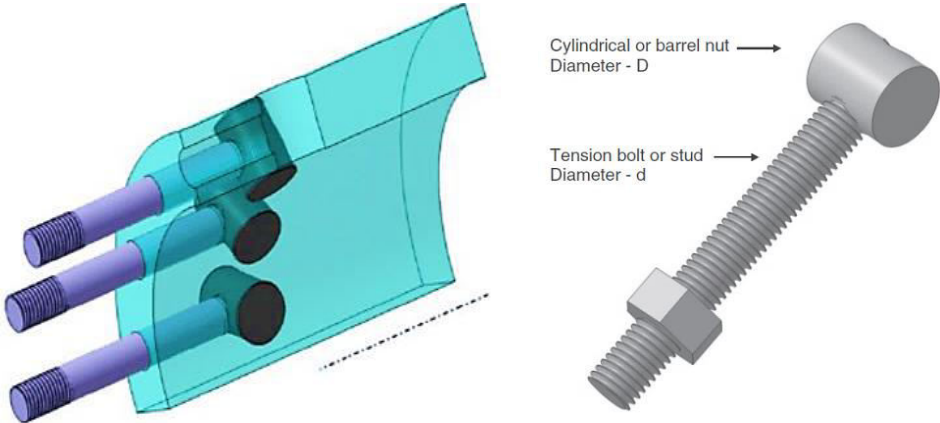
Figure 34: Blade root connector using T-bolt attachment [113]

- **Hütter attachment**: This method is known as the Hütter design, named after its inventor, the German wind energy pioneer Ulrich Hütter. In this method, long fiberglass strands are

bonded into the lower part of the blade as shown in figure 35. Circular metal flanges are provided at the base of the blade, and attached to these flanges are circular hollow spacers. The fiberglass strands are wrapped around the spacers and brought back into the rest of the blade. Resin keeps all the strands and the flanges in place. The blades are eventually attached to the hub via bolts through the flanges and spacers. This root design is most applicable to fixed-pitch rotors [1].
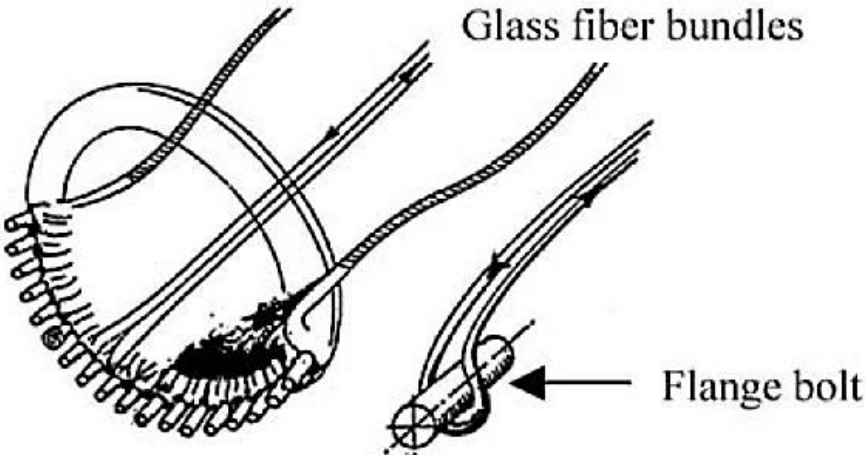
Figure 35: Blade root connector using based on Hütter design [1]

• **Metal-stud root attachment:** In this method, studs or threaded inserts bonded directly into the blades. The use of studs was originally developed in conjunction with wood–epoxy blades, but it has proven applicable to fiberglass blades as well. Fixed-pitch wind turbine blades normally are fastened to the hub with bolts or studs which are aligned radially, and perpendicular to the bottom of the blade root. These fasteners must withstand all the loads arising from the blades [1]. Figure 36 gives an example of a blade root stud design.
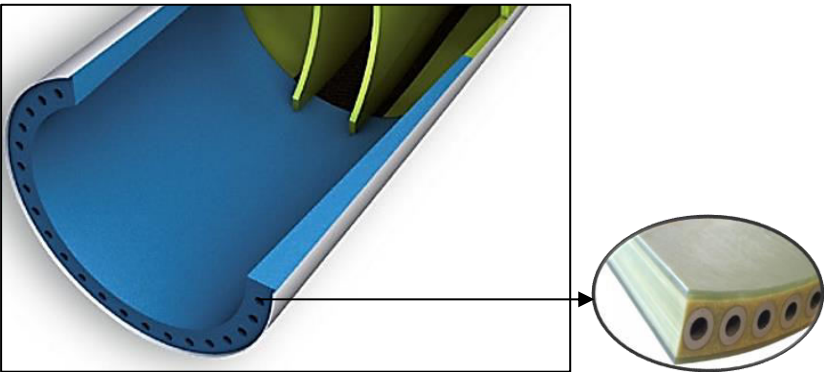
Figure 36: Example of a blade root stud design

• **Metal root:** This method is used only for small wind turbines. The root is thickened and flated, and bolts are placed through the root and a matching part on the hub. The bolts are perpendicular to both the long axis and chord of the blade.

To ensure a good connection between the rotor blade and the hub, **a circular shape with T-bolt attachment was selected for the present blade root design**. This choice can be justified by the fact that this connection form has demonstrated its ability to withstand different loadings during normal and extreme operating conditions. Furthermore, it has the advantage of not using adhesive material, and more importantly, it allows replacing damaged studs and barrel nuts. Finally, Particular attention should be paid to the manufacturing process of this blade part, especially because the root region is generally subject to fatigue loads which tend to loosen the matrix resin, allowing relative motion of the fiberglass.

Figure 37: Example of a flat blade root

4.6.2 Blade root cross-section design

Damages related to the bending moments (in the flapwise and the edgewise directions) are one of the common causes of failure in small wind turbine blade, especially when the root region is not well design. In order to avoid structural failures, the blade root connection must be able to withstand the loads in steady and unsteady wind conditions (i.e. high wind speeds and gusts). In the determination of the blade root diameter, the aerodynamic loads are considered as the main causes of flapwise bending of the wind turbine blades [111, 114]. These loads are suggested to be critical (operating in the extreme wind conditions), and are calculated using a wind speed of U_{e50} which is the 3s-50-year extreme wind speed. The maximum applied normal stress is determined using the drag force which is used to calculate the maximum bending moment in the root region for a parked wind turbine. This maximum bending is taken from IEC 61400-2 load case H (Parked Wind Loading) as shown in equation 72 [41].

$$M_{root} = \frac{1}{4}.C_d.\rho.U^2_{e50}.A_{proj,B}.R = \mathbf{2393.02\ N.m} \tag{72}$$

Where:

C_d: The drag coefficient taken as 1.5;
$A_{proj,B}$: The projected area of the blades taken as 0.54 m²;

The extreme wind speed, U_{e50}, is the design survival wind speed that represents a three-second gust with a recurrence period of 50 years. This value is recommended by the IEC 61400-2 and can be determined using the following formula:

$$U_{e50} = 1.4 * V_{ref} \tag{73}$$

Where, V_{ref} is the reference wind speed. This is a basic parameter for wind speed used for defining small wind turbine classes. As mentioned earlier, wind turbine class III was selected. This corresponds to a reference wind speed of 37.5 m/s. Therefore, the design survival wind speed will be 52.5 m/s. To calculate the blade root diameter, we have conducted the following formulations: First, we assumed that the blade root is a solid cylinder.

The corresponding stress is calculated using the flexure formula:

$$\sigma_{root} = \frac{M_{root} * r_{root}}{I_{root}} \tag{74}$$

Where I_{root} is the area moment of inertia of the blade root, and which is calculated using equation 75.

$$I_{root} = \frac{\pi . D_{root}^4}{64} \tag{75}$$

To make sure that the blade will operate safely without any risk of damage, it is necessary that the applied equivalent stress is less than the allowable stress. In the case of this study, the maximum allowable stress is taken to be the ultimate tensile strength of the blade composite material. By using a blade root laminate stacking sequence of $[(\pm 45)_3/0_{12}/(\pm 45)_3/0_{12}/(\pm 45)_3]_s$, the ten-percent rule of mixture gives a composite's ultimate tensile strength, σ_{dr}, of 576 MPa. The material is assumed to be minimal characterized so that the appropriate partial safety factor is 3 for both material characterization and ultimate strength load [41]. The blade root will operate safely if the following condition is satisfied:

$$\sigma_{root} < \frac{\sigma_{dr}}{\gamma_m . \gamma_f} \tag{76}$$

Where γ_f is the load partial safety factor taken as 3 and γ_m is the partial safety factor for the material taken as 3. By substituting σ_{root} by its expression in equation 76, the minimum shaft diameter that satisfies all design conditions is given by the following equation:

$$D_{root} \geq \sqrt[3]{\frac{32. M_{root} . \gamma_m . \gamma_f}{\pi . \sigma_{dr}}} \tag{77}$$

To maintain this condition valid, the minimum diameter of the blade root must be **72 mm**. To make sure that the blade root will be able to withstand the loads and forces applied in different load cases (e.g. centrifugal loading), the root diameter is taken to be **150 mm**. In order to save weight, the blade root will be made hollow. In this case, the outer diameter is used as a variable and the inner diameter chosen to provide inertia equal to a solid root of comparable strength. The inner diameter should be fixed and is taken to be $\mathbf{D_i = 84\ mm}$ (the root section

will have a thickness of 33 mm). For the solid diameter, the area moment of inertia is given by:

$$I_{solid} = \frac{\pi}{4} \cdot \left(\frac{D_{solid}}{2}\right)^4 = 2.48 * 10^{-5} \text{ m}^4 \tag{78}$$

By equating the inertias the sections and assuming a fixed inner diameter, the outer diameter of the blade root can be determined using the following equation:

$$D_{outer,min} = \left[\frac{64. I_{solid}}{\pi} + D_i^4\right]^{\frac{1}{4}} = 0.153 \text{ m} \tag{79}$$

To ensure a proper functioning of the blade with respect to the maximum allowable stress, which enables the blade to withstand extreme loads without any eventual damage, the root cross section in the case of this project is defined by: $D_0 = 153$ mm, $D_i = 84$ mm.

4.7 Internal beam structure design

Throughout their lifetime service, small wind turbine blades may undergo different external loads (in normal and extreme conditions). In order to avoid catastrophic failures and ensure a proper operation of the turbine machine, the blade structure must be able to withstand all the different load scenarios. In a most basic simplification, a turbine blade can be represented by a cantilever beam rotating about its rotor axis. Therefore, high mechanical properties are required to prevent the blade from hitting the tower when spinning under high wind conditions (minimizing the blade deflection). Generally, the outer surface of the blade (shell thickness) is governed by the aerodynamic considerations. However, the blade shell thickness has limited ability to withstand shear loads because of its hollow form. When the blade skin (relatively thin skin) is subject to compressive loads, there is a possibility of localized buckling. This buckling can remain in the elastic region and contributes to fatigue damage, or move into the plastic region and cause localized skin failure. Because of the high life-cycle of the blade, its structural design must take into consideration local buckling, and therefore, stiffening of the blade is essential to resist bending [115].

Two blisters of reinforcing material are used to provide local stiffening: one on the upwind face (pressure side of the blade) and another one on the downwind face (suction side of the blade). However, to provide the essential shear strength these two parts need to be structurally joined by a construction called a shear web [83].

For small scale turbine blades, the two main configurations that are commonly used are: two pieces of blister caps made up of carbon fiber paired with foam or a shear web with two spar caps (located at the top and bottom of the blade) made up of fiberglass (E-glass in this case) laminas as shown in figure 38.
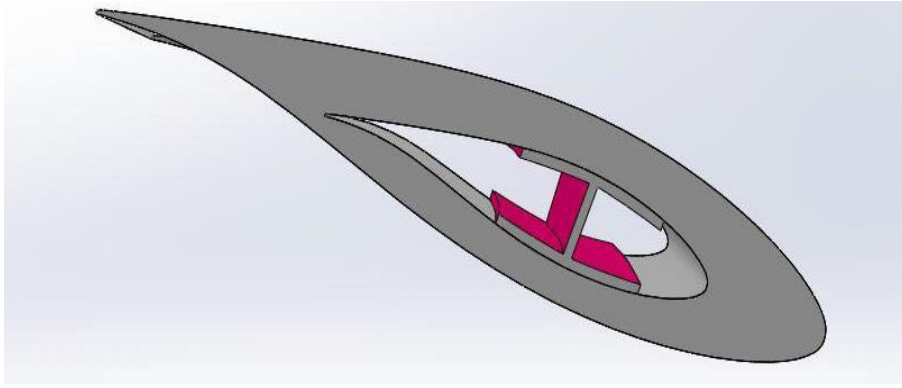
Figure 38: Small wind turbine blade cross section with spar caps and shear web

The first option consists in using caps manufactured in carbon fiber composites used with core material (foam). With the specific stiffness of carbon being more than twice higher than for glass fiber, there is a high possibility of weight reduction. However, carbon fibers are more expensive than are glass (by approximately a factor of 8) [1]. Besides, manufacturing and dealing with carbon fiber represents a serious challenge requiring more strict precautions to be taken than when dealing with the glass fiber. The interest in this technology is limited, as the necessary precautions require very high quality in the manufacturing process and the associated risks are more serious than in case of the glass fiber construction. In carbon design, a big attention is put on ensuring carbon fiber straightness. Any misalignments, or waviness may results in significant reduction of already low ultimate compression strain. The quality plays the most important role in carbon structure [116]. **Therefore; this solution has been ruled out.**

The second option, which was retained for this project, consists in using glass fiber for blade reinforcement (E-glass in this case). This material presents significant advantages [116] such as raw material availability and low cost, robustness of manufacturing techniques, ease of handling and repairs and finally well-known manufacturing procedures which are compatible with different resin systems and other blade material composition.

The design of the blade internal structure is based on the assumption that the wind turbine blade has a form of a cantilever beam that is deflected by the action of the wind. When deflected, one side of the blade will be stressed in tension and the opposite side in compression. The blade spar caps are separated by a shear web. This structure has the same principle as an I-beam where the flanges are replaced by the spar caps and the web is represented by the shear web. To support the applied loads, the spar caps and the shear web are made up of **tri-axial E-glass fibers with epoxy resin**. In comparison to composite materials with unidirectional and biaxial fiber orientations, triaxial fabrics provide structures with high tensile and compressive strength. The spar caps incorporate biaxial plies **(±45°)** to

transfer load between the unidirectional fibers by including extra plies [3]. Particular attention should be paid to the connection between the internal beam parts in order to ensure sufficient overlap of the caps with the shear web. This allows transferring the entire load through the adhesive (usually made up from epoxy) that bonds the components together [117]. Table 34 gives the lay-up schedule of the spar caps and the shear web over the blade span.

Component	Radius %	Location (m)	Layup schedule	Airfoil	Thickness (m)
Spar caps	14.2 to 32	0.500 to 1.121	$[(\pm45)_2/0_4/(\pm45)_2/0_4/(\pm45)_2]_s$	DU 93-W-210	0.014
	32 to 40.8	1.121 to 1.431	$[(\pm45)_2/0_3/(\pm45)_2/0_3/(\pm45)_2]_s$	DU 93-W-210	0.012
	40.8 to 49.7	1.431 to 1.741	$[(\pm45)_2/0_2/(\pm45)_2/0_2/(\pm45)_2]_s$	DU 93-W-210	0.01
	49.7 to 70.4	1.741 to 2.466	$[(\pm45)/0_2/(\pm45)/0_2/(\pm45)]_s$	DU 93-W-210	0.007
	70.4 to 100	2.466 to 3.500	$[(\pm45)/0_2/(\pm45)]_s$	DU 93-W-210	0.004
Shear Web	14.2 to 73.4	0.500 to 2.569	$[(\pm45)/0_6/(\pm45)]$	_	0.004

Table 34: Lay-up schedule of the blade spar caps and the shear web

In the case of this project, the shear web runs from **14.2% to 78% of the blade length**. In all chord stations, **a single web positioned at 32% of the chord** length (near the maximum thickness position) seems to be the ideal configuration. To ensure good connection between the spar caps and the shear web, two common ways can be used: either the spar caps are built as part of the shell and a separate shear web is bonded between them, or the shear web and spar caps are built together and glued into the shell. In these two cases, the connection between webs and caps is to be verified in details, as the integrity of the wind blade is highly dependent on the bond quality between the shear web and the shells [83]. To have a clear idea of the material composition, analysis of adhesives cannot be neglected as loss of their structural functionality may result in a catastrophic failure of the entire blade. Adhesive joints are used to connect webs and caps. Its main objective is to ensure proper load transfer within blade structure. In order to properly estimate the strength and durability of the adhesive joint, the glue line is assumed to have fixed constraints on the geometry. The thickness is assumed to have a thickness of **1 mm in the case of this design process**, and the bond is assumed to be continuous [116]. The adhesive used in this project will include a commercial structural adhesive used by blade manufacturers (fiberglass reinforced epoxy or polyester). The use of spar caps and shear web in the blade structural design allows increasing the stiffness of the blade without changing its shape (by making the caps thicker or thinner). This structural design could be done with minimum cost. If the blade is made thinner, it may perform better aerodynamically (thinner structure will decrease the blade mass). Thicker spar caps provide better stiffness to the whole structure, but it will make the blade more expensive. Figure 39

shows the internal structure of the blade with the spanwise placement of the caps and the shear web.
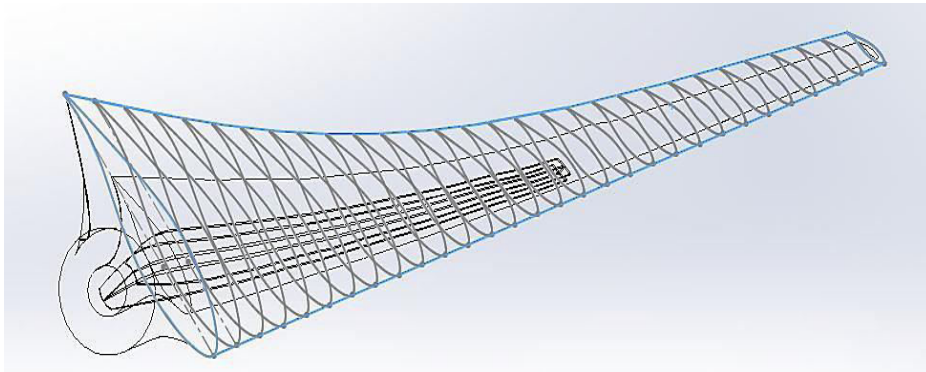
Figure 39: Internal structure of the small wind turbine blade

For manufacturing process, two different approaches can be used to manufacture the turbine blade. The first one consists in manufacturing the upper and the bottom blade shells separately. The upper shell forms the suction side of the profile. It represents the largest element of the rotor blade. For manufacture, first a negative mould is produced and the positive form taken from it. The E-glass fiber non-woven or the weave is inserted into it and soaked in resin. The bottom shell forms the pressure side of the profile. Its manufacturing process is similar to the upper one [3]. If the upper and lower shells as well as spars are manufactured separately, then they must be assembled. The spars are first glued into the upper and lower shells. Then, adhesive is applied to the front rear edge of the two shells as well as the upper surface of the spar caps, and the second shell is placed on the first one. Once the three main parts are assembled, the rotor blade is closed and there will be no possibility to check the adhesive surface from inside. The second approach consists in manufacturing the two shells in one single piece. For this purpose, hinged moulds are used that are folded together after inserting the fibers. The fibers are pressed against the forms using one or more inflatable balloons and the resin is injected afterwards. The balloons can be removed subsequently. According to A.P.Schaffarczyk [3], this production method has the advantages of removing the later gluing of the two shells. Therefore, the weak spots in the rotor blade are eliminated. However, this method presents difficulties in building spar caps for reinforcement.

4.8 Blade tip transition

The wind turbine blade tip has significant effects on the blade aerodynamic (especially aerodynamic damping) and aerocaustic performances. In fact, the aerodynamic optimization of the tip region does not differ from that of the rest of the blade except that the aerodynamic models (BEM in the current project) cannot resolve the details of the complex flow in this

region, due to the complex, three dimensional flow fields. It has been found that an optimization of the entire blade leads to a slender tip with the chord length decreasing to zero. Generally, the blade design based on multipoint optimization procedures (the case of this project) lead to more slender blades at the tip region. This is due to the constraints on the parameters involved in the objective functions [118].

Until now, many different blade tip designs have been proposed and used in wind energy industry. Commercial wind turbine blades are mainly designed with one of these three tip shapes: standard tip, swept tip and taper tip. Figure 40 shows an example of the different tip designs.
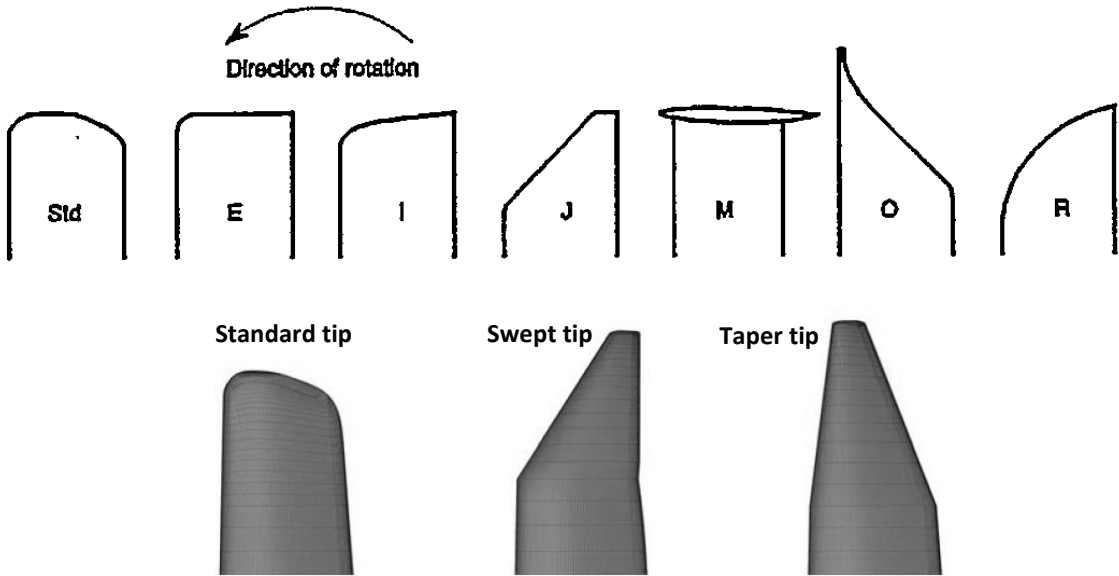
Figure 40: Different tip shapes for wind turbine blades

To select an appropriate blade tip shape, a number of requirements can be defined. These include low noise emission, low flapwise and edgewise vibrations, optimal aerodynamic performance and good aesthetics. An investigation of the complex flow around the tip of a rotating wind turbine blade has been performed by Jeppe Johansen and Niels N. Sørensen [119]. Using Computational Fluid Dynamics (CFD), it has been found that the lift coefficient for the standard tips decreased approaching the tip, while the two tapered tips kept at a more constant lift level. The drag coefficients actually decreased for the two tapered tips, and even become negative for the swept tip. Therefore, the lift to drag ratio will be maximized by using slender tip shapes. The results of the analysis show that three-dimensional effects are more pronounced for the standard tip compared to the two tapered tips. In other words, more concentrated tip vortex for standard tip, leading to a steeper gradient on both tangential and normal force when approaching the tip, whereas the swept and the taper tips show more flat behavior. For relatively high wind speeds (at 12 m/s), the swept tip experiences a decrease of

the lift coefficient and an increase of the drag coefficient. This is mainly because of the flow separation at the tip. The taper tip keeps the higher loading causing the flapwise bending moment to be higher. It has been also deduced that the two tapered tips have a slightly larger loading at the tip indicating that a tapered tip is more efficient based on power production at low wind speeds.

Regarding the aeroacaustic aspect of the blade tip, as the tip noise arises from the separation of the tip vortex, there seems to be two different design directions to choose in order to limit the tip noise [118]. First, the tip vortex strength must be reduced as much as possible. Secondly, the separation of the tip vortex must be reduced or removed by designing the tip in a way that no separation occurs at the tip. Decreasing both the chord and the effective angle of attack using a local twist of the blade tip will reduce these two parameters, and thus the blade tip noise [118].

At high wind conditions, stall regulated wind turbine blades can, eventually, experience some undesirable unstable vibrations, called stall induced vibrations. The aerodynamic damping phenomenon is associated with the amount of total damping of the turbine. This total damping consists of the structural and aerodynamic damping. The latter is strongly dependent on wind speed. In some cases, negative aerodynamic damping exceeds the positive structural damping resulting in a total damping being negative, which again causes the wind turbine to vibrate in an unstable condition. This phenomenon has been investigated for the already mentioned tip shapes and it has been found that the standard tip seems to be slightly less damped with respect to the flapwise vibrations, but no particular differences have been observed with respect to the edgewise vibrations [119].

Balancing all the aforementioned considerations, a taper tip shape demonstrates the ability to improve the aerodynamic performance and to make the blade structure more stable during the turbine operation. **Therefore, it was selected for the present project.**

By using this typical tip shape, the chord goes smoothly from its optimal value to the zero value at the tip position. The leading edge is almost straight out to the tip and the smooth decrease in chord length to zero at the tip gives a trailing edge line which is bending to the leading edge.

To draw an initial shape of the design small wind turbine blade, the chord and the twist angle distributions (obtained from a multi-variable optimization using the SWRDC program) were exported to a 3D CAD design software SOLIDWORKS and used to generate a three dimensional solid model. In this design, to connect the blade root section to the rest of the blade, mixed airfoils were used. As the design of the root section does not involve any aerodynamic consideration (as it is mainly used to generate the required starting torque at low

wind speed), the chord length at this blade part was defined using a linear relationship of the chord lengths from the root/hub connection to the active position at 14% of the blade length. This smooth transition was performed by decreasing gradually the chord length and increasing the thickness of the airfoil sections. **The airfoils that were used are the DU 91-W2-250 airfoil and the DU 97-W-300 airfoil (their corresponding thicknesses are 25% and 30% respectively)**. For example, the chord length of the airfoil at 12% position (on the blade span) was determined using a linear polynomial relationship between the chord of the root cylinder, at 11.4% position, and the chord length of the airfoil at 14% position. It should be noted that a smooth transition from the hub to the active part of the blade presents three major advantages. First, thick root transitions are needed to generate the starting torque at low wind speed. Secondly, the manufacturing process of such linear forms does not present any difficulties, and more importantly, thick airfoils in the root region are required to withstand the bending moments and the centrifugal forces from the wind. Figure 41 shows the placement of the airfoils along the blade span.
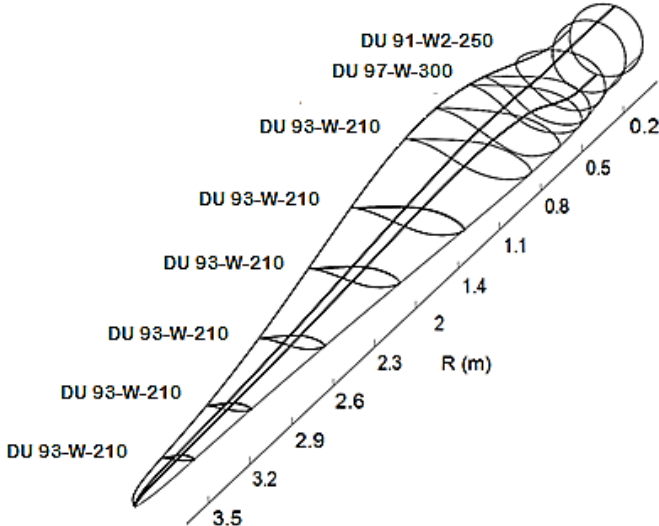
Figure 41: Detailed spanwise placement of the airfoils on the blade span

4.9 Blade tip clearance calculation

Small wind turbine blades are generally subject to fluctuating loads from the wind. This is especially the case when the turbine machine is installed in geographical locations where extreme winds and turbulences are dominant. The wind cyclic loadings result in structural deformations of the blade (with respect to the flapwise and the edgewise directions), and may cause excessive displacements that make the blade hit the tower. Under high wind conditions, turbine blades experience tip deflection. This is defined as the displacement of the blade tip caused by wind loads comparing with the blade static condition. When the wind loads act in the flapwise direction, blades can experience tip deflections up to about 10% of the blade

radius [120]. Therefore, Special attention should be paid to the blade tip deflection to avoid any risk of blade/tower collisions in the case of upwind wind turbines.

Aerodynamic loads are the main causes of the flapwise bending moments (which results in flapwise deflection). During extreme conditions, when the blade airfoil is subject to high wind speeds, components of lift and drag are induced due to the aerodynamic properties of the airfoil. These aerodynamic forces are resolved into useful force (lift) acting in the direction of rotation and reaction forces which are acting in the flapwise bending plane, and must be tolerated by the blade with limited deformation [65].

In a wind turbine design, blade tip clearance is a critical parameter that must be determined in order to prevent catastrophic failures caused by blade striking the tower. This static blade displacement is defined as the distance between the blade tip and the tower edge when a blade is parallel with the tower. The sum of blade tip deflection and blade tip to tower clearance is a constant, which is equal to the blade tip to tower clearance when the blade is in unloaded condition [121]. In order to avoid any contact of the blades and the tower, manufacturers of wind turbine machines rely on several techniques such as increasing the initial tip clearance by putting the rotor further upwind of the tower, tilting the rotor out at the bottom (an angle of 5° is added between the nacelle and the drive shaft) or pre-bending the blades or "coning" (angling all the blades upwind relative to the flat rotor plane). All these approaches are used to an extent but each has a cost associated with it, either in aerodynamic losses or higher manufacturing costs. For example, a greater clearance between the rotor the tower requires that the yaw bearing must be stronger [83]. Generally small turbines have a larger distance between the tower axis and the blade attachment point than do large turbines, when expressed as a fraction of the blade radius, so such contact between the tower and the blade is less likely. Nevertheless, it is still necessary to demonstrate clearance [41].

Regarding the maximum allowable blade tip deflection, the Germanischer Lloyd, GL [122] states that the quasi-static tip deflection under the extreme unfactored operational loading is not to exceed 50% of the clearance without blade deflection. This implies using a load safety factor of 2. IEC standard for design and safety of small wind turbines (IEC 61400-2) requires that the maximum predicted tip deflection multiplied by the appropriate partial load factor shall not exceed the no-load clearance between the blade and the tower.

Typical minimum clearance between the blade tip and the tower should not exceed 30% of the unloaded clearance under the worst-case loading [83, 123]. This value corresponds to the minimum tip deflection required by the IEC 61400-2 standard if a partial safety factor of $\gamma_f = 3$ is applied (safety factor for ultimate load in the case of simple load calculation, SLM). In

the present work, determination of the tip clearance of the turbine blade will be based on these requirements.

To have a first approximation of the wind turbine blade maximum deflection, analytical approach was used. This simulates the wind turbine blade as a beam of a finite length (3.5m) and a cross section defined by the blade airfoil cross sectional geometry [124, 125, 126]. This approximation assumes that the blade is a cantilever beam, fixed at one end and subject to a triangular distribution of the drag force as shown in figure 42.
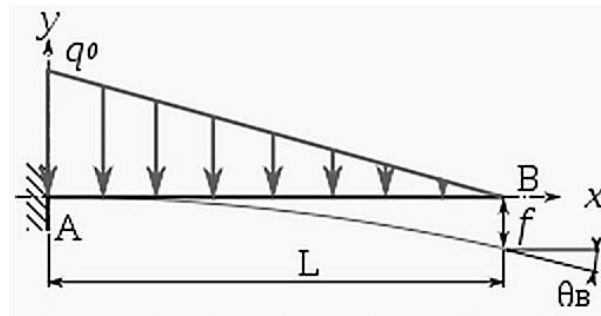
Figure 42: Load distribution on the cantilever beam

Assuming small deflections and applying appropriate boundary conditions at the end of the cantilever beam, a single static analysis using Macaulay's method can be used to estimate the displacement of the blade tip [127]. This approach which is knowns also by the double integration method, is a technique that is widely employed in structural analysis to determine the deflection of Euler-Bernoulli beams. The Macaulay's technique is very useful for load cases of discontinuous and/or discrete loading. Typically partial uniformly distributed loads and uniformly varying loads over the span of a cantilever beam. By double integrating the equation 80, the blade tip displacement formula and the maximum tip deflection are given by equations 81 and 82.

$$\text{EI } \frac{d^2y}{dz^2} = M \tag{80}$$

$$y = \frac{q_0 . x^2}{120.\text{E.I.L}} \left(x^3 - 5.\text{L}.x^2 + 10.\text{L}^2 . x - 10.\text{L}^3 \right) \tag{81}$$

$$D_f = \frac{q_0 . \text{L}^4}{30.\text{E.I}} \tag{82}$$

Where E is the tensile modulus of the composite (N/m^2), I is the second moment of inertia of the area (m^4), and M is the bending moment (N.m), L is the length of the beam, q_0 is the load on the beam and x is the position along the beam span.

Figure 43 shows the deflection along the blade span.
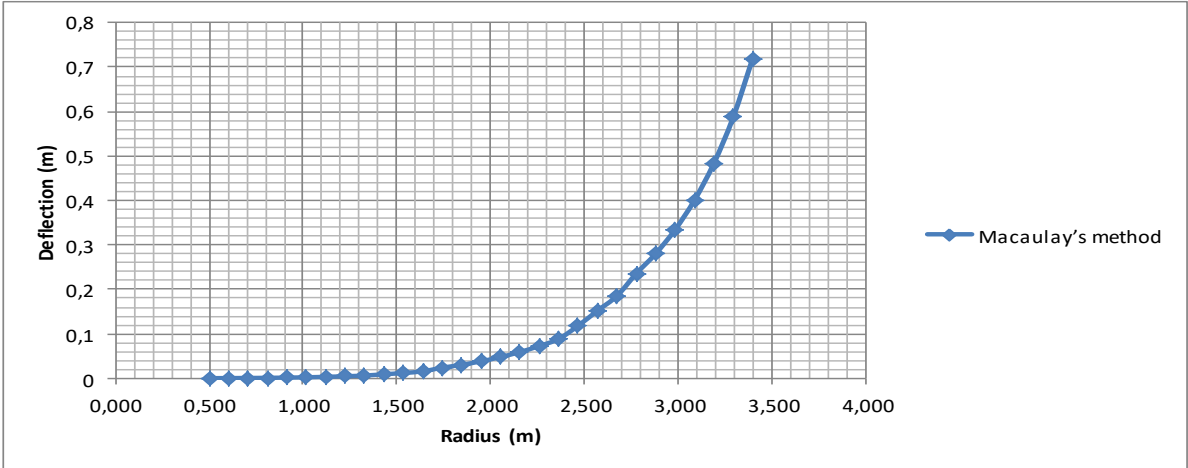
Figure 43: Blade deflection over the blade length using Macaulay's method

Using the Macaulay's method, the maximum blade tip deflection is found to be **719 mm**. This value should be taken as an approximation since the used analytical approach does not consider the real geometry of the blade.

To validate this result the SWRDC (Small Wind-Turbine Rotor Design Code) program for the design of small wind turbines rotor was used. This code allows calculating the deflection along the blade span, under two different load cases. The first load case is concerned with the parked conditions. These consider several separate loads acting on a parked turbine. That is, a turbine whose rotor is not producing power (it is not necessary for the blades to be stationary while parked). Parked load case simulates a hurricane whereby the rotor is stationary and is subject to an extreme wind speed in all directions (i.e. 0°-360° around the blade axis). The second load case considers overspeed conditions. This simulates an incoming wind normal to the rotor plane that will cause the rotor to rotate beyond the maximum allowable rotational speed of the generator. Parked rotor scenario is adopted as it allows simulating the worst scenario the turbine machine may encounter. The main loads involved in this case are due to drag. To simulate the deflection, the wind loading will be assumed to be applied to the wind turbine with a survival wind speed of U_{e50}= **52.5 m/s** (the 3s-50-year extreme wind speed). Also, it was assumed that the turbine has furled and the blades are effectively stationary. The loads associated with the extreme wind speed will be multiplied by a load safety factor of γ_f = **3**. Figure 44 gives a screen shot of the load case data panel of the SWRDC code. This contains the load case, the safety factor and the applied wind speed.
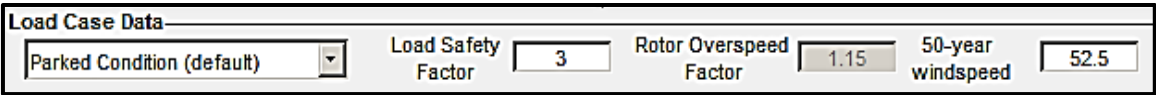
Figure 44: Input data for load case data panel

Taking into account all the aforementioned requirements, figure 45 depicts the tip deflection with respect to the flapwise and edgewise directions.
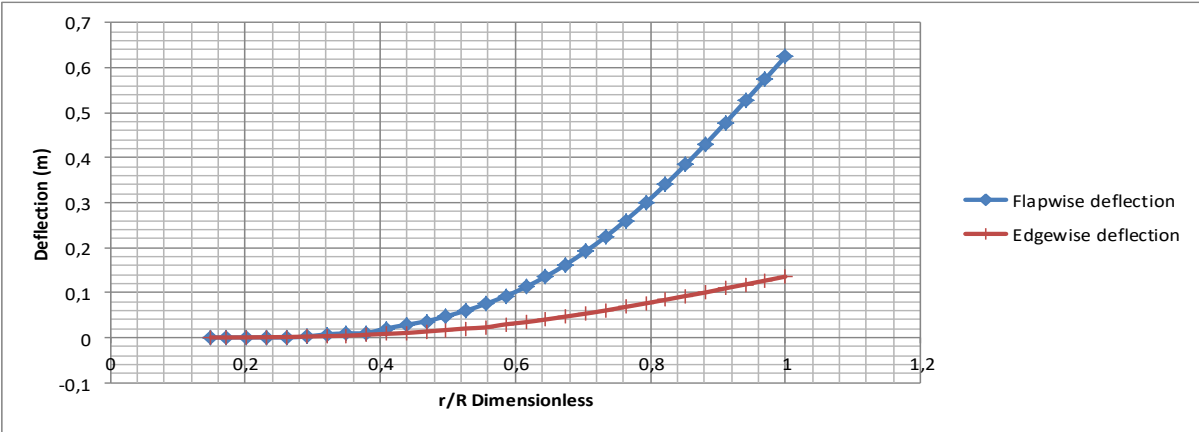
Figure 45: Blade tip deflection in the flapwise and edgewise directions

Under the worst load case, the E-glass blades have a maximum tip displacement of **624 mm**, with respect to the flapwise direction. This tip deflection represents 18 % of the blade length. To avoid mechanical interference between the blade and tower, the blade tip displacement shall not exceed the no-load clearance between the blade and tower (according to the IEC 61400-2 standard). It should be noted that the estimated tip deflection did not take into consideration the contribution of the spar cap and shear web which enable major reductions of the tip deflection by increasing the flexural rigidity of the blade.

To make sure that the rotor blades will never hit the tower, more accurate deflection analysis should be processed. For instance, finite element analysis is highly recommended when complicated three-dimensional shapes are simulated and which involve local effects such as stiffness jumps, stress concentration and force deviation [3]. To accurately estimate the blade tip deflection, Fatigue, Aerodynamics, Structures and Turbulence (or simply FAST) code was used [128]. This is a powerful code, developed by the National Renewable Energy Laboratory (NREL) and used to predict both the extreme and the fatigue loads of two- and three-bladed horizontal-axis wind turbines (HAWTs). The main advantage of FAST is that it considers the real geometry of the blade (outer and internal shapes) when calculating the blade deflection.

FAST simulation is based on six input files which are the primary input file, the aerodynamic file, the blade file, the tower file, the platform file and the furling input file. These input files are used to generate time-series data on the aerodynamic loads as well as loads and deflections of the structural members. In the blade input file, which is used to model the blade geometry, several input parameters are required. These include blade parameters and blade adjusted factors (simple data to process), distributed blade properties and blade mode shapes.

Static tests are still the most effective way to make sure that a blade bending during high winds will not compromise the safety of the system. These tests measure deflection against load, and provide reliable values of the blade structural deformation.

To compute the distributed blade properties, PreComp code was used [129]. This is a code developed by NREL and used to provide span-variant structural properties for composite blades. PreComp computes these properties with a novel approach that integrates a modified classic laminate theory with a shear-flow approach. The computed properties include cross-coupled stiffness properties, inertia properties, and offsets of the blade shear center, tension center and center of mass with respect to the blade pitch axis. PreComp requires that the blade external shape and the internal layup of composite laminates be described for inputs. The external shape is specified in terms of the chord, twist, and airfoil geometry variation along the blade. The internal structural layup is specified in terms of the laminates schedule, orientation of fibers in each laminate and the laminate constituent properties. The code allows for a general layup of composite laminates, both spanwise and chordwise, and an arbitrary number of webs.

The simulation of the blade mode shapes was performed using BModes code [130]. BModes is a finite-element code that provides coupled modes for a turbine blade or a tower. BModes allows computation of coupled modes for both the blade and the tower. A coupled mode implies presence of coupled flexural, axial and torsion motions in a natural mode of vibration. In BModes' input file, each one of rotor speed, blade geometry, precone, pitch control setting and structural properties distribution along the blade need to be defined. These properties are incorporated in two files an auxiliary which contains distributed properties of the blade obtained from PreComp and main input file which are user designated data.

Finally, to simulate the wind speed variation, TurbSim simulator was used [131]. This is a stochastic, full-field, turbulent-wind simulator. It uses a statistical model (as opposed to a physics-based model) to numerically simulate time series of three-component wind speed vectors at points in a two-dimensional vertical rectangular grid that is fixed in space. For tip deflection analysis in the present study, Extreme Wind Speed Model (EWM) was used. This model is based on 10-minute average wind speed with a recurrence period of 50 years (worst scenario with an extreme wind speed of 52.5 m/s). Once both the blade geometry and the wind profile were defined, the input files are entered to FAST and time-series data can be generated. **Based on the actual blade geometry, a maximum tip deflection of 386 mm was found.** This value is very low compared to the results obtained from both the analytical method and the SWRDC code. This is not surprising as the two first methods do not consider the contribution of the spar cap and the shear web which have major reduction of the tip

deflection by increasing the flexural rigidity of the blade. By adding an angle of **5°** to the nacelle frame and the drive shaft (equivalent to 30 cm), it is reasonable that a tip clearance of $\mathbf{T_{cl} = 0.6\ m}$ guarantees that the blade will never hit the tower even under worst conditions.

4.10   Conclusion

The first part of the fourth chapter was devoted to the design and analysis of the wind turbine rotor blades. An optimum aerodynamic shape of the blade was determined using both the optimum rotor theory and the SWRDC code. The chord length and the twist angle distribution along the blade span were determined such that power coefficient of the wind turbine at a design tip speed ratio of 6 will be maximum.

The second part of the present chapter covered a design optimization of the blade geometry by using the Small Wind turbine Rotor Design Code (**SWRDC**). In order to validate the results given by this software, the blade chord and twist angle distributions was also be determined using Q-blade software. Finally, a comparison of the two distributions was made.

The third part was concerned with selection process of an appropriate composite blade material. The mechanical properties of the selected fiber composite materials were also discussed and an E-glass/Epoxy composite was adopted of the blade manufacture. By using the Laminator software, which is based on the classical laminate theory, an ultimate tensile strength of 215 MPa was found for the blade composite material whil multidirictional fibers.

The wind turbine blade design was completed by a preliminary tentative design of the blade internal structure (shear web and spar caps), the blade tip transition and the blade root connection.

For safe operation, the final subsection of the wind turbine blade design discussed the blade tip deflection and the required minimum tip clearance. In wind turbines operation, many failure cases are mainly caused by the event that blade tip hits the tower. Thus, one of the most important indicators in a wind turbine design is the tip deflection estimation. Usually, the maximum tip deflection possibly occurs in some extreme conditions during wind turbine operation; therefore, study of the tip displacement must be conducted for the worst wind conditions (generally at three-second gust with a recurrence period of 50 years). Based on the worst operations scenarios, a minimum blade tip clearance of 885 mm was selected.

CHAPTER 5: ROTOR AND NACELLE COMPONENENTS DESIGN

For an effictive design of the wind conversion system, a tentative design of the rotor and the nacelle components must be developed. For this to be done, the wind turbine system will be subdivided into different subsystems. The following subsystems will be designed:

➢ Rotor components that composes the rotor hub and front nose cone;

➢ Nacelle structure that composes the main frame and nacelle cover ;

➢ Drive train components that composes the main shaft, shaft coupling, and the main shaft bearings;

➢ Generator and safety system the is composed of the generator and the brake system;

➢ Yaw system that is composed of the yaw bearings or slewing bearing;

➢ Furling system that is composed of the tail fin and the tail boom;

5.1 Front nose cone design

A component which the majority of the wind turbines have, and which is closely attached to the nacelle cover, is the spinner or nose cone. This is the cover for the hub. The spinner provides environmental protection to the hub. Typically, the spinner is made from glass fiber in sections and is bolted together with a galvanized steel support [132]. Unlike nacelle cover, nose cones seldom provide any engineering utility. They are an aesthetic adornment. Ideally, the nose cone carries the horizontal lines of the nacelle past the blades to break up the vertical lines of the rotor. Wind turbines without well designed nose cones have a negative visual impact and may affect the airflow circulation around rotor blades, especially in the root region [133]. The nose cone provides an aerodynamic shape to the design of the nacelle cover. The selected nose cone has a simple structure that can be clipped onto the hub. Also, it presents the advantage of being easy to assemble and cheap to manufacture. This design consists in a simple hemispherical shape that lets the air flows smoothly over the back of the turbine as shown in figure 46.
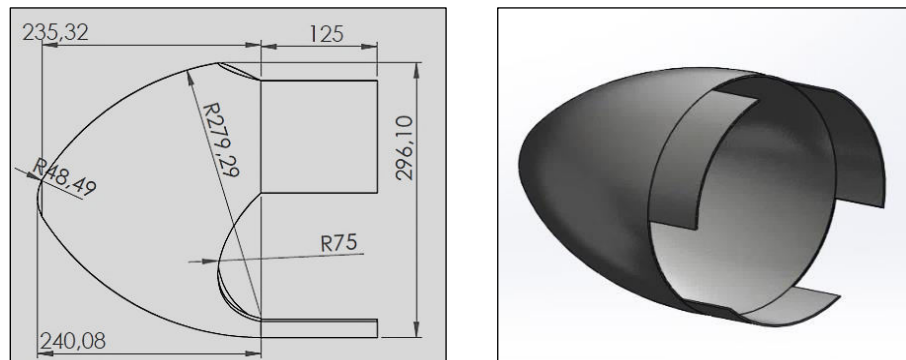
Figure 46: Wind turbine nose cone design

5.2 Rotor hub design

The wind turbine rotor hub connects the blades to the main shaft and ultimately to the rest of the drive train. The hub is an important constituent of the overall layout. It transmits the aerodynamic loads to the shaft and withstands the loads generated by the blades. Details in hubs differ considerably depending on the overall design philosophy of the turbine. In general, three basic types of hubs are commonly used by the wind turbines manufacturers. These are rigid hubs, teetering hubs and hubs for hinged blades [1]. Rigid hub is the most common design which is nearly universal for machines with three (or more) blades. This type is designed to keep all major parts of the blade in a fixed position relative to the main shaft. The selection of a hub design, in the present study, was driven by the recommendations of the IEC 61400-2. This states that the Simple Load Model (SLM), for the wind turbine load analysis, is only applicable for wind turbines with rigid hub [7]. **Therefore this option was adopted for rotor design**. Figure 47 gives the structure of the selected hub.
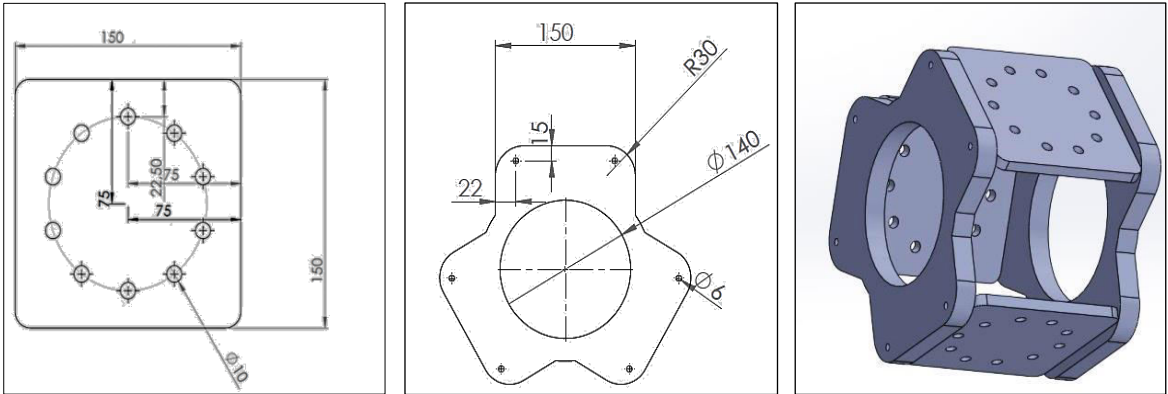
Figure 47: Small wind turbine rotor hub design

The selected hub has the advantage of being simple and easy to manufacture. By using this structure, strong connection between the blade root and the turbine frame can be made. Additionally, this typical design enables the blades to be easily mounted on their positions. The connection between the hub parts (that hold the blades) and side parts (that hold the main shaft) will be bolt connection. Regarding the attachment bolts, stainless steel hexagon socket head cap screws, in accordance with DIN 912/ISO 4762 in the 10.9 strength grade (ISO 4762:2004) are suitable for bolting the hub parts.

The hub frame provides the structural support for the three blade roots and connects the shaft to the rotor. It must be structurally strong enough to manage the load between the rotor and the shaft which is mainly experiencing bending and torsional loading. Hubs are generally made of steel, either welded or cast. For the present design and analysis, the hub frame will be manufactured from C55/1.0535 (EN 10083-2) medium carbon steel.

5.3 Nacelle cover design and manufacture

5.3.1 Nacelle cover design

The outward appearance of a wind turbine is, to a considerable degree, determined by the external shape of the nacelle. The shape of the rotor is determined by the aerodynamic considerations. Apart from the contour of the tower, the shape of the wind turbine is mainly determined by the shape of the nacelle. The main objective of the nacelle cover is to provide weather protection for the wind turbine components which are located inside the nacelle. These include specifically the electrical and mechanical components that could be affected by sunlight, rain, ice and snow [1]. Another important functional requirement of the nacelle consists in orienting and affixing the main components in their proper positions relative to each other [134]. These components are the yaw bearings, the rotor shaft bearings, the furling axis bearings, the turbine generator, the brake system, the rotor speed sensors, the main controller (MPPT & charge controller) and finally the slip ring.

On small and medium-size wind turbines, the nacelle cover is normally attached to the main frame in such a way that it can be easily opened for access to items inside. Generally, the nose cone and the nacelle should be kept as small as possible to limit aerodynamic drag in the rotor wake (which may reduce the power coefficient of the wind turbine system) [135]. This is the only aerodynamic consideration that should be taken into consideration when designing the nacelle cover. However, the space created by the nose and nacelle needs to be large enough to accommodate all the nacelle components. Therefore, an optimal trade-off between the functional performance (aerodynamic and structural stiffness) and the aesthetics of the structure should be set in order to achieve an optimal design for the nacelle as whole.

The most recent research has shown that the design of the nacelle can be used to improve the airflow in the root region of the rotor blades. The acceleration of the flow around the nacelle minimizes the separation of the airflow in the inner part of the rotor blades. Thus, minimizing the effect of the nacelle leads to a noticeable increase in the performance of the rotor with the given flow around the nacelle [136]. It should be noted that the functional constraints concerning the shape of the nacelle exist only to a limited extent and should not be over emphasized.

Regarding the nacelle form, configurations of wind turbine nacelles are classified into 4 types [137]: rectangular, cylinder, globe and disk form. The rectangular form is the commonly used configuration. However, the cylinder shape, and specifically the streamlined form, presents further advantages. These include the fact that the wind flow through the rotor is hardly disturbed by having to pass around the nacelle, which takes place in the hub region of the rotor. Aside from limiting drag in the rotor wake, this streamlined nacelle design is supposed

to have an additional benefit of minimizing the nacelle wake influence on the operation of the furling tail. **Therefore, this shape was selected for the current project.**

In order to build a nacelle with minimum aerodynamic effects, the following aerodynamic considerations should be taken into account:

- Maintaining a smooth low frontal profile which hides behind the spinner and allows the airflow to pass around the nacelle

- Using a continuing aerodynamic profile form chosen spinner to the nacelle: The nacelle is slightly larger than the hub to lessen inefficiencies as air flows over the nacelle and to the blades;

- Using a faired tower section which encases the position of the tower/nacelle assembly and allows for less turbulent flow across the turbine tower. This minimizes vortex shedding as wind flows over the trailing edge of the tower and reduces inefficiencies as the turbine blades pass behind the tower. Also, this aerodynamic casing can be integrated into the nacelle design to create a sleek and aesthetically appealing design;

- Minimizing the size of the wake by using a tapered shape at the rear: by keeping flow attached as long as possible, adverse pressure gradients are avoided and streamlines are moving gradually together behind the nacelle resulting in minimum pressure drag;

In addition to these geometric and loading constraints, the nacelle must provide weather protection to the nacelle components while allowing adequate cooling for the generator and the controller. Considering the operating temperature ranges of the wind turbine components, the nacelle must not be heated or actively cooled. The components only need to be protected from harsh external conditions by the nacelle and venting must be provided to the controller and generator. In fact, any mechanical components will produce heat through friction, so managing heat generated from rotating machinery is crucial for wind turbines to function properly. Thermal management in itself is necessary to prevent damage to components, but another issue for heat generation is the resulting power losses that can occur as a result of a heat build-up. Any power loss can greatly impact on the profitability of a turbine, so mitigating such risks is extremely important. Thus, the eventual power losses require a thermal management system that would have to drive away generated heat. Therefore, **the nacelle should allow airflow to suck hot air out of the nacelle by creating an internal air circulation through a passive cooling system. Besides, Provisions for drainage holes should be included for good measure in order to evacuate trapped condensation.**

Regarding the manufacturing process, innovative materials and new technologies have been explored in order to improve the structure of the nacelle covers and make them more lightweight, easy to transport and to install. The manufacturing process of the nacelle is

generally based on three different materials: Glass Reinforced Plastic (GRP), steel or aluminum [138]. Glass fiber composites are widely used because of their main advantages: (1) ease of fabrication into the desired aerodynamic shape, (2) high strength, and (3) high stiffness to weight ratio. **For the present project, the nacelle cover is made of E-Glass composite and designed in such a way that the internal components are fully protected against various ambient conditions.**

Aside from the aforementioned performance requirements, cost, reliability and simplicity are the additional factors which should be considered when designing the nacelle cover. The reliability aspect is addressed by adopting a "zero-maintenance" requirement for the nacelle component itself, and ensuring that the affixed components can be easily accessed for easy of assembly (to reduce cost) and ease of maintenance. The anemometer and the aircraft warning lights are generally mounted on the roof of the nacelle cover. The air flow around the nacelle needs to be considered in the context of positioning the anemometer [136].

In order to increase the inertia of the nacelle with respect to the yaw axis, the center of gravity of the system can be shifted downstream. In this case, the nacelle is horizontal but an angle of 5° will be added to the nacelle and the drive shaft. This angle allows avoiding any contact of the blades with the tower in strong wind conditions [139].

5.3.2 Nacelle cover manufacture

For an initial design, a two-piece construction for the nacelle was selected. This is composed of the following parts: the first part is an outer fairing cover which consists of two subparts (upper and lower) and made from E-Glass composite. The manufacturing process of this part will be based on a cheap, rapid and easy technique, i.e. **vacuum formed thermoplastic**. The second part is a supporting structure box (nacelle main frame) used as a reinforcing base. This reinforcing structure is known as "bed frame" and will be the central assembly platform at the tower head. This housing system is composed of several plummer and blocks to accommodate the rotor bearing support, the yaw axis, the rear bearing, the generator bolt circle and the furling bearing plane. The nacelle frame provides structural support for both the hub and the rotor blades. The bed frame must be structurally strong to withstand the loads exerted by the weight of the rotor and subsequent torsional loads as it rotates. The generator should be positioned directly behind the rotor hub and directly connected to it through the main shaft. For the first guess, it was thought that **160 mm** would have to be reserved for the location of the generator. An initial design attempt of the main frame is shown in figure 48:
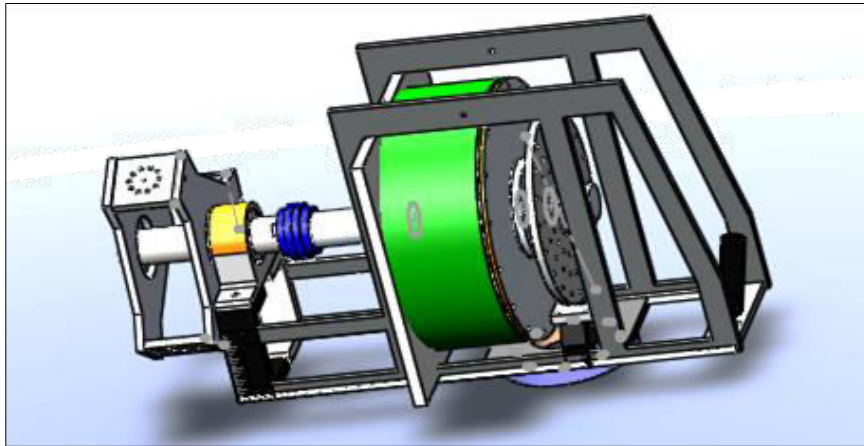
Figure 48: Small wind turbine nacelle main frame

The nacelle frame will be manufactured from C55/1.0535 (EN 10083-2), which is an unalloyed medium carbon steel. This type of steel is suitable for the manufacture of wind turbine parts such as hubs, shafts, bolts and studs. Table 35 gives the material properties for the main frame.

Material properties	Value
Ultimate tensile stress (MPa)	**700**
Yield stress (MPa)	**450**
Young's modulus, stiffness (GPa)	**210**

Table 35: Mechanical properties of typical medium carbon steel

The closed top and bottom of the box structure must resist bending moments from the rotor while being able to support the self-weight of the nacelle components. The bearing and the other components are attached to their Plummer blocks (in the bed frame) using bolts and nuts. These latter will be fixed through drilled holes in the nacelle cover. This concept should fulfill both aerodynamic and structural requirements of the design. Compared to potential alternatives such as castings, stamping, welding, or injection molding, the tools used in this process are cost effective (for both prototyping and hypothetical small-series production). Also, the material and the labor costs are not significantly high.

Taking into account the design considerations mentioned above, figure 49 shows the first design of the nacelle.
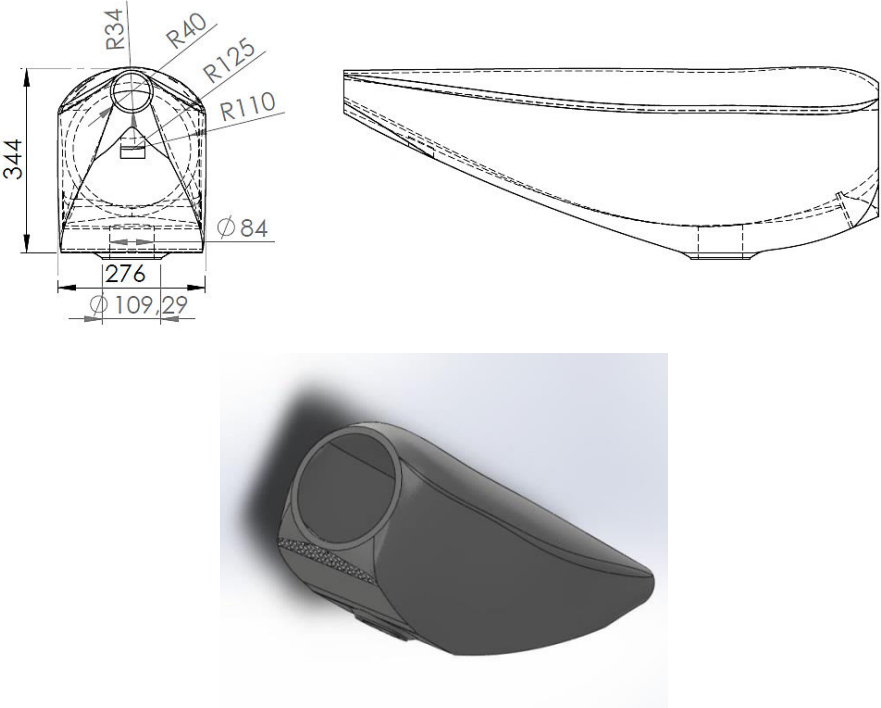
Figure 49: Small wind turbine nacelle cover

5.4 Wind turbine drivetrain design

5.4.1 Main shaft design

Direct drive small wind turbines have a main shaft (sometimes referred to as the low-speed or rotor shaft) which represents the core rotating element of the turbine system. This component transfers the torque generated by the rotor to the rest of the drive train. It also supports the blades' weight while transferring the different applied loads to the fixed main frame of the nacelle. The rotor shaft is important as the main load bearing structure in the assembly and as a primary mean of transmitting the torque generated from the wind energy. Therefore, the design of the shaft must be rigid and stiff to resist both bending and torsion. These features are can be achieved by an appropriate selection of the shaft material.

The shaft design must consider both static and fatigue failure possibilities; it should take into account the combined loads of torque (torsion) and bending [1]. This combined loading is often time-varying, so fatigue is an important consideration. Shafts also have resonant natural frequencies at critical speeds. Operation near such speeds is to be avoided; otherwise, large vibrations can occur. The main shaft should be designed for the worst operating conditions. These can occur in the case of a direct short across the output terminals of the generator or in

the case of an emergency stop of the turbine. In designing a wind turbine main shaft, several constraints should be taken into consideration [140]:

- Minimize both deflections and stresses. The shaft length should be kept as short as possible and overhangs minimized. This overhang is taken as the distance from the rotor center to the first bearing (L_{rb}). **To minimize the shaft deflection, this distance was set to L_{rb}= 0.1 m.**

- A cantilever beam will have a larger deflection than a simply supported one for the same length, load, and cross section, so the main shaft should be supported (bearings) unless a cantilever shaft is imposed by design constraints;

- General low carbon steel is just as good as higher strength steels (since deflection is typical the design limiting issue);

- If axial thrust loads are present, they should be taken to ground through a single thrust bearing per load direction;

- The first natural frequency of the shaft should be at least three times the highest forcing frequency expected in service, and preferably much more. (A factor of ten times or more is preferred, but this is often difficult to achieve);

- A hollow shaft has a better stiffness/mass ratio (specific stiffness) and higher natural frequencies than a comparably stiff or strong solid shaft, but will be more expensive and larger in diameter;

For a shaft design, the two major variables that should be taken into consideration are the inertial properties of the shaft and the shaft's material properties. Therefore, the design variables that would be analyzed for their effects on the shaft performance are the shaft diameter (since diameter controls inertia) and material.

In designing a rotor shaft, the worst conditions should be considered. In the case of this design analysis, an emergency stop (emergency brake) is assumed to be the relevant load case. The determination of the characteristic values of the individual loads is made according to the equation given by IEC Simple Load Model for small wind turbines (**especially, load case G: shutdown**). The objective of this design procedure is to establish the minimum shaft diameter that satisfies all design requirements. Due to its importance in the torque transmission, the rotor shaft will be designed with very large safety factors. Following the IEC 61400-2 recommendations, a value of 9 is taken in this study. This includes the partial safety factor for both applied loads and shaft material. Different cases can be used to evaluate the shaft design and which are namely [141]:

- Shaft subjected to twisting moment or torque only;

- Shaft subjected to bending moment only;

- Shaft subjected to combined twisting and bending moments;

- Shaft subjected to axial loads in addition to combined torsional and bending loads;

In the current design process, the case of combined torsion, bending moment and axial loading is used. This case of study implies that the shaft will be designed on the basis of three different loadings simultaneously. Various theories have been suggested to account for the elastic failure of the materials when they are subjected to various types of combined stresses. The three main theories that can be used for the design of a component subjected to combined stresses are:

• **Maximum Normal Stress Theory:** this simplest theory ignores any interaction between the normal principal stresses, and assumes that failure occurs when either of the normal stresses exceeds the ultimate stress.

• **Maximum Distortion Energy Theory (MDE) or von Mises' Yield Criterion:** this theory looks at the total energy at failure and compares that with the total energy in a uniaxial test at failure. This states that failure occurs when the von Mises stress, in the component being designed, equals the von Mises stress in a uniaxial tensile test at the yield stress. According to the MED, the smallest shaft diameter where failure occurs is given by the following equation **[142]**:

$$\frac{4}{\pi. D_s^3} \cdot \sqrt{(8M_s + T_{hmax}. D_s)^2 + 48T_{ds}^2} = \frac{F_y}{n} \tag{83}$$

Where n is the combined safety factor which is taken as 3. The total safety factor combines both the safety factors for ultimate loads (n_1=3) and material characterization (n_2=1), F_y is the yield strength of the used material, M_s is the bending moment acting on the shaft, T_{ds} is the dynamic torque acting on the shaft and T_{hmax} is the maximum wind thrust.

• **Maximum Shear Stress Theory (MSST) or Guest's theory**: this approach is the most used method. It states that failure occurs when the maximum shear stress in the component being designed equals the maximum shear stress in a uniaxial tensile test at the yield stress. According to the MSST, the smallest shaft diameter where failure occurs is given by the following equation **[142]**.

$$\frac{4}{\pi. D_s^3} \cdot \sqrt{(8M_s + T_{hmax}. D_s)^2 + 64T_{ds}^2} = \frac{F_y}{n} \tag{84}$$

This theory will be used in the present design procedure as it enables the design to be conservative when compared to the distortion energy theory. By using equations 83 and 84, an explicit expression of the shaft diameter cannot be obtained. Therefore, numerical methods must be used. For the case of the current design, the optimum shaft diameter is determined using the Microsoft excel solver. This solver uses the Generalized Reduced Gradient (GRG)

Algorithm for optimizing nonlinear problems, which has been developed by Leon Lasdon et al. [143].

Based on this method, the value of the shaft diameter is set as the adjustable variable (x), and the equation 85 is fixed as the target formula. Then, the optimum shaft diameter will be defined by the corresponding minimum values of the adjustable variable ($x=D_s$) that gives the exact solution of the equation $F(x) = 0$.

$$F(x) = \frac{4n}{\pi . F_y} . \sqrt{(8M_s + T_{hmax}. D_s)^2 + 64T_{ds}^2} - D_s^3 \tag{85}$$

Figure 50 is used to identify loads and reactions that the main shaft is subjected to. Under normal conditions, reactions in the shaft can be obtained from equilibrium considerations.
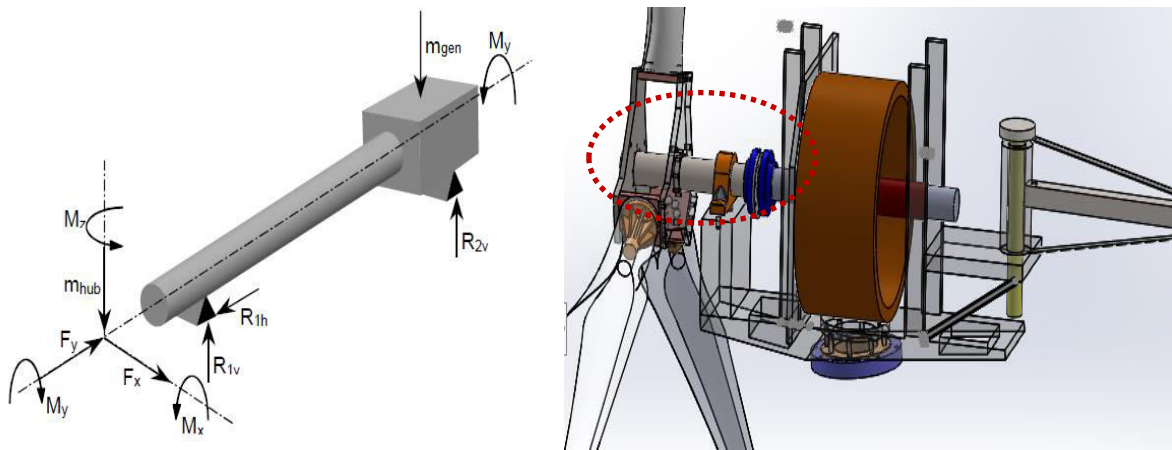
Figure 50: Loads and reactions on the rotor main shaft [144]

To determine the bending moment (static moment) on the shaft, the system is modeled as a cantilever beam. The forces acting on the beam are the weight of the rotor (wind turbine blades and the hub) and the reaction force R_b of the bearing on the fixed end of the shaft. This model is pictured in the figure 51.
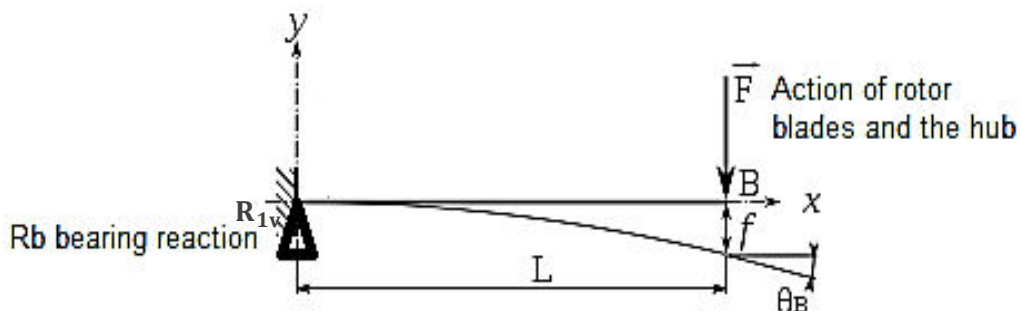
Figure 51: Free body diagram of the main shaft

Where f is the maximum deflection of the shaft and L is the distance from the rotor center to first bearing. **This distance should be as short as possible and was taken as 0.1 m.**

The maximum bending moment is determined using equation 86:

$$M_{shaft} = B. \omega_{max}. \Omega. J_B + m_r. g. L_{rb} + \frac{R}{6}\Delta F_{X-shaft} = 7517.08 \text{ Nm} \quad (86)$$

Where m_r is the rotor mass including the hub mass and the bolts which was taken as 93.82 Kg and g is the acceleration due to the gravity. Equation 86 combines three terms which are: the first term concerns the cyclic gyroscopic load. The second term gives the magnitude of the bending moment from the rotor blades and hub, and the last term approximates the effect of wind shear. n order to determine the maximum dynamic torque acting on the shaft, the total brake toque will be considered (highest torque). **According to IEC 61400-2,** the total torque in **case of a shutdown (load case G)** is given by:

$$T_{ds} = Q_{design} + T_{B,total} = 2717.88 \text{ N.m} \quad (87)$$

Where $T_{B,total}$ is the maximum permissible braking torque on the rotor shaft. Q_{design} is the design shaft torque of the wind turbine. This can be determined using the following equation:

$$Q_{design} = \frac{30 \, P_{design}}{\eta. \pi. \Omega_{design}} = 932.38 \text{ N. m} \quad (88)$$

According to IEC 61400-2, the wind turbine drive train efficiency, η, can be computed using equation 89.

$$\eta = 0.6 + 0.005 * P_{design} = 0.655 \quad (89)$$

The maximum thrust on the shaft is taken from IEC 61400-2 load case H (Parked Wind Loading). This load case considers the thrust caused by the wind loading on the turbine rotor of a parked wind turbine (the case of a spinning rotor).

$$T_{hmax} = 0.17 \, B \, A_{proj,B} \, \lambda^2_{e50} \, \rho \, U^2_{e50} = 2719.01 \text{ N} \quad (90)$$

Where λ_{e50} is the tip speed ratio for the 3s-50 year survival wind speed:

$$\lambda_{e50} = \frac{\Omega_{max}. \pi. R}{30. U_{e50}} = 1.71 \quad (91)$$

The maximum rotational speed is determined based on the wind speed at which the furling system intervenes to turns the nacelle away from high wind speeds directions. For the present design process, the cut-out wind speed, V_{cout}, is taken as 15 m/s. Therefore, the maximum rotational speed is calculated using equation 92.

$$\Omega_{max} = \frac{30. \lambda_{design}. V_{cout}}{\pi. R} = 245.55 \text{ RPM} \quad (92)$$

Regarding the shaft material selection and specification, the selected material should meet some requirements such as high strength, good machinability, low notch sensitivity factor,

good heat treatment properties and high wear resistant properties. In a wind turbine application, steel is one of the most widely used materials in wind turbine fabrication. It is used for many structural components including the tower, hub, main frame, shafts, etc. [1].

It was assumed that the main shafts will be manufactured from C55/1.0535 (EN 10083-2), which is an unalloyed medium carbon steel (ideally, heat-treated steel of high strength). The selected material is an unalloyed medium carbon steel with good tensile strength which is suitable for the manufacture of parts such as general purpose axles and shafts, gears, bolts and studs [145]. Table 36 gives the mechanical properties of the selected material.

Material properties	Value
Ultimate tensile stress (MPa)	700
Yield stress (MPa)	450
Young's modulus, stiffness (GPa)	210

Table 36: Mechanical properties of C55/1.0535 (EN 10083-2) medium carbon steel

By using equation 85, the minimum shaft diameter for maximum transmitted torque is found to be $D_{solid} = 82$ **mm**. In order to save weight, the rotor shaft will be made hollow. In this case, the outer diameter is used as a variable and the inner diameter chosen to provide inertia equal to a solid shaft of comparable strength. The inner diameter should be fixed and is taken as $D_i = 50$ **mm**. For the solid diameter, the area moment of inertia is given by:

$$I_{solid} = \frac{\pi}{4} \cdot \left(\frac{D_{solid}}{2}\right)^4 = 2.21 \ 10^{-6} \ m^4 \tag{93}$$

By equating the inertias of the shafts assuming a fixed inner diameter for the hollow shaft, the shaft outer diameter can be determined:

$$D_{outer,min} = \left[\frac{64. \, I_{solid}}{\pi} + D_i{}^4\right]^{\frac{1}{4}} = 84.6 \ mm \tag{94}$$

Considering diameters and tolerances for standard semi-finished goods according to DIN EN 10060 [146], a minimal shaft diameter of **82 mm** is appropriate. However, to prevent any eventual failure due to the largest loads acting on the rotor shaft (Example of the Coriolis component on the shaft load), **a common shaft diameter of 90 mm is chosen**.

Having calculated the forces acting on the main shaft, the maximum tip deflection can be determined using the following equation:

$$D_f = \frac{F. \, L^3}{3. \, E. \, I} = 4.55 \ 10^{-6} \ mm \tag{95}$$

Where E is the Young's modulus of carbon steel which is taken as 210 GPa and I is the area moment of inertia of the shaft, taken as $2.21 \ 10^{-6} \ m^4$.

Additionally to the aforementioned considerations, a small wind turbine can be exposed to large transient loads. Therefore, it has to be considered whether the chosen structural material possesses the necessary ductility. This is particularly important if the turbine is to be operated at low temperatures. Since corrosion may imply a considerable reduction of the assumed fatigue capacity, the shaft must be protected against corrosion. Suitable quality assurance should be implemented to make sure that: the geometrical and mechanical assumptions for the design are fulfilled, e.g. surface roughness, the specified values of material parameters are met, and the imperfections of the material do not exceed any critical level. This detailed analysis can be conducted using computerized methods like finite element analysis (FEA).

5.4.2 Shaft coupling design

In a wind turbine conversion system, mechanical couplings are mainly used to connect shafts that are assembled separately, so one can transmit the rotational power to the other. A typical use of couplings in direct drive small wind turbines is to connect the generator to the rotor main shaft. Mechanical couplings consist usually of two major pieces, one of which is attached to each shaft. They are often kept from rotating relative to the shaft by means of a key. The two pieces are, in turn, connected to each other by bolts (example of disc coupling).

When selecting a shaft coupling for a small wind turbine application, there is a large number of factors that must be considered. These include lower life cycle cost, easy connection and disconnection, full power transmission from the rotor blades to the generator shaft, perfect alignment of the two involved shafts, ability to withstand relative misalignment while remaining torsionally stiff, reduction of the shock loads transmission from one shaft to another, lightweight design and ease of installation and suitability for use in wind turbines operating in areas with a wide range of environmental conditions (high temperature, dust, and moisture).

In selecting a coupling for a small wind turbine, four design parameters must be specified. First, the topology of the coupling must be selected. The selection of a specific type of coupling is normally governed by the general requirements of the application in which it will be used. Secondly, the size of the coupling must be determined. This is driven primarily by the shaft size and by the torque requirements of the system. The material of the coupling must also be chosen based on both coupling's torque rating and coupling's mass. Finally, bore type and shaft attachment option must be specified.

• **Coupling type**: in power transmission systems, shaft couplings are divided into two categories. The first category consists of **rigid couplings**. This type is convenient when the shafts are already positioned in precise lateral and angular alignment. Their design does not

allow for any misalignment between the connected shafts. Given the fact that some misalignment could eventually occur during wind turbine assembly and operation (which could be generated from assembly inaccuracy, turbine's oscillating load or from thermal expansion during operation), the use of rigid couplings can result in unbalancing and vibration problems that can increase wear on multiple parts, such as the main shaft bearings. Therefore, the rigid coupling is not suitable to be used in mechanical power transmission systems of wind turbines. As can be seen in figure 52, three different types of misalignment could be encountered in wind turbine transmission systems. The center lines of the shafts might be parallel with an offset, the centerlines might form an angle (or the distance between the shaft-end faces may vary when running), and finally a possible combination of these two types.
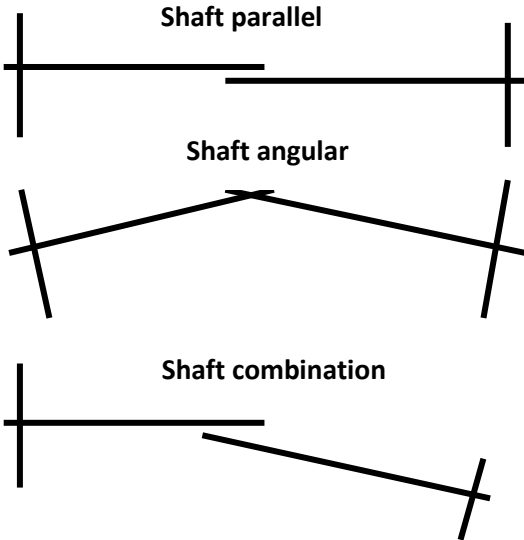
Figure 52: Types of shaft misalignment

In a wind turbine application the coupling is supposed to tolerate these misalignments while ensuring full power transmission between the rotor and generator. However, if a rigid mechanical coupling is used; damaging loads can be transferred from one shaft to another, which in turn, could result in a wear inside the shaft bearings that might lead them to fail prematurely.

The second category consists of **flexible couplings**. The main advantage of this category is their ability to balance radial, axial, and angular displacements while maintaining high torsional stiffness of the power transmission system. Flexible coupling has three main advantages. First, it allows full transmission of the rotational power from the rotor shaft to the generator (figure 53.a). Secondly, it is able accommodate any misalignment (figure 53.b), and finally, it compensates for end movements (figure 53.c). Figure 53 gives the three basic functions of a flexible coupling [147].
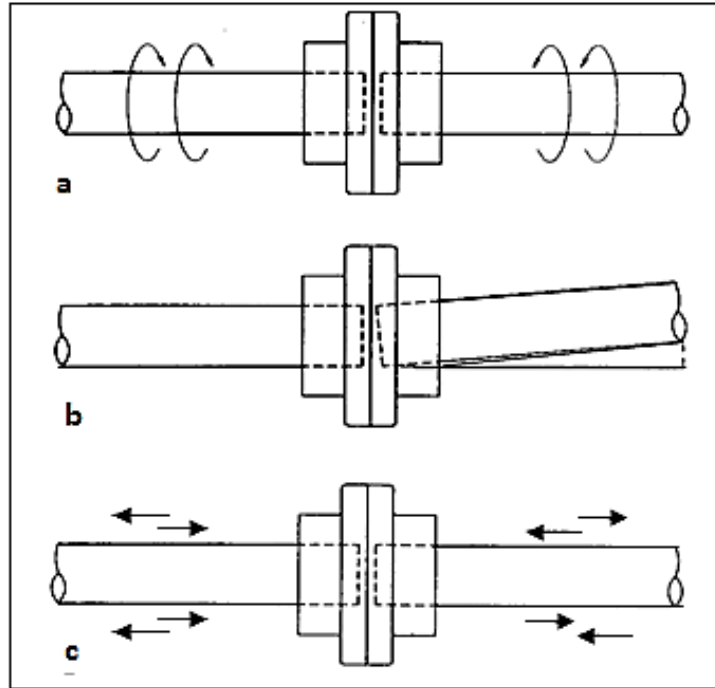
Figure 53: Basic functions of a flexible coupling **[147]**

Given the fact that perfect alignment is not practical in wind turbine applications as some level of misalignment will always occur, flexible couplings are commonly used by wind turbine manufactures **[1, 120, 123]**. **Therefore, this option was selected for the current design process.**

• **Size of coupling**: the coupling size must be large enough to accommodate both generator and rotor shaft ends. The coupling can be modeled as a hollow cylinder whose inner diameter is the same as that of the involved shafts. As a general rule, the shaft diameter must not exceed the coupling's maximum bore. For the case of the present design process, the selected coupling must have a 90 mm maximum bore. This value is exactly the same as the main shaft diameter (the generator shaft is supposed to have the same diameter as the main shaft). Another design parameter of a coupling is the nominal and the design torque. Torque requirements can be calculated from either the torque of the driven component or from the power and rotational speed of the driving side (rotor blades in this case).

The nominal torque can be determined using equation 96 **[148]**.

$$T_{cnom} = \frac{9549 \, P_{design}}{\Omega_{design}} = 610.69 \, Nm \tag{96}$$

Where T_{cnom} is the nominal torque to be transmitted by the coupling, P_{design} is the design power output which is taken as 11 kW and Ω_{design} is the design rotational speed which was set to 172 RPM.

While the nominal toque application is important to know, this torque is not the parameter to be used in the coupling selection. Rather, the application torque must be multiplied by a service factor (application specific), F_{sc}, to make sure that the coupling is robust enough to handle the unique challenges of that specific system. A service factor is used to account for the high operating torque conditions of the equipment to which the coupling is connected. This service factor should be applied to the normal operating torque (equation 96) of the system. Different service factors are used or recommended depending on the severity of the application. The service factor must be applied to continuing operating conditions rather being used to account for starting torques, short circuit conditions, or similar transient conditions [148]. In order to determine an adequate service factor for a specific application, many manufacturers use the American Gear Manufacturers Association (AGMA) standard: Load classification and service factors for flexible couplings [149]. According to this standard, when a flexible coupling is used to connect a standard electric turbine (driving machine) and an electrical generator (driven machine), a service factor of 1.5 to 2 can be used. **To cover uncertainties in the coupling design, a value of 2 will be used**. Thus, the design torque that will be used to select the coupling is given by equation 97.

$$T_{cdesign} = T_{cnom}.F_{sc} = 1221 \text{ Nm} \qquad (97)$$

• **Coupling materials:** proper selection of materials allows the coupling to resist aggressive environmental conditions (especially high temperature) while transmitting the mechanical torque. Hubs of flexible couplings are typically available in stainless steel, alloy steel, brass, and advanced thermoplastics. Each material has a set of advantages. For example, stainless steel couplings offer good corrosion resistance and high strength over a wide range of temperatures, but this solution will increases the cost. However, alloy steel and brass couplings are worth considering when cost is the primary consideration [150].

• **Bore types and shaft attachment options:** the coupling's bore is normally selected to fit the driver (rotor shaft) and the driven shafts. Cylindrical bore is selected in the present project since the generators are always offered with cylindrical shafts. For cylindrical bores three types can be used. The first type is known as **through-bores**. This is the most common option; they have a big advantage in ease of mounting, because the hub can be slid back over the shaft and out of the way to insert the midsection, then slid back and locked down, so that the coupling can be installed without moving either the driving or driven component. The second type is **blind bores**. This category of bores offers the potential advantage of giving a bottom of the bore for the shaft to push against, helping to axially locate the hub relative to the shaft. The third type is **the keyed bores**, which can be either through-bores or blind bores.

A keyway is broached into the bore to accept standard inch or metric keys that also seat in a keyway in the shaft. This helps to transmit torque from the shaft to the hub, preventing shaft slippage, even at very high torques **[150]**. Balancing the above mentioned considerations, table 37 summarizes the main requirements on which the selection of a coupling for the current design small wind turbine will be based.

Design parameter	Specification
Type of coupling	**Flexible coupling**
Coupling's maximum bore	**90 mm**
Bore type	**Keyed bore**
Coupling material	**Stainless steel (EN 1.4028, ASTM TYPE 420)**
Coupling design torque	**1221 Nm**

Table 37: Main requirements of the selected flexible coupling

Another feature that can be added to the coupling's requirements is the torque limitation device. Actually, wind turbine couplings can incorporate a mechanical slip device to provide a maximum limit of 150% to 200% for the forward torques, which inherently provides the same limit in reverse. This provides some protection against generator short circuits, emergency stops and other transient load events. For a first tentative design, disc flexible shaft coupling (Crossflex disc flexible coupling from cross+Morse Company) is selected for the present project. This product is particularly suited for systems operating in poor environmental conditions. Additionally, it provides reliable and accurate transmission of mechanical power for applications requiring low maintenance and no lubrication. The selected disc coupling presents the following performance characteristics:

- **Backlash Free**: ensures accuracy of control on all positioning applications, particularly essential for drives with frequent stop and starts;

- **Torsionally stiff**: the disc pack design ensures high torsional stiffness;

- **High temperature**: this Coupling is manufactured entirely from steel, enabling operating temperatures up to 240 °C in difficult environmental conditions;

- **High operating speeds**: close tolerances and precision machining provide accurate concentricity enabling high speed operation;

- **Long maintenance free life**: the design of the Crossflex coupling ensures there is almost no wear enabling a very long service life. As there are no moving parts within the system no lubrication or maintenance are required;

Figure 54 and tables 38 and 39 give the dimensions and the technical specifications of the selected disc coupling.
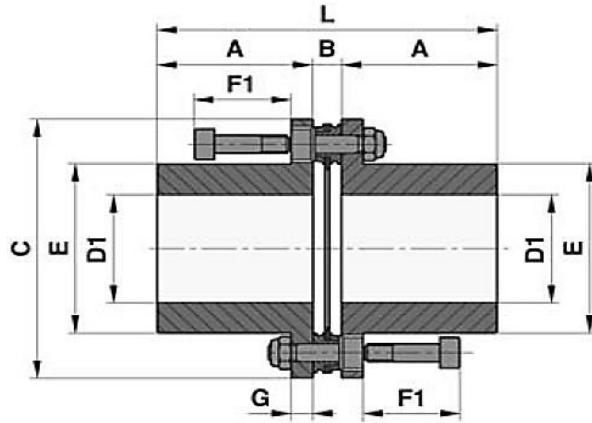
Figure 54: Crossflex single disc flexible coupling

A (mm)	B (mm)	C (mm)	D_1 (mm)	E (mm)	F_1 (mm)	G (mm)	L (mm)
75	13	166.5	90	118	55	12	162.7

Table 38: Dimensions of the selected disc flexible coupling

Nominal torque (Nm)	Maximum speed (RPM)	Maximum misalignment (mm)			Inertia (kg.m²)	Torsional stiffness (KNm/rad)
		radial	axial	angular		
2400	4300	0	1.2	1	0.03513	710

Table 39: Technical specifications of the selected disc flexible coupling

5.4.3 Rotor shaft bearing design and analysis

Rotor shaft bearing is one of the most important components in a small wind turbine system. Its design requires specific attention to achieve maximum reliability and efficiency. The main shaft bearing has two major functions. First it must support the main shaft (including the wind turbine rotor weight) and transmits the reactions from the rotor loads to the nacelle frame. The second function consists in transmitting the mechanical torque to the generator with minimum heat and friction losses. Usually, the performance of a shaft bearing can impact upon efficiency, reliability, noise and maintenance. In its design process, several requirements have to be taken into consideration:

- The lifetime of the bearing should be at least 20 years;

- The main bearing must be able to accommodate axial as well as radial forces from the rotor;

- The bearing must allow misalignment from deflection of the shaft and the support (misalignment of ± 5° needs to be taken into account);

- Due to the external operating conditions, the bearing configuration should compensate temperature-related material stretching and shrinking;

- To keep losses at a minimum, bearing friction should be low;

- As small wind turbines usually operate onshore and might even operate close to residential areas, a quiet operation is favorable;

For the combined axial and radial loads, which are generated in the rotor side, single bearing design is an appropriate solution. This bearing configuration is a well-proven solution which is able to accommodate different loads in one multiple-row bearing [151]. In this system, the bearing is arranged at one end of the shaft (rotor side) to locate the shaft axially and radially. The opposite end of the shaft will be directly connected to the generator. **The solution adopted in this design process consists in using one spherical roller bearing**. This type of bearings is usually designed to work in applications where severe misalignment exists, whether from mounting or shaft deflection and with relatively heavy radial loads and some axial loads in either direction (similar conditions for direct drive small wind turbines). Also, they are extremely resistant to shock loads and their self-aligning feature allows full capacity loading despite shaft deflection. Spherical roller bearings are designed to be more robust at lower rotational speeds. These bearings have barrel-shaped rollers between the inner ring, which has two raceways, and the outer ring which has one spherical raceway. Based on their features, spherical roller bearing configuration seems to be suitable for a direct drive wind turbine machine [152]. According to the experts, the single bearing configuration is suitable when two conditions are met. The first condition states that the generator must have an integrated bearing that supports the reaction forces. That is, the generator must have some torque stays or something flexible in order to not carry parasitic loads. Then it will work like a three point suspension turbine. The second condition requires that the connection between the main shaft and generator shaft must be rigid. In case these conditions are not satisfied, another bearing, in the generator side (usually cylindrical bearing), is necessary. As shown in figure 55, the bearing will be positioned close to the shaft/hub flange connection (0.1 m from the hub) in order to minimize the gravity moment due to the cantilevered rotor mass.
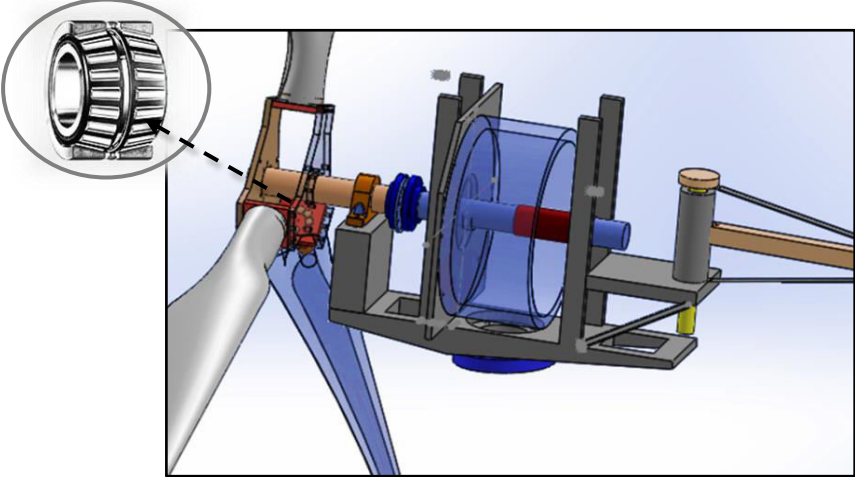
Figure 55: Spherical roller bearing for the main shaft position

For the present project, a spherical roller bearing from SKF Company was selected [153]. The dimensions of the selected bearing are given in the figure 56.
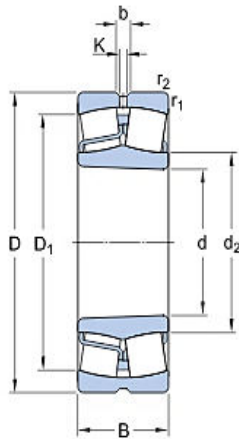
d		90	mm
D		160	mm
B		40	mm
d_2	≈	106	mm
D_1	≈	141	mm
b		6	mm
K		3	mm
$r_{1,2}$	min.	2	mm

Tapered bore, taper 1:12

Figure 56: Spherical roller bearing dimensions [153]

The design of the shaft bearing should start by determination of the requisite minimum radial load that must be applied to the bearing. In order to achieve satisfactory operation, spherical bearing must always be minimal loaded. The necessity of applying a minimum load increases in applications when there are rapid accelerations or rapid starts and stops, and when shaft speeds exceed 50% of the limiting speeds of the bearing's components. If minimum load requirements cannot be met, NoWear coated bearings should be considered. This is a wear-resistant carbon coating that can be applied to the rolling elements and to the inner ring raceways of a bearing or only on the rolling elements: a physical vapor deposition process applies the wear-resistant carbon coating ranging from 1 to 3 μm depending on the size of the bearing. NoWear coated bearing surfaces retain the toughness of the underlying material while adopting the hardness, improved friction properties and wear-resistance of the coating. During the running-in period, minute amounts of the coating material are transferred to the counter surfaces. This transfer reduces friction and improves resistance against wear and smearing, even in bearings where only the rolling elements are coated. This substance is mainly used to extend service life and to withstand severe operating conditions including light loadings. A general "rule of thumb" indicates that minimum loads of $0.01\ C_0$ should be imposed on roller bearing. That is, the requisite minimum radial load is given by:

$$F_{rm} = 0.01 \cdot C_0 = 0.01 \cdot 375 = 3.75\ \text{kN} \tag{98}$$

Where C_0 is the basic static load rating (this data can be found in the product's data sheet). For the current design, the radial force acting on the bearing is given by:

$$F_r = m_{rot} \cdot g = 919.436\ \text{N} \tag{99}$$

Where m_{rot} is the total rotor mass and g is the acceleration due to the gravity. As can be seen, the minimum load requirements are not meet. Therefore, NoWear coated bearings should be considered. For the selected bearing configuration, static and dynamic structural safety is calculated.

The maximum rotor axial load is taken from IEC 61400-2 load case H (Parked Wind Loading). This load case considers the thrust caused by the wind loading on the blades of a parked wind turbine:

$$F_a = \frac{1}{2}.B.C_d.\rho.U_{e50}^2.A_{proj,B} = 4102.33 \text{ N} \tag{100}$$

Where B is the blade number, C_d is the drag coefficient taken to be 1.5, ρ the air density which is taken to be 1.225 kg/m³, U_{e50} is the 3s 50-year extreme wind speed which is taken as 52.5 m/s and $A_{proj,B}$ is the projected area of the blades which can be taken as the planform area. For a spherical roller bearing, the equivalent static bearing load, P_0, is given by:

$$P_0 = F_r + Y_0.F_a = 12405.87 \text{ N} \tag{101}$$

The permissible static equivalent load on bearings depends on both the basic static load rating C_0 and the operating conditions of the bearing. This permissible load is generally expressed as a ratio of the basic static load rating (intrinsic characteristics) and the equivalent static load on the bearing (applied loads).

The permissible static load factor S_0 is a safety factor that is applied to the basic static load rating and is defined by the following ratio.

$$S_0 = \frac{C_0}{P_0} = 30.22 \tag{102}$$

For a quiet running of single spherical roller bearings (low noise application), the structural safety factor of at least 4 is required [154]. Because the permissible static load factor is higher, a quiet running of the bearing can be expected.

The dynamic structural safety is determined by assuming that the dynamic forces are equal to the normal operating forces according to IEC61400-2 Load Case A. The dynamic equivalent bearing loads are calculated as follows:

First, the axial load is calculated using equation 103:

$$F_a = \frac{3}{2}.\frac{\lambda_{design}.Q_{design}}{R} = 2397.54 \text{ N} \tag{103}$$

Where λ_{design} is the design tip speed ratio which is taken as 6 and Q_{design} is the design shaft torque which is taken as 932.38 N.m.

The radial force is calculated by assuming the centrifugal force acting on the blade root:

$$F_r = 2. m_B. R_{cog}. \Omega_{design}^2 = 19.617 \text{ KN} \tag{104}$$

Where m_B is the blade mass (21.6 Kg), R_{cog} is the radial distance from hub center to blade center of gravity (1.4 m) and Ω_{design} is the design rotational speed (18.01 rad/s).

Secondly, the ratio of the combined loads is computed using the following equation:

$$\frac{F_a}{F_r} = 0.12 \tag{105}$$

As the ratio of these two combined load is less than the given calculation factor e (which is given as e = 0.24), the dynamic equivalent bearing load P_d is given by:

$$P_d = F_r + Y_1. F_a = 26.33 \text{ KN} \tag{106}$$

Where Y_1 is the calculation factor given by the bearing manufacturer which is considered as 2.8.

With a bearing dynamic load rating of $C = 331$ kN, the dynamic structural safety factor is:

$$S = \frac{C}{P_d} = 12.57 \tag{107}$$

As all the safety factors exceed the minimum design values, the bearing unit meets the structural requirements. The basic rating life of the locating bearing is given by:

$$L_{10h} = \left(\frac{C}{P_d}\right)^{10/3}. 10^6. \frac{1}{\Omega_{design}. 60} = 447\ 477 \text{ hour} \tag{108}$$

After determining the bearing size, the comparison between the estimated rating life and the specification life of the application (or the requisite rating life) is necessary. This later usually depends on the type of the machine and the lubrication requirements. In the absence of previous experience, the guideline values given by SKF Company [154] are used. For wind energy machinery (which includes main shaft, yaw and generator bearings), the specification life of the bearings should be between 30,000 and 100,000 operating hours. Therefore, the estimated lifetime of the bearing exceeds the specification life. Based on SKF design application, the results of the bearing life calculation are summarized in table 40.

SKF rating life, L_{10mh}	>1000000 hour
SKF life modification factor, a_{skf}	4.9
Viscosity ratio, k_r	1.09
Equivalent dynamic bearing load, P_d	26.3 KN
Factor for contamination level, η_c	0.5

Required kinematic viscosity for k=1, γ_1	47.7 mm²/s
Basic rating life, L_{10h}	449 300 hour
Load ratio, C/P_d	12.6

Table 40: Bearing life calculation of the locating bearings

In order to increase the reliability of the selected bearing, an appropriate bearing housing is needed. When selecting a bearings housing, many factors should be considered. The selection process depends not only on the bearing type and size but also on the ability of the housing to safely accommodate the magnitude of the applied loads. Additionally, further important considerations must be taken into account such as easy mounting, low maintenance and sealing options. The main purpose of a bearing housing is to support the bearing while transmitting the static and the dynamic loads to the bed frame, protect the bearing and lubricant from contaminants, contain the lubricant and accommodate lubrication system components, accommodate monitoring system components and maximize the performance of the bearing by improving the service life of the incorporated components. In the present project, **the selected housing is a two bolt pillow block roller bearing** which is the most commonly used type of mounted units. These housings are developed to be the first choice because of their quality and their cost effectiveness. Pillow block housings are designed to provide shaft support where the mounting surface is parallel to the shaft axis as shown in figure 57. This type of housing enables the incorporated bearings to achieve maximum service life while minimizing the maintenance.
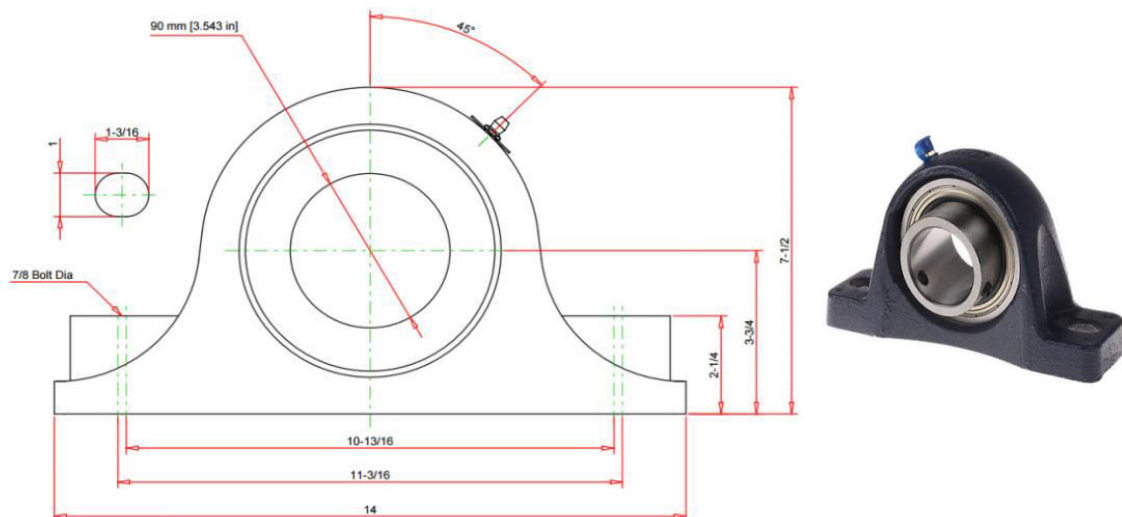
Figure 57: Two bolt pillow block roller bearing unit [155]

The connection between the bearing housing and the nacelle frame will be a bolt connection. This connection should be capable of transferring the combination of axial and radial forces from the bearing to the main frame by friction or by shear in bolts by tight fit, depending on

the geometry of the connection. In order to improve their operating conditions, an appropriate lubrication process should be provided. The type of lubrication depends on the bearing concept and the sealing technique used [3].

5.5 Wind turbine generator design

Electric generator represents a core component in a wind power generation system. Its good operation is a guarantee of reliability and efficiency of the whole system. As the wind energy conversion system is demanded to be more cost-effective, so that a comparison of different wind generator systems is necessary.

5.5.1 Wind turbine generator technology

Generally, there are three main types of wind turbine generators that can be considered for wind turbine systems, these being direct current (DC), alternating current (AC) synchronous and AC asynchronous generators [156].

Generally, DC wind turbine generators are unusual in wind turbine applications and especially used in low power demand situations where the load is physically close to the wind turbine, in heating applications or in battery charging [156, 157, 158]. In addition, Brushed DC generators have a lot of maintenance need with the brushes and were quickly eliminated as an option for the present design process [134].

Asynchronous generators (induction generators) are usually used in a grid connected wind turbine systems. Because this type of generators operates only in a narrow range around the synchronous speed, the wind turbine equipped with this type of generator is often called the fixed-speed wind turbine. Since the asynchronous generators always draw reactive power from the grid, the concept of this machine was extended with a capacitor bank for reactive power compensation. The well-known advantages of the asynchronous generator are its robustness and its cost-effectiveness for mass production. Additionally, it enables stall-regulated machines to operate at a constant speed when it is connected to a large grid, which provides a stable control frequency [159].

An asynchronous generator for a fixed speed wind turbine concept has several disadvantages [160]: the speed is not controllable and variable only over a very narrow range, in which only speeds higher than the synchronous speed are possible for generator operation. Additionally, the fixed speed concept means that wind speed fluctuations are directly translated into electromechanical torque variations, this causes high mechanical and fatigue tresses on the system (turbine blades, gearbox and generator). Also, a gearbox in the drive train is necessary for this wind turbine concept. Gearboxes represent a large mass in the nacelle, and also a large

fraction of the investment costs. Besides, the gearbox has a high failure rate, especially oil leakage, while running. So it makes maintenance workload increasing and available work hours to reduce. Based on the aforementioned considerations, asynchronous machine is not an appropriate solution for the present project.

Permanent Magnetic Synchronous Generators (PMSG) are widely used in the variable speed wind turbine systems, especially in the small or medium power range, which increases the conversion efficiency and reduces the maintenance cost due to brushless design [161]. The reliability of the variable speed wind energy systems can be improved significantly by using a permanent magnet synchronous generator (PMSG). This type of generators has several advantages such as simple structure they have, the ability of operation at slow speed, and the self-excitation capability leading to high power factor and high efficiency operation. With low speed of PMSG operation there is no need for a gearbox which often suffers from faults and requires regular maintenance making the system unreliable [162].

According to the literature, PMSG machines present many advantages such as high efficiency and energy yield, no additional power supply for the magnet field excitation, improvement in the thermal characteristics of the PM machine due to the absence of the field losses, higher reliability due to the absence of mechanical components such as slip rings, and lighter and therefore higher power to weight ratio [160-163]. This type of generators has also some drawbacks such as high cost of PM material, difficulties to handle in manufacture, and finally, demagnetization of the permanent magnet at high temperatures. This is the reason why the temperature of a PMSG machine must be supervised and an appropriate cooling system is necessary. An analysis of the commercially available 10 kW and 11 kW small wind turbine generators has been conducted. It is found that a direct-drive permanent magnet generator is the most widely used solution. This is due to the fact that this topology offers high reliability for the full drive train. In addition, it requires less assembly labor than competing designs and provides a reduction in overall maintenance. Also, the elimination of the gearbox allows an improvement of the efficiency of the whole system.

Due to the fact that the performance of PMs is improving and the cost of PM is decreasing in recent years, gearless direct-drive PM machines is an attractive solution for small scale wind turbines [160]. This type of generators is becoming the most common solution for the stand alone direct drive wind turbine systems [164]. Figure 58 shows the available options for small wind turbine generators.
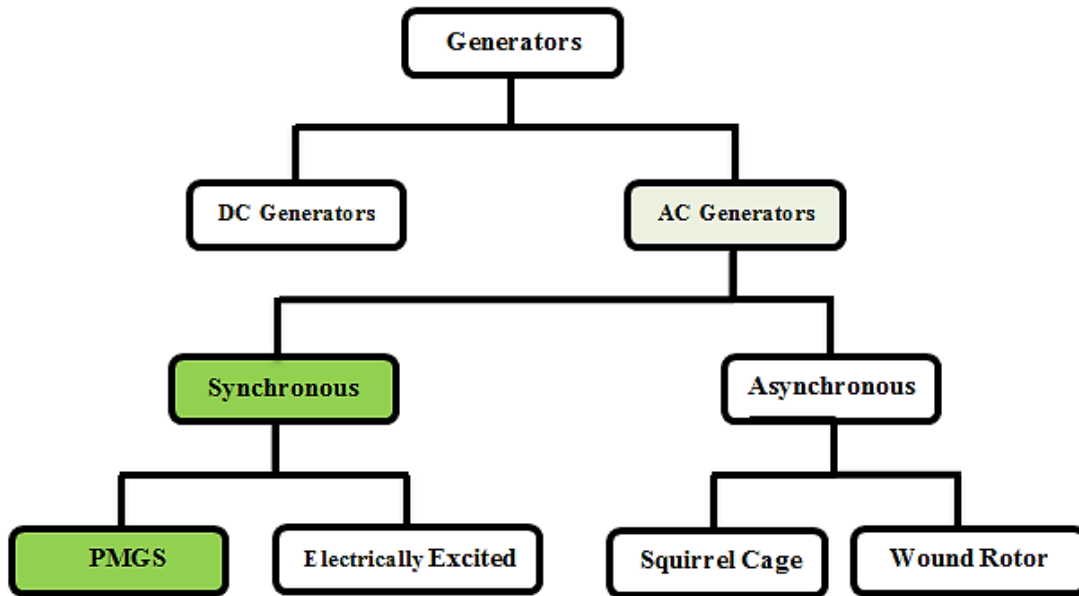
Figure 58: Types of the small wind turbine generators

Balancing all these parameters, Permanent magnetic synchronous generators was selected for the present project. Figure 59 gives a simplified scheme of a direct-drive PMSG system:
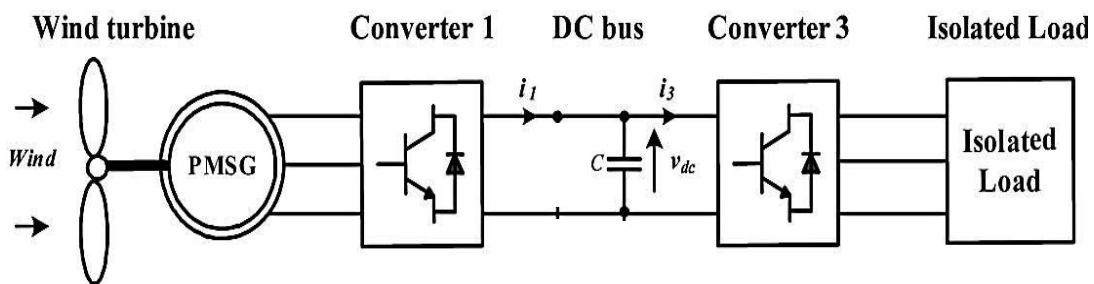
Figure 59: Scheme of a direct-drive PMSG system

5.5.2 Wind turine generator topology

Permanent magnet generators are not standard machines, but they allow a great deal of flexibility in their geometry, so that various topologies may be used. PM machines can be classified into the following types: radial flux (RFM) machines, axial flux (AFM) machines and the transversal flux (TFM) machines, based on the direction of flux penetration [165]. AFMs have many advantages over RFMs. First, they can be designed to have a higher power-to-weight ratio resulting in less core material and higher efficiency. Secondly, they are smaller in size than their radial flux counterparts and have disc shaped rotor and stator structures. This is an important feature of axial flux machines because suitable shape and size to match the space limitation is crucial for some applications such as small scale wind turbine applications. Also, they have planar and adjustable air gaps, which radial flux machines do not have. Moreover, the noise and vibration levels are less than the conventional machines [166].

This type of machines (especially Double Rotor Slotted Axial-Flux Machines and Axial-Flux Machine with Toroidal Winding or Torus machines) is for use in small-scale stand-alone generating systems in remote areas. For such applications, which are characterized by low speed of rotation, the axial flux permanent magnet generator is particularly suited since it can be designed with a large pole number and high torque density [167,168]. The reduction of the cost of high energy permanent-magnet materials is expected to open up applications for the axial-flux machines [169]. Figure 60 shows an example of axial-flux machine structure with toroidal winding:
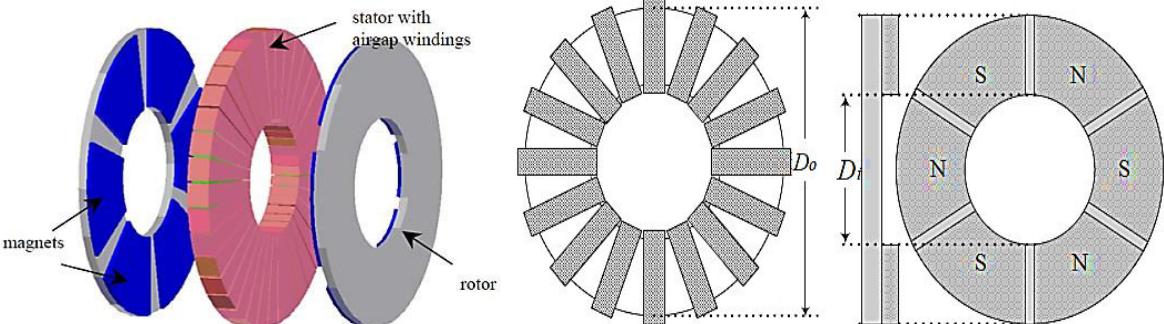
Figure 60: Torus machine structure

A comparative study between the axial-flux and radial-flux permanent-magnet synchronous generators, for a small wind turbine application, has been conducted by Augustin POP et al. [170]. The comparison is made on the basis of the generators efficiency and active material's estimated cost. The results show that the axial-flux PMSG is the best solution for small scale wind turbine application. Yicheng Chen et al. [171] have conducted a comparison among permanent magnet (PM) wind generators of different topologies and have shown that axial-flux PMSGs, direct-drive stand-alone machines (Double Rotor Slotted Axial-Flux Machines and Axial-Flux Machine with Toroidal Winding) present the following advantages:

- High torque density;
- Magnet weight versus power (they use less magnet material for their construction for which the price still very high);
- Lamination weight versus power (they require less lamination);
- Total volume versus power (axial-flux machines require the least space);
- Efficiency versus power (axial-flux machines have maximum efficiency);

Keeping in mind all the aforementioned considerations, the axial flux permanent magnet generator represents an advantageous option in small scale wind turbine applications. Therefore, it was selected for the present design process.

The rated power output of the selected generator should be 11.000 W at a rated wind speed of 10.5 m/s. The generator rated power should be produced at a rotor rotational speed of 172

RPM (which corresponds to the design rotational speed). In addition, the generator should tolerate up to 20% of its maximum output power (which is equal to 13.2 kW in the case of this project) before the stall regime takes place, particularly when the wind speed is above the rated speed (V_{rated} = 10.5 m/s). This will ensure that the maximum rotational speed of the rotor blades will not exceed the generator maximum overloading.

As the frequency, f, of the induced voltage in the stator of a PMG is directly proportional to the RPM (that's why they are known as synchronous), the relationship can be expressed with the following formula [74]:

$$\Omega = \frac{60.\,f}{P_{pole}} \tag{109}$$

Where Ω is the rotor rotational speed and P_{pole} is the number of magnetic rotor pole pairs.

As the energy transmission chain in the present work consists in a direct coupling of the synchronous PMG to the wind turbine rotor, it is necessary to match between the power turbine curves and the generator. The maximum power is extracted from the wind and fed to the load if only a matching the mechanical output characteristic of the wind turbine to the characteristic of the synchronous generator. PREDESCU et al. [74, 164] give two design methods of the generator for maximum power transfer from wind to the load. In the case of this project, the matching of the turbine rotor and the generator curves is ensured by the optimal control strategy for the fixed-pitch variable speed wind turbine.

The ERNEO A535S-3-14 is the permanent magnet generator that has been selected for the current design process. This generator has rated power of 16 kW at rated rotational speed of 200 RPM. It should be noted that this generator can operate at 175 RPM with a corresponding output power of 11 kW. This generator has 70 poles (or 35 pole pairs) with a low RPM operating range, which makes it an ideal option for direct drive system. A picture of the A535S-3-14 generator is shown in Figure 61, and the specification sheet can be found in the Appendices.
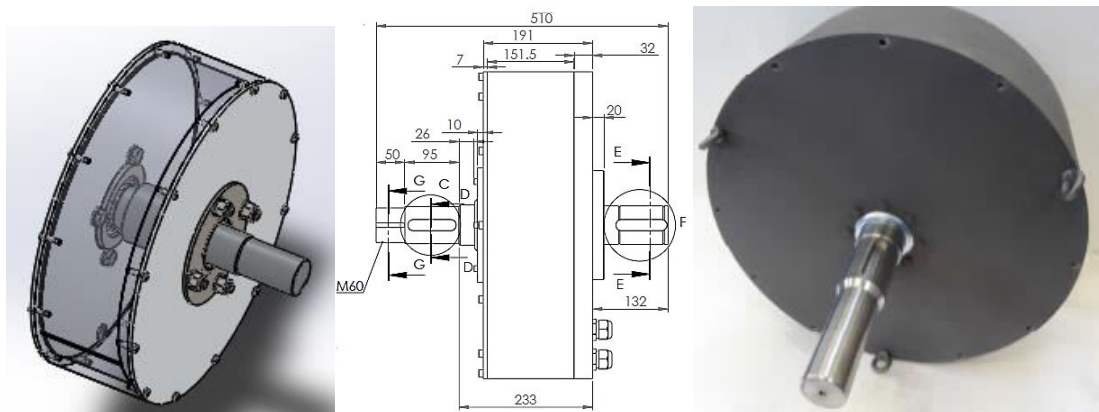
Figure 61: A535S-3-14 permanent magnet generator [172]

5.6 Wind turbine control system design

5.6.1 Wind turbine operation mode

Small wind turbines have to cope with the intermittent and seasonal variability of the wind while attempting to achieve maximum power production over a wide range of wind speeds. For maximum power extraction, wind turbine machines must be designed to operate at their maximum power coefficient from cut-in wind speed to rated wind speed. Beyond the rated wind speed, they must include some mechanisms to limit the captured power at high wind speeds to prevent overloading. In order to limit excessive power under strong winds, small and medium-size wind turbines have two common torque controls: **fixed-pitch and pitch-controlled topologies [173]**. **The fixed pitch** or the stall control strategy is based on a specific design of the blades so that stall occurs when the wind speed exceeds a certain level; it means that the captured power is automatically limited in the rated power range. This method is simple, robust and cheap but it has low efficiency at low wind speed. Passive stall is mostly used in small wind turbine systems **[174]**.

In case of **pitch control**, blades can be turned away from or into the wind as the captured power becomes too high or too low; this is performed by rotating the blades, or part of them, with respect to their longitudinal axes. Below rated wind speed, blades are pitched for optimum power extraction whereas above the rated wind speed, blades are pitched to small angle of attack for limiting the power. Advantages of this type of control are good power control performance, assisted start-up and emergency power reduction; the biggest disadvantage is the cost and the extra complexity due to the pitch mechanism **[175]**. Pitch adjustment is usually used for multi-megawatt class and rarely used in small scale wind turbines **[3, 41]**.

Beyond the captured power controllability, another feature is the speed controllability. Based on this, small wind turbines are classified into two main categories: **fixed speed and variable speed operation modes [161]**.

Fixed-speed wind turbines are generally equipped with an induction generator and usually used for grid connection, with a soft-starter and a capacitor bank for reducing reactive power compensation. For constant-speed small wind turbines, the rotor blades are designed to operate near maximum efficiency (C_{pmax}) at wind speeds that occur most frequently at sites. The rotor speed varies by only a few percent (the slip) above the synchronous speed of the induction generator, but the wind speed varies over a wide range. Therefore, the operating point is rarely, and randomly, at the tip speed ratio (TSR), λ, for C_{pmax} **[176]**. That is, one argument for operating a wind turbine at variable rotational speed is that it is possible to operate at maximum power coefficient over a range of wind speeds. The fixed-speed wind

turbine has the advantage of being simple, robust and reliable and well proven. Its disadvantages are an uncontrollable reactive power consumption, mechanical stress and limited power quality control. Owing to its fixed-speed operation, all fluctuations in the wind speed are further transmitted as fluctuations in the mechanical torque and then as fluctuations in the output electrical power [159].

Variable-speed wind turbines are designed to achieve maximum aerodynamic efficiency over a wide range of wind speeds. In order to extract maximum power from the wind, the turbine rotor speed needs to be changed proportional to wind speed. Most modern wind turbines are designed for variable speed operation [177]. In comparison to the fixed speed operation, variable speed systems offer some advantages including increased energy capture, operation at maximum power point, improved efficiency, power quality, reduced mechanical stresses and audible noise at low wind speed [159, 176].

Fixed-pitch variable speed (FPVS) wind energy conversion systems are generally more efficient compared to fix-speed counterparts, and hence are becoming increasingly popular, particularly in small scale applications [174]. **Therefore, FPVS approach is the selected solution for the current project.** The potential benefit of this topology in comparison to variable pitch systems is a lower cost of energy resulting from lower capital cost, improved reliability and reduced maintenance expense.

5.6.2 Wind turbine control strategy

To achieve maximum power extraction from winds with fluctuating behavior, the common used control strategies are summarized in the following points:

• **Power/torque tracking strategy by controlling the generator frequency**: this control strategy uses either a Peak Power Tracking (PPT), which tracks the target power curve in the lower frequency range and extracts maximum power from the wind turbine generator, or by using a fully controlled frequency converter [178, 179, 180]. This method is generally used with an induction generator connected directly to the power grid. The control uses a simple Voltage/frequency scheme with the frequency being set based on the speed of the turbine and the optimum power the turbine can produce at that speed.

• **Control strategies using wind speed measurement to obtain the desired rotor speed in order to vary the generator speed**. This option requires anemometer-based control strategy, which increases cost and reduces the reliability of the overall system. These control strategies are not suitable or too expensive for a small-scale wind turbine [181].

• **Control strategy using current vector of an interior type permanent-magnet synchronous generator (IPMSG)**: The armature current vector of the IPMSG is optimally

controlled according to the generator speed in order to maximize the generated power from the wind [182].

• **Power control strategy, within the whole wind velocity range,** for a commonly used permanent magnet synchronous generator (PMSG) based VSFP concept wind power system; this method uses an aerodynamic power feedback (by using an aerodynamic power observer) along with an adaptive PI-like fuzzy logic controller [183]. Constant speed stalling operation and constant power soft-stalling operation are all realized in order to achieve maximum power extraction.

For the present design process, **a control strategy for the generator-side converter with output maximization of a generator-based small-scale wind turbine is used**. A Generator-side Switch Mode Rectifier, SMR, is controlled to achieve maximum power from the wind. This method requires a position sensor to measure the generator's rotational speed along with one active switching device (insulated gate bipolar transistor (IGBT) for example) which is used to control the generator torque to extract maximum power. This solution was selected because of its simplicity, effectiveness and for its low cost. Using this method, the wind speed is not required to be monitored, and, therefore, it is a simple output-maximization control method without wind-speed sensor (anemometer).The wind turbine conversion system topology with the control block diagram of the control strategy is shown in figures 62 and 63:
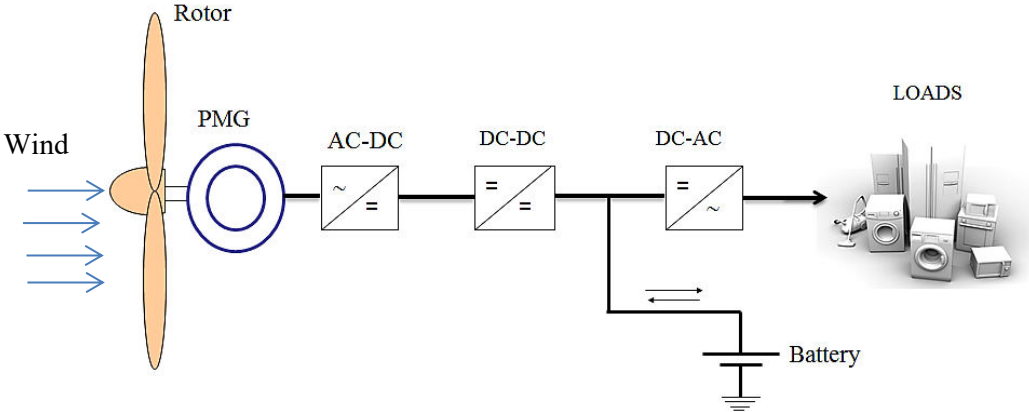
Figure 62: Schematic of a small wind energy conversion system
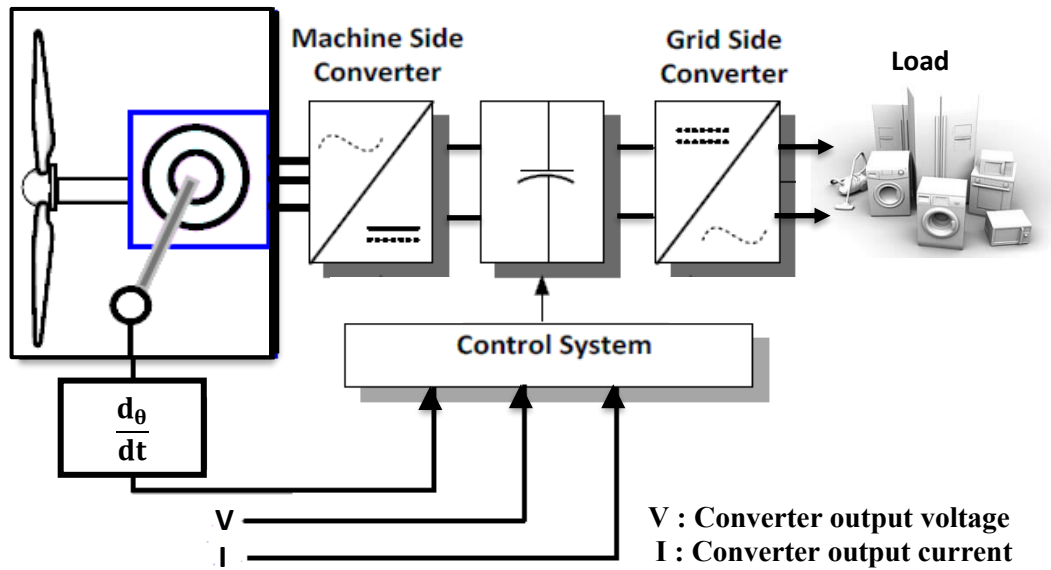
Figure 63: Wind turbine conversion system with the main control loop

In this control method, the turbine is controlled to operate near maximum efficiency in low and moderate wind speeds. To keep the rotor speed at an optimum value of the tip speed ratio in low and moderate wins speeds, the rotational speed is controlled by specifying the demanded generator torque. The generator output is controlled by the power converter to follow the optimum RPM-power curve. The generator should respond to the torque demand instantaneously. At high wind speeds, the turbine is controlled to limit its rotational speed and output power. This can be accomplished by forcing the rotor into an aerodynamically stalled condition (soft stall is required as this regulation type allows that the mechanical loading on the wind turbine components is not significantly increased). Figure 64 shows the difference between the power curves of a pitch and stall controlled wind turbine systems.
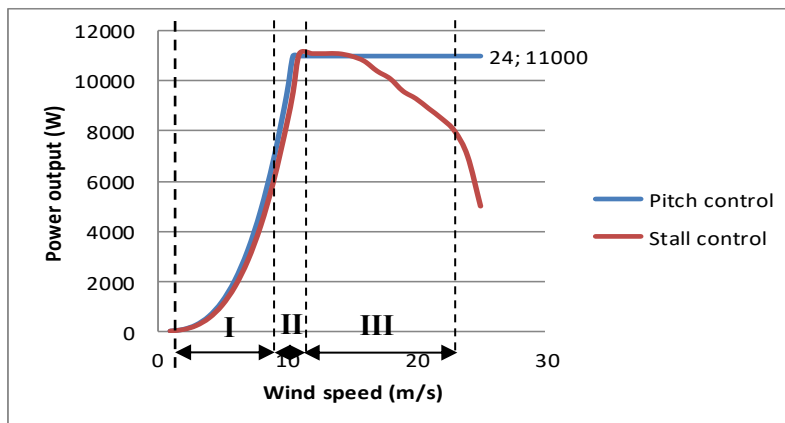
Figure 64: Power curves of a stall and pitch controlled wind turbines [184, 185]

As can be seen from the figure above, for a fixed-pitch variable speed wind turbine, four wind speeds separate the turbine operation into three operating regions, which represents a typical

power curve of a wind turbine. The first region is delimited by the cut-in wind speed and a transition wind speed. The cut-in speed is defined as the wind speed at which the turbine starts to generate the power. Below this wind speed, the wind turbine is supposed to be stationary and no power is produced. The transition speed is the wind speed that the operating point starts to move from maximum power curve of region I to the rated power in region III. The transition region is included to allow the machine to reach rated torque at rated speed. If there were no transition region and the wind turbine was not allowed to exceed rated speed, the rated power of the turbine will be too low. Usually, this region begins at a rotor speed Ω_1 and reaches the rated torque at rated speed or slightly below rated speed Ω_2. Here, the rated speed corresponds to the wind speed at which the turbine reaches its rated power. The cut-out wind speed is the maximum wind speed at which the wind turbine can still generate power. Beyond this wind speed, the rotor has to be furled to keep the blades, the electrical generator and other components from reaching damage [186]. The control objective here is to vary the generator torque (by varying the speed of the turbine) in order to maintain an optimum tip speed ratio in the region I, thus maintaining maximum power coefficient which maximizes the power output. In above rated wind speed (region III), the generator torque is held constant (or decreasing slightly as the blades come into the stall regime) until reaching the cut-out wind speed. At this specific wind speed, the turbine is supposed to furl by turning the system away from the main wind directions.

To control the generator torque, a single-switch three-phase switch-mode rectifier (SMR) is used to convert the AC output voltage of the generator to a constant DC voltage before conversion to AC voltage via an inverter. The single-switch three-phase switch-mode rectifier consists of a three phase diode bridge rectifier and DC/DC boost converter. The structure of the proposed control strategy is shown in figure 65 which consists of a wind turbine generator, single-switch three-phase switch mode rectifier, a vector-controlled PWM (Pulse Width Modulation), and switch mode rectifier control.
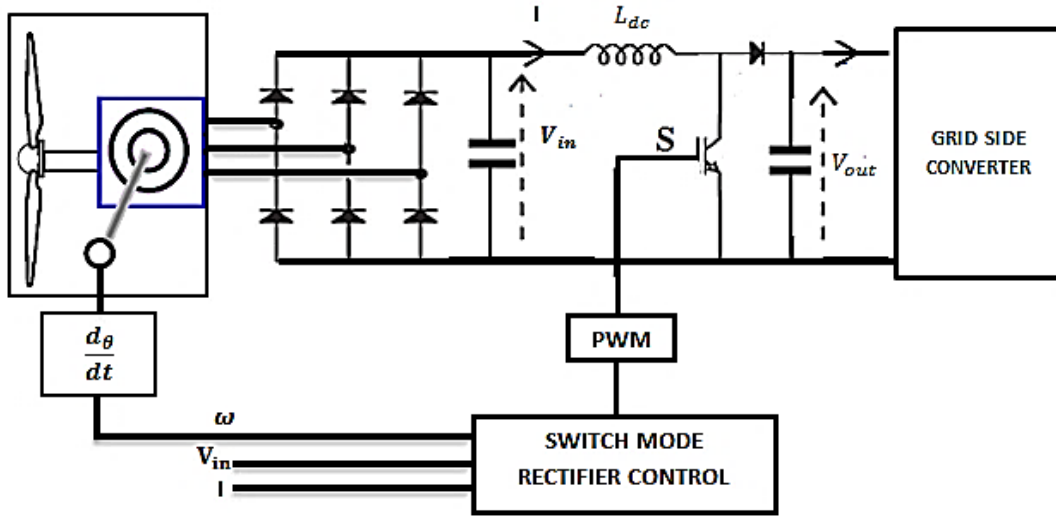
Figure 65: Structure of the control device for the small wind turbine system

5.6.3 Detail analysis of the selected control strategy

According to the aerodynamics, the power that can be extracted from the wind turbine can be expressed in equation 110. In the present analysis, the equation represents the net electrical power after considering the aerodynamic efficiency of the rotor blades and the mechanical and electrical system losses [187].

$$P = C_p \cdot \frac{1}{2} \cdot \rho \cdot \pi \cdot R^2 \cdot V^3 \tag{110}$$

Where ρ is the mass density of the air, R is the rotor radius, V is the wind speed (m/s) and C_p is the wind turbine power coefficient. The power coefficient of a wind turbine is influenced by the tip-speed to wind-speed ratio, which is given by:

$$TSR = \lambda = \frac{\omega \cdot R}{V} \tag{111}$$

In case of a fixed-pitch variable-speed wind turbine, the objective is to operate near maximum efficiency, where the resulting target power can be expressed as:

$$P_{opt} = C_{opt} \cdot \frac{1}{2} \cdot \rho \cdot \pi \cdot R^2 \cdot \left(\frac{\omega.R}{\lambda_{opt}}\right)^3 = K_{opt} \cdot \omega^3 \tag{112}$$

Where:

$$K_{opt} = C_{opt} \cdot \frac{1}{2} \cdot \rho \cdot \pi \cdot R^2 \cdot \left(\frac{R}{\lambda_{opt}}\right)^3 \tag{113}$$

Based on equation 113, the value of K_{opt} is 1.87 N.m.s².

Therefore, the target optimum torque can be given by equation 114.

$$T_{opt} = \frac{P_{opt}}{\omega} = K_{opt} \cdot \omega^2 \tag{114}$$

Thus, in the region I, the generator torque can be expressed as:

$$T_{opt} = 1.87 \, \omega^2 \tag{115}$$

Taking into account that the generator rectification voltage (V_{dc}) is proportional to the rotor speed (ω) for the generator [188], that is:

$$V_{dc} = K_u . \omega \tag{116}$$

The control objective is to control the duty cycle of the switch (**switch S in the figure 64)** in order to extract maximum power from the variable-speed wind turbine and transfer the power to the load. The method requires only one active switching device (insulated gate bipolar transistor- IGBT in this case), which is used to control the generator torque and to regulate the DC link voltage. The IGBT is usually used because of its advantageous characteristics. This switching device can be totally controlled by a low voltage. Also, it has low on-state losses and large blocking voltages. The control algorithm includes the following steps:

1. Measure of the generator speed, Ω;

2. Determination of the reference torque (T_{opt}) by using the equation 114;

3. The reference torque is then used to calculate the dc current reference (I_{opt}) by measuring the rectifier output voltage V_{in} as given by :

$$I_{opt} = (T_{opt} . \omega) / V_{in} \tag{117}$$

4. The difference between the reference dc current (I_{opt}) and measured dc current, I_r, is used to vary the duty cycle of the switch (using a current loop controller) to regulate the output of the switch-mode rectifier and the generator torque through a hysteresis or proportional–integral (PI) controller. The generator torque is controlled in the optimum torque using the switch mode rectifier controller as shown in figure 66:
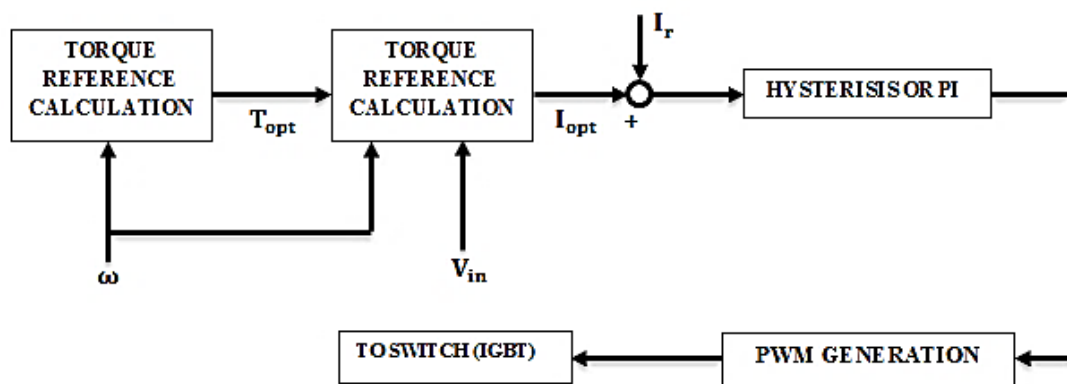
Figure 66: Structural configuration the proposed switch mode rectifier control

The boost converter is located after the diode rectifier block. The DC/DC converter controls the output current from the rectifier, I_r, which is directly related to currents in the generators.

Hence the electrical torque of the generator is controlled. The output capacitor is large so it is possible to assume $V_{out}(t) = V_{out}$. The value of the input inductor, L_{dc}, is made large enough for the converter to always work Continuous Conduction Mode (CCM). The CCM means that the current in the energy transfer inductor never goes to zero between switching cycles. To make sure the converter always works in CCM, equation 118 is used to describe the boundary conditions between CCM and DCM, Discontinues Conduction Mode. I_{max} is the maximal load current through the inductor and T_s is the switching time period [189].

$$L_{dc} = \frac{T_s . V_{out}}{2 . I_{max}} . D_u (1 - D_u)^2 \tag{118}$$

Where D_u is the duty cycle of the switch control.

When the IGBT is turned on, t_{on}, the energy of the generator is being stored in the inductor. During this time the diode is reversed biased, hence it does not conduct any current. When the IGBT is turned off, t_{off}, the stored energy in the inductor flows through diode transferring it to the load. It is assumed that the input voltage, V, and the output voltage, V_{out}, stays constant during each switching periods. The increase in the input current to the converter is stated as [190, 191]:

$$\Delta_i = i_{t0+T_s} - i_{t0} = \frac{T_s}{L_{dc}} . (V_{in} - V_{out} . (1 - D_u)) \tag{119}$$

The control signal can be written as:

$$V_{control} = \frac{L_{dc} . \Delta_i}{T_s} \tag{120}$$

From equations 117 and 118, the duty cycle can be expressed as:

$$D_u = \frac{1}{V_{out}} . (V_{control} - V_{in}) + 1 \tag{121}$$

The control signal is compared with a periodic triangular pulse with a constant switching frequency, and then a PWM signal is produced controlling the IGBT switch.

The acceleration or deceleration of the generator is determined by the difference of the turbine torque T_{opt} and generator torque $T_{electric}$. If the generator speed is less than the optimal speed, the turbine torque is larger than the generator torque and the generator will be accelerated. The generator will be decelerated if the generator speed is higher than the optimal speed. Therefore, the turbine torque and generator torque settle down to the optimum torque point at any wind speed. The rotor acceleration is be made zero when the power extracted from the wind, less drivetrain losses, is equal to the electric power output of the generator.

This relationship is described by Equation 122 in terms of torque.

$$\frac{d\Omega}{dt} = \frac{(T_{rotor} - T_{electric})}{J} \tag{122}$$

The rotor acceleration ($\frac{d\Omega}{dt}$) is inversely proportional to the inertia of the rotating system, essentially the rotor inertia (J), and directly proportional to the difference between the torque applied by the wind (T_{rotor}) and the electric torque of the generator ($T_{electric}$) [192].

In the region II, we want the generator torque to be equal to the rated torque at the rated speed. This region must be inserted depending linearly on the rotor speed. It starts at a rotational speed Ω_1 and reaches the rated torque at or slightly below rated speed Ω_2 [193]. The generator torque in this region can be expressed by the following equation:

$$T_g = Q_1 + \frac{Q_{rated} - Q_1}{\Omega_2 - \Omega_1} \cdot (\Omega - \Omega_1) \tag{123}$$

Where Ω is the rotor speed, Q_1 is the generator torque at the rotor speed in which this region starts (Ω_1), Q_{rated} is the rated torque, and Ω_2 is the rotor speed at which the rated torque reached.

The region II of the power curve is illustrated in figure 67.
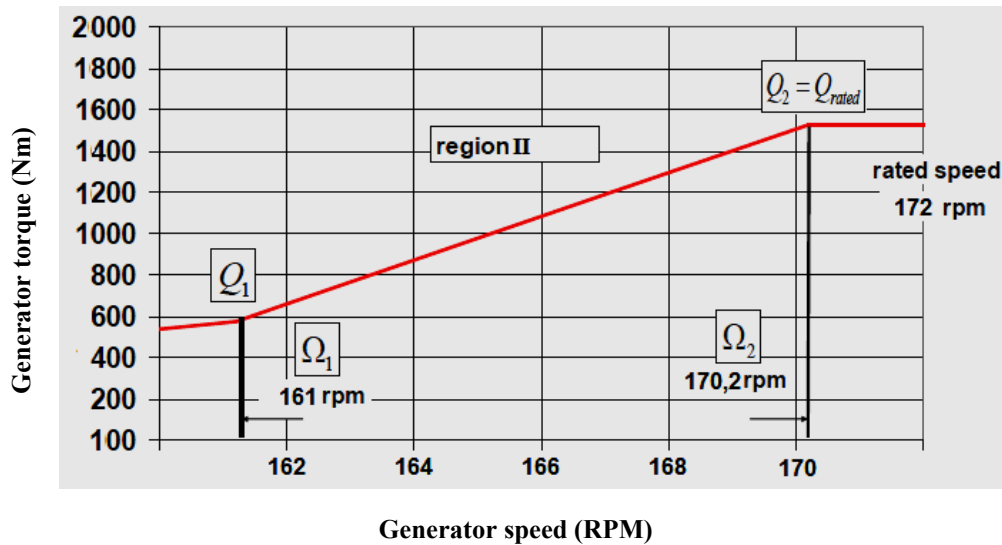
Figure 67: Details of the region II in the wind turbine power curve

For example considering figure 67, if the generator operating at point 'A' and wind speed increases from V1 to V2 (point B), the additional power and hence torque causes the generator to accelerate. The accelerating torque is the difference between the turbine mechanical torque and the torque given by the optimum curve. Finally, the generator will reach the point 'B' where the accelerating torque is zero as shown in figure 68. A similar situation occurs when the wind velocity decreases.
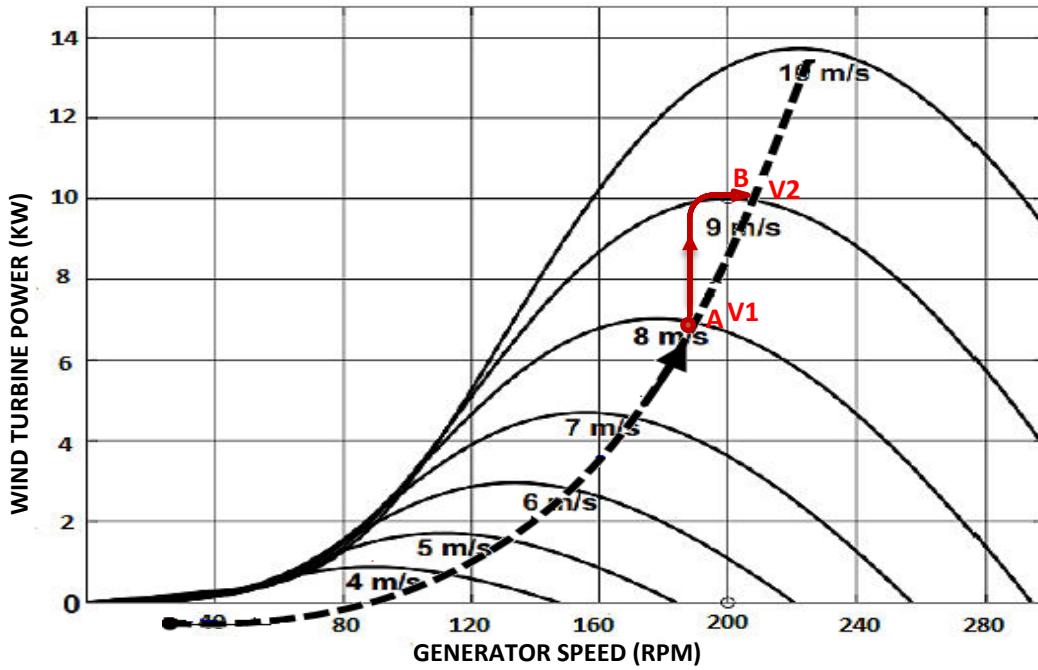
Figure 68: Power output as a function of generator rotational speed

This control method will be used in the present design by including its design parameters in the primary input file of the FAST code. Table 41 summarizes the inputs parameters in the turbine control section of the primary input file.

Parameter	Description	Value
VSContrl	Variable-speed control mode {0: none, 1: simple VS, 2: user-defined from routine UserVSCont, 3: user-defined from Simulink/Labview} (switch)	1
VS_RtGnSp (rpm)	Rated generator speed for simple variable-speed generator control [used only when VSContrl=1]	170.27
VS_RtTq (Nm)	Rated generator torque/constant generator torque in Region 3 for simple variable-speed generator control [used only when VSContrl=1]	610.71
VS_Rgn2K (Nm/RPM²)	Generator torque constant in Region 1 for simple variable-speed generator control [used only when VSContrl=1]	0.0206
VS_SlPc (%)	Rated generator slip percentage in Region 2 for simple variable-speed generator control [used only when VSContrl=1]	74.38

Table 41: Design parameters of the variable speed control in FAST

In the FAST simulation, the rated generator torque was chosen to be equal to Ω_2 (170.27) instead of the rated speed of 172 RPM. Actually FAST does not distinguish between rated generator speed and Ω_2, the end point of the region II is set using a linear interpolation. For small differences between these two values, this should not be a serious limitation.

5.7 Wind turbine brake system design

Generally, small wind turbines are exposed to high wind conditions, and eventual damage may be caused when the design limitations are exceeded. Without an appropriate control mechanism, the wind turbine generator could speed up immensely, presenting its full swept surface area to enormous forces (e.g. high thrust). The combination of these forces can easily damage, if not destroy the whole system. For this reason, special attention must be paid to the design of the wind turbine safety system in order to avoid any failure of this particular component, which, in turn, can lead to catastrophic consequences. Therefore, an appropriate design of the safety system is a major factor to be considered in order to achieve safe and efficient operation of the small wind turbine system.

5.7.1 Safety system control strategy

The used control strategy for the small wind turbine safety system has to meet several requirements. In the present design process, these requirements are specified in accordance with the IEC standard for small wind turbines (**IEC 61400-2**). The technical requirements that have been identified in this study are summarized in the following points:

- Safety system should be independent and can operate independently of the wind turbine operating conditions (e.g. the microcontroller should be powered despite of any eventual failure of the system);

- Safety system must limit the rotational speed (rotor and generator) and ensure power production within the limited design condition for all load cases;

- Safety system must operate automatically;

- Safety system must protect the wind turbine from single failures or fault of any component as well as from faults in load connection;

- Additionally to the automatic control and protection, the safety system should provide a manual emergency stop;

- Safety system must be able to block the rotor whenever it is necessary, within a short period of time (typically from 0.01s to few seconds as mentioned in IEC standard);

In order to fulfill all the above mentioned requirements, the small wind turbine must be equipped with a safety system which features the following components:

• **An aerodynamic brake which essentially consists of passive stall power control of the wind turbine blades**. Normally, the small wind turbine has its blades designed so that when wind speeds are high, the rotational speed or the aerodynamic torque, and thus the power production, decreases with increasing wind speed above a certain value. The decrease in power with increasing wind speeds is due to aerodynamic effects on the turbine blades. The

blades are designed so that they will perform worse (in terms of energy extraction) in high wind speeds to protect the wind turbine without the need for active controls **[194]**.

• **An electrically released fail safe brake (e.g. permanent magnet brake or a caliper brake)**. The rotor brake controls overspeed and provides parking and emergency braking. Caliper brakes are an example of the brake systems that can be used in small scale wind turbines. The brake is usually mounted as close as possible to the shaft. When no current is flowing in the coil, the rotor is broken by two compression springs squeezing the brake pads and the brake rotor together. Friction between the pads and rotor slows the disc down. When current flows into the core, it counteracts the piston force, pulling the brake pads towards it, and the brake is released. A lot of friction is generated during braking, and this creates heat in the system. Therefore, the brake parts must be able to withstand high temperatures and should be exposed to air and be ventilated adequately. In addition, the used brake system should produce high torques at small dimensions of the disc. Due to the fact that the brake must operate automatically in installations that are largely unmanned, often in remote areas that make access for maintenance both difficult and costly, the selected brake should operate reliably in the most challenging environmental conditions (this means absolute reliability when located in sites in salt atmospheres or desert sites subject to dust) **[195]**.

The above two types of braking systems are necessary in the design system as the IEC standard for small wind turbine (IEC 61400-2) requires two independent braking systems, one of which is usually aerodynamic and the other of which is positioned in the drive train.

• **A monitoring system based on a microcontroller, powered by an independent source of energy (small battery) and equipped with input peripheral devices (mainly wind speed sensor, position sensor and voltage measurement devices).** The main task of the microcontroller is to actuate the emergency brake in case of a failure or fault of any component and to control the maximum power point tracker system (MPPT) which is used for a maximum energy extraction as described in section (5.6.3) of this report. A centralized control system including safety features and maximum power tracking will be more efficient and would results in a significant reduction in the cost. In order to ensure safe operating conditions to the stand alone small wind turbine system, the microcontroller has **three main program steps**:

➢ The first step consists in activating the brake system whenever the microcontroller cannot supply voltage on the power output for the brake e.g. due to an electrical fault, a programming fault or when the brake is disconnected from the turbine or battery.

➢ The second step consists in measuring the voltage at the battery and the battery controller. Based on these measurements, it can be determined if e.g. the battery is disconnected from the

turbine system or the battery controller suffers an electrical fault. In either of these cases, the emergency disc brake gets activated immediately. The case when the main battery is fully charged and disconnected from the generator shouldn't be taken into account in this step because it represents a normal operating situation. But the problem arises when the battery is fully charged (disconnected) and there is no connected load to the inverter. In this case, the wind generator becomes unloaded and starts to spin at high speeds. To avoid this situation, a dumping load box could be added to dissipate the extra power as heat.

➤ The last program step consists in measuring the rotational speed of the rotor and compares it to the maximum allowable overspeed value which represents the design limit of the turbine. If this value is exceeded, the emergency brake is engaged. The overspeed can be caused by a loss of the electrical load, a failure of the main shaft or a failure in the furling system.

If none of the three criteria mentioned above is true, the emergency brake of the turbine can be disengaged and hence the rotor is unblocked, in case the brake has been engaged before.

In order to satisfy the requirement of an uninterruptible power supply for the safety system, the power source of the microcontroller has also to be independent from the turbine generator. Hence, the system selectively operates from an external DC input (main battery) and an internal back up battery circuit: Firstly, the microcontroller is connected to its own battery circuit being able to maintain it in operational state for at least one day (uninterrupted power supply–UPS). Secondly, the microcontroller is connected to the main battery such that the controller can be fed from a second source. The choice on an autonomy of one day results from the assumption that this period is far enough for a situation without proper operation (e.g. no wind) with empty main battery. The microcontroller has its own load regulator to charge its own battery via the power from the main battery, converting the voltage (typically 24 or 48V) from the main battery to a suitable charging voltage via a Universal Battery Elimination Circuit (UBEC).

As a microcontroller board for the current project, a microcontroller from ARM Cortex M4 family, Arduino or a DSP 1103-1104 controller board can be chosen. They are relatively cheap and can fulfill all the required safety functions. These microcontrollers have a wide range of high-performance analog and digital inputs which can be used to measure the rotor rotational speed, voltage and other required input signals.

➤ **An emergency stop function:** this represents an interrupt function which interrupts the program flow of the microcontroller which is become activated once a certain input signal reaches a certain value, independently of the current step of the main program the controller is running. This ensures that whenever the emergency stop button is pressed, the emergency disc

brake will be activated immediately. This function is initiated by a single human action using a manual button to block the wind turbine generator.

➢ **A furling system:** for this system, the braking is achieved by mechanically furling the wind turbine, which turns the nacelle away from high wind speeds directions. This control system uses the upwind rotor configuration with a tail fin for passive yaw control. Typically, the tail fin is hinged, allowing the rotor to furl (turn) in high winds, providing both power regulation and over-speed protection. The furling system should start to act whenever the wind speed becomes higher than the cut-out wind speed (15 m/s in the case of this project). In case the furling system fails (e.g. due to blocking of the furling tail fin by ice), the emergency brake is activated by the microcontroller at the maximum allowable rotor speed as described above.

Another option widely used in small wind turbine braking systems is the electrodynamic braking. This is a method that involves short-circuiting the generator stator windings. A short-circuit results in a large back-torque whose magnitude depends on the rate of rotation of the generator and the dimensions and configuration of the generator; two principal configurations are radial or axial flux designs. In general, turbine manufacturers that use electrodynamic braking expect that the magnitude of this back-torque, a negative quantity by convention, will be larger than the magnitude of the wind turbine rotor torque, positive by convention. The acceleration of the wind turbine rotor depends on the net torque: a net positive torque will cause the rotor to accelerate; a net negative torque will result in deceleration. The problem with this method is that in high wind speeds, the magnitude of the rotor torque will often exceed that of the back-torque at normal rates of rotation. In some cases, it will be impossible for electrodynamic braking to bring the turbine to a stop or even to slow it down. This results directly from the observation that the electrical generator has one peak short-circuit torque while the rotor has a different peak torque for every possible wind speed [196].

5.7.2 Rotor rotational speed measurement

The rotor rotational speed has a major influence on the safety system operation. Thus, a particular attention should be paid to its measurement. While the stator voltage frequency could be used to measure the rotational speed (as the voltage frequency ω_s is proportional to the shaft (or rotor) rotational speed ω : $\omega_s = \omega \cdot P_{pole}$, this solution still dependent on the drivetrain state. That is, if the shaft fails and the furling system fails to regulate the rotational speed in high wind conditions, the rotor blades could experience high centrifugal forces that may cause the blades to be detached from the hub and may result in damage to its environment. Therefore, measurements of the rotor speed should be attached as close as

possible to the rotor. The simplest solution consists in using a sensor for precise and reliable position measurements which will be located right after the first bearing. The same measurement will be used as an input signal for the control strategy of the maximum power extraction program.

5.7.3 Brake design requirements

In general, four main parameters should be taken into account when selecting a brake for a wind turbine [1]. These are the maximum braking torque, the brake response time, the total energy consumption, and the operating temperature of the brake disc.

The main task of a brake system in a wind turbine is to stop the rotor (or the generator) by exerting a torque in excess of what could plausibly be expected to originate from the rotor. Different standards recommend that a brake design torque should be equal to the maximum design torque of the wind turbine. The action time of the brake should be immediate, and should ramp up to full torque within a few seconds (from 0.01s to few seconds as mentioned in the IEC standard). The action time selected is a balance between instantaneous (which would apply a very high transient load to the drive train) and so slow that acceleration of the rotor and heating of the brake during deceleration could be of concern. Normally, the entire braking event, from initiation until the rotor is stopped, is less than five seconds [1]. Furthermore, the brake must be able to absorb all the kinetic energy in the rotor when turning at its maximum possible speed. It must also be able to absorb any additional energy that the rotor could acquire during the stopping period.

In order to fulfill the general safety requirements as described above, the turbine has to be protected against overspeed which can occur by different failures such as high wind speed conditions, loss of electrical load or failure of the main shaft. If one of these incidents occurs and the furling system fails to limit the rotor speed, the brake must get activated immediately. The brake is monitored by the microcontroller, which determines the overspeed conditions by a set of sensors. This solution has an advantage to be independent of any human intervention and covers all the requirements set in the IEC standard. However, the only disadvantage of the system is the continuously energy needed to keep the brake released.

5.7.4 Brake torque calculation

The braking torque level for the rotor brake is a crucial design parameter that must be determined during initial stages of a brake design. The maximum permissible braking torque on the rotor shaft is usually imposed by three main parts: the necessary torque to break down the inertia of the moving parts of the machine, the torque to break down the energy input of

the wind (or the aerodynamic torque) and the frictional resistance. Therefore, the braking torque is given by equation 124.

$$T_{B,total} = T_{B,friction} + T_{B,inertia} + T_{B,Aero} \qquad (124)$$

Generally, the effects of friction can be neglected. The aerodynamic torque (or the braking torque to break down the energy input of the wind) is calculated by assuming a maximum input power of 13.2 kW, which corresponds to the generator maximum overloading (about 120% of the generator rated power).

$$P_{input} = T_{B,Aero} \cdot \frac{2.\pi.\Omega}{60} \qquad (125)$$

Where P_{input} is the maximum input power, $T_{B,Aero}$ is the aerodynamic torque, and Ω is the rotational speed .

For a maximum power input of 13 200 W with a corresponding rotational speed of 183 RPM, the necessary torque to brake down the energy input of the wind is $T_{B,Aero} = 688.8$ N.m.

The inertia of the moving parts of the machine can be determined by the following method: It was assumed that a fault in the safety system or a furling delay leads to an overspeed condition reaching the cut-out wind speed (15 m/s in the case of this project) with a maximum rotor speed of $\Omega_{max} = 245.55$ RPM. The brake must completely stop the rotor during the first three seconds t=3s. This assumption is made in addition to IEC 61400-2 Load Case G to fulfill the customer's high safety requirements. Also, this response time ensures a complete shutdown of the system before the generator reaches the runaway point.

It should be noted that the calculation of the rotational speed for the given cut-out wind speed is based on the assumption that the wind turbine system operates at its maximum efficiency (at a constant tip speed ratio of λ=6) between the rated wind speed and the cut-out wind speed. With the calculated blade inertia of (given by the 3D design software SOLIDWORKS) J_B=42.33 kg.m2, the generator inertia of J_g= 1.2 kg.m^2 (which is given by the generator manufacturer), and an estimated inertia taking into consideration other hub components as spinner and shaft (given by the CAD software) J_O= 0.0225 kg.m², the total inertia is given by equation 126.

$$J_{total} = 3.J_B + J_g + J_o = 128.2 \text{ kg.m}^2 \qquad (126)$$

The brake torque, $M_{B,inertia}$, is calculated taking the angular velocity into account:

$$T_{B,inertia} = J_{total} \cdot \frac{2.\pi.\Omega_{max}}{60.t} \qquad (127)$$

The brake is activated once the overspeed limit has been triggered.

The required torque to break the rotor in 3 seconds is given by the following equation:

$$T_{B,total} = P_{input}.\frac{60}{2.\pi.\Omega} + J_{total}.\frac{2.\pi.\Omega_{max}}{60.t} = 1785.2 \text{ N.m} \qquad (128)$$

This torque can be lowered by assuming higher braking times. The calculated brake torque gives the range that the brake should be able to cover.

5.7.5 Brake system selection

Rotor brakes are operated either electrically or hydraulically. The selected brake for this project is a spring applied hydraulic brake (fail safe mode) which is designed for small scale wind turbines. This solution offers a cost effective solution for holding, static and/or emergency stops. Besides, it is characterized by high torques with low power consumption. Figure 69 shows an example of small wind turbines spring applied caliper brake. The brake disc is normally from steel [3]. This engages to prevent shaft rotation when electrical power is removed for any reason. When power is restored, the brake releases and stays in the off position.
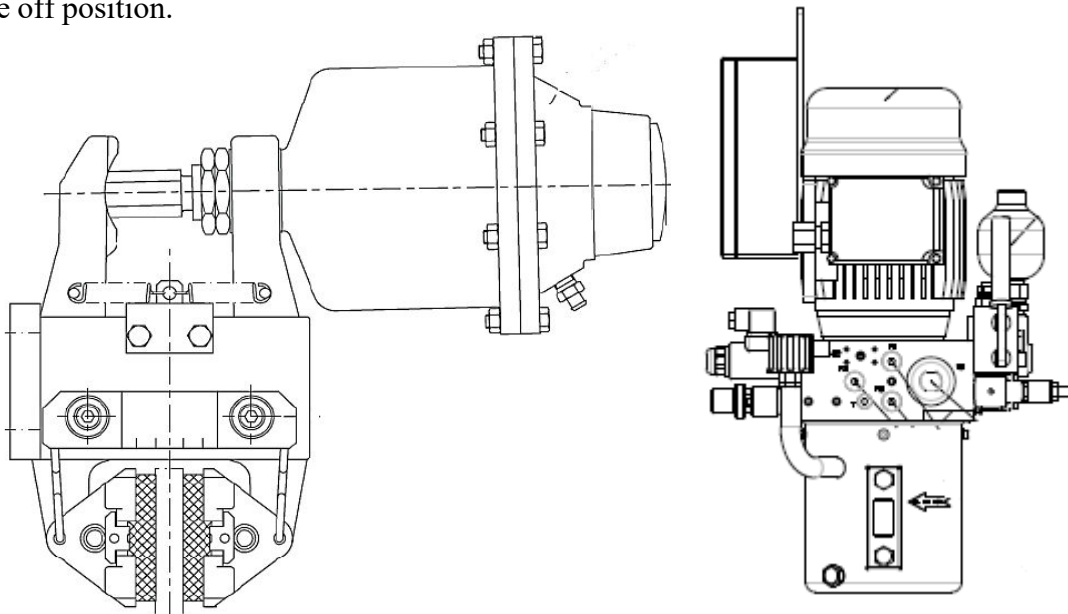
Figure 69: Spring applied hydraulic brake for wind turbine applications

5.8 Wind turbine furling system design and analysis

5.8.1 Furling type selection

The first objective of a furling system is to automatically force the wind turbine blades out of the direction of winds for which the wind speed ranges from cut-out speed to overspeed. A fully furled turbine blade, when stopped, has the edge of the blade facing into the wind (with a minimum surface area facing the wind, and then the turbine will not over-spinning). Furling happens without motors or special devices which make this solution cost effective and simple

to implement. It works because the rotor axis is offset from the furling axis. When the wind exceeds a determined force on the rotor, the rotor rotates around the furling hinge or pin, either vertically or horizontally. As the wind speed slows, the turbine rotor turns back into the wind. The other solution consists in using a blade pitch system. **This technology is not suitable for small wind turbines because of its cost, maintenance requirements, and for its complexity [41]**.

Two type of furling mechanism can be used in a small wind turbine system: horizontal and vertical. Vertical furling is achieved by moving the rotor upward. In high winds, the force of the wind tilts the rotor up, while the tail fin stays oriented downwind. This reduces the frontal area of the rotor and reduces its speed **[197]**. When the wind speed declines, the rotor returns to its normal position. This type of furling usually uses springs to control the wind speed at which the rotor begins to furl. That is, the wind speed at which the rotor begins to pitch back is governed by the tension of the spring. This furling system has a major disadvantage of increasing fatigue loads on the system as the rotor and the generator rock back and forth whenever the furling is activated. Gusty wind, for example, can cause the rotor to tip up, and then quickly rock forwards, dropping the rotor and the generator onto the wind turbine's frame, and severely striking the blades on the rotor main shaft **[198].** Additionally, since the entire system must tilt back with the blades, the output wiring can be exposed to repeated stresses if care does not taken in the design.

The simplest way of furling a small wind turbine is a horizontal system in which the turbine is yawed sideways away from the wind as high wind speeds are reached. According to Md. Arifujjaman et al. **[199]**, this solution is the most commonly used control method in small wind turbines. This system is simple to implement and has the advantage of combining the overspeed protection of the turbine with a system that controls the yaw of the turbine in accordance with the wind direction. In addition, this furling system does not need extra material like shock absorber and counterbalancing weight for dampening actions. **Therefore, the option of horizontal furling was selected for this project**.

The main disadvantage of a horizontal furling system is the effects of yaw error on the turbine power production. The yaw control system must be designed to minimize the yaw error (Δ_θ), which is defined as the angle between the turbine's axis and the wind direction **[200]**. This yaw error reduces the wind turbine output power by a factor of $Cos^2\theta$ **[41, 201]**, and its effect is significant even for moderate values of θ. The power loss proportional to the yaw angle is depicted in figure 70.
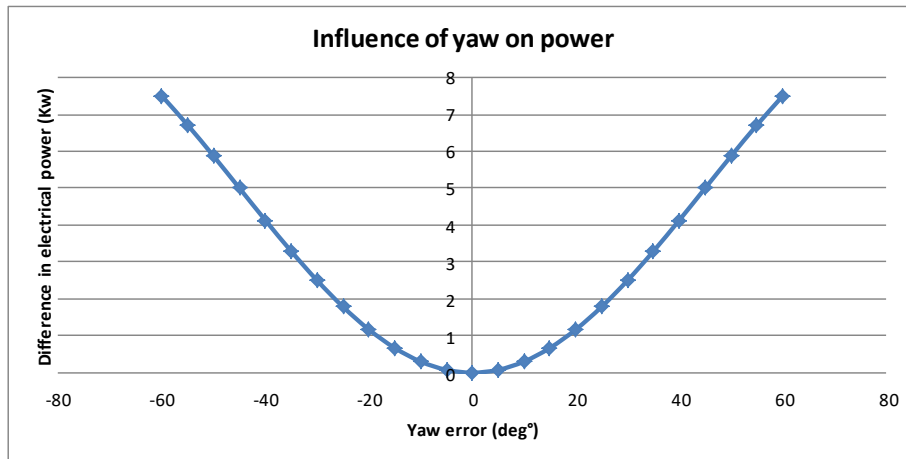
Figure 70: Influence of yaw error on wind turbine electrical power output

As shown in figure 69, a 20° yaw error reduces the power by a significant percentage of 12%. The load calculation which involves yaw error angle is cover by the IEC simple load model calculation (SLM-load case C which considers a single yaw error of $\Delta_\theta = 30°$).

5.8.2 Horizontal furling mechanism

In the case of a horizontal furling system, the wind turbine main frame is designed with a lateral offset. That is, the center of rotation of the blades is not on the same vertical line as the yaw axis around which the nacelle turns in order to face the wind direction: the tail fin is offset at an angle, and is hinged at the position where it joins the main frame. Generally, the horizontal furling operates according to two situations: in low and moderate wind speeds, the force of the wind on the blades tends to rotate the machine around the yaw axis. However, the tail fin resists to this rotation and keeps the rotor facing into the wind.

When the wind speed increases and reaches the cut out wind speed, the rotor thrust produces a high moment about the yaw axis. Furling occurs when the thrust force on the blades overcome the weight of the tail. At the cut-out wind speed, the rotor pivots relatively to the tail fin (at the articulating position in which it is hinged) with the effect of turning the rotor to face away from the prevailing wind direction. Consequently, the tail fin folds on itself and the blades end up facing the side at an angle to the wind, reducing the frontal area of the rotor. As the tip speed ratio is kept constant, the rotor rotational speed decreases and the system is protected from overspeed. When the wind speed is below the critical point, the tail drops back into normal configuration via gravity. Horizontal furling systems have the advantage to be nearly foolproof, with no mechanical components that can ice up, rust or fatigue.

5.8.3 Furling system design parameters

The geometry of a furling system is characterized by several parameters and angles as shown in figures 71 and 72. The distance L_1 describes the lateral distance between the yaw and the furling axis in the rotor plane, whereas L_2 is the distance between these two axes in the direction perpendicular to the rotor plane. L_3 is the distance between the furling axis and the center of gravity of the tail. L_4 and L_5, represent the distances of the center of mass of the rotor from the yaw axis measured perpendicular and parallel to the rotor plane, respectively. The angles β and V are, respectively, the backward tilt of the furling axis (for positive β values) and the lateral tilt of the furling axis.
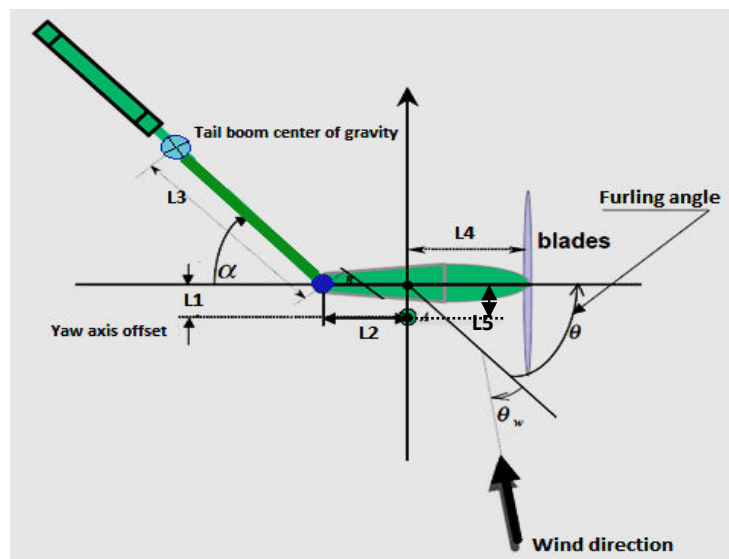
Figure 71: Top view of the small wind turbine furling system **[202]**
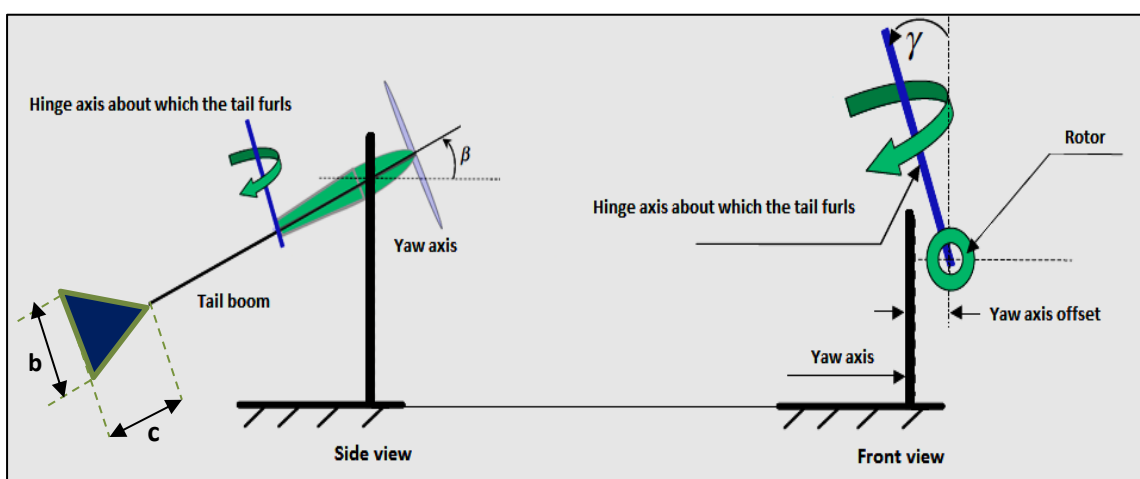
Figure 72: Side and front view of the small wind turbine furling system **[202]**

Etienne Audierne et al. **[203]** have conducted an analysis of the furling behavior of small wind turbines by using a model of the dynamics of gravity-controlled furling systems based on Lagrangian formalism. They found that the furling behavior is governed by several

parameters. The impact of the different design parameters on the onset and leaving the furling regime can be summarized by the following points:

- **Influence of the mass of the tail vane M$_{tail}$**

- The mass of the tail vane has a considerable influence on the onset of the yawing/furling regime, since it directly controls the gravity-induced restoring torque around the furling;

- The value of the tail mass is a convenient parameter for controlling the transition to the furling regime;

- For low values of the mass of the tail vane, the turbines starts to yaw at low wind speed values with linearly increasing onset wind speed values for increasing tail masses;

- The value of the tail mass has a linear effect on the onset of the furling regime and the return to normal operation;

- A hysteresis between onset and return to the unfurled position was observed, and the difference between the onset and return values is approximately constant for all tail mass values studied;

- **Furling characteristic time**

The furling characteristic time is defined as the time required (for the yaw angle to reach 90% of the final position) for the onset of furling. It was observed that the tail mass does not affect the furling time. It can be concluded that the dynamics of the transition is mostly determined by the yaw moment caused by the rotor thrust.

- **Influence of the tilt angle β**

- The tilt angle β is critically important for the transition to and from the furling regime;

- A marked asymmetry between the onset and the return situation has been identified;

- The return to aligned operation is critically dependent on the precise value of β;

- For negative values of β, corresponding to an inclination of the furling axis towards the rotor, the rotor practically jumps to the stop position, leaving little room for a continuous adjustment of the turbine output power. On the other hand, once the turbine has reached its yawed/furled position it is very difficult for it to return to unfurled operation. Clearly, such a large hysteresis is detrimental to energy capture;

- A slightly positive value of the tilt angle, which corresponds to a backwards leaning furling axis, not only reduces the hysterias between the onset of furling and return to normal operation, but also allows for a smoother transition between the two regimes, thereby allowing to consider the furling mechanism for continuous output power control;

- **Influence of the lateral inclination angle V̆**

- The lateral inclination of the furling axis has a less dramatic influence on the system behavior under stationary wind speed conditions;

- The impact of V is similar to the one caused by a varying tail mass, since a variation of V leads to an almost linear response of threshold values, with low values causing an earlier onset of yawing/furling and a smoother transition;
- A hysteresis occurs for switching between the two regimes, but this hysteresis depends little on the value of V chosen;

• **Influence of the transverse displacement L_1**

- L_1 measures the transverse displacement between yaw and furling axes and can assume both positive and negative values, with positive values corresponding to the rotor and the furling axis being on opposite sides of the yaw axis, while negative values indicate a position of the furling axis on the same side as the rotor center of mass;
- The effect of L_1 on the onset of yawing is generally small, even though the transition is somewhat smoother for positive values of L_1 as opposed to negative values. The return to normal operation is smoother than the onset and no qualitative difference is observed for negative and positive values of L_1;
- Negative values of L_1 will allow for a restoring torque and therefore a stable operation only if L_2 is sufficiently large. Otherwise, the torque produced by the aerodynamic forces on the tail vane will actually act in the same counterclockwise direction as the rotor torque. Note that for rotor initially aligned with the wind direction, a small rotation of the rotor around the yaw axis is required to take advantage of the lever distance L_2 which helps invert the sense of the vane torque and stabilize the system;

• **Influence of the longitudinal displacement L_2**

L_2 is the longitudinal distance between the yaw and the furling axis. Under normal conditions, where the tail vane and the rotor axis are essentially aligned, this distance basically adds to the distance L_3 between the furling axis and the aerodynamic center of the tail vane, therefore causing a similar effect as L_3 on the onset of yawing/furling.

• **Influence of the tail lever distance L_3**

- The value of L_3 has a critical importance in maintaining a simultaneous balance of the torques acting on both the yaw and the furling axes;
- For large values of L_3, the aerodynamic force acting on the tail vane causes a large torque for clockwise rotation around the yaw axis, requiring a large torque for counter-clockwise rotation caused by the rotor thrust in order for furling to occur;
- For small values of L_3, the rotor can be seen to stabilize at positive yaw angles even at small wind speeds. In this case, the torque formed by the rotor thrust and the lever L_1 is strong enough to overcome the pull from the tail vane and force both tail and rotor to settle on a rotated position;

- **Influence of the lever distance L_4**

- The lever distance L_4 is directly related with the torque caused by the aerodynamic thrust acting on the rotor. The appropriate choice of these values is critical to the design of a furling system;

- L_4 largely determines the torque under yawed conditions and therefore the return from the furling regime. The value of L_4 is important for the length of the transition regime and therefore the softness of the onset of yawing/furling;

- While for large values of L_4, an almost immediate transition to the stop position occurs, a continuous adjustment of the yaw angle as a function of steady-state wind speed is found for the case of smaller L_4 values.

- A hysteresis occurs for the return to normal operation, but as opposed to the effect of other design parameters the difference between the onset and return transitions is strongly dependent on the exact value of L_4;

- **Influence of the lever distance L_5**

- The transverse distance of the rotor center of mass from the yaw axis fully determines the rotor torque at zero yaw angles and therefore the onset value of the wind speed. It can be seen from figure 71 that this distance is similar to L_1, but viewed from rotor side;

- A hysteresis occurs for the return to aligned conditions, where the hysteresis values were observed to be lower than in the case of increasing wind speeds;

- For high values of L_5 an alignment error for low wind speeds occurs, being of the order of 20° for a value of 0.2 m;

5.8.4 Furling system design tips

The geometry of the furling system is a critical factor in having a wind turbine remains facing into the wind during normal and turbulent conditions. If not sized properly, the turbine will shift away from the core wind direction causing a drop in RPM and a loss of power.

According to the literature review, there are a few rules of thumb that are developed through many years of turbine design and testing and which can be used for a first guess at how to design a furling system and which can be summarized as follows:

- The offset between the furling and the yaw bearings should be at least $\frac{1}{12}$ the length of a single blade;

- The easiest way to establish the optimum tail vane area is to relate it to the sweep area of the wind turbine: The surface area of the tail fin should be between 5 and 10% of the rotor swept area;

- The tail boom length should be about the same length of one blade;

- The shape of the tail fin is not a big factor, but is it is better to keep the tail fin taller than its wide. A good rule of thumb is the tail height should be approximately twice the length in order to be the most effective. In general, an "arrow shaped" vane with a leading edge that sweeps rearward is a bit more effective. Usually a stronger driving factor is to establish a tail vane shape that matches the overall wind turbine look that is shooting for. Aside from being aesthetically pleasing, easily manufactured, and strong delta wings have favorable and well-known aerodynamic characteristics. **For this reason, the theory of tail fins is developed in terms of delta wing aerodynamics in the present design process**. The most notable feature of delta wings is their high stall angle, which in the context of a tail fin suggests high restoring moments on the turbine up to yaw angles of around 40°;

- The tail vane should be centered with the tail boom, with half the tail vane area above the boom and the other half below the boom;

- Metal is an appropriate material for tail fin. **Thus, the tail boom and the vane can be made from stainless steel or carbon steel with strong anti-corrosion performances**. The shape and the structure of the tail vane should reduce vibration in the tail boom, and resist to failure cracking;

5.8.5 Furling system design

In order to summarize all the above mentioned considerations in a roadmap useful for the design of furling systems: three of the design parameters, β, L_4 and L_5 have more pronounced effect on the overall patterns for transitioning to and from the furling regime, whereas the other parameters (m_{tail}, V, L_1, L_2, and L_3) can be used to adjust the wind speed values for the onset of furling and the return to unfolded operation as they have little effects on the transition system.

The most important step in this design process of the furling system is the determination of the furling (or the onset for furling) point at which the system starts to folds up. The wind speed at which the tail fin begins to rise depends on a number of factors which can be summarized as follows [204]:

- The lateral distance between the yaw axis and the rotor axis of rotation L_5;

- How far forward the yaw axis the blades are mounted L_4;

- The angle of the tail boom V;

- The size of the tail fin;

- The weight of the tail assembly;

The main objectives that have been identified for the design of the furling system in this project are:

- Well-defined furl-in wind speed of 15 m/s;

- Low hysteresis between furl-in and furl-out speed;

- Low oscillation of the system to prevent high rotor and shaft loads;

- Low yaw angle error to prevent high power loss;

Based on the previous aforementioned considerations, the following steps were used to determine the geometry of the furling system:

• **Estimate the values of β, L_4, and the Lateral tilt of the furling axis V:** As mentioned previously in the nacelle cover design section, the center of gravity of the system will be shifted downstream with an angle of **β=5°**. This backward title angle was chosen on purpose to increase the inertia of the nacelle with respect to the yaw axis. The value of L_4 was fixed when the blades tip clearance was discussed (section of tip clearance). In order to ensure that the blade will never hit the tower even under worst conditions, a value of **L_4= 0.6 m** was selected. Regarding the value of lateral tilt angle of the furling axis, a small value of **V=8°** was selected since low values of V cause an earlier onset of yawing/furling and a smoother transition.

• **Estimation of the rotor thrust:** the wind thrust on the wind turbine rotor which provides a part of the yawing moment is given by equation 129:

$$F_{thrust} = \frac{1}{2}.\rho.C_T.A.V_y{}^2 \tag{129}$$

Where C_T is the thrust coefficient, which taken as 0.5 and **A** is the swept area of the turbine blades. If Δ_θ (yaw error) denotes the angle between the wind direction and the rotor axis, the effective wind speed in the equation 129 can be thought of as given by:

$$V_y = V.\cos\Delta_\theta \tag{130}$$

Therefore the rotor thrust can be expressed as follows:

$$F_{thrust} = \frac{1}{2}.\rho.C_T.A.(V.\cos\Delta_\theta)^2 \tag{131}$$

• **Choose L_1, L_2, L_5, and A_{tail} (the surface area of the tail vane), using the equilibrium condition around the yaw axis and assuming a constant yaw error of $\Delta_\theta = 8°$:**

The equation of the equilibrium of moments around the yaw axis is given by the thrust force F_{thrust} and the moment induced by the aerodynamic lift and drag applied on the furling tail, M_T, both depend on the wind speed V_{wind} and the yaw error angle Δ_θ:

$$F_{thrust}.L_5 + M_T = 0 \tag{132}$$

The tail aerodynamic yaw moments is given by equation 133.

$$M_T = \frac{1}{2}.\rho.V^2_{wake}.A_{tail}.\{L_1.[\cos \Delta_\theta.C_D - \sin \Delta_\theta.C_L] - (L_{ac} + L_2).[\sin \Delta_\theta.C_D + \cos \Delta_\theta.C_L]\}$$

(133)

Where L_{ac} is the distance between the yaw axis and the aerodynamic center of the tail. Theoretically, the center of pressure on a delta wing is $2c/3$ from the apex. C_L and C_D are the lift and the drag coefficients of delta wing tail vane respectively.

As the location of the tail fin is in the rotor wake, the lift and the drag forces will change due to the changing wind direction and speed [41]. One assumption is that the tail fin is located in the ''near wake'' region of the rotor wake, so that, V_{wake}, the wind speed experienced by the tail is:

$$V_{wake} = V.(1 - a)$$

(134)

In order to determine the value of the wind speed V_{wake}, we assumed an optimum turbine operation. That is, the axial induction factor is given as a = 0.33. Therefore, equation 133 becomes:

$$M_T = \frac{1}{2}.\rho.(0.67.V)^2.A_{tail}.\{L_1.[\cos \Delta_\theta.C_D - \sin \Delta_\theta.C_L] - (L_{ac} + L_2).[\sin \Delta_\theta.C_D + \cos \Delta_\theta.C_L]\}$$

(135)

Polhamus et al. [205,206] have derived the following equations for the lift and the drag coefficients of delta wings:

$$C_L = K_p.\sin \alpha.\cos^2 \alpha + K_v.\cos \alpha.\sin^2 \alpha$$

(136)

$$C_D = C_L.\tan \alpha$$

(137)

Where α is the apparent angle of attack of the flow as seen by an observer attached to the tail. K_p, K_v are the coefficients that depend on the aspect ratio $AR = \frac{2.b}{c}$. In the case of this project, an aspect ratio of 4 is chosen. The corresponding values of K_p and K_v are 3.4 and 3.45 respectively.

By substituting $\mathbf{F_{thrust}}$ and $\mathbf{M_T}$ by their expressions in the equation 132, the equilibrium of moments around the yaw axis, which is used to determine the aforementioned design parameters, is given by:

$$C_T.A.\cos^2 \Delta_\theta.L_5 + 0.67^2.A_{tail}.\{\{L_1.[\cos \Delta_\theta.C_D - \sin \Delta_\theta.C_L] - (L_{ac} + L_2).[\sin \Delta_\theta.C_D + \cos \Delta_\theta.C_L]\} = 0$$

(138)

- **Choose L_3 and m_{tail}, using the equilibrium moments around the furling axis and assuming a constant yaw error of $\Delta_\theta = 8°$:**

As gravity is chosen as the restoring force (in case of a gravity controlled furling system), the equilibrium of moments around the furling axis is derived from the gravitational force of the tail fin and the aerodynamic force induced by the wind on the furling tail.

This equilibrium moment gives a solution of the furl-in wind speed, V_{furl}, at which the small wind turbine start to turn away from prevalent wind direction:

$$V_{furl} = \sqrt{\frac{m_{tail}. \, g. \, L_3. \sin V. \cos \beta}{\frac{1}{2}. \rho. \, A_{tail}. \, L_{ac}. \cos \beta . (C_L. \cos \Delta_\theta + C_D. \sin \Delta_\theta)}} \qquad (139)$$

Since the furl-in wind speed was previously defined as the cut-out wind speed (which is given as **V_{furl} =15 m/s**), equation 139 can be used to determine the required tail mass for which the system starts to furl at the desired wind speed. Keeping in mind all the above mentioned considerations, table 42 summarizes the values of the furling system design parameters:

parameter	Value	Explanation
Distance between yaw and furl axis – L_1	**0.085 m**	-
Longitudinal distance between the yaw and the furling axis – L_2	**0.4 m**	- The longitudinal distance has less influence on the furling system operation – Small values will reduce the nacelle material costs
Distance between the furling axis and the center of mass of the vane – L_3	**1.64 m**	- This value is set on the basis of the equilibrium conditions around the yaw axis
Distance between the yaw axis and the rotor center of mass L_4	**0.6 m**	- This value is determined in the section of tip clearance design and analysis
Distance between the yaw axis and the rotor center of mass L_5	**0.085 m**	- Low values of L_5 avoid an alignment error for low wind speeds
Backward tilt of the furling axis β	**5°**	- This value was set in the section of nacelle cover design - Slightly positive value of β reduces hysteresis and allow a smooth transition between onset and return regime
Lateral tilt of the furling axis V	**8°**	- The value of this design parameter is fixed on the basis of previous experiences - Low values cause an earlier onset of yawing/furling and a smoother transition
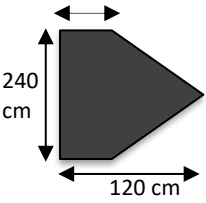
Tail boom dimensions and weight	$M_b = 68$ Kg 270 cm x 60 cm x 30 cm	- These values are fixed on the basis of literature review and previous experiences - Tail boom will be made from structural steel **EN 10025-5:2004 S 235J0W** (atmosphere corrosion resistance steel which is a steel with improved atmospheric corrosion resistance)
Tail fin dimensions and weight	$M_V = 20$ Kg 240 cm x 120 cm x 40 40 cm**cm** 240 cm 120 cm	- The weight of the tail assembly, **88 Kg**, is evaluated on the basis of the required wind speed for the onset for furling - The dimensions, on the other hand, are set on the basis of the equilibrium around the yawing axis - Tail boom will be made from structural steel **EN 10025-5:2004 S 235J0W** (atmosphere corrosion resistance steel which is a steel with improved atmospheric corrosion resistance)

Table 42: Values of the furling system design parameters

It is worth noting that most of these design parameters will be defined when the frame is welded together, and can be determined by trial and error. Therefore, the value of some furling design parameters (especially the mass of the tail vane) could be adjusted after the final assembly of the system to account for calculation and manufacture errors.

5.9 Wind turbine yaw mechanism design

5.9.1 Yaw bearing type selection

The yaw bearing is the component that supports the nacelle weight in a horizontal axis wind turbine. It is located between the rotating nacelle and the stationary tower and transmits wind loads from the nacelle to the tower. The yaw bearing is the most crucial and cost intensive component of a yaw system of modern horizontal axis wind turbines. This component must cope with enormous static and dynamic loads and moments during normal operation of a small wind turbine. Also, it must provide smooth rotational characteristics for the orientation of the nacelle under all wind conditions. Furthermore, its materiel must be corrosion and wear resistant and extremely long lasting while being cost effective. In most small wind turbine systems, free yaw is used because of its simplicity, reliability and for its cost effectiveness. In free yaw systems, there is nothing more than the yaw bearing. Some other wind turbines, however, include a yaw damper. This is used to slow the yaw rate, helping to reduce gyroscopic loads, and they are most useful for machines that have a relatively small polar moment of inertia about the yaw axis [1]. The tower head bearing in most cases consists

of large ball bearings with internal or external gears designed as a four point bearings, either single or double [3]. The main requirements that the yaw bearing must fulfill are increasing the turbine reliability even in harsh environments, extending seal and bearing service life, reducing operation and maintenance costs and reducing installation and replacement time.

When selecting a yaw bearing for a small wind turbine, the most factors that must be considered are running accuracy, magnitude and direction of loads (this is the factor that determine the size of the bearing to be used), permissible operating temperatures (generally the permissible operating temperature typically ranges from –25 to +70°C), vibration (small wind turbine operation is subjected to vibrations), operating speed, and sealing (the selection of a seal is vital to the performance of a yaw bearing as it provides the required protection against moisture and contaminants and a reliable retention of the lubricant).

In order to fulfill all the above mentioned requirements, four-point contact ball slewing bearing, from SKF Company, is selected for this design process. This type of yaw bearing is a common technical solution that has been used by many wind turbine manufacturers as it offers low turning friction and smooth rotation of the nacelle. The slewing yaw bearings can accommodate axial and radial loads, as well as moment acting either singly or in combination and in any direction. Besides, they are able to withstand heavy and shock loads that can vary in magnitude and direction.

5.9.2 Yaw bearing design

The size of the yaw bearing is based on the dynamic and static load ratings, which are related to the applied loads and the requirements regarding reliability and service life. Values for the axial dynamic load rating, C, and the axial static load rating, C_0, are given by the bearing manufacturer. The loads and moments acting on the yaw bearing from the inherent weight of the nacelle, and from the radial force (which is generated by the wind thrust) can be calculated assuming the conditions shown in figure 73.
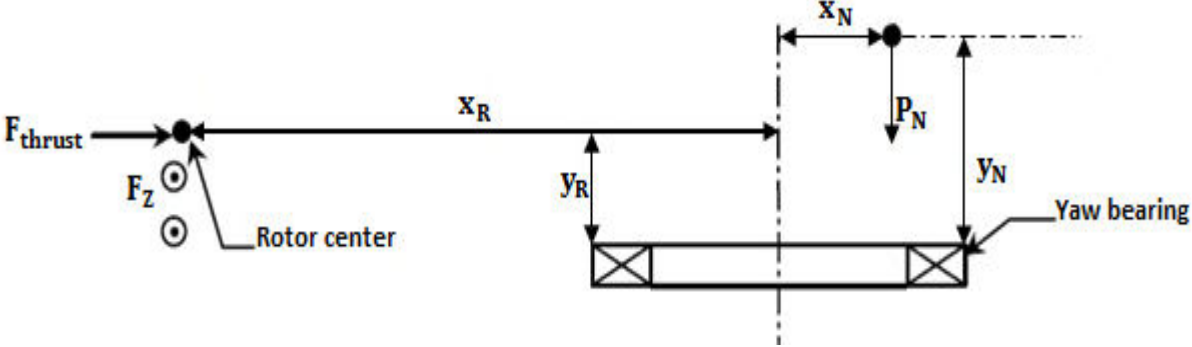
Figure 73: Loads and moments acting on slewing bearing [207]

Where P_N is the weight of the nacelle, y_N is the vertical distance to the nacelle center of gravity (c.o.g), x_N is the horizontal distance to the nacelle c.o.g, y_R is the vertical distance to the rotor c.o.g, x_R is the horizontal distance to the rotor c.o.g, and F_Z is the side force on the rotor and nacelle.

The radial load, in the case of the current study, is taken as the maximum rotor thrust. This load case is taken from IEC 61400-2 load case H (Parked Wind Loading) and considers the thrust force caused by the wind loading on the blades of a parked wind turbine:

$$F_{thrust} = \frac{1}{2}.N.C_d.\rho.U_{e50}^2.A_{proj,B} = 4.102 \text{ KN} \tag{140}$$

The wind force acting on the nacelle side is given by:

$$F_Z = \frac{1}{2}.C_{ST}.\rho.U_{e50}^2.A_{proj,N} = 1.35 \text{ KN} \tag{141}$$

Where C_{ST} is the nacelle side-on force coefficient which is taken as 1.5, and $A_{proj,N}$ is the projected area of nacelle (side-on) which is taken as 0.535 m². The resulting loads and moments acting on the bearing can be estimated, using following equations:

$$F_r = \sqrt{F_Z^2 + F_{thrust}^2} = 4.31 \text{ KN} \tag{142}$$

$$F_a = M_{tt}.g = 4.68 \text{ KN} \tag{143}$$

Where M_{tt} is the nacelle mass (including the rotor blades) which is taken as 478 Kg and g is the acceleration due to the gravity (m/s²).

$$M_{tilt} = \sqrt{M_1^2 + M_2^2} = 1999.49 \text{ Nm} \tag{144}$$

Where

$$M_1 = F_Z.y_N + F_a.L_1 + Q_{design} = 1691.3 \text{ Nm} \tag{145}$$

$$M_2 = F_{thrust}.0.26 = 1066.52 \text{ Nm} \tag{146}$$

As the resulting axial bearing load and the magnitude of the tilting moment are determined, it is now possible to determine the size of the slewing bearing by using the static limiting load diagram, which gives the relationship between the maximum rated tilt moment and the maximum rated axial load [144]. In using the static limiting load diagram, the applied loads and moments should consider the type and mode of operation of the machine. The operational requirements regarding service life and reliability can be considered by multiplying the resulting axial load and tilting moment (in equations 143 and 144) by a load factor F_L which is taken as **1.7** in the current study [144]. Therefore, the maximum rated axial load and the maximum rated tilting moments are given by:

$$F_{ar} = F_a.F_L = 7.95 \text{ KN} \tag{147}$$

$$M_{tr} = M_{tilt}. F_L = 3399.1 \text{ Nm} \qquad (148)$$

The static limiting load diagram contains two curves per bearing (figure 74); the solid line shows the raceway capacity, which is defined as the maximum static load that can be accommodated by the slewing bearing without detrimental effects on its running behavior, and the dotted line shows the bolting capacity, which gives the strength of the bolts used to bolt the bearing to its supporting structure. The points where the plotlines of rated axial load F_{ar} and the rated tilting moment M_{tr} intersect must always be below the capacity curves.

1) Not suitable, insufficient bolting capacity
2) Meets the requirements
3) Not suitable, insufficient raceway capacity

M_{tr} (Nm)

F_{ar} (N)
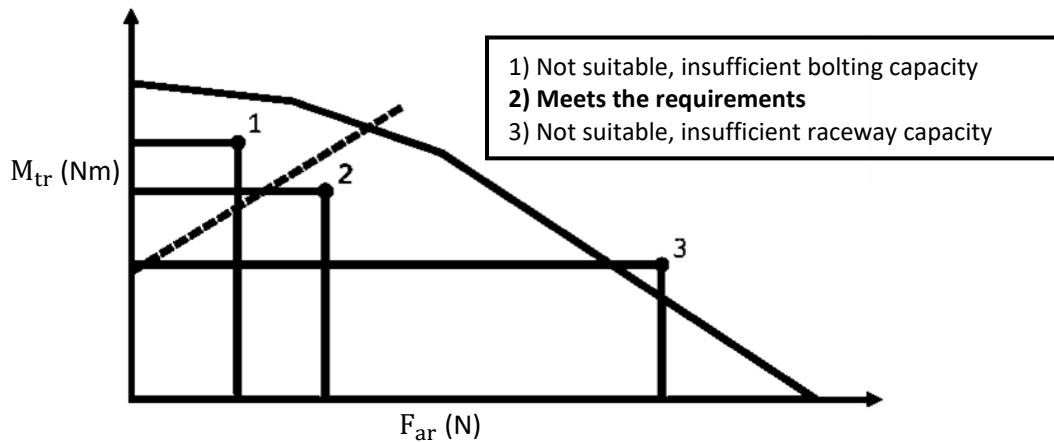
Figure 74: Static limiting load diagram for slewing bearing selection **[207]**

Based on the maximum rated axial load, F_{ar}, and the maximum rated tilting moment, M_{tr}, a **four-point contact ball slewing bearing without a gear is selected as a solution for this wind project application.** This type of slewing bearings features a good combination of load carrying ability and speed capability. Also, it provides a cost-effective solution for light to medium-duty arrangements that do not require high precision. Schematic of the selected slewing yaw bearing is shown in figure 75.
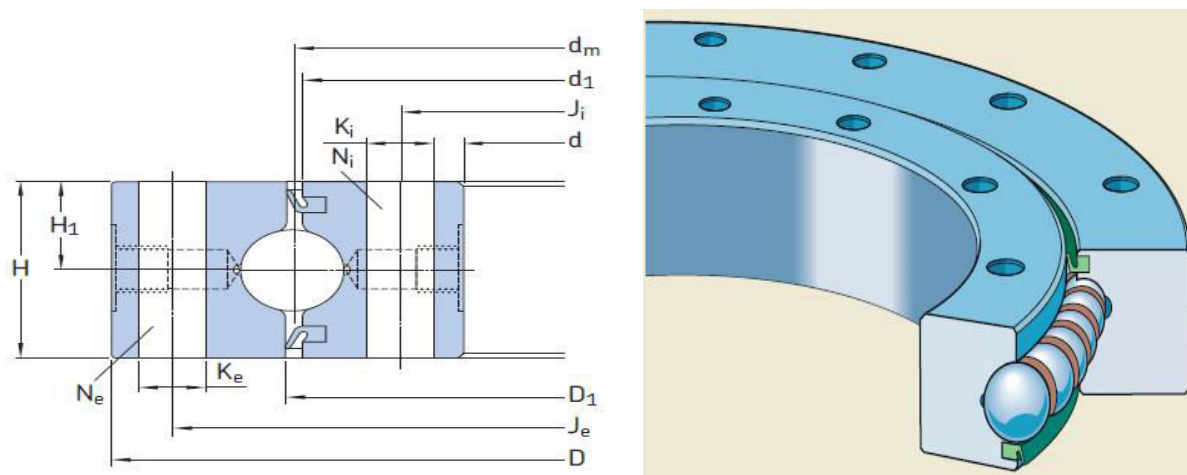
Figure 75: Geometry of the medium size four-point contact ball slewing bearing **[207]**

Tables 43 and 44 give the dimensions and the basic load ratings of the selected slewing yaw bearing, respectively:

Dimensions					Attachment bolt holes Outer ring			Inner ring			Mass
d_m	D	D_1	d	d_1	H	H_1	J_e	K_e	N_e	J_i	Kg
mm					mm		-	mm		-	
179	234	180	125	178	25	12.5	214	11	24	144.5	6

Table 43: Dimensions of the medium size four-point contact ball slewing bearing

Basic load ratings	
Axial dynamic load C (KN)	**Axial static load C_0 (KN)**
80	280

Table 44: Load ratings of point contact ball slewing bearing

As shown in figure 74, the inner and outer rings have a standardized number of equally spaced holes that allow the bearing to be bolted directly to the nacelle frame and the tower supporting surface. To facilitate proper functioning of a slewing bearing arrangement, the support structure of the tower must be sufficiently strong and rigid. Additionally, the flatness of the support surfaces must be within defined limits. In the case of the present design process, the tolerance of the overall flatness, in a circumferential direction of the tower support surface, is limited to:

$$t_c = \frac{d_m + 1000}{10000} = 0.117 \text{ mm} \tag{149}$$

Where t_c is the maximum permissible deviation from flatness, and d_m is the mean raceway diameter of the bearing. The flange must support the bearing ring across its entire side face and the thickness of the support flange (tower and nacelle frame, in figure 76) should be in accordance with the following guideline value:

$$S \geq 0.05 * d_m = 8.95 \text{ mm} \tag{150}$$

The requisite minimum wall thickness (figure 76) of the structure can be estimated using:

$$S_1 = 0.35 * S = 3.5 \text{ mm} \tag{151}$$
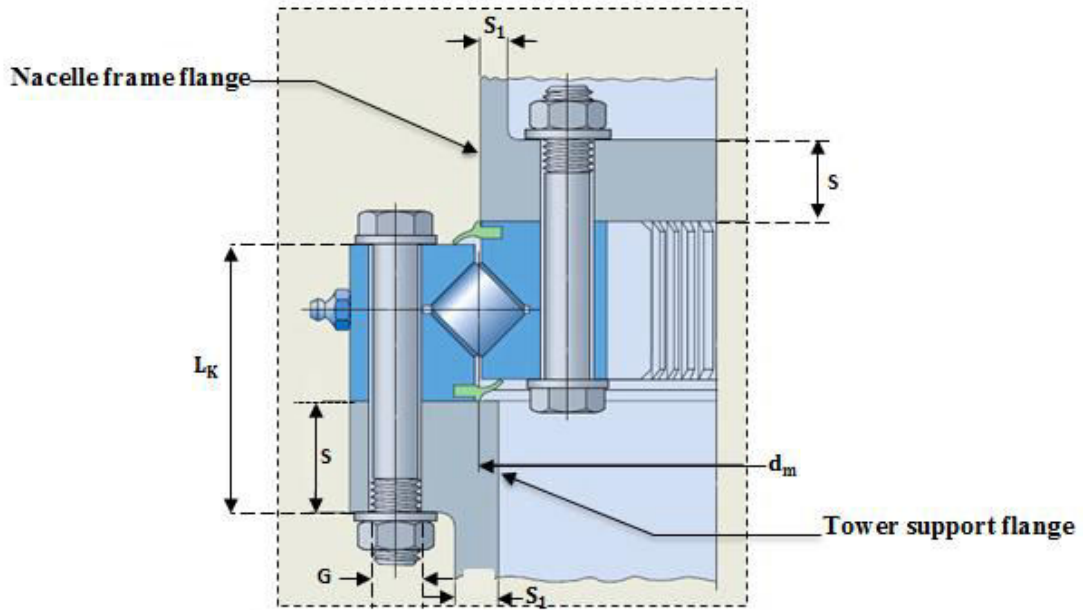
Figure 76: Support flange and wall thickness

Where S_1 is the wall thickness of the structure, S is the thickness of the support flange, d_m is the mean raceway diameter of the bearing. Regarding the attachment bolts, hexagonal head bolts in accordance with DIN EN ISO 4014:1999 in the 10.9 strength grade (EN ISO 898) are suitable for securing slewing bearings to their support structures **[208, 209]**. **The minimum clamp length of bolted joints (figure 76) should be:**

$$L_K = 5. G_b = 55 \text{ mm} \tag{152}$$

Where L_K is the minimum length of the bolt joint in mm, and G_b is the bolt thread diameter in mm. For the 10.9 bolts and nuts class, **hardened or quenched and tempered flat washers** will be used beneath the bolt head and nuts. This avoids excessive surface pressure on the support surfaces. In order to improve the efficiency of the yaw mechanism, the slewing bearing is normally equipped with a seal mechanism which prevents solid contaminants and moisture from penetrating into the bearing. A second protection can be ensured by the faired tower section, which is a part of the nacelle cover, and which encases the position of the tower/nacelle connection.

5.10 Conclusion

Chapter five was devoted to the design of the nacelle compoenents. Throughout this chapter, a detailed design and analysis of the rotor components (rotor hub and front nose cone), nacelle structure (main frame and nacelle cover), drive train components (main shaft, shaft coupling, and main shaft bearings), generator and safety system (Generator and brake system), yaw system (yaw bearings) and furling system (tail fin and tail boom) were presented.

The conceptual design in this chapter was based on a trade-off between technical and economic considerations. Some considerations that have been taken into account include the cost-effectiveness of the turbine components, the structural stability of the system, the strength and rigidity of the components, the visual aesthetics of the turbine's nacelle, the efficient manufacturing methods and the aerodynamic considerations for the design of some nacelle components (nacelle cover design for example). The final part of the present chapter discussed two major aspects of the wind turbine operation which are the wind turbine operation mode and the wind turbine control strategy for maximum power extraction. A particular attention was given to this subsection since the major goal of a wind turbine control strategy is to optimize the power production: below the rated wind speed, the goal is to maximize energy production, and above rated wind speed the goal is to limit the power production.

CHAPTER 6: TOWER DESIGN AND ANALYSIS

The tower of a wind turbine has a structural support function. The main function of this component is to provide strength to the entire system while carrying the weight of the wind turbine (the nacelle and the rotor blades). Generally, lattice and guyed-towers are the most common types, but the widespread deployment of grid-connected small turbines has led to monopoles taking over, largely because they do not need guy-wires [41].

Basically, lattice towers come in two different types: those made from steel angle or other sections which are assembled on site and tubular lattice towers that are pre-fabricated in sections. Lattice towers are manufactured using steel welded profiles. The main advantage of lattice towers is their low prices as they require only half the material used for tubular towers with similar stiffness. Furthermore, lattice towers are cheap to transport and easy to assemble on the site. However, the biggest drawback of this type of towers is their relatively short lifetime and corrosion that usually starts in the section joints. For guyed towers option, a large number of small wind turbines are built with narrow towers supported by guy wires. This tower shape reduces the material, and therefore the cost of the tower. The difficulty in getting access to terrain just around the tower is the main drawback of guyed towers. This disadvantage makes it unsuitable for farmlands. Another disadvantage is that the guyed towers are more vulnerable to vandalism, which could compromise the overall safety of the construction. For monopole towers, which are the most common type [3], they are manufactured in sections with flanges (or slip fitting option) at each end and bolted together on the site. These towers are tapered. That is, their diameter increases toward the base. This increases their strength and save material at the same time [210]. Monopole towers are well suited to farmlands. Also, their generic form can be analyzed without Finite Element Analysis, FEA. This solution has the disadvantages of being expensive to make and transport. **In a first stage of the present study, the tower design will be concerned with a multi-sectioned monopole tower with different thicknesses. The multi-sectioned option is used to reduce tower mass and cost.** The design of the other options (guyed and lattice towers) should be conducted, since the wind turbine system is normally manufactured and commercialized with all the three options. This gives the customer the possibility to select the wind turbine with the tower that meets his needs.

6.1 Optimum tower height and material

The productivity of wind turbines (the power output or the annual energy production) is strongly dependent on the wind sources. These latter can vary significantly with the tower

height. Therefore, determination of an optimum hub height is a critical step in any wind turbine design process. The reason this is so important is because small wind turbine systems are usually located where the power is required or adjacent to the owner's home, and which may not be a windiest location. Generally, there are two important parameters that can diminish the wind resource for small wind turbines, and which have to be considered when selecting an optimum tower height [211]. The first parameter is the surface roughness which generates friction drag; this occurs between the surface of the earth and air masses that flow over it. The more cluttered the landscape (with trees and buildings), the greater the ground drag will be in a given area. Frictional drag reduces the wind speed, and then reduces its kinetic energy. The second parameter is the turbulence, which is caused by the obstacles that clutter the earth. The turbulence intensity depends on the roughness of the terrain (varies from 0.1 to 0.2 for a smooth terrain or more for a relatively rough terrain) [3, 24]. The turbulence intensity depends also on the height; they generally decrease with increasing height. Turbulence can influence both the power and the loads on a wind turbine. These two critical parameters depend on the height, and usually decrease with increasing the turbine tower height.

Several optimization approaches have been used in the literature to determine an optimum tower height. An example of these methods consists in using differentiation to carry out the optimization. According to Jaehwan Lee et al. [212], an optimum tower height can be determined using a formulated objective function, expressed in terms of both the annual energy production and the wind turbine cost. This objective function can be differentiated with respect to the hub height. Another approach was given by Wood [213], which consists in maximizing the ratio of the average power output to the total capital cost of both the turbine and the tower in order to determine an optimum tower height.

To make effective use of the wind, small turbine towers must be at least 18 m high and well above obstacles (such as trees). Generally, for residential application systems with a power generation of 5 to 15 kW, turbines need to be on towers with heights from 24 to 36 m tall [214]. Some rules of thumb can also be used. These include the general rule stating that the entire rotor of the wind turbine must be at least 9 m above anything within 150 m far from the tower [215]. As a first approximation, the tower height can be estimated by assuming that security and turbulence issues are taken into account when the distance between the tip of the blade and the ground is equal or greater than 15 m [216].

$$\frac{D_t}{2} + 15 \leq H_{hub} \qquad (153)$$

Where D_t is the rotor diameter.

By using this approximation, the wind turbine rotor must be located at a minimum height of **18.5 m**. To achieve better performance while minimizing the total cost, an optimization approach was used. This considers the determination of an optimum tower height which maximizes the average energy output per unit price, PR_{total}. The total price is defined by the price of both the turbine and the tower. This approach has demonstrated its ability to optimize the tower geometry while minimizing the cost. According to wood [217], the wind turbine total price can be expressed as:

$$PR_{total} = R_t + R_{tu}.h \qquad (154)$$

Where R_t is the cost of the turbine and R_{tu} is the cost of the tower per unit meter. The cost of the turbine was based on the average capital cost of commercially available small turbines that are similar to the present wind turbine (same power output and same drive train topology). A wind turbine capital cost of **US \$30.000** (cost including the inverter) was considered in the design process [218]. The tower cost per unit meter was taken as **US \$690/m**. This value represents an average capital cost of the of the commercially available monopole towers for small wind turbines. The optimization approach used here was carried out with some assumptions. These are given as follows: 1) The terrain is relatively rough around the turbine and the roughness is constant. In this case, the wind shear power law exponent, m, **was taken as 0.2.** This corresponds to a roughness length of approximately **0.10 m** (agricultural land with some houses and 8 m high hedges with spacing of approximately 1250m) [3]. Additionally, a value of 0.2 is recommended by **IEC 61400-2** when no specific values are available. 2) The main wind speed, U_{10}, at a reference height of **10 m, was taken as 3.55 m/s**. This value represents an average wind speed of wind data collected from 45 regions in Morocco, and which have been taken at a reference height of 10 m. 3) The offset wind speed, U_0, was taken as **1.95 m/s** at a reference height of 10 m. This value is defined as the difference between the average and the minimum wind speed for the already considered (more details can be found in the section of the small wind turbine class).

By taking into consideration these specific conditions, the ratio to be optimized is proportional to [41]:

$$\frac{U_{10}.\left(h/10\right)^m - U_0}{R_t + R_{tu}.h} \qquad (155)$$

Differentiating 148 with respect to h, and equating the result to zero, gives the optimum tower height, h_{opt}:

$$\frac{m.R_t}{R_{tu}.h_{opt}} + m - 1 + \frac{U_0}{U_{10}}\left(\frac{10}{h_{opt}}\right)^m = 0 \qquad (156)$$

Increasing m and U_0 and decreasing U_{10}, all increase the optimum height. This equation is evaluated using matlab's function fzero, which is a function that is used to solve single variable nonlinear equations. Typical distributions of the optimum height, h_{opt}, as a function of the power law exponent, m, are plotted in figure 77. The tower height was computed for U_{10}=3.55 m/s and 6.39 m/s, which are the mean and the maximum wind speeds at a reference height of 10 m respectively. As it can be seen, the tower height varies linearly with the power law exponent. That is, rough terrains need tall towers and vice-versa. **For the site specific conditions considered in this study, the used optimization method gives an optimum height of 25 m. A standard height of 24 m will be adopted (three different sections of 8 m each)**. This value will be used in the next section to determine the base diameter, D_{b0}, and the corresponding thickness of each section.

For the tower material, most of the wind turbine towers are manufactured from steel [1, 3, 120]. The tower material has to fulfill the requirements regarding safety and reliability. Steel grades S235 and S355 are widely used for tubular towers [219]. **For the current design process, the wind turbine tower will be manufactured from the non-alloy structural steels S355JR, in accordance with the European standard EN10025-2:2004 [220].**

Having high strength, stiffness, toughness, and ductile properties, this structural steel is the most common materials in commercial and industrial building construction. Furthermore, structural steel can be developed into nearly any shape, which are either bolted or welded together in construction. Also, structural steel can be erected as soon as the materials are delivered on site [221, 222].
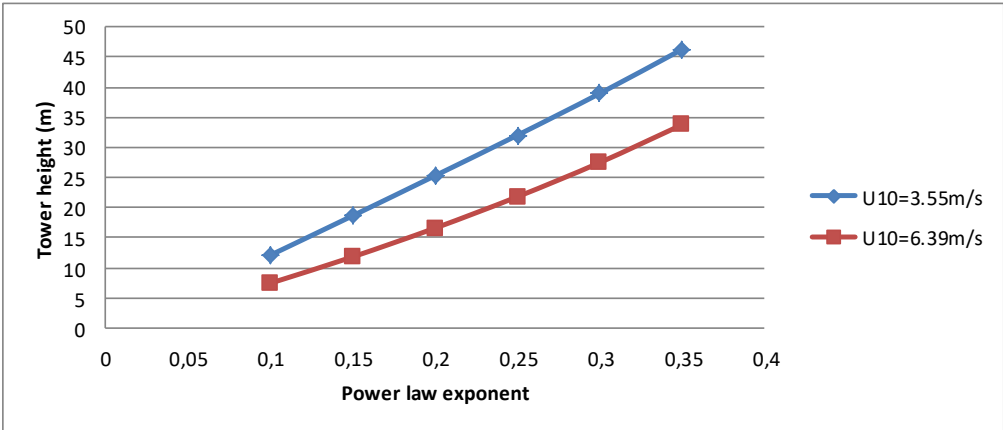
Figure 77: Optimum tower height as a function of the power law exponent

6.2 Tower design and optimization

The basic parameters that must be determined here are the cross-sectional shape of the tower, the wall thickness in each section, t, and the base diameter, D_{b0}. For the top diameter, it is

assumed that the wind turbine and the tower connection define the minimum diameter, D_{h0}. The tower geometry must be able to withstand the loads from the turbine and from the tower self-weight. Additionally, it is necessary to calculate the horizontal force and the base overturning moment, M_h, in order to make sure that the tower will never fail under extreme wind conditions.

The first parameter in the tower design is the tower shape. Usually, the horizontal force on the tower due to an extreme wind speeds (typical wind speed is 52.5m/s) is much larger than the maximum thrust, T_{hmax}. Therefore, particular attention should be paid to the tower shape in order to reduce the drag force, which is the main loading on a stationary wind turbine rotor. The most widely used forms are the circular and the octagonal cross sections. **An octagonal cross-section, tapered towards the top, was selected for the present design project. This shape has a major advantage of being easy to manufacture**. However, It has been shown that wind turbine tower with an octagonal cross section has the highest wind force coefficients [7, 223]. The tower diameter will be taken as the distance across the flats on the outside of the tower, as shown in figure 78.
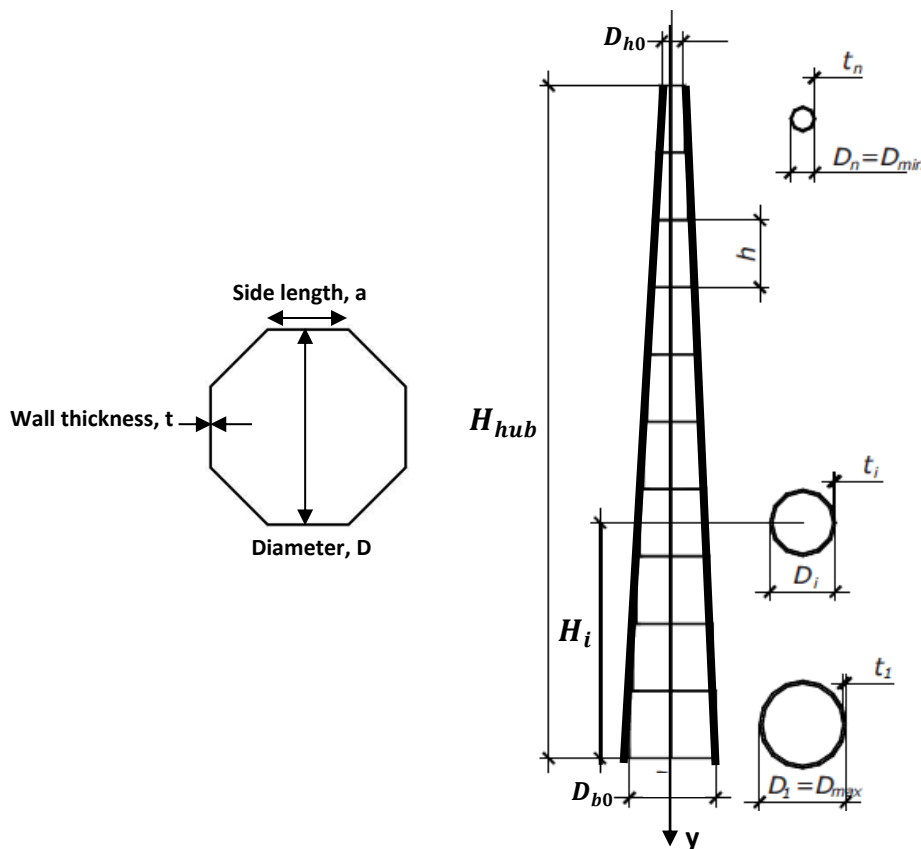
Figure 78: Diameter and thickness of an octagonal cross-section

The main objective of this section is to determine an optimal tower shape with the first aim of minimizing the tower mass which is closely associated with the cost of manufacture,

transport, and foundation. However, the optimization of a tapered tower with different sections is not possible analytically. Therefore, an evolutionary strategy will be used. This optimization method can combine minimizing tower mass, maximizing the capacity factor, **CF**, (which is defined as the ratio of the maximum applied stress on the tower to the maximum allowable stress), and maximizing the tower natural frequency. The objective function can be written as [224]:

$$\text{fitness(ci)} = a_m \frac{\min(m_t)}{m_t(ci)} + a_{CF} \frac{CF(ci)}{\max(CF)} + (1 - a_m - a_{CF}) \frac{n_1(ci)}{\max(n_1)} \quad (157)$$

Where a_m and a_{CF} are the objective weight factors. The sum of this weight factors must be equal to one and each weight must be strictly positive. **The current tower has been designed to meet a capacity factor of 0.6 for a welded connection of general purpose category, as given by the Australian Standard Steel Structures [225]**. Therefore, the base diameter, D_{b0}, and the wall thicknesses will be chosen to keep the capacity factor less than 0.6. Table 45 summarizes the input parameters for the tower optimization.

Parameter	Value
Number of tower sections, N_{se}	3
Tower mass weight factor, a_m	0.5
Maximum thickness, t	50 mm
Maximum diameter, d_0	0.9 m
Population size	3000
Maximum capacity factor, CF_{max}	0.6
Capacity factor weight factor, a_{CF}	0.5
Minimum thickness, t	2 mm
Crossover factor, CR	0.1
Number of generations	100

Table 45: Input parameters for the optimization program

This optimization process is carried out using a suite of Matlab programs based on the work of Clifton Smith and David Wood. According to D. H. Wood [224], the differential evolution method has shown to successfully design an 18 m minimal mass self-supporting wind turbine tower for a 5kW wind turbine, whilst retaining the required strength, stability, and manufacturability using a linear taper and constant wall thickness for each section. As can be seen in table 46, the tower optimization was carried out with four different top tower diameters, d_0. The range of the selected values represents an average diameter for monopole towers that have been designed for 10 kW and 11 KW horizontal axis small wind turbines.

d_{min} (m)	D_{h0} (m)	D_{b0} (m)	CF_{max}	Mass (Kg)	t_0 (mm)	t_1 (mm)	t_2 (mm)
0.2	0.2	0.527	0.6	1 136	3.5	4.8	6.2
0.25	**0.25**	**0.548**	**0.6**	**1 318**	**4.3**	**5.1**	**6.3**
0.3	0.3	0.525	0.6	1 444	4.4	5.1	7.2
0.35	0.35	0.580	0.6	1 600	4	4.8	7.5

Table 46: Results of tower optimization

It was observed that the minimum diameter has a large effect on the tower mass. In all cases, the maximum CF reached the limit value of 0.6, and the top diameter converges to d_{min}. This is because the tower top contributes significantly to the bending moment at the base, and the magnitude of the moments is fixed by the diameter. It should be noted that the calculated tower mass does not include the connection flanges and the baseplate.

As mentioned before, the minimum diameter of the tower top section is determined by the turbine/tower connection. Normally, the value of the top diameter is defined by the topology of the yaw mechanism, especially by the yaw bearing diameter, D_1 (as shown in figure 75). **Keeping in mind this specific detail, a tower top diameter of 250 mm was selected.**

The tower top section flange must support the yaw bearing ring across its entire side face and its thickness should be more than 8.95 mm (section yaw bearing design). By adding all the uncertainties during the manufacturing process, a flange thickness of 10 mm is suitable for the tower top section. The turbine and the tower connection will be ensured by hexagonal head bolts in accordance with DIN EN ISO 4014:1999 in the 10.9 strength grade (as described in the previous section of yaw bearing design). The flange of the two lower sections will have a thickness of 20 mm. These sections will be flanged and bolted without slip-fitting, to minimize movement due to fluctuating turbine loads and to prevent disassembly during rising and lowering. To reduce stress acting on the weakest and critical zones in the section with flange connections, gusset plates will be used, especially in the baseplate. Finally, it is worth mentioning that the results of the current optimization process still require validation by using more accurate structural analysis (full three-dimensional Finite Element Analysis, FEA), to ensure that no component will fail under any type of load.

6.3 Tower analysis

In designing a small wind turbine tower, the key design requirements are to ensure that the maximum design stress is below the allowable material stress, no tower member in compression will buckle, the tower lowest frequency is not likely to be significantly excited by blade passing frequencies, and the top tower maximum deflection should be small enough to justify the assumption that the structural shape does not alter under the load. Normally, the

IEC 61400-2 simple load model, SLM, mandates only the first requirement. For the present tower analysis, the following considerations are to be taken into account:

- Three IEC load cases are considered: load case A for fatigue during normal operation, load case B for yawing, and load case H for parked wind loading where it will be assumed that the rotor is stationary;

- A wind speed of **52.5 m/s** will be used as a typical value from the IEC safety standards, which is the 50-year extreme wind speed. This wind speed is chosen because the wind turbine system should be designed for the worst possible scenario;

- The main tower-top loads are the maximum thrust, $\mathbf{T_{hmax}}$, and the nacelle weight, $\mathbf{m_{tt}}$;

- For simplicity purposes, the analysis will be restricted to static-linear behavior. That is, the tower material is assumed to respond linearly to the imposed load that the deflections are small enough to make the original shape sufficiently accurate for stress analysis;

- The structural elements of the tower have the same material properties;

- The analysis considers only the general form of the tower and no details such as turbine mounting flange and baseplate;

6.3.1 Tower bending stress calculation

The tower maximum bending stress analysis is conducted by considering the co-ordinate, **y**, in the negative vertical direction with origin at the tower top. The horizontal drag per unit height on the tower section is given at y is given by:

$$D(y) = \frac{1}{2} . \rho . U^2(y) . C_d . d(y) \tag{158}$$

Where $d(y)$ is the diameter and $U(y)$ the wind speed which is assumed to be constant for all heights in this case.

The drag coefficient for an octagonal section, C_d, is taken as 1.4. This value is given by the Australian standard AS 1170.2 **[226]**. The selected drag coefficient value is larger than that given by the **IEC 61400-2**, which is equal to 1.2. This value is used for geometries with characteristic lengths greater than 0.1 m. A higher value is selected because the tower design should be the most conservative possible. Higher drag coefficient allows the design to meet the **IEC 61400-2** requirements as well as relevant local codes. By deriving the formula of the applied shear force and the corresponding moment on the tower, the diameter and the total moment at a given height are given by equations 159 and 160, respectively:

$$D(y) = D_{h0} + \frac{D_{b0} - D_{h0}}{H_{hub}} . y = D_{h0} + d_1 . y \tag{159}$$

$$M(y) = M_0 + T_{hmax} . y + \frac{1}{2} . \rho . U^2 . C_d . \left(\frac{D_{h0}}{2} y^2 + \frac{d_1}{6} y^3 \right) \tag{160}$$

With M_0, a moment acting on the tower, and which can arise from a number of causes such as gyroscopic or cyclic loads on the turbine main shaft or a significant overhang of the tower top center of mass. In order to simplify the analysis, it is assumed that T_{max} and M_0 act at the tower top position. At any height, the maximum bending stress that occurs at a distance of $d/2$ from the centroid is given by:

$$\sigma_b = \frac{M(y).d(y)}{2.I(y)} \tag{161}$$

Where, I is the second moment of area for a regular octagon section with a wall thickness t. The second moment of inertia can be computed using equation 162. The thickness is assumed to be constant for each section.

$$I(y) = 0.05474.[d^4(y) - (d(y) - 2t)^4] \tag{162}$$

The total bending stress is found by adding axial loading due to the turbine and the tower self-weight.

$$\sigma_{max} = \sigma_b + \frac{[m_{tt} + m_t(y)].g}{A(y)} \tag{163}$$

Where g is the acceleration due to gravity, and $A(y)$ is the tower cross-sectional area, which is given by:

$$A(y) = 3.3137.[d(y) - t] \tag{164}$$

The maximum stress in each section occurs at the start of its lower zone and the increase in the stress with height (y) generally requires the wall thickness to be increased in the lower sections of the tower. **Using equations 151 and 153, and assuming that the moment on tower due to the turbine, M_0, is equal to zero**, **the horizontal force on tower is 22.17 KN, and the base overturning moment gives a value of 331.38 KNm.**

6.3.2 Tower local buckling

When the wind turbine rotor faces the prevailing wind direction, the upwind face of the rotor is in tension and the downwind face is in compression. In this case, the tower could buckle and this must be designed against. Usually, the axial load will make the maximum compressive stress larger in magnitude than the maximum tensile stress. For buckling analysis, American Society of Civil Engineering (ASCE) guidelines for regular polygon sections are used. These correlate the results of experiments to determine the limiting values of L/t (the side length over thickness). For an octagonal section with a specified maximum yield stress, F_y, the basic condition is:

$$\frac{L}{t}\sqrt{F_y} < \begin{cases} 680 \text{ for } \sigma_a < 6.9 \text{ MPa} \\ 630 \quad \text{Otherwise} \end{cases} \tag{165}$$

Where L is the side length of the octagonal section, which is given by:

$$L = \frac{d}{1 + \sqrt{2}} \tag{166}$$

The axial stress, σ_a, is due to the axial load of both the turbine and tower. If the inequality holds, then F_y may be used for the design and there will be no buckling. However, if the axial stress is larger than the specified limits but still smaller than 960, then the allowable stress considering the local buckling strength of the structure is given by:

$$F_a < \left(\begin{array}{c} 1.42 F_y. \left(1 - 4.34 \times 10^{-4} \frac{L}{t}\sqrt{F_y}\right) \text{ for } \sigma_a < 6.9 \text{MPa} \\ 1.45 F_y. \left(1 - 4.91 \times 10^{-4} \frac{L}{t}\sqrt{F_y}\right) \text{ Otherwise} \end{array} \right) \tag{167}$$

The tests did not extend to values $\frac{L}{t}\sqrt{F_y} > 960$. By comparing this correlation to the FEA determination of the linear buckling factor, the ratio of the load required to induce elastic buckling divided by the maximum load, Clifton smith and Wood [224] found that the equation 167 over-predict F_a for $t < 4.3 \times 10^{-4}$ m approximately. Then they suggested the following modification:

$$F_{a,corr} < \left(\begin{array}{c} (414t - 0.7842)F_a \text{ for } t < 4.3 \times 10^{-4} \\ F_a \qquad\qquad\qquad \text{otherwise} \end{array} \right) \tag{168}$$

This modified allowable stress will be used in the present analysis. The buckling analysis will also involve a capacity factor, **CF**. For the present study, the maximum allowable stress, F_A, is taken to be the minimum of the yield stress and the allowable stress, and given by equation 169.

$$F_A = \min (F_Y, F_a) \tag{169}$$

Then the capacity factor can be written as:

$$CF = \frac{\sigma_{max}}{F_A} \tag{170}$$

As mentioned before, a typical value of 0.6 will be used for the capacity factor and the ultimate tensile strength will be considered. Based on Matlab programs given by Clifton Smith and Wood, **the maximum, CF, for both buckling and maximum stress is 0.596**. Therefore, the tower would be safe against buckling.

6.3.3 Tower top deflection

The tower top deflection is considered as the maximum deflection of the turbine and the tower. This must remain small to justify the assumption that the structural shape does not alter under the load and hence does not alter the loads. The deflection, in the case of the tower analysis, can be calculated according to the standard beam theory as:

$$\frac{d^2x}{dy^2} = \frac{M(y)}{EI(y)} \tag{171}$$

Regarding the difficulties in analytically determining the double integral, the problem may be solved under the restriction of $t \ll d_0$, for which the second moment of inertia is given by:

$$I(y) = 0.43792.\,t.\,(D_{h0} + d_1 y)^3 \tag{172}$$

The equation 171 can be written as two first order ordinary differential equations and solved using Matlab's built-in Runge-Kutta routines. Based on Matlab programs given by Clifton Smith and Wood, **the tower top maximum deflection is 1.24 m**. It should be noted that this deflection is given for extreme wind conditions with a survival wind speed of 52.5m/s.

6.3.4 Tower natural frequency

An important step in the current design process is to check whether there will likely to be any resonance caused by blade passing frequencies matching the tower lowest natural frequency. The reason this is so important is because this matching is almost guaranteed for variable-speed small wind turbines, for which the rotational speed varies to match the wind speed in order to keep the tip speed ratio constant. Also, the natural frequency is necessary to determine whether static or dynamic is required. For example, AS 1170.2 [226] allows a static analysis for structures with natural frequency $f_1 > 1Hz$ and mandates a modified analysis for lower values using increased wind loads. The most important consideration in the tower design is to avoid resonance. In order to do this, the tower natural frequency, f_0, must not coincide with the frequency of the cyclical loading resulting from the rotor frequency, f_r, and the frequency for the blades passing in front of the tower, f_b. Generally, towers and wind turbine systems are classified as soft–soft, soft–stiff, or stiff–stiff, depending if the tower's natural frequency is less than the rotor frequency ($f_0 < f_r$), greater than the rotor frequency but less than the blade passing frequency ($f_r < f_0 < f_b$), or greater than the blade passing frequency ($f_0 > f_b$), respectively. The majority of wind turbines are designed for the soft–stiff regime. Soft–soft or soft–stiff are preferred over stiff–stiff because much more material and cost are required for this later approach [227]. For either a soft-soft or soft–stiff tower, the

tower can be excited during start-up or shutdown of the turbine. As a first approximation, the tower lowest natural frequency can be determined using Baumeister's equation [228, 229].

$$f_0 = \frac{1}{2\pi} \cdot \sqrt{\frac{3.E.I}{(0.23m_t + m_{tt}).H_{hub}{}^3}} \tag{173}$$

Where f_0 the lowest natural frequency (Hz), E is the modulus of elasticity, I is the moment of inertia, and H_{hub} is the tower height. This equation gives a first approximation of **0.79 HZ**.

In the present analysis, two different methods have been used to determine the tower lower frequency: the first method approximates the stiffness as the total horizontal force divided by the turbine deflection, and then the natural frequency is found as the square root of stiffness divided by tower mass. This method is more accurate for the combined turbine and tower. This is because the turbine mass is concentrated at the top of the tower. The second method undertakes the same approach but suggests that the effective mass of the tower is set to 0.23 m_t . This factor comes from the standard analysis of the natural frequency of concentrated mass and force on top of a constant diameter column [230]. **Based on Matlab programs given by Clifton Smith and Wood, the estimated natural frequencies are:**

- For the tower and the turbine (first method): 0.546 Hz;

- For the 0.23*tower + turbine (second method): 0.828 Hz;

For the present design, the wind turbine is considered has a rated rotational speed of 172 RPM which gives an equivalent frequency of $f_r = 2.86\,\text{Hz}$. The corresponding blade passing frequency, denoted 1P, is given by:

$$f_b = \frac{B.\Omega_{design}}{60} = 8.6\,\text{Hz} \tag{174}$$

Therefore, it is almost certain that the turbine will excite the tower natural frequency during some part of its operation. Fortunately, the wind thrust at a rotational speed corresponding to about 1 Hz is low so that a well-designed tower should not show significant resonance and the blades will be stationary when the maximum thrust occurs under load case H of **IEC 61400-2**.

6.3.5 Tower fatigue loading

The load case A, from the **IEC** Simple Load Model (SLM), is the only load case that covers fatigue behavior during normal operation. Using the normal operation conditions, equation 175 gives the peak to peak fatigue loads on the turbine shaft [7].

$$\Delta F_{X-shaft} = \frac{3.\,\lambda_{design}.\,Q_{design}}{2R} = 2397.54\,\text{N} \tag{175}$$

As mentioned above, all the equations, in the this specific load case, define peak-to-peak loads generated by the assumed cycling between 1.5 times and 0.5 times the design values of the angular velocity and torque. Therefore the average thrust is **2397.54 N** and the maximum is **3596.31 N**. Using the same load case, the shaft moment against the first bearing is given by [7]:

$$\Delta M_{shaft} = 2.\, m_r.\, g.\, L_{rb} + \frac{R}{6} \Delta F_{X-shaft} = 1582.63 \text{ Nm} \tag{176}$$

This specific moment is assumed to be the moment M_0 acting on the tower. Using the Matlab programs given by Clifton Smith and Wood, table 47 shows the stresses resulting from the maximum and the mean of the cyclic load from SLM load case A.

Parameter	Maximum cyclic load	Mean cyclic load
Horizontal force on the tower (KN)	0.89	**0.89**
Base overturning moment (N.m)	97.21	**68.44**
Maximum CF for buckling	0.21	**0.14**
Maximum CF for stress	0.21	**0.14**

Table 47: Maximum and mean cyclic loading for SLM load case A

However, it is necessary to see the effect of non-zero mean stress which will reduce the fatigue life of structural steel. The effect can be assessed using Gerber's relation [231] and assuming en endurance limit of $\sigma_l = 200$ MPa. Gerber's relation for the allowable maximum stress, σ_n, can be written as:

$$\sigma_n = \frac{F_Y}{2}.\left(\sqrt{\left(\frac{F_Y}{\sigma_l}\right)^2 + 4} - \frac{F_Y}{\sigma_l}\right) = 158.81 \text{ MPa} \tag{177}$$

The yield stress in this case is used as the ultimate stress. The reduction in the allowable stress is very small. **Since the maximum stress for fatigue load (51.79 MPa for load case A) is well below the allowable maximum stress σ_n, the tower will not fatigue.**

6.3.6 Tower and gyroscopic loading

To analyze the effect of the gyroscopic loading on the tower structure, the moment,M_0, acting on the tower is assumed to be the bending moment on the main shaft, **M_{shaft}** , which can be calculated using equation 178 [7].

$$M_{shaft} = B.\, \omega_{max}.\, \Omega.\, J_B + m_r.\, g.\, L_{rb} + \frac{R}{6} \Delta F_{X-shaft} = 7517.93 \text{ Nm} \tag{178}$$

Where, $\omega_{yaw,max}$ is the maximum yaw rate which is defined as the maximum speed of yaw movement of the rotor around the yaw axis.

This can be determined using equation 179.

$$\omega_{yaw,max} = 3 - 0.01 * (A - 2) = 2.635 \text{ rad/s} \qquad (179)$$

Where A is the rotor swept area which is taken as 38.48 m², m_r is the rotor mass (93.82 Kg), J_B is the blade inertia which is taken as 42.33 Kg.m², and L_{rb} is the distance between rotor center and first bearing (0.1 m).

The main results of the analysis are given in table 48.

Parameter	Value
The horizontal force on tower	**0.89 kN**
The base overturning moment (kNm)	**74.38 KNm**
The maximum CF for buckling	**0.18**
The maximum CF for stress	**0.18**

Table 48: Results for gyroscopic loading

As can be seen, the tower is safe against buckling and stress loading. Finally, it is worth noting that the analysis, undertaken in the present design process, still requires further critical calculations to accurately determine the exact response of the tower structure to the bending, fatigue, deflection, and buckling loads. Finite element analysis technique (FEA) is the most effective way to make sure that tower structure will be able to withstand all the loads to which it will be subjected throughout its intended life span. In this case, FEA can be used to analyze the static and dynamic structural responses in terms of the stress distribution, deflection, stability, and modal analysis of the tower structure.

Finally, for easy installation and maintenance, the tower of some the wind turbine could be equipped with a hydraulic lifting system. This is a very popular solution that enables erecting and lowering the tower during installation and maintenance without any need to a crane or other lifting equipments. The hydraulic system is very necessary in windy areas where the customer needs to lower his wind turbine to avoid catastrophic failure under extreme wind conditions (typhoon, storm, or cyclone). Using the hydraulic lifting system, the tower and the turbine can be erected or laid down within 5 or 15 minutes. However, It worth mentioning that it could be very dangerous to attempt to lower a turbine in high wind condition. If this will be the case, the turbine must be designed to withstand the high winds when erect. Another cheaper and safe alternarive is to use a tractor. The use of a tractor eliminates the

extra cost and complexity of a hydraulic system which would not be warranted. Figure 79 illustrates how the hydraulic system of wind turbine tower works.
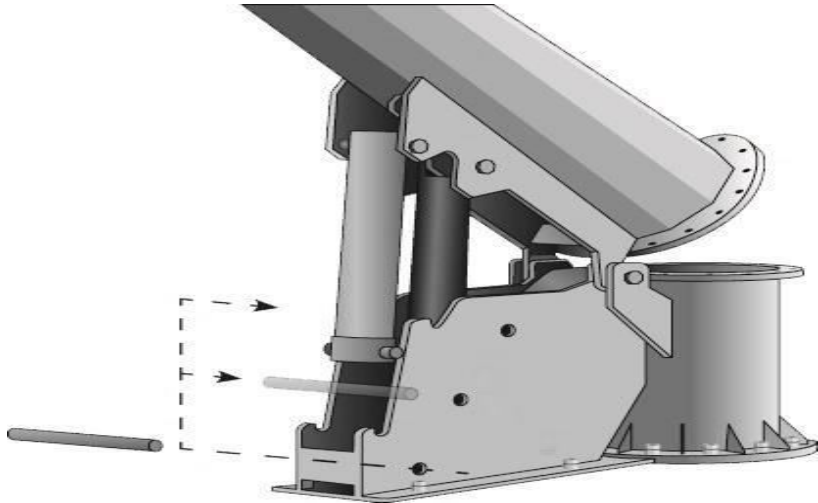
Figure 79: Wind turbine tower with a hydraulic system

6.4 Conclusion

For an effective design of the small wind turbine, the design and analysis of the tower structure must be included in the design process. This chapter discussed the tower design and its structural analysis. In a wind turbine design, it is necessary to find an optimum design for the tower by taking considering different external conditions (loads from the wind and dead loads applied by the nacelle components). The first part of the present chapter coverd the tower type selection, the tower height and its geometry. A single monopole tower (three sections that will be mounted on the site) with an optimum hub height of 24 m was selected. The material that was found to be used for twoer design is S355JR, in accordance with the European standard EN10025-2:2004. This is a structural micro-alloyed grade used for a great variety of applications that include wind turbine systems. The same material was selected for the manufacturing of the turbine tower.

For an optimum design of the tower geometry, a multivariable design optimization was usued. This optimization process was carried out using several Matlab programs based on the work of Clifton Smith and David Wood. This simulation tool analyzes the effects of some design parameters on the tower structure. These parameters include the hub height, the tower diameters and the wall thickness of the tower sections. The optimum geometry of the tower was specified by the top and the base diameter as well as optimal wall thickness of the tower sections. The final part of the present chapter was devoted to the strurual analysis of the tower for the different load scenarios.

CHAPTER 7: WIND TURBINE FOUNDATION DESIGN

During normal operation, small wind turbines are subject to different types of loads. For instance, the wind force (which is basically used to produce useful electricity) acts in an unpredictable manner thereby creating an environment prone to material fatigue. Furthermore, as the turbine nacelle is located on relatively high tower, the system becomes more affected by complex aeroelastic interplay which involves vibrations, cyclic loadings, and resonances. The combination of these loads creates large dynamic load components on the structure. From such complex operating conditions, rises the problematic of designing a tower foundation which will be able to sustain various loads without failure. In addition to these operating conditions, soil stability related issues, such as substantial pore water pressure under the foundation, can be added as a governing factor that must be considered when designing a wind turbine foundation **[232]**. The first task of a wind turbine foundation is to ensure functional stability for the wind turbine during its lifetime. This can be done by designing a solid structure that will able to transfer and spread the loads to the ground while preventing the tower from overturning. The vertical force acting on the foundation is mainly due to the dead loads from the tower and the nacelle, but the most significant loads come from the wind. Because wind turbines are usually mounted on relatively high towers, horizontal forces from the wind can generate considerably high overturning moments (through wind thrust and drag force). These are transferred to the foundation, and may lead to an overturning of the whole structure. Various types of foundations are designed depending on geotechnical conditions of the terrain and the design requirements of the system. Generally, wind turbine foundations can be divided into two major subgroups; **spread foundations and piled foundations**. Both of them have some kind of interface that connects them to the tower. **Piled foundations** are commonly used in case stiff soil (bedrock) is found at great depths and the loads are counterbalanced by a combination of friction and end bearing **[233]**. This is the raison why pile supported foundations are attractive when the top soil is of a softer quality and the loads need to be transferred to larger depths where stronger soils are present to absorb the loads **[144]**.

Spread foundation, which also called **slab foundation**, is composed of a big plate that makes use of the big area for spreading the loads to the ground. This type of foundation is suitable for strong and stiff soils that don't give large settlements. This is the reason why this type of foundation is mostly used on friction soils with high friction angle, or moraine and not clays, salty clays, fillings, organic soils or other soils with low modulus of elasticity and/or

low strength [234]. According to A.P.Schaffarczyk [3], the gravity foundation is the standard solution for the foundation of wind turbines. This type of foundation is footed some distance down in the soil. Thus, some soil has to be excavated and filling material is replaced above the foundation after it is constructed. If strong and stiff soils are overlaid with top layers of soft soils, such as clays, it can be a good idea to excavate these layers and put the foundation on the better soil. If this is the case, the weight of the filling soil above the foundation is preventing the tower from turning over and the area of the plate can be reduced. This foundation has the advantage of reducing the amount of used concrete, but instead requires major excavation and refilling work. The gravity base foundation provides sufficient resistance against sliding and sufficient vertical pressure. Furthermore, this solution promises cost efficient installation. Therefore, gravity foundation type, with a square area, is selected for the present design project.

Several gravity foundations can be designed depending on the geometry of the base (rectangular, circular or octagonal form) and the type of connection between the steel tower and the foundation. To ensure a proper transfer of loads between the tower and the foundation, two different alternatives are commonly used. The first type is a so-called double flange joint, where a massive I-girder-bent is used to form a ring which is cast inside the concrete. In this case, the steel tower is attached to a special connection flange with pre-stressed bolts.

The second option presents a connection through a Pre-stressed anchor bolt cage, as shown in figure 80. A steel flange is embedded in the slab before concreting, and on the top of the foundation another ring shaped T-girder is placed. The bolts are then stressed against both flanges. Fastening of the steel tower follows the same manner as with the previous variant. The main advantage of the second option is that it allows a better transmission of loads to the concrete. The Pre-stressed anchor cage can be built with a set of bolts, which are hold together by an inferior and superior steel rings. It normally arrives disassembled to the site, and it is mounted and installed easily within a short period of time. This solution was selected for the present design process.

The turbine foundation will be built using reinforced concrete. According to Manuel JF et al. [1], the reinforced concrete is frequently used for the foundations of wind turbines. This is a composite material in which concrete (with relatively low tensile strength and low ductility) is counteracted by the inclusion of reinforcement having higher tensile strength and high ductility. The reinforcement, in this case of this project, is the pre-stressed anchor cage, which is embedded passively in the concrete before the concrete sets. The reinforcing scheme will be

designed to resist tensile stresses that might cause unacceptable cracks or whole structural failure.
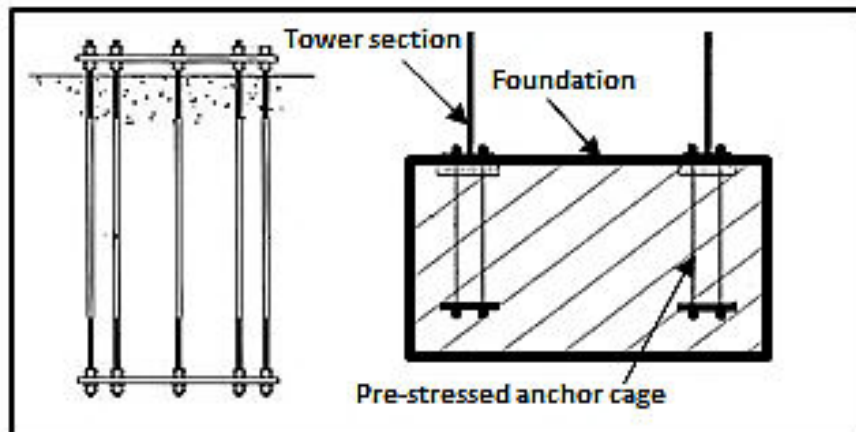
Figure 80: Gravity foundation with Pre-stressed anchor bolt cage

7.1 Soil and structure interaction

The structural design of a wind turbine foundation is strongly dependent on the nature of the contact pressure with the soil. As the major objective of a foundation slab is to distribute more or less concentrated load into a large area so that the soil can carry it without destructive damages (Bearing failure of the soil and excessive settlement), it is the resulting soil pressure that causes the bending moments and shear forces in the slab. Therefore, the form of the soil pressure distribution has a decisive impact on the magnitude of the internal forces on the structure itself. According to MacGregor JG **[235]**, the distribution of soil pressure under a foundation is a function of both the type of soil and the relative rigidity of the soil and the foundation pad. For example, a rigid foundation slab on a sandy soil will have pressure distribution with a convex form, as shown in figure 81.a. The sand near the edges of the foundation tends to displace laterally when the footing is loaded, causing a decrease in soil pressure near the edges. However, for a clayey soil, the pressure distribution under a foundation will have a concave form, as shown if Figure 81.b. As the foundation is loaded, the soil under it deflects in a bowl-shaped depression, relieving the pressure under the middle. Generally, elaboration of elastic-plastic behaviour of a given soil requires too much time, that is why simplifications can be used.
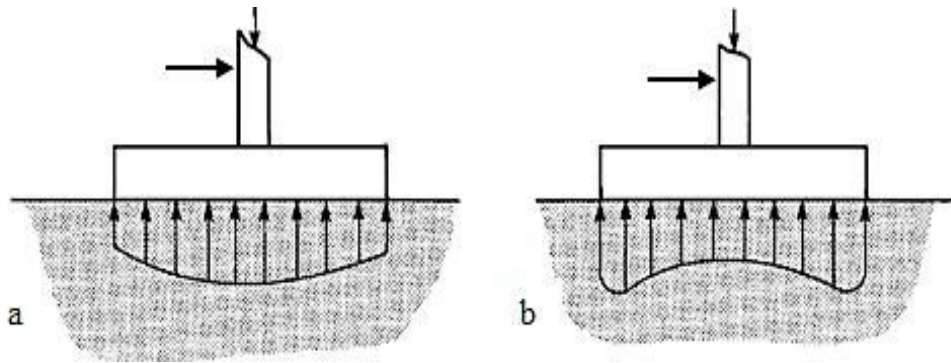
Figure 81: Soil pressure distribution under rigid foundations [235]

Linearly varying soil pressure distribution is an example of simplified models that can be used for analytical calculation. This model describes the distribution of soil pressure under a foundation slab by assuming no interaction between the structure and soil, as shown in figure 82. The use of elasticity theory for beams results in a linear soil pressure distribution that depends on both the magnitude of the applied loads and the surface area of the foundation. For small and in proportion somewhat stiff foundations, this method gives rather good approximation [232].
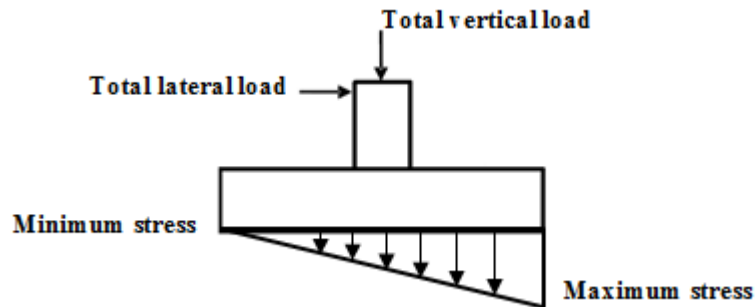
Figure 82: Model assuming linear pressure distribution

As the present small wind turbine is basically designed for remote areas to meet individual household's electricity needs including water pumping systems, sandy clay soil will be considered for the wind turbine foundation design. This choice is due to the fact that this soil type is fairly common in agricultural areas. Additionally, sandy clay soil represents a suitable choice for a conservative design. Typical properties of a sandy clay soil are given in table 49.

Soil type	Sandy clay
Soil cohesion, c' (KN/m²)	23.94
Unit weight of the soil, V_s (KN/m³)	15.71
Soil friction angle, ϕ_s (Deg.°)	25°
Soil Poisson's ratio	0.3
Undrained shear strength (KPa)	150
Inclination of the load on the foundation, β_s (Deg.°)	0

Table 49: Typical geotechnical properties of sandy clay soil

The main objective of this design procedure is to examine the foundation for possibility of tilting, overturning, and sliding. These dynamic phenomena occur when the load intensity imposed by foundation being in excess of the ultimate capacity of the soil. Therefore, the foundation must remain stable under all the possible combinations of loads to which it is likely to be subjected under the most stringent conditions. The type and the size of a wind turbine foundation is generally governed by the geotechnical conditions of the site, the maximum power of the turbine (which directly related to the size of the wind turbine), and the type of the tower. In designing a wind turbine foundation, there are four major requirements that must be satisfied. First, the calculated bearing pressure needs to be less than the allowable bearing capacity of the soil under the foundation. By definition, soil bearing capacity is the maximum average contact pressure between the foundation and the soil that should not produce shear failure in the soil. This parameter is usually measured in units of force per unit area. The second requirement is that the calculated settlement of the foundation, due to applied loads, needs to be less than the allowable settlement. Settlement is the vertically downward movement of the foundation due to the compression of underlying soil because of increased loads. Generally, settlement is not considered when designing a small wind turbine foundation because the contact pressure on the soil from vertical loads is relatively low and typically causes less than 2.5 cm of settlement in soils having adequate bearing capacity and stiffness [236]. Therefore, the settlement calculation will be excluded from the present analysis. The third requirement is that the foundation needs to have sufficient capacity to resist sliding caused by any horizontal loads. Finally, the foundation needs to be sufficiently stable to resist overturning loads. These overturning loads are commonly caused by horizontal forces applied above the foundation base (such as the horizontal force on the tower and the maximum thrust of the rotor blades).

During normal conditions, wind turbine foundations are generally subject to both lateral (which generate the base overturning moments) and vertical loads. The combination of these two loads causes an eccentricity of the applied loading. Consequently, the distribution of pressure by the foundation on the soil is not uniform. The eccentricity is measured from center of the foundation to the point of application normal to the axis of the foundation, and can be found using equation 180.

$$e = \frac{M_h}{Q} \tag{180}$$

Where Q is the total vertical load. This load is the sum of both the vertical forces acting on the foundation (which is composed of the nacelle and tower mass) and the self-weight of the foundation itself, m_f.

$$Q = (m_{tt} + m_t + m_f).g \qquad (181)$$

Where m_{tt} is tower top mass which is taken as 478 Kg, m_t is the tower mass, and m_f is the foundation mass in Kg. The moment, M_h, is the total overturning moment measured at the bottom of the footing, including horizontal loads times the vertical distance from the load application location to the bottom of the foundation. In the present design process, the total overturning moment will be taken as **360.19 KNm**. This value was determined in the previous section of the tower design and analysis (equation 160). Figure 83 shows an example of an eccentrically loaded foundation, which results in a non-uniform pressure distribution.
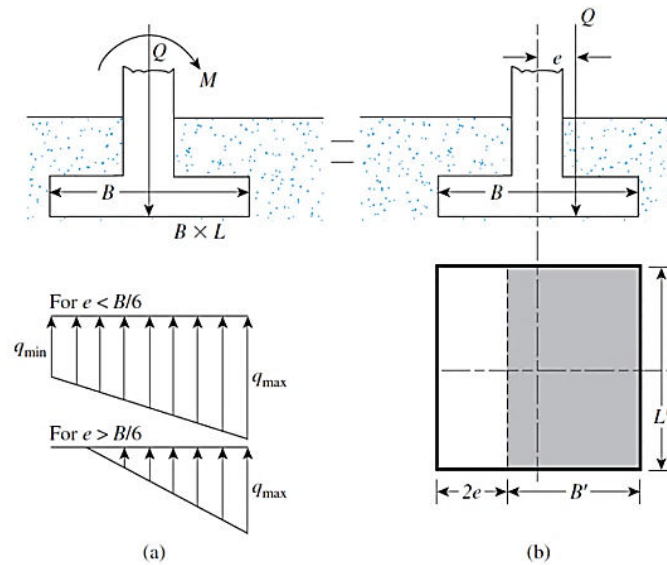
Figure 83: Non-uniform pressure distribution on an eccentrically loaded foundation [237]

According to DAS B. [237], the nominal pressure distribution is given by:

$$q_{max} = \frac{Q}{B_f.L_f}.\left(1 + \frac{6e}{B_f}\right) \qquad (182)$$

$$q_{min} = \frac{Q}{B_f.L_f}.\left(1 - \frac{6e}{B_f}\right) \qquad (183)$$

Where B_f is the foundation's width (m), L_f is the turbine foundation's length (m), and e is the load eccentricity (m). When the eccentricity e becomes $\frac{B_f}{6}$, q_{min} is zero. For $e \geq \frac{B_f}{6}$, q_{min} will be negative, which means that tension will develop. Because soil cannot take any tension, there will then be a separation between the foundation and the soil underlying it. The nature of the pressure distribution on the soil will be as the one shown in Figure 79.a.

The value of q_{max} is then:

$$q_{max} = \frac{4Q}{3L_f.(B_f - 2e)}$$ (184)

7.2 Ultimate bearing capacity

The soil supporting the wind turbine foundation must be able to carry the loads from the turbine structure placed upon it without a shear failure and with the resulting settlements being tolerable for the turbine structure. The main engineering concern, in this case, is to ensure that the soil structure under the foundation slab is effectively mobilized to restrain ground displacements and can secure the structural stability with an appropriate factor of safety, F_s. The safety factor and the maximum pressure on the soil, Q, determine the ultimate net bearing capacity, Q_{ult}, according to equation 185.

$$F_s = \frac{Q_{ult}}{Q}$$ (185)

In general, the minimum required safety factor against bearing failure of a shallow foundation is in the range of 2.5 to 3.5. For most applications, a minimum factor of safety of 3.0 is adequate **[238, 239]**. The IEC 61400-2 standard recommended the same partial safety factor for ultimate loads when the SLM model is used for the wind turbine structure analysis. **Therefore, a safety factor of 3 will be used in the present design and analysis.**

The process that is commonly used to calculate the ultimate bearing capacity of a given soil, for eccentrically loaded foundations, is known as the Meyerhof or effective area method **[240, 241]**. This model involves the following general steps: a) First, with a set of arbitrary initial values, choose the first dimensions for the wind turbine foundation. These include the foundation's width, B_f, the side length, L_f, the depth, D_d, and the foundation's area, A_f. The values of the first selection will be based on the dimensions of the commercially available small wind turbine foundations. B) Determine the eccentricity of the loading on the foundation and use it to calculate the effective width, B′, length, L′, and area of the foundation, A′. To consider the effect of the eccentricity in the calculation of ultimate bearing capacity calculation, Meyerhof suggested taking the effective dimensions of the foundation as follows:

$$L' = L_f$$ (186)

$$B' = B_f - 2e$$ (187)

The effective area is given by:

$$A' = B'.L'$$ (188)

In the case of the present design process, the foundation is assumed to be loaded with one way eccentricity. This means that the eccentricity of the load is included in design by reducing the width of the footing, B_f, by twice the eccentricity, 2e, thus reducing the effective width to 2e. The effective length will be taken as the actual foundation's length.

a) Calculate the Meyerhof's general ultimate bearing capacity, q_u'.

$$q_u' = c'N_cN_{cs}N_{cd}N_{ci} + (V_s'D_d)N_qF_{qs}F_{qd}F_{qi} + 0.5V_sB'N_VN_{Vs}N_{Vd}N_{Vi} \qquad (189)$$

Where N_c, N_q, N_V are the Meyerhof's bearing capacity factors (Their values depend on the soil friction angle ϕ_s). N_{cs}, N_{qs}, N_{Vs} are Meyerhof's shape factors. N_{cd}, N_{qd}, N_{Vd} are the Meyerhof's depth factors. N_{ci}, N_{qi}, N_{Vi} are the Meyerhof's inclination factors. D_d is the wind turbine foundation depth (m), V_s' is the effective unit weight above the base level of the foundation, and V_s is the effective unit weight of soil below foundation base.

The Meyerhof's factors, involved in the general ultimate bearing capacity calculation, can be determined using the following equations:

$$N_q = \tan^2(45 + \tfrac{\phi_s}{2})\, e^{\pi \tan \phi_s} \qquad (190)$$

$$N_c = (N_q - 1)\cot\phi_s \qquad (191)$$

$$N_V = 2(N_q + 1)\tan\phi_s \qquad (192)$$

$$F_{cs} = 1 + \left(\frac{B'}{L'}\right)\left(\frac{N_q}{N_c}\right) \qquad (193)$$

$$F_{cs} = 1 + \left(\frac{B'}{L'}\right)\tan\phi_s \qquad (194)$$

$$F_{Vs} = 1 - 0.4\left(\frac{B'}{L'}\right) \qquad (195)$$

$$F_{cd} = \begin{cases} 1 + 0.4\left(\frac{D_d}{B_f}\right), & \frac{D_d}{B_f} \le 1 \\ 1 + 0.4\tan^{-1}\left(\frac{D_d}{B_f}\right), & \frac{D_d}{B_f} > 1 \end{cases} \qquad (196)$$

$$F_{qd} = \begin{cases} 1 + 2\tan\phi_s(1 - \sin\phi_s)^2\left(\frac{D_d}{B_f}\right), & \frac{D_d}{B_f} \le 1 \\ 1 + 2\tan\phi_s(1 - \sin\phi_s)^2 \tan^{-1}\left(\frac{D_d}{B_f}\right), & \frac{D_d}{B_f} > 1 \end{cases} \qquad (197)$$

$$F_{Vd} = 1 \qquad (198)$$

$$F_{ci} = F_{qi} = \left(1 - \frac{\beta_s}{90°}\right)^2 \qquad (199)$$

$$F_{Vi} = \left(1 - \frac{\beta_s}{\phi_s}\right)^2 \qquad (200)$$

b) Compute the total ultimate load and ensure that the factor of safety against bearing capacity failure meets the requirements. This can be done using equation 201.

$$Q_{ult} = q_u'.A' \qquad (201)$$

c) Check the safety factor against the maximum pressure on the soil.

$$F_s = \frac{q_u'}{q_{max}} \qquad (202)$$

d) If the safety factor is higher than the target value (3 in this case), then decrease the selected baseline and repeat all the steps above. The optimum geometry of the foundation will be defined by the minimum values that give the required safety factor. Keeping in mind all the above mentioned considerations, table 50 summarizes the results of the calculation.

Parameter	Final values
Foundation depth (m)	1.5
Foundation length (m)	4
Foundation width (m)	4
Eccentricity (m)	0.63
Allowable eccentricity (m)	0.67
Maximum pressure on the soil (KN/m²)	70.92
Ultimate bearing capacity (KN/m²)	1311.39
Safety factor	18.48

Table 50: Optimal values of the wind turbine foundation parameters

As the ultimate bearing capacity of the soil is greater than the maximum pressure from the turbine components (with a safety factor of 18.48), the soil supporting the small wind turbine foundation can sustain the applied loads without any risk of failure.

7.3 Overturning calculation

Wind turbine foundations are usually subject to large overturning moments. For this reason, the turbine structure must be examined for possible overturning, especially when it operates under extreme wind conditions. In designing a wind turbine foundation, the overturning is considered using a safety factor. This is defined as the ratio the total moments that tend to resist overturning, $\sum M_R$, to the base overturning moment, M_h.

$$F_{so} = \frac{\sum M_R}{M_h} \qquad (203)$$

The usual minimum value of the safety factor, with respect to overturning, is taken as 2 or 3 [237]. As both the resisting and the overturning moments on the structure are well defined, the safety factor for overturning can be computed.

The overturning analysis will be based on the assumption that all vertical loads are stabilizing loads that produce the required stabilizing moment whereas lateral shear and moments will act to de-stabilize the structure. Resisting and overturning moments are calculated at the toe of the foundation (point C in figure 84). Normally, the axis about which the event of overturning takes places passes through this specific point. The total resisting moment is the total vertical load multiplied by one-half of the foundation's width.

$$\sum M_R = Q \cdot \frac{B}{2} \qquad (204)$$
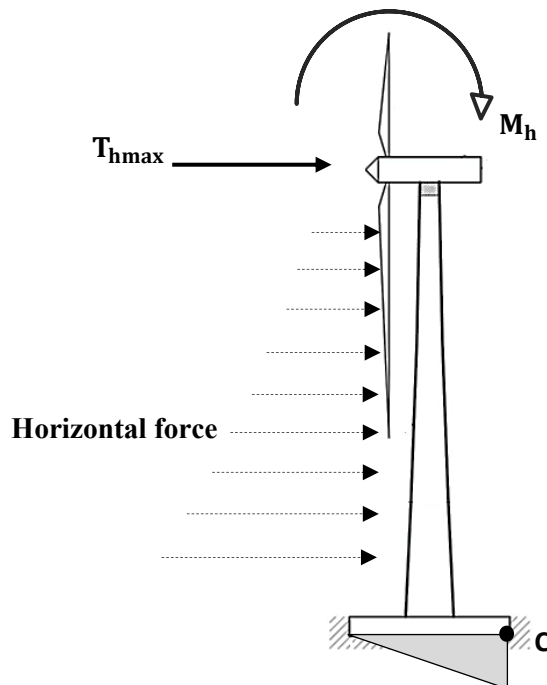
Figure 84: Check for overturning, assuming linear pressure distribution

By taking into consideration all the aforementioned considerations, table 51 summarizes the results of the overturning analysis.

Width (m)	Length (m)	Depth (m)	Resisting moments (KNm)	Overturning moment (KNm)	Safety factor for overturning
4	4	1.5	1165.34	367.57	3.17

Table 51: Safety factor for foundation overturning

Since the sum of the resisting moments is greater than the base overturning moment (with a safety factor of 3), the wind turbine foundation is safe against overturning.

7.4 Conclusion

The main objective in this chapter is to study and analyze different types of foundation methods for land based wind turbines and choose the most appropriate one for the small wind turbine design. The target of the design procedure to determine an optimal foundation geometry that will be able to support the tower and nacelle structures and withstand heavy loads and moments due to extreme wind conditions. The analysis of the foundation was carried out based on the Meyerhof or effective area method. A comparison of the foundation types was done first and a gravity foundation with Pre-stressed anchor bolt cage was selected. As the small wind turbine machine is mainly designed to be installed in remote area and agricultural sites, typical agricultural soil was selected for the design process. Once the foundation type and the geotechnical characteristics of the supporting soil were identified, the foundation geometry was determined using the ultimate bearing capacity calculation. Finally, given the design loads and the soil properties, design checks of the bearing capacity, overturning and rotational stiffness were performed.

CHAPTER 8: WIND TURBINE NOISE ANALYSIS

Small wind turbines provide clean, non-polluting, inexhaustible energy. In most places they are viewed with sympathy. However, the acoustic noise produced during their normal operation is becoming one of the main concerns. Actually, the amount of acoustic noise that a turbine emits becomes one of the significant drivers for small wind turbine design. This issue is particularly important because small wind turbines are usually placed in a rural environment (associated to the owner's home), where the background noise is relatively low and they can therefore be heard. Small wind turbines may be grid-connected or stand-alone systems. Due to their proximity of human activity, these applications could potentially result in noise complaints. Additionally, small wind turbines are in many cases louder than large turbines [242]. This is because they operate at higher tip speeds or turned partially out of the wind (furling operation system). These operating modes may aggravate sound generation. Then, it is very important to be able to understand, to model, and to predict the aeroacaustic noise for a given wind turbine and to make design changes before prototypes are built and tested.

8.1 Sound pressure level prediction

Generally, small wind turbines produce noise with two different distinct ways [243]: the first one is mechanical noise from the rotating machinery in the nacelle, and the other is aerodynamic noise produced by motion of air around the blade (blade swish, inflow turbulence, trailing edge noise, and vortex shedding). The sound technology is, generally, based on the following primary elements: noise sources, propagation paths, and receivers [244], as shown in figure 85. Concerns about noise depend on the level of intensity, frequency, frequency distribution, and patterns of the noise source; background noise levels, terrain between emitter and receptor, and the nature of the noise receptor.

Noise Sources :	Propagation path :	Receivers:
- Aerodynamic	- Distance	- Ambiant noise
- Mechanical	- Absorption	- Indoor/outdoor
	- Terrain	exposure
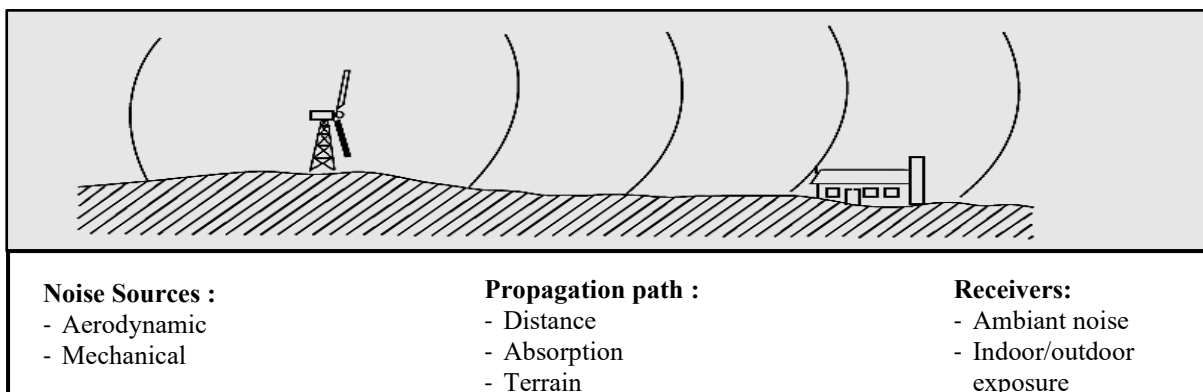
Figure 85: Primary elements contributing to wind turbines acoustic noise

Regarding the noise types, there are four types of noise that can be generated by small wind turbines which are tonal noise, broadband noise, low-frequency noise, and impulsive noise [245]:

• **Tonal**: tonal noise is defined as noise at discrete frequencies. It is caused by wind turbine components such as meshing gears, nonlinear boundary layer instabilities interacting with a rotor blade surface, by vortex shedding from a blunt trailing edge, or unstable flows over holes or slits.

• **Broadband**: this noise is characterized by a continuous distribution of sound pressure with frequencies greater than 100 Hz. It is often caused by the interaction of wind turbine blades with atmospheric turbulence, and is also described as a characteristic 'swishing' or 'whooshing' sound.

• **Low-frequency**: this describes noise with frequencies in the range of 20 to 100 Hz mostly associated with downwind turbines. It is caused when the turbine blade encounters localized flow deficiencies due to the flow around a tower, wakes shed from other blades, etc.

• **Impulsive**: short acoustic impulses or thumping sounds that vary in amplitude with time characterize this noise. They may be caused by the interaction of wind turbine blades with disturbed air flow around the tower of a downwind machine, and/or the sudden deployment of tip breaks or actuators.

The prediction of noise from a single wind turbine under expected operating conditions is an important part of an environmental noise assessment. Many analytical models and computational codes for the noise prediction of single wind turbines have been developed. In general, these models can be divided into the following three categories [123]:

• **Category I models**; this class of models gives a simple estimate of the overall sound power level as a function of the basic wind turbine parameters (e.g., rotor diameter, power, and wind speed). Models in this class represent rules of thumb which are simple and easy to use.

• **Category II models;** these models are semi-empirical relationships which predict the total sound pressure level and spectral shape taking into account the various noise generation mechanisms. These represent the current turbine state of the art.

• **Category III models;** these models use refined models describing the noise-generation mechanisms and relate them to a detailed description of the rotor geometry and aerodynamics.

For the Class I models (which will be used as a first approach in the present analysis), there are empirical equations that have been used to estimate the sound power level. For example, one simple data correlation for the sound power level, L_w , gives [246]:

$$L_w \approx 10^{-7}.P \qquad (205)$$

That is one-ten millionth of the turbine's power is output as noise. For this reason, a well-designed small wind turbine is almost guaranteed to be quiet. Another correlation that is more accurate in some cases is given by [40]:

$$L_w \approx 50 \, \log_{10} \Omega. R + 10 \log_{10} R - 1 \qquad (206)$$

Where Ω is the blade angular velocity in rad/s, so ΩR is the circumferential velocity of the blade tip in m/s, and R is the rotor radius measured in m.

In order to predict the sound pressure level at a distance from a source with a known power level, the sound waves propagation should be considered. Generally, for the case of a stand-alone wind turbine, the sound pressure level is calculated by assuming a spherical spreading, which means that the sound pressure level is reduced by 6 dB per doubling of distance. However, if the source is on a perfectly flat and reflecting surface, then hemispherical spreading has to be assumed, which leads to a 3 dB reduction per doubling of distance [123]. Furthermore, the effects of atmospheric absorption and the ground effect, both dependent on frequency and the distance between the source and observer, have to be considered. The ground effect is a function of the reflection coefficient of the ground and the height of the emission point.

Wind turbine noise also exhibits some special features. First, the height of the source is generally higher than conventional noise sources by an order of magnitude, which leads to less importance of noise screening. In addition, the wind speed has a strong influence on the generated noise. The prevailing wind directions can also cause considerable differences in sound pressure levels between upwind and downwind positions.

For the present study, the noise level at any point around the turbine is determined using a simple model based on hemispherical noise propagation over a reflective surface, including air absorption, and which is given by the following equations [3, 40, 247]:

$$L_p \approx L_w - 10\log_{10}(2.\pi. d_L{}^2) - \alpha_l. d_L \qquad (207)$$

$$L_p \approx L_w - 20\log_{10}\sqrt{H_{hub}{}^2 + d_L{}^2} - \alpha_l. \sqrt{H_{hub}{}^2 + d_L{}^2} - 8 \qquad (208)$$

Where L_p is the sound pressure level or the noise level expressed in (dB), d_L is the distance from a noise source radiating, L_w the sound power level expressed in (dB), and α_l is the frequency-dependent sound absorption coefficient which is taken as 0.005 dB(A)/m.

Taking into account all the above mentioned considerations, the prediction of the noise for the present design process, under expected operating conditions, can be computed. The noise assessment study is conducted by following the four major parts of information:

1. **An estimation of the existing ambient background noise levels**: a noise impact assessment for any proposed wind turbine project requires an evaluation of the environmental sound levels at the site to establish what minimum level of natural masking noise is consistently present to obscure noise from the project. Adverse impacts occur when the new noise from a project significantly exceeds the background level at sensitive receptors and becomes clearly audible **[248]**. Because of the importance of background noise in determining the acceptability of the overall noise level, it is crucial to measure the background ambient noise levels for all the wind conditions in which the wind turbine will be operating. Determining what background level to use as a design basis is strongly dependent on wind speed, since wind turbines only generate noise under windy conditions. Generally, in rural areas, the major environmental sounds produced by wind are grass, crop, and tree-leaf rustle. Assuming that the small wind turbine location is surrounded by flat area without any major highway noise sources nearby (farmland), the sound level could reach 42 dB(A). This value is assumed at wind speed of 8 m/s, at an IEC standardized height of 10 m **[248]**.

Determination of the background level to use as a design basis is strongly dependent on the wind speed, since wind turbines only generate noise under windy conditions. Because background levels also increase during windy conditions, an extensive sound level test is usually necessary so that measured levels can be correlated to a range of wind speeds. In general, a regression plot of sound level versus wind speed needs to be developed. For a typical wind speed of 5 m/s, in a given site, an average value of 35 dB(A) was found for the residual ambient sound level for wintertime conditions **[248].** This value represents the minimum residual ambient level for the entire year as it was measured during wintertime when the trees are bare, crops have been harvested, and there is no insect noise. For the rest of this analysis, the value of 35 dB(A) will be taken as the background sound levels, measured during the nighttime, over a specified period exceeded 90% of the time, L_{90}.

2. **Sound power level determination:** in order to calculate noise levels heard at different distances, the reference sound levels need to be determined. According to the IEC 61400-2, the apparent sound power level at 8.0 m/s at the hub height shall be used for noise assessment. However, for most wind turbine operation, wind speed usually ranges between 4 and 5 m/s. Therefore, a typical value of 5 m/s will be adopted for the sound power level assessment (most propbable wind speed on the site during normal wind conditions). Based on this requirement and using equation 208, the noise level of the actual design small wind turbine is **78.29 dB(A)**.

3. **Sound propagation model:** sound propagation is a function of the source sound characteristics (directivity, height), distance, air absorption, reflection and absorption by the

ground and nearby objects. Using equations 207 and 208 and assuming hemispherical noise propagation, the sound pressure level (noise level) at a slant distance of 60 m (expected observer distance for small wind turbine) **[249]**, for a reference wind speed between 5 m/s, is around **34 dB(A)**. Figure 86 shows the predicted sound pressure level at different distances from the small wind turbine source.
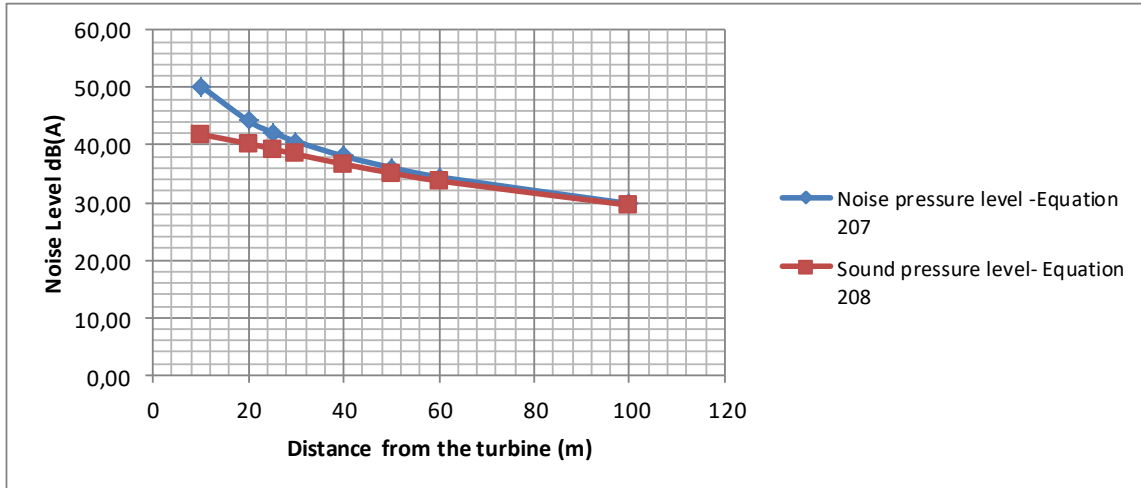
Figure 86: Noise level as a function of the distance from noise source

4. **Cumulative noise level:** the background noise environment consists of a multitude of distant sources of sound. When a new nearby source is introduced, the new background noise level would be increased. Any proposed or existing turbine within 2 km of the wind turbine development must be taken into account when establishing cumulative noise impact, where the proposed turbine produces noise emissions within 10 dB of any existing, consented or proposed (within the planning process) turbine noise emissions **[249]**. The addition of a new source with a noise level of 10 dB(A) below the existing background would increase the new background by 0.4 dB(A). If the new source has the same noise level as the existing background then the new background is increased by 3.0 dB(A). However, if the new source is 3.3 dB above the existing background then the new background would have increased by 5 dB(A). Lastly, when the difference between the source and the existing background is greater than 15 dB(A), the addition of the lower level has negligible effects **[1]**. The relation between the new noise sources and the existing background can be generalized as follows:

$$L_{total} = 10\log_{10} \sum_{i=1}^{N} 10^{\frac{L_i}{10}} \tag{209}$$

Where L_i is the sound pressure level of the ith source. The total sound pressure level a distance of 60, for a reference wind speed of 5 m/s, is **37.44 dB(A)**. Table 52 summarizes the results of the noise assessment of the actual design small wind turbine:

Turbine Parameters	Turbine sound power level (dBA)	Turbine tower height (m)	Atmospheric absorption coefficient (dBA/m)	Distance from turbine (m)	Calculated noise level (dBA) Equation 207	Calculated noise level (dBA) Equation 208	Background noise (dBA)	Total Noise (dBA)
Rotor angular velocity (rad/s)	78,29	24	0,005	10	50,26	41,86	35	42,68
8,57	78,29	24	0,005	20	44,19	40,24	35	41,38
	78,29	24	0,005	25	42,23	39,32	35	40,69
Blade radius (m)	78,29	24	0,005	30	40,62	38,41	35	40,04
3,5	78,29	24	0,005	40	38,07	36,68	35	38,93
	78,29	24	0,005	50	36,08	35,14	35	38,08
	78,29	24	0,005	60	34,45	33,76	35	37,44
	78,29	24	0,005	100	29,81	29,54	35	36,09

Table 52: Noise levels of the actual design small wind turbine

8.2 Noise limit determination

The analysis of the wind turbine noise should be considered as an important aspect during the planning stage of any wind turbine project. When developing new policy or regulation, governing authorities are interested in reliable references from other countries in order to define their own specific needs, and then to setup their noise regulation limits. Noise limits are established are regulated by applying specific noise metrics to ensure the quality of life within the local communities. The noise metrics used to regulate noise from wind turbines have shown a large disparity between countries. Regarding the community standards for determining acceptable sound pressure levels, at the present time, there are no common international noise standards or regulations [250]. In most countries, however, noise regulations define upper bounds for the noise to which people may be exposed. These limits depend on the country and are often different for daytime and nighttime. To give a sense to the disparity of wind turbine noise code regulations, an overview is presented in figure 87 summarizing the threshold limits as published by a variety of different countries. These values are given by the noise metric L_{Aeq}, which is defined as the average A-weighted sound pressure level which gives the same total energy as the varying sound level during the measurement period of time. This is the most common used noise metric.
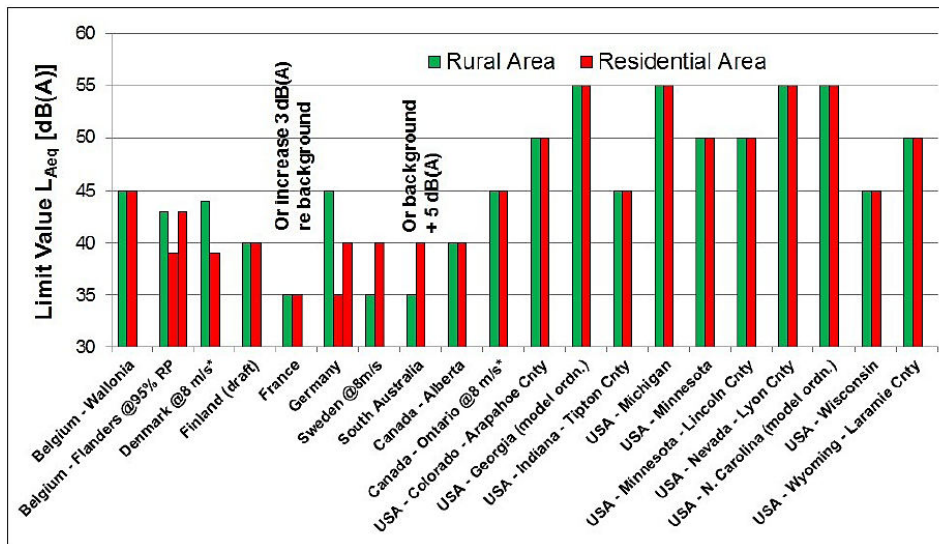
Figure 87: Noise limits for rural and residential areas, **[250]**

Countries like France, Sweden, South Australia and New Zealand have more strict noise limits for rural areas with relatively low background noise levels than for residential areas. In contrary, Belgium (Flanders region), Denmark and Germany in general allow high noise levels at dwelling in rural areas than at residential areas. Haugen, Kathryn M. B. **[251]** has conducted a similar comparison study of the acceptable noise limits between different countries. Figure 88 represents the noise limits at residences in countries and regions that have required or recommended noise limits at residences near wind turbines. The blue bars represent the lower noise limits, and the blue plus green bars represent the upper noise limits at residences near wind turbines. The average lower noise limit is approximately **35 dB(A)**, and the average upper noise limit is **45 dB(A)**. For farmhouses, the most important benchmark is **45 dB(A)**, which is to be adhered to at night in mixed area **[3]**.
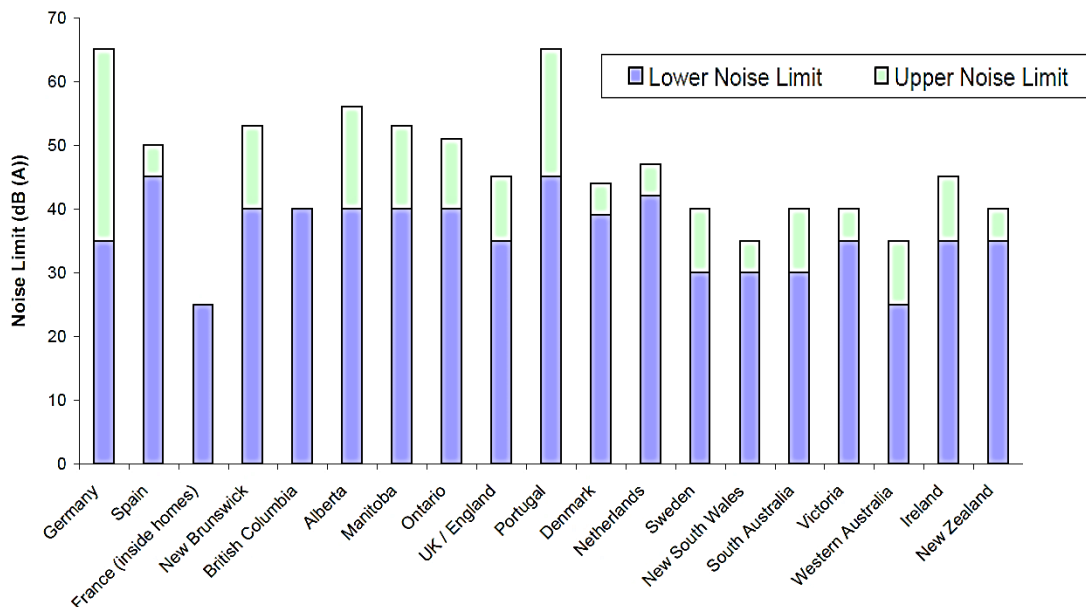
Figure 88: Noise limits at residences near wind turbines in different countries, **[251]**

A common approach that is usually used to determine an acceptable noise limit consists of using the existing background sound levels for each area as the basis for establishing the sound level limits for the wind turbine project [252]. This method has the advantage of adjusting the allowable limits for various background soundscapes. It makes use of a standard method for assessing background sound levels by measuring over a specified period of observation to determine the sound level exceeded 90% of the time (L_{90}) during the night. The night is important because it is the most likely time for sleep disturbance. Then, by using the background sound level as the base, the wind turbine system is allowed to increase it by 5 dB(A) for both day and nighttime. That is, the allowable noise limit is L_{90} + 5 dB(A). This method is adopted for the criteria in this document. Therefore, the acceptable noise limit in the case of the present study is 40 dB(A). Finally, it can be concluded that the actual design small wind turbine meets the noise requirements in the both rural and residential areas, and the system can be placed safely 25 m away from the owner's home without any noise disturbance.

It is worth noting that this analysis is based on the category I models, which predict the global emitted noise as a function of main wind turbine parameters (rated power, rotor diameter, blade area, tip speed, etc.). These Category I models are simple and fast, however they are by far not universal. Therefore, further more accurate models (category II and category III models) should be used to accurately determine the exact noise emissions from the wind turbine system.

Measurements and tests still the most effective way to make sure that the noise emissions from the small wind turbine will not exceed the required limits. Measurement of noise emission from small wind turbines is guided by the international standard **IEC 61400-11** [253]. This provides methods and conditions under which the sound power levels and spectra of wind turbines are to be determined. It includes measurement at ground level at various distances from the tower, both upwind and downwind, over a range of wind speeds, and uses a ground reflection board for the mounting of the microphone to increase the signal to noise ratio. All suppliers of small wind turbines provide sound power level and spectral data measured according to this standard [254].

8.3 Conclusion

Wind turbines emit a relatively weak but characteristic noise. The noise is mainly generated by the movement of the blades through the air. This produces a swishing sound in rate with the rotation of the blades, as well as noise from the turbine machinery. Machine noise can have a tonal character which is particularly annoying. Therefore, noise assessment is an

important part of the present design processs since the small wind energy system is originally designed for residential areas and farmers' households. According to the Literatrue, noise emissions should be measured under both very windy conditions (8 m/s at 10 m height) and less windy conditions (6 m/s) to reflect the two sets of noise limits. The calculation of the amount of noise emitted to neighbouring properties is very simple, because the noise is emitted from a significant height. Throughout this chapter, the sound power level of the wind turbine system and the noise level at a given distance from the source were determined using a prediction model based on simple equations that involve the main wind turbine parameters (rated power, rotor diameter, blade area, tip speed, etc.). Based on the results obtained, the actual design small wind turbine meets the noise requirements in the both rural and residential areas, and the system can be placed safely 50 m away from the owner's home without any noise disturbance.

CHAPTER 9: WIND TURBINE STRUCTURE AND LOADING

Small wind turbines are generally exposed to fluctuating winds and variable forces. This is especially the case if they are installed on sites that are characterized by extreme winds and turbulences. These operational constraints impose that the wind turbine design must take into consideration the resistance, the dynamic behavior and the fatigue properties of the materials used in construction of the entire structure. In normal operation, the components of a wind turbine are subjected to repeated bending and fatigue loads. This is mainly due to the random variation in wind speed. For example, the rotor blades when they are subjected to repeated loads, they can develop some cracks which can eventually break the component. Therefore, in designing a wind turbine, it is extremely important to calculate in advance how different components vibrate, both individually and together. It is also important to calculate the forces involved in bending or tension of each component.

Different numerical models are developed in order to analyze the behavior of the entire structure of a wind turbine. Currently, the wind energy industry makes use of these models to design safe machines which can operate safely whatever the climatic and environmental conditions of the sites [7]. The most commonly models, which are recommended by the international standard **IEC-64100-2** (International Electrotechnical Commission), are:

- **Simple load model, SLM:** this model is based on simple equations to calculate the bending moments and fatigue loads. As its name suggests, this model is a very simple design methodology.

- **Aeroelastic model**: allowing a more accurate computer modeling of different loads on the turbine in response to stochastic inputs such as changes in wind directions and wind gusts. This model is commonly used for large wind turbines. The main problem with the aeroelastic modeling seems to be the high cost of software and the time required for its implementation. This method is rarely used in the design of small wind turbines.

- **Measurements of loads and extrapolation for extreme conditions:** This model requires testing in the field.

The main objective of this section is to determine the different loads (fatigue, bending, compression and torsion) applied on both the turbine blades and the main shaft. **These loads will be assessed using the simple Load Model (SLM)**. In this perspective, an overview of the model as well as the different load cases will be presented. After, determination of the applied forces, according to each load case, will be conducted. The results will be then converted into equivalent stresses (σ_{eq}) that must be compared with the allowable stresses of

the corresponding components (σ_a) [40]. So that a component operates safely without risk of damage, it is necessary that the equivalent stress that is applied is less than the allowable stress:

$$\sigma_{eq} < \sigma_a \qquad (210)$$

9.1 Simple Load Model-SLM

A good location in a windy site can expose the wind turbine to high winds which could make it turn at high speeds exceeding the limits set by its design (typically at 15 m/s). Strong winds can cause premature wear, damage of the nacelle or in the worst scenarios a complete destruction of the wind turbine. To guarantee a proper functioning of the entire system, the various components of the wind turbine must be designed in a way that they can withstand the loads without damage. Loads applied to each element must be assessed by calculation or by testing in order to determine if the integrity of the structure satisfies the security requirements. Calculation of the stresses on the small wind turbine in this study will be based on the simple load model (SLM). Compared to the other models (aeroelastic model and the mechanical laboratory testing), this model has the advantage of being simple and reliable. However, the other models require expensive tools and sophisticated approaches which are not affordable at this stage of the design process. The wind turbines for which the simple load model (SLM) can be used must meet many requirements. These are: turbine with horizontal axis rotor, turbines with two or more blades, rotor with cantilevered blades and rigid hub, upwind or downwind rotor, operation at constant or variable speeds, turbines with active or passive pitch mechanism, as well as fixed pitch, and turbines with vertical or horizontal furling, or intermediate axes, as well as turbine with no furling system. If the configuration of the wind turbine does not meet these requirements, the aeroelastic models or measurements of loads by extrapolation for extreme conditions should be used.

9.2 Simple load model loading

The evaluation of the applied stresses on a wind turbine must consider the following loads [114]:

- Vibration, inertial and gravitational loads: these loads are generally generated by centrifugal forces, gyroscopic effects, and by gravity loads represented by weight of the blades and the nacelle;

- Aerodynamic loads: these loads are associated with the forces generated by all the overpressure and the depression caused by airflow and its interaction with the fixed and moving parts of the wind turbine.

- Operational loads: this type of loads is a result of the operation and control of the turbine system. Operational loads can be generated by the wind turbine orientation system (yaw drive) or by the braking system (furling) as they can be caused by the aerodynamic control systems such as the pitch control system;

- Other loads: other loads may be generated by environmental conditions or by special use of wind turbine. These loads must be taken into account when calculating the stresses on the structure (loads of snow, wake, transport, installation, maintenance etc.);

Figure 89 summarizes the applied loads on wind turbines' components:
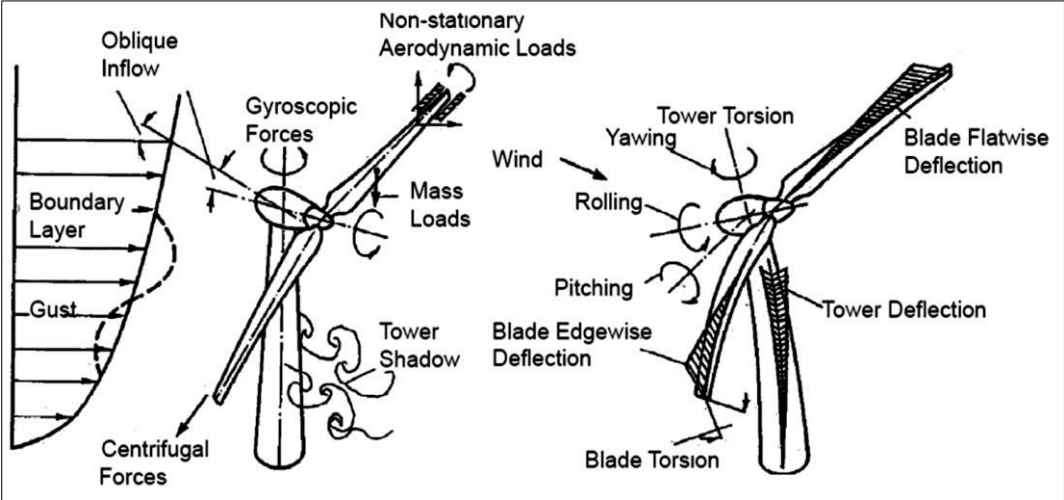
Figure 89: Forces and moments applied to a wind turbine components **[255]**

For design purposes, the life cycle of a wind turbine can be represented by a set of design situations covering all the most important external conditions which the wind turbine is supposed to face. All relevant load cases with reasonable probability of occurrence are to be considered in assessing the behavior of the structure in extreme wind conditions. Generally, the design scenarios that can be used to analyse the structure of a small wind turbine are as follows: wind turbine operation without fault and with normal external conditions, wind turbine operation without fault and with extreme external conditions, wind turbine operation with fault and appropriate external conditions, and finally general situations including transportation, installation and maintenance **[7]**. In every design situation, several load cases must be considered. Table 53 gives all the load cases considered in the simple load model analysis **[40]**:

LOCATION DESIGN		LOAD CASE	WIND SPEED USED	TYPE OF ANALYSIS
Energy production	**A**	Normal Operation		F
	B	Yawing	$V_{hub} = V_{design}$	U
	C	Yaw Error	$V_{hub} = V_{design}$	U
	D	Maximum Thrust	$V_{hub} = 2.5\ V_{ave}$	U

		Maximum Rotational Speed		U
Power production plus occurrence of fault	E	Maximum Rotational Speed		U
	F	Short at Load Connection	$V_{hub} = V_{design}$	U
Shutdown	G	Shutdown (Braking)	$V_{hub} = V_{design}$	U
Parked (idling or standstill)	H	Parked Wind Loading	$V_{hub} = V_{e50}$	U
Parked and fault conditions	I	Parked Wind Loading, Maximum Exposure	$V_{hub} = V_{Ref}$	U
Transport, assembly, maintenance and repair	J	To be stated by manufacturer		U

Table 53: Load cases of simple load model

For each design situation, the appropriate type of analysis is stated by "**F**" and "**U**" in the table 53. **F** refers to analysis of fatigue loads, to be used in the assessment of fatigue strength. **U** refers to the analysis of ultimate loads such as analysis of exceeding the maximum material strength, analysis of tip deflection, and stability analysis.

9.3 Coordinate system

To define the directions of the loads of a horizontal axis wind turbine (HAWT), the system of axes given by IEC standard and shown in Figure 90 is used. x_{blade} is such that a positive moment about the x-axis acts in the rotational direction y_{blade} is such that a positive moment acts to bend the blade tip downwind zblade is positive towards blade tip the blade coordinate system follows the right-hand convention for a rotor that spins clockwise and the left-hand convention for a rotor that spins counter clockwise when viewed from an upwind location.
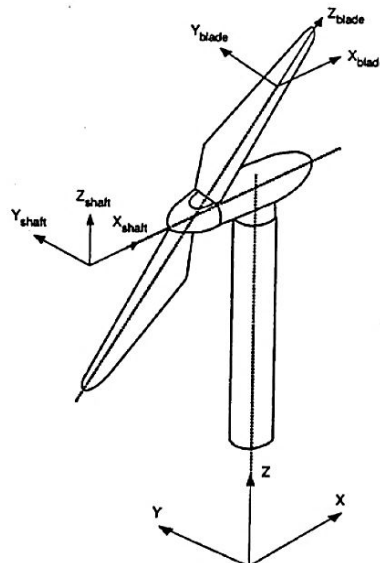
Figure 90: Coordinate system for load calculation

9.4 Design parameters for load calculation

Before using the SLM model for load analysis, some design parameters must be defined. These are determined based on both the site conditions (external conditions) and the structure of the wind turbine. The site conditions are mainly specified by the wind turbine class which specifies the design wind speeds and the turbulence intensity. Based on the previously conducted wind data analysis (wind speeds at different heights), **a wind turbine class III was selected**. Therefore, table 54 summarized the design conditions considered in the present design and analysis.

Design parameters	Values
Wind turbine class	**Class III**
Temperature range	**-20 °C to +50 °C**
Air density	**1.3943 Kg/m^3 to 1.0932 Kg/m^3**

Table 54: Basic environmental design parameters

On the basis of the selected wind turbine class and through a verification process of the structural integrity of the components in the critical load paths (from the rotor blades to the generator), a verification can be conducted to check if the wind turbine can withstand the most severe external conditions during its entire lifetime. In Addition to the environmental conditions, simple load model requires a set of additional design parameters. The first step in the load calculation process consists in defining the design parameters given in table 55.

Design Parameter	Value
Design wind speed (m/s)	**10.5**
Average wind speed (m/s)	**7.5**
Design power (kW)	**11**
Design rotational speed (RPM)	**172**
Drive train efficiency	**0.655**
Maximum yaw rate (rad/s)	**2.635**
Maximum rotational speed (RPM)	**245.55**
Design shaft torque (Nm)	**932.38**

Table 55: Fundamental design parameters

With the exception of the maximum yaw rate, the determination of these parameters is normally based on tests. The full list of the primary design parameters that are required to perform a load analysis using SLM model is given in table 56.

Description	Input Value	Units	Symbol
Air density	1,2250	kg/m^3	ρ
Gravitational acceleration	9,8100	m/s^2	g
Reference Wind Speed	37,5000	m/s	V_ref
Average Wind Speed	7,5000	m/s	V_ave
Number of Blades	3	n/a	B
Blade Tip Radius	3,5000	m	R
Total Planform Area of the Blade	0,5400	m^2	A_proj,B
Drag Coefficient of the Blades	1,5000	n/a	C_d
Max Lift Coefficient of the Blades	2,0000	n/a	C_l,max
Thrust Coefficient	0,5000	n/a	C_T
Maximum Rotor Speed	245,5500	rpm	n_max
Design Rotor Speed	172,0000	rpm	n_design
Second Moment of Inertia for each Blade	42,3360	kgm^2	I_B
Single Blade Mass	21,6000	kg	m_B
Rotor Mass (All Blades plus Hub)	93,8200	kg	m_r
Distance from Blade centre of gravity to rotor axis	1,4000	m	R_cog
Distance Between Rotor Centre and First Bearing	0,1000	m	L_rb
Distance Between the Rotor Centre and the yaw axis	0,6000	m	L_rt
Gearbox Ratio (enter 1.0 for no gearbox)	1,0000	n/a	Gear
Enter "Y" if brake is on high speed side of gearbox, otherwise "N"	N	n/a	n/a
Brake torque (enter 0.0 for no brake)	1785,2000	Nm	M_brake
Design Power	11,0000	kW	P_design
Short Circuit Torque Factor	2,0000	n/a	G
Type "Y" if blades are stationary during parking, otherwise "N"	Y	n/a	n/a

Table 56: Design parameters for load calculation

Table 57 gives additional design parameters which are deduced from data given in the table above.

Description	Value	Units	Symbol
Design Wind Speed	10,50	m/s	V_design
50 year extreme wind speed	52,50	m/s	V_e50
50yr extreme tip speed ratio	1,71	n/a	λ_e50
Design Tip Speed Ratio	6,00	n/a	λ_design
Drive Train Efficiency	0,655	n/a	ή
Design Torque	932,38	Nm	Q_design
Projected Area (turbine swept area)	38,48	m^2	A_proj
Design Rotational Speed of the Rotor	18,01	rad/s	ω_n,design
Maximum Possible Rotor Speed	25,71	rad/s	ω_n,max
Max Yaw Rate	2,635	rad/s	ω_yaw,max
50yr extreme tip speed ratio	1,71	n/a	λ_e50
Ecentricity of the Rotor Centre of Mass	1,75E-02	m	e_r
Effective brake torque	1785,20	Nm	M_brake

Table 57: Additional design parameters

9.5 Load cases

9.5.1 Load case A: Normal operation

The first load case covers fatigue behavior during normal operation of the turbine and is the only fatigue load case. All the equations in this sub-section define peak-to-peak loads generated by the assumed cycling between 1.5 times and 0.5 times the design values of the angular velocity and torque. Loads (applied on the blades and main shaft) that make up this load case will be forwarded to the tower.

$m_B = 21.6$ Kg
$R_{cog} = 1.4$ m
$L_{rb} = 0.1$ m
$B = 3$

The first load is the centrifugal force:

$$\Delta F_{ZB} = 2. \, m_B. \, R_{cog}. \, \Omega^2 = 19617.29 \text{ N} \tag{211}$$

The lead-lag (in the direction of rotation) and flapwise moment (in the direction of the wind; alternatively, out of the plane of rotation) are calculated using the following equations:

$$\Delta M_{xB} = \frac{Q_{design}}{B} + \, 2. \, m_B. \, g. \, R_{cog} = 904.1 \text{ N. m} \tag{212}$$

$$\Delta M_{yB} = \frac{\lambda_{design}. \, Q_{design}}{B} = 1864.76 \text{ N. m} \tag{213}$$

Where R_{cog} is the radial distance from hub center to blade center of gravity.

The next three equations give the peak to peak fatigue loads on the turbine shaft. This load is assumed to occur at the first shaft bearing (nearest to the rotor):

$m_r = 93.82$ Kg
$e_r = 0.005 \, R = 0.0175$

$$\Delta F_{X-shaft} = \frac{3. \, \lambda_{design}. \, Q_{design}}{2R} = 2397.54 \text{ N} \tag{214}$$

$$\Delta M_{X-shaft} = Q_{design} + \, 2. \, m_r. \, g. \, e_r = 964.54 \text{ N. m} \tag{215}$$

$$\Delta M_{shaft} = 2. \, m_r. \, g. \, L_{rb} + \frac{R}{6} \Delta F_{X-shaft} = 1582.63 \tag{216}$$

Where e_r is the default eccentricity in the rotor center of mass.

9.5.2 Load case B: Yaw (Yawing)

The loads due to the bending moment M_{yB} and the bending moment on the main shaft M_{shaft} must be calculated using equations 217 and 218.

$L_{rt} = 0.6$ m
$J_B = 42.33$ Kg.m²
$\omega_{max} = 2.635$ rad/s

$$M_{yB} = m_B . \omega^2_{max} . L_{rt} . R_{cog} + 2 . \omega_{max} . J_B . \Omega + \frac{R}{9} \Delta F_{X-shaft} = 5076 \text{ N.m} \qquad (217)$$

Where L_{rt} is the distance between the rotor and the yaw axis (the tower axis), and J_B is the blade moment of inertia. For the shaft, the loads are dependent on the number of blades. Thus, for a three-bladed rotor or more, the shaft bending moment is given by:

$$M_{shaft} = B . \omega_{max} . \Omega . J_B + m_r . g . L_{rb} + \frac{R}{6} \Delta F_{X-shaft} = 7517.08 \qquad (218)$$

9.5.3 Load case C: Yaw error

All wind turbines operate with a certain yaw error. In this load case, a yaw error of 30° is considered. The flapwise bending moment caused by the yaw error is given by equation 219.

$C_{lmax} = 2$
$A_{proj,B} = 0.54$ m²

$$M_{yB} = \frac{1}{8} \rho . A_{proj,B} . C_{l,max} . R^3 . \Omega^2_{design} \left[1 + \frac{4}{3 . \lambda_{design}} + (\frac{1}{\lambda_{design}})^2 \right] = 2874.82 \text{ N.m} \quad (219)$$

Where $A_{proj,B}$ is the projected area of the blades, and $C_{l,max}$ is the maximum lift coefficient. If no value is specified, a value of 2 shall be used.

9.5.4 Load case D: Maximum thrust

The small wind turbine can be exposed to high thrust loads on the rotor. The thrust load acts parallel to the rotor shaft and has a maximum value given by:

$C_{Th} = 0.5$
$V_{ave} = 7.5$ m/s

$$F_{x-shaft} = 3,125 . C_{Th} . \rho . V^2_{ave} . \pi . R^2 = 4143.47 \text{ N} \qquad (220)$$

Where C_{Th} is the thrust coefficient which is taken equal to 0.5.
This is a critical load since it increases with the square of the wind speed, so that operation at a sufficiently high speed will produce very high loads. The thrust must also be transmitted to

the tower, making it, along with the turbine weight, and the gyroscopic loads described above, the main ways in which the turbine loads influence the tower loads.

9.5.5 Load case E: Maximum rotational speed

The centrifugal loading on the blades and especially the blade hub can become extremely large at high rotational velocities. The centrifugal load in the blade root is calculated using equation 221.

$$\mathbf{F_{ZB} = m_B.\, \Omega^2{}_{max}.\, R_{cog} = 19988.76\ N} \tag{221}$$

The bending moment on the main shaft due to the small rotor imbalances can be calculated using equation 222.

$$\mathbf{M_{shaft} = m_r.\, g.\, L_{rb} + m_r.\, e_r.\, \Omega^2{}_{max}.\, L_{rb} = 200.56\ N.\,m} \tag{222}$$

9.5.6 Load case F: Short at load connection

In the case of a direct electrical short at the output of the small wind turbine or internal short in the generator, a high moment is created about the rotor shaft due to the short circuit torque of the alternator. In the absence of any values proven to be more accurate, two times the design torque is to be taken as the short circuit torque acting on the generator shaft:

$$\mathbf{M_{X-shaft} = G.\, Q_{design} = 1864.76\ N.\,m} \tag{223}$$

With **G** is the numerical factor taken equal to 2.0 unless a more accurate value is established.

$$\mathbf{M_{XB} = \frac{M_{X-shaft}}{B} = 621.58\ N.\,m} \tag{224}$$

9.5.7 Load case G: Braking

In the case of wind turbines with a mechanical or electrical braking system in the drive train, the braking moment can be greater than the maximum driving moment. In these cases, the braking moment, $\mathbf{T_{Brake}}$, derived from testing or calculations, shall be used in the design calculations of the small wind turbine. The maximum shaft torque is assumed to be equal to the brake plus the design torque (thus assuming that the brake is applied while the generator still delivers design torque). The bending moment is given by:

$$\mathbf{M_{X-shaft} = T_{Brake} + Q_{design} = 2717.58\ N.\,m} \tag{225}$$

The blade load during shutdown is assumed to be determined by the shaft torque and blade mass. Thus being:

$$\mathbf{M_{xB} = \frac{M_{X-shaft}}{B} + m_B.\, g.\, R_{cog} = 1202.51\ N.\,m} \tag{226}$$

9.5.8 Load case H: Parked wind loading

This load case considers several separate loads acting on a parked turbine, that is, a turbine whose rotor is not producing power. It is not necessary for the blades to be stationary while parked. The loads are calculated using a wind speed of U_{e50}, the 3s 50-year extreme wind speed. The main loading on a stationary rotor is due to drag:

$C_d = 1.5$
$U_{e50} = 52.5$ m/s

$$M_{yB} = \frac{1}{4} . C_d . \rho . U^2_{e50} . A_{proj,B} . R = 2393.02 \text{ N.m} \tag{227}$$

Where C_d is the drag coefficient.

If the rotor is rotating, M_{yB} is due to the lift created on the blades due to changes in wind direction:

$$M_{yB} = \frac{1}{6} . C_{l,max} . \rho . U^2_{e50} . A_{proj,B} . R = 2127.13 \text{ N.m} \tag{228}$$

For a parked rotor the shaft thrust load is calculated as given by equation 229:

$$F_{X-shaft} = \frac{1}{2} . B . C_d . \rho . U^2_{e50} . A_{proj,B} = 4102.33 \text{ N} \tag{229}$$

For a spinning rotor the thrust force is given by:

$$F_{X-shaft} = 0,17 \ B . A_{proj,B} . \lambda^2_{e50} . \rho . U^2_{e50} = 2719.01 \tag{230}$$

Table 58 summarizes the SLM loads with reference to the relevant equations in IEC 61400-2.

Load Case A - Fatigue Loads on Blades and Rotor Shaft

Equation	Description	SLM Value	Units	Symbol
	Blade Loads			
9.4 (IEC 21)	Centrifugal Force at the Blade Root (z-axis)	19621,22	N	ΔF_zB
9.5 (IEC 22)	Lead-lag Root Bending Moment (x-axis)	904,10	Nm	ΔM_xB
9.6 (IEC 23)	Flapwise Root Bending Moment (y-axis)	1865,99	Nm	ΔM_yB
	Shaft Loads			
9.7 (IEC 24)	Thrust on shaft (x-axis)	2399,13	N	ΔF_x-shaft
9.8 (IEC 25)	Shaft Moment about x-axis	964,60	Nm	ΔM_x-shaft
9.9 (IEC 26)	Shaft Moment	1583,57	Nm	ΔM_shaft

Load Case B - Blade and Rotor Shaft Loads during Yaw

Equation	Description	SLM Value	Units	Symbol
9.16 (IEC 28)	Flapwise Root Bending Moment (y-axis)	5077,60	Nm	M_yB
9.11,12 (IEC 29,30)	Bending moment on the shaft	7519,47	Nm	M_shaft

Load Case C - Yaw Error Load on Blades

Equation	Description	SLM Value	Units	Symbol
9.13 (IEC 31)	Flapwise Root Bending Moment (y-axis)	2874,98	Nm	M_yB

Load Case D - Maximum Thrust on Shaft

Equation	Description	SLM Value	Units	Symbol
9.14 (IEC 32)	Maximum Thrust on Shaft	4143,47	N	F_x-shaft

Load Case E - Maximum Rotational Speed

Equation	Description	SLM Value	Units	Symbol
9.15 (IEC 33)	Centrifugal Force at the Blade Root (z-axis)	19994,88	N	F_zB
9.16 (IEC 34)	Bending Moment on the shaft	200,60	Nm	M_shaft

Load Case F - Short at Load Connection

Equation	Description	SLM Value	Units	Symbol
9.17 (IEC 35)	Bending Moment on Shaft	1864,77	Nm	M_x-shaft
9.18 (IEC 36)	Lead-lag Root Bending Moment (x-axis)	621,59	Nm	M_xB

Load Case G - Shutdown Braking

Equation	Description	SLM Value	Units	Symbol
9.19 (IEC 37)	Bending Moment on Shaft	2717,58	Nm	M_x-shaft
9.20 (IEC 38)	Lead-lag Root Bending Moment (x-axis)	1202,52	Nm	M_xB

Load Case H - Parked Wind Loads during Idling

Equation	Description	SLM Value	Units	Symbol
9.23,24 (IEC 39,40)	Flapwise Root Bending Moment (y-axis)	2393,03	Nm	M_yB
9.25,26 (IEC 41,42)	Maximum Thrust on Shaft	4102,33	N	F_x-shaft

Table 58: SLM load calculation

9.6 Equivalent components stresses and safety factors

9.6.1 Equivalent components stresses

Loads calculated in the previous paragraph shall be converted into equivalent stresses. To ensure that the structure of the wind turbine can withstand the forces applied to it, a comparison between the equivalent stresses (σ_{eq}) and allowable stresses (σ_a) of different components must be done. In order to convert the SLM loads into equivalent stresses, another set of design parameters are required. The additional design parameters are given in table 59.

Description	Value	Units	Symbol
Diameter of the Shaft	9,0000E-02	m	
Cross Sectional Area of the Shaft	4,3982E-03	m^2	A_shaft
The second moment of inertia for the shaft	2,9138E-06	m^4	I_x-shaft
Section modulus for the shaft	6,4752E-05	m^3	W_shaft
Cross Sectional Area of the Blade Root	1,2130E-02	m^2	A_B
Ixx for the blade	2,2407E-05	m^4	I_xxB
x-distance from blade centroid to the maximum stress point	7,5000E-02	m	c_xB
Iyy for the blade	2,2407E-05	m^4	I_yyB
y-distance from blade centroid to the maximum stress point	7,5000E-02	m	c_yB
Blade x-section modulus	2,9875E-04	m^3	W_xB
Blade y-section modulus	2,9875E-04	m^3	W_yB
Ultimate Material Strength for the Blades	3,7500E+02	MPa	f_kB
Ultimate Material Strength for the Shaft	4,5000E+02	MPa	f_k-shaft

Table 59: Additional data input for load calculation

Table 60 shows the equations used to calculate the equivalent stresses for the blade root and the main shaft:

	Circular blade root	Main shaft
Axial load	$\sigma_{ZB} = \dfrac{F_{zb}}{A_B}$	$\sigma_{x-shaft} = \dfrac{F_{x-shaft}}{A_B}$
Bending moment	$\sigma_{MB} = \dfrac{\sqrt{M^2_{xB} - M^2_{yB}}}{W_R}$	$\sigma_{M-shaft} = \dfrac{M_{shaft}}{W_{shaft}}$
Shear	**Negligible**	$\mathcal{T}_{M-shaft} = \dfrac{M_{x-shaft}}{2W_{shaft}}$
Combined load (bending moment and axial load)	$\sigma_{eqB} = \sigma_{ZB} + \sigma_{MB}$	$\sigma_{eq} = \sqrt{(\sigma_{x-shaft} + \sigma_{M-shaft} + 3\mathcal{T}^2_{M-shaft}}$

Table 60: Equivalent stresses for SLM loads

The equivalent stresses acting on the wind turbine components are calculated and the results are summarized in table 61.

Description	Equivalent Stress (MPa)
Load Case A - Fatigue Loads on Blades and Rotor Shaft	
Blades	8,56
Shaft	28,13
Load Case B - Blade and Rotor Shaft Loads during Yaw	
Blades	17,00
Shaft	116,13
Load Case C - Yaw Error Load on Blades	
Blades	9,62
Load Case D - Maximum Thrust on Shaft	
Shaft	0,94
Load Case E - Maximum Rotational Speed	
Blades	1,65
Shaft	3,10
Load Case F - Short at Load Connection	
Blades	2,08
Shaft	24,94
Load Case G - Shutdown Braking	
Blades	4,03
Shaft	0,01
Load Case H - Parked Wind Loads during Idling	
Blades	8,01
Shaft	0,93

Table 61: Equivalent stresses calculation

9.6.2 Partial safety factors

To assess the allowable stresses for various components of a wind turbine, the **IEC 61400-2** standard define partial safety factors for all the load cases. Table 62 shows the safety factors for fatigue and ultimate loads. Load factors are used to account for uncertainties in the assessment process of the loads. Their values vary according to the model used.

Model	Safety factor for fatigue loads (γ_f)	Safety factor for ultimate loads (γ_f)
Simple Load Model	1	3

Table 62: Partial safety factors for SLM load cases

Table 63 contains the partial safety factors for material characterization. To use the full characterization factors, that is to say low safety factors, the material properties must have been estimated with 95% probability at a 95% confidence level. Additionally, the use of a full material characterization requires that: the properties have been obtained from materials and configurations representative of the final structure, the test samples come from the same process as the final product, the static and the fatigue testing have been done with appropriate load spectrum and rate effects, the environmental effects, such as ultra-violet degradation, have been included, and finally, any other appropriate geometry effects, such as fiberglass orientation in composite; blades, have been adequately accounted for.

Actually, full characterization of physical properties requires deep knowledge of both the material properties and the manufacturing process. This is not the case for the present project, especially at the current stage of design process. Therefore, blade material is assumed to be minimal characterized so that the appropriate material safety factors are 10 for fatigue loads and 3 for ultimate strength. For the shaft material, it was assumed to be well characterized as no specific knowledge is needed. Therefore, its partial safety factor for fatigue and ultimate strength are 1.25 and 1.1, respectively.

Condition	Full characterization (γ_m)	Minimal characterization (γ_m)
Fatigue	**1.25**	**10**
Ultimate strength	**1.1**	**3**

Table 63: Partial safety factors for material characterization

In order to determine the equivalent stresses. It is assumed that the shaft and other metal components are made from C55/1.0535 (EN 10083-2) medium carbon steel with a yield stress of **450 MPa** and the composite blades have an ultimate strength of **374 MPa**. Assuming minimal characterization of the blade material and full characterization for the shaft material, and by using the corresponding load safety factors for each material, the rotor blades will be safe in ultimate loads if the equivalent stress is less than **41.61 MPa** and the steel components if their stress is less than **136.36 MPa**.

Table 64 gives the results abtianed from SLM calculations. The main shaft and the rotor blade pass successfully all the load scenarios. However, the results of stress analysis show large gap between stress limits and calculated tress for the majority of the load scenarios. This is due to the fact that SLM is associated with high safety factors and increased conservatism. The stress analysis demonstrates that SLM still presenting a barrier to small wind developers.

Load Case B - Blade and Rotor Shaft Loads during Yaw			
	Material Stress Limit (MPa)	**Calculated Stress (MPa)**	**Conclusion**
Blades	41,67	17,00	SAFE
Shaft	136,36	116,13	SAFE
Load Case C - Yaw Error Load on Blades			
	Material Stress Limit (MPa)	**Calculated Stress (MPa)**	**Conclusion**
Blades	41,67	9,62	SAFE
Load Case D - Maximum Thrust on Shaft			
	Material Stress Limit (MPa)	**Calculated Stress (MPa)**	**Conclusion**
Shaft	41,67	0,94	SAFE
Load Case E - Maximum Rotational Speed			
	Material Stress Limit (MPa)	**Calculated Stress (MPa)**	**Conclusion**
Blades	41,67	3,10	SAFE
Shaft	136,36	1,65	SAFE
Load Case F - Short at Load Connection			
	Material Stress Limit (MPa)	**Calculated Stress (MPa)**	**Conclusion**
Blades	41,67	2,08	SAFE
Shaft	136,36	24,94	SAFE
Load Case G - Shutdown Braking			
	Material Stress Limit (MPa)	**Calculated Stress (MPa)**	**Conclusion**
Blades	41,67	4,03	SAFE
Shaft	136,36	0,01	SAFE
Load Case H - Parked Wind Loads during Idling			
	Material Stress Limit (MPa)	**Calculated Stress (MPa)**	**Conclusion**
Blades	41,67	0,93	SAFE
Shaft	136,36	8,01	SAFE

Table 64: Results of stress analysis using SLM

To validate the results obtained SLM, Finite Element method using ANSYS was conducted for the load case H (Parked wind loads during idling). The coordinates of the airfoil, the chord and the twist distribution and the thicknesses are imported to the 3-D CAD design software SOLIDWORKS. Computational fluid dynamic (CFD) approach was performed by simulating the airflow for a wind velocity of 52.5 m/s ANSYS (same wind conditions as SLM). The pressure distribution was exported to the structural analysis model in ANSYS to evaluate the maximum stress. As the equations of the SLM model computes the stress in the blade root, a comparison of the maximum stress from ANSYS (7.13 MPa) and SLM (8.01 MPa) shows that SLM model gives good results the stress on the blade structure. Figure 91 shows that the maximum stress is distributed along the length of the blade where the spar cap was integrated into the blade shell. This is not surprising given that the spar cap are the stiffest part of the blade (suction and pressure sides) which is mainly used to withstand the extreme flap-wise bending moments on the blade structure, and then to minimize the blade tip deflection. The use of spar caps and shear web in the blade structural design allows increasing the stiffness of the blade without changing its shape. Figure 91 shows the stress distribution on the blade structure (von-Mises stress).
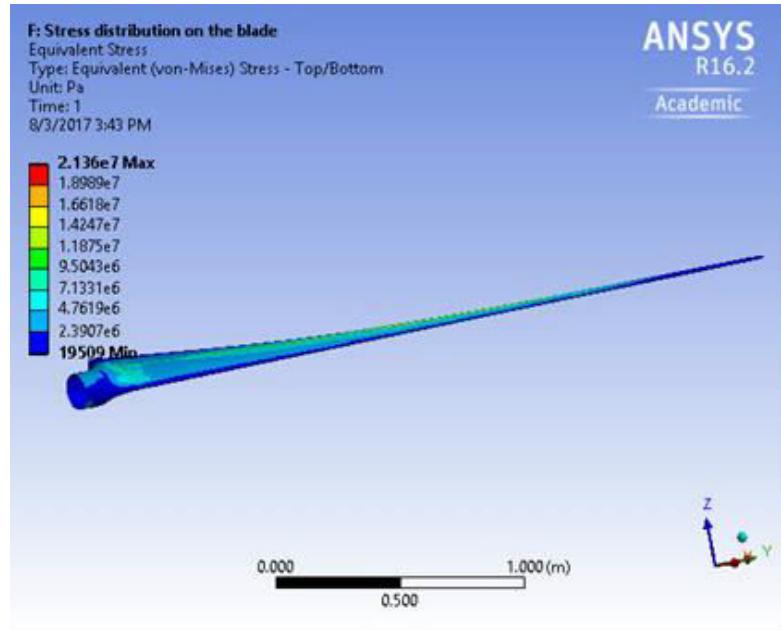
Figure 91: Stress distribution on the blade structure

9.7 Blade fatigue analysis

9.7.1 Blade fatigue analysis using SLM model

Small wind turbines are fatigue critical machines that are typically subjected to various cyclic loads. Therefore, their design process should take into consideration this important structural condition which includes high numbers of fatigue cycles. The fatigue loading varies between tension, compression and reversed tension-compression loads according to the particular loads spectrum for the turbine and the wind conditions **[256]**. The most fatigue critical part of a wind turbine is the rotor blades and their connection to the hub. In a design life extending over more than **20 years**, the system has to endure high cycle fatigue loading **($> 10^8$)** of variable amplitude due to gusts, wind shear, and start/stop procedures etc. **[257]**. In order to allow a safe and economic design of wind turbines it is necessary to determine the high cycle fatigue properties of materials and substructures used in the rotor blades.

To evaluate the fatigue damage on a wind turbine structure, the **IEC 61400-2** recommends the use of the Miner's law for cumulative damage. This linear accumulation law predicts the failure of a component under variable loading. The damage of a component is calculated by using the equation 231:

$$D_m = \sum_i \frac{n_i}{N_{cycle}(\gamma_f \cdot \gamma_m \cdot S_i)} \tag{231}$$

Where i is the level loading index, n_i is the number of cycles performed for loading i, N_{cycle} is the number of cycles to failure, S_i is the stress level of the fatigue cycles, γ_f is the partial

safety factor for the corresponding load case, and γ_m is the Partial safety factor for material characterization. The parameter between parentheses in the denominator is called the associated stress level. For the SLM model, there is a single bin 'i' for which the number of fatigue cycles is given by:

$$n = \frac{B \, \Omega_{design} \, T_d}{60} = 5.43 \; 10^9 \tag{232}$$

Where T_d is the design life of the wind turbine (20 years) in seconds.

Under the Miner's law, a component is supposed to be broken when the damage is unity. In order to determine the number of cycles to failure (N_{cycle}), the S-N curve characterization for composite materials (maximum stress versus cycles to failure) is used. As discussed by many authors [258, 259, 260], the S-N behavior of composite materials at a constant R_S (minimum stress over maximum stress) fit to an exponential relationship which is linear on a maximum stress versus log cycles to fail basis, yielding, for a static strength, S_0. A stress ratio of $R_S=0.1$ is used in the present fatigue analysis as it simulates the turbine blades operational conditions [261].

$$\frac{S}{S_0} = 1 - b \log N_{cycle} \tag{233}$$

Where S is the maximum cyclic stress (or the stress level), N_{cycle} is the number of cycles to failure, and b is the fatigue coefficient; the slope of the normalized S-N curve [262].
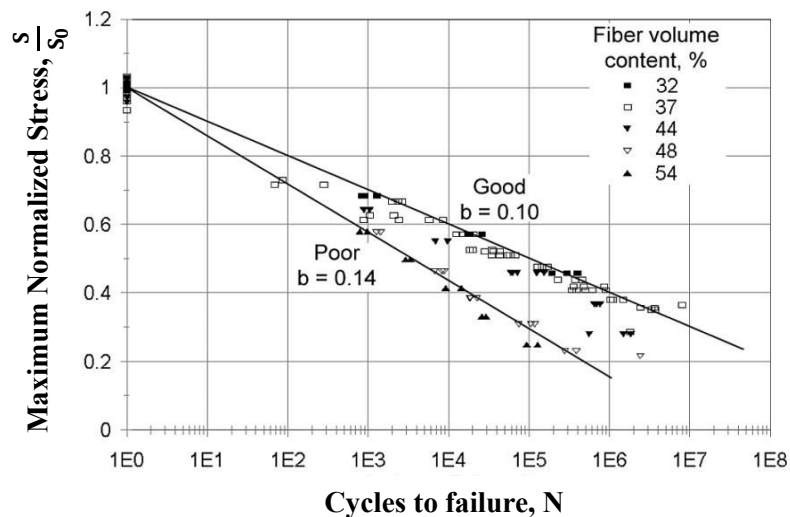
Figure 92: Normalized tensile fatigue data for composite materials $[0/\pm45/0]_S$, $R_S=0.1$

As shown in Figure 92, the fatigue coefficient, b, varied significantly in tension. The best glass fiber composites have a value of b close to **0.10**, while the worst have a value close to **0.14**. The good materials in this figure are approaching the best fatigue-behavior that can be

obtained for fiberglass materials in tensile fatigue, while the poor materials do not perform nearly as well. The small appearing variation in the fatigue slope b produces significant differences in fatigue performance. A small difference in the fatigue coefficient can represent a difference in cycles to failure of about a factor of 100 [263]. The value of the fatigue coefficient depends on the construction techniques used in the triax material. Normally, **the composite materials can be made from stitched or unstitched laminates**. In the case of a stitched-triax material, the material contains 0° and ±45° layers that are stitched together with organic fibers at the factory to save handling costs during blade fabrication. Although stitching makes fiber layers and bundles easier to handle in the manufacturing process, they degrade the fatigue behavior of the composite system (b around 0.14 as shown in figure 90).The unstitched-triax material is made by separating the 0° and ± 45° layers. The experiment results show that when the stitching is removed, the unstitched-triax behaves as one of the best materials [263]. In the present design process, as the selected blade laminate orientation in the blade (the weakest part of the blade spar cap) was a triaxial E-glass fabric $[(\pm45)°/0_2/(\pm45)°]_s$, with a fiber volume fraction of $V_f = 50\%$, a fatigue coefficient of 0.1 was selected [264]. According to Germanischer Lloyd (GL), this value can be applied for laminates with a fibre content of at least 30% and at most 55% by volume without further verification. For other fibre volume contents and matrix resins, an appropriate analysis (S/N curve) shall be performed [122]. In order to determine the associated blade stress level, S, the blade material is assumed to be minimal characterized so that the appropriate material safety factors are $\gamma_m = 10$ for material and $\gamma_f = 1$ for fatigue load. The blade associated stress level is given by:

$$S = \gamma_f . \gamma_m . S_i = 85.58\ \text{MPa} \tag{234}$$

Where S_i is the stress level of the fatigue cycles. Using equation 235, the number to cycles to failure is:

$$N_{cycle} = 10^{\frac{1 - S/S_0}{b}} = 10^{7,71} \tag{235}$$

The required data for fatigue analysis of the small wind turbine blades and the rotor shaft are given in table 65.

Description	Value	Units	Symbol
Design life of the turbine	20	Years	
	631152000	s	T_d
Number of Fatigue Cycles	5,43E+09	n/a	n_i
Number of Cycles to Failure as a Function of Stress (Shaft)	Inf	n/a	N_shaft
Number of Cycles to Failure as a Function of Stress (Blade)	5,22E+07	n/a	N_blade

Table 65: Fatigue data for the small wind turbine blades

Using the Miner's rule (given by equation 231) and taking into consideration an estimated design life-span of 20 years, the accumulated theoretical fatigue damage of the small wind turbine blades is **D = 105**. **As the cumulative damage is well above the assigned limit of unity, the wind turbine blade seems not be safe in fatigue**. However, it worth noting that the approach used is the present analysis requires an adequate S-N curve, which gives an accurate number of cycles to failure as a function of the actual maximum normalized stress. Therefore, more accurate analysis of the blade fatigue is mandatory. This will be performed using FAST code which is a comprehensive aeroelastic simulator that has been evaluated by the Germanischer Lloyd WindEnergie and found suitable for the calculation of onshore wind turbine loads for design and certification.

For fatigue analysis of the main shaft, as the number of cycles to failure can be considered infinite for carbon steel martial, the main shaft is easily safe in fatigue. Typical curves for fatigue of metals are shown in figure 93 [7]. As can be seen, most steel alloys exhibit the infinite life property.
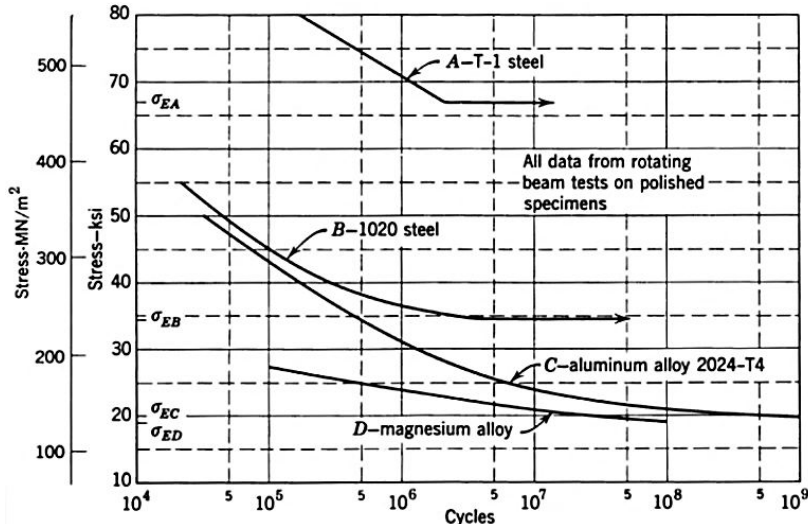
Figure 93: Input data for the cumulative damage calculation (Miner's Rule)

Table 66 shows the outcome of the SLM calculations. The main shaft and the rotor blade pass successfully the entire load cases except for blade fatigue. This latter will be further discussed in the section below.

Load Case A - Fatigue Loads on Blades and Rotor Shaft			
	Fatigue Stress Limit (Mpa)	Calculated Stress (MPa)	Conclusion
Blades	1,00	1,04E+02	FAIL
Shaft	1,00	Infinite Life	SAFE

Table 66: Results of fatigue analysis using SLM

According to the SLM model, the rotor blades will just stand for 70 days before breaking under cyclic loading. In order to make the blade pass the fatigue analysis, two major

modifications are needed; full material characterization must be adopted and a minimum ultimate tensile strength of 404 MPa must be used for the blade material. However, the use of low safety factors (full characterization) requires a strong knowledge of the blade material properties which is difficult to achieve in our design case. Besides, an ultimate tensile strength of 404 MPa for triaxial stitching patterns is regarded as high. Therefore, full computational analysis of fatigue damage is required.

It can be seen that **IEC 61400-2** provides a very useful methodology for designing safe small turbines and the spreadsheet described in this paper facilitates the analysis. The SLM is a good starting point for turbine structural analysis, but it is only a starting point. More accurate models for the analysis of small wind turbine structure, which are recommended by the international standard **IEC-64100-2**, should be used. This type of models will allow more accurate computer modeling of different loads on the turbine in response to stochastic inputs such as fatigue, changes in wind directions and wind gusts.

9.7.2 Blade fatigue analysis using FAST

9.7.2.1 FAST input files

As discussed in the last section, the results of the fatigue analysis using SLM model showed that the small wind turbine blades are not able to withstand the fatigue loads from the wind. Therefore, more accurate analysis is necessary. The most common tool that has been used in this case is FAST code. This is a comprehensive aeroelastic simulator capable of predicting both extreme and fatigue loads of horizontal-axis wind turbines. FAST is able to model most common wind turbine configurations including two- or three-blade horizontal-axis rotor, pitch or stall regulation, rigid or teetering hub, upwind or downwind rotor, and lattice or tubular tower. This code is based on advanced engineering models--derived from fundamental laws, but with appropriate simplifications and assumptions, and supplemented where applicable with computational solutions and test data. It represents a reliable, simple, and free of charge code that can model a three-bladed HAWT with 24 degrees of freedom under time variant wind conditions and allows for specified pitch and yaw maneuvers, as well as generator control, brake application, and a multitude of other possibilities. In 2005, FAST code was evaluated by the Germanischer Lloyd WindEnergie and found suitable for the calculation of onshore wind turbine loads for design and certification.

Through this section, an overview of the fatigue analysis that was performed for the small wind turbine blades, will be presented. Based on the fact that the rotor blades are the main components that are mostly affected by the repetitive or the cyclic loads, an accurate fatigue analysis required in order to check whether these rotating parts will withstand the wind loads

over a lifespan of 20 years. Based on FAST, the outputs of the simulation are mainly the time-series data on the aerodynamic loads as well as the loads and the deflections of the structural members of the wind turbine. These outputs will be used to predict the accumulated damage on the wind turbine blades. FAST is normally composed of six different input file which are namely: primary input file, blade input file, tower input file, furling input file, aerodynamic input file, and finally platform input file. Each of these input files requires a list of parameters that must be defined. The general structure of the FAST code is given in figure 94.
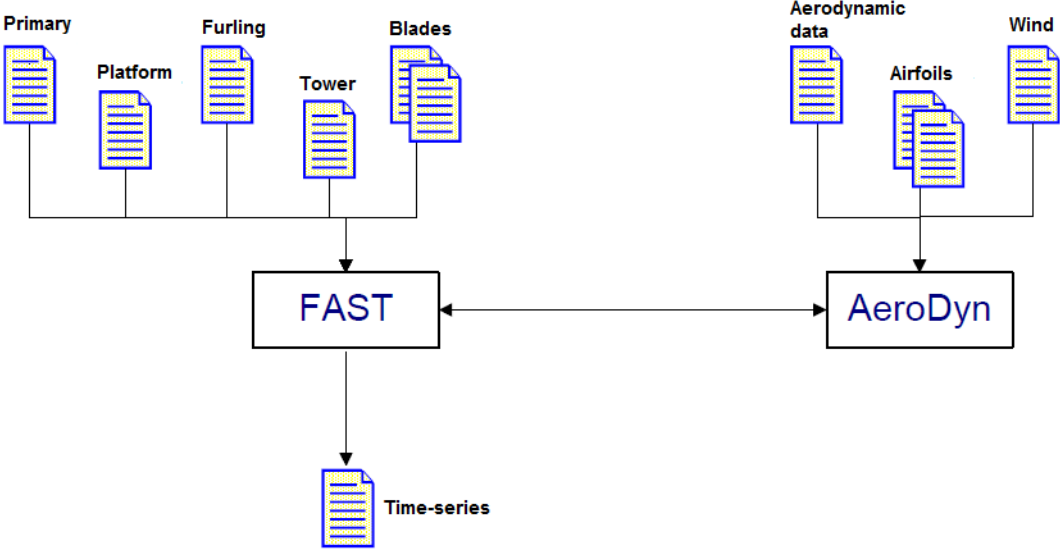
Figure 94: Structure of the FAST code

The primary input file is used to describe the wind turbine operating parameters as well as the basic geometry of the turbine machine. The parameters that are not described in this main input file will be detailed in the other files (blade, tower, furling, aerodynamic parameters, and wind-time histories). Some parameters do not apply to two-bladed turbines, and others do not apply to three-bladed turbines. The mean feature of the primary input file is that it enables defining the structure of the output file containing the time-series data. The structure of a

time-series file is mainly defined by the channels (columns) containing the values the fatigue loads for different wind speeds. An example of fatigue channels is shown in figure 95.

```
"uWind, vwind, wwind"                        - Downwind, crosswind, and vertical wind speeds
"RotSpeed, TSR"                              - Rotor speed and blade tip speed ratio
"RotThrust"                                  - Rotor thrust
"TipClrnc1, TipClrnc2, TipClrnc3"            - Tip-to-tower clearances of each blade
"TipDxb1,TipDyb1"                            - Blade 1 flapwise and edgewise tip deflections
"TipDxb2,TipDyb2"                            - Blade 2 flapwise and edgewise tip deflections
"TipDxb3,TipDyb3"                            - Blade 3 flapwise and edgewise tip deflections
"RootMEdg1,RootMFlp1"                        - Blade 1 root edgewise and flapwise bending moments
"RootMEdg2,RootMFlp2"                        - Blade 2 root edgewise and flapwise bending moments
"RootMEdg3,RootMFlp3"                        - Blade 3 root edgewise and flapwise bending moments
"RootFxb1,RootFyb1"                          - Blade-1 root flapwise and edgewise shears
"RootFxb2,RootFyb2"                          - Blade-2 root flapwise and edgewise shears
"RootFxb3,RootFyb3"                          - Blade-3 root flapwise and edgewise shears
"RootFxc1,RootFyc1,RootFzc1"                 - Blade 1 root forces
"RootFxc2,RootFyc2,RootFzc2"                 - Blade 2 root forces
"RootFxc3,RootFyc3,RootFzc3"                 - Blade 3 root forces
"RotCq, RotCp, RotCt"                        - Rotor torque, power, and thrust coefficients
END of FAST input file (the word "END" must appear in the first 3 columns of this last line).
-----------------------------------------------------------------------------------------------
```

Figure 95: Channels to be printed in the output file of the FAST code

In the blade input file, multiple input parameters are required. These include the blade parameters, the blade adjusted factors, the distributed blade properties, and the blade mode shapes. PreComp, which is a preprocessor for computing the blade composite properties, was used to compute the properties that are required to properly evaluate the model flexible components of the blades **[129]**. PreComp requires as inputs the blade internal structure and the external (outer) shape of composite laminates. The external shape (or aerodynamic shape) is mainly defined by the chord, and the twist angle of each section along the blade span. The internal structural layup is defined by the lay-up schedule of both the spar caps and the shear web. PreComp give as a result the distributed blade properties which include the cross-coupled stiffness properties, inertia properties, and offsets of the blade shear center, tension center and center of mass with respect to the blade pitch axis. These section properties will be used as input for both the FAST blade input file and the BModes input file. BModes, which is software developed by NREL, is a finite-element code that provides dynamically coupled modes for a beam **[130]**. In BModes's input file, each one of the rotor speed, the blade geometry, the rotor precone, the pitch control setting, and the blade structural properties must be defined.

The tower input file is composed of four different subsections which are tower parameters, tower adjustment factors, distributed tower properties, and tower mode shapes. The section of the distributed properties includes the tower section mass per unit length, the tower section fore-aft stiffness, the tower section side-to-side stiffness, and the tower section torsion stiffness. As for the blade input file, BModes is used to generate the mode shape for the tower. The section properties of the tower need to be specified by the user and it has the same format as the blade-section properties file as shown in figure 96.

```
------------------ DISTRIBUTED TOWER PROPERTIES --------------------------
HtFract       TMassDen      TwFAStif      TwSSStif      TwGJStif      TwEAStif      TwFAIner
  (-)          (kg/m)       (Nm^2)        (Nm^2)        (Nm^2)         (N)          (kg m)
0.0000       0.8565E+02   0.7743E+08   0.7741E+08   0.6188E+08   0.2196E+10      0.000
0.2000       0.6472E+02   0.4671E+08   0.4670E+08   0.3733E+08   0.1659E+10      0.000
0.4000       0.4971E+02   0.2779E+08   0.2779E+08   0.2221E+08   0.1275E+10      0.000
0.6000       0.3757E+02   0.1567E+08   0.1566E+08   0.1252E+08   0.9633E+09      0.000
0.8000       0.2637E+02   0.7804E+07   0.7802E+07   0.6236E+07   0.6762E+09      0.000
1.0000       0.2143E+02   0.4167E+07   0.4166E+07   0.3330E+07   0.5495E+09      0.000
```

Figure 96: Input data for the tower input file for FAST

In the furling input file, the core configuration of the furling mechanism of the small wind turbine is defined. The parameters available in the furling input file are unique to small wind turbine machines since this control mechanism is not applied to medium and large wind turbines. The furling input file is organized into sections similar to those available in the primary input file. Actually, the furling file is simply a continuation and expansion of the core configuration definition designations available in the primary file. In this input file, an exact value of the furling initial conditions, the turbine configuration, the mass and the inertia of the furling components, as well as the tail fin aerodynamics need to be defined. FAST only reads the furling input file if the model is designated as a furling machine.

The platform input file contains all the design parameters of to the wind turbine's support foundation. This input file contains data related to the initial conditions of the platform, the turbine configuration, as well as the mass and the inertia of the foundation.

The AeroDyn input file includes all of the parameters related to the aerodynamics of the small wind turbine. This input file contains three main sections. In the first section, the values of the settings that control the different flags are defined. These include the system unit flag (SI), the pitch moments flag, the dynamic stall flag, and the dynamic inflow flag. In this same section, a set of input parameters is required such as the tower height, the air density, the kinematic viscosity of the air, and the number of the airfoils to be used in the blade structure. The most important parameter in the first section is the wind file. Normally, the user chooses whether to use a hub height wind file (specifies hub-height wind data that also includes wind shears and gusts) or full field turbulence wind files (in a binary form). For the case of this study, a full field wind data was created with NREL's TurbSim code. This is a stochastic inflow turbulence tool that has been developed to provide a numerical simulation of a full-field flow that contains coherent turbulence structures that reflect the proper spatiotemporal turbulent velocity field relationships seen in instabilities associated with nocturnal boundary layer flows and which are not represented well by the IEC Normal Turbulence Models (NTM) [131]. A series of wind files with a mean wind speed, that are taken at a reference height and varying between the cut-in wind speed (3 m/s) and cut-out wind speed (15 m/s), were generated. FAST will simulate the aerodynamic loads for each single wind file and will generate a single time-series file. The number of time-series needed for fatigue simulation is

specified by the wind turbine design standards (IEC in this case). For example, the load-case 1.2 for fatigue during normal operation should involve at least six 10-minute simulations per 2-m/s wind speed bin from cut-in to cut-out wind speed (typically 600 seconds long, after removal of start-up transients). Each 10 minutes simulation should use different random seeds for the wind file and wave data.

The second section of the aerodynamic input file gives the names of the files containing the aerodynamic data of the used airfoils. The aerodynamic data are mainly the lift and the drag coefficients for different angles of attack. The third section describes the blade geometry in details. The 3.5 meters blade was divided into multiple sections. In this study, the blade length was divided into 32 blade stations. For each blade section, the chord length, the twist angle, and the airfoil identification are specified.

9.7.2.2 Fatigue analysis using Mlife codes

Once the input files are given and the design parameters are well defined, fatigue analysis can then be performed. This step was processed using Mlife code. This is a Matlab-based tool created to post-process results from wind turbine tests, aero-elastic, and dynamic simulations. Mlife includes three generalized Design Load Cases (DLC) which are intended to encompass the required fatigue-related DLCs of the IEC standard IEC 61400-1. These load cases are Power Production load case (IEC DLC 1.2), Parked load case (IEC DLC 6.4), and Discrete Events (IEC DLCs 2.4, 3.1, and 4.1) [122]. For each of this load cases, MLife computes statistical information and fatigue estimates for one or more time-series. The statistical calculations include minimum and maximum value, mean, standard deviation, skewness, kurtosis, and maximum range of the selected channels. MLife uses as inputs the time-series from each load-case (typically forces and moments) at specific cross sections such as the blade root, shaft, tower-top, and tower-bottom, as well as blade-tip-to-tower clearance. For the present study, only fatigue analysis of the power production load case was conducted. The two other load cases are judged not having significant contribution in the fatigue of the turbine blades.

The fatigue calculations are based on the entire set of the input files, a design lifetime period, an availability factor (an availability of 1 indicates the turbine is always online and producing power when the wind speed is in the range $[V_{in} - V_{out}]$), and a wind speed distribution on a typical site (based on Weibull or Rayleigh distribution function). The results of the fatigue simulation are given as the lifetime Damage Equivalent Load (DEL) which is a constant-amplitude fatigue-load that occurs at a fixed load-mean and frequency and produces the equivalent damage as the variable spectrum loads, the lifetime damage, and the time until

failure. MLife follows the techniques outlined in the IEC standard for design requirements, IEC 61400-1 [265]. The program accumulates fatigue damage due to fluctuating loads over the design life of the wind turbine. These fluctuating loads are broken down into individual hysteresis cycles by matching local minima with local maxima in the time-series using rainflow counting algorithm [266, 267]. As the time-series data derived from the analytical simulations must be converted into cycle count matrices. A number of numerical techniques have been used. The technique typically used in the wind turbine industry is the rainflow counting algorithm [268]. Rainflow counting processes the variable amplitude loads into a form that is compatible with design life calculations. This algorithm has demonstrated good agreement with measured fatigue lives when compared to other counting algorithms.

Mlife processes the random signals for fatigue analysis by characterizing the cycles by a load-mean and a range and assumes linear accumulation of the damage with each of these cycles according to the Miner's Rule (Palmgren and Miner). The total damage from all cycles is given by:

$$D_m = \sum_i \frac{n_i}{N_i(L_i^{RF})} \tag{236}$$

Where N_i denotes the number of cycles to failure, n_i is the cycle count (number of fatigue cycle that the components will experience), and L_i^{RF} is the cycle's load range about a fixed load-mean value. The relationship between load range and cycles to failure (S-N curve) is modeled by:

$$N_i = \left(\frac{L^{ult} - L^{MF}}{\frac{1}{2} L_i^{RF}} \right)^m \tag{237}$$

Where L^{ult} is the ultimate design load of the component, L^{MF} is the fixed load-mean, and the Whöler exponent (the inverse of the fatigue coefficient, b), m, is specific to the component under consideration. Typically, the ultimate design load is taken as the maximum value of the load channel to be processed multiplied by a load factor between 1.5 and 4.5 [269, 270]. In the present study, an ultimate load factor of 5 was adopted. For fatigue verification, a partial safety factor of 1.48 should be used for the blade material. This typical value is recommended by GL standard and can be computed using equation 238.

$$\gamma_m = 1.35 \prod_i C_{ib} \tag{238}$$

Where C_b are the reduction factors that are given in table 67.

Reduction factor	Designation	Value
$C_{1b} = N^{\frac{1}{m}}$	Curve of high-cycle fatigue for the load cycle number N and slope parameter m	1
C_{2b}	Temperature effect	1.1
C_{3b}	Effect of fiber orientation	1
C_{4b}	Post-cured laminate	1
C_{5b}	Partial safety factor for the blade trailing edge	1

Table 67: Reduction factors for material safety factor

Actually, the above formulations assume the fatigue cycles occur over a constant, or fixed, load-mean. However, the actual load cycles will occur over a spectrum of load means. Therefore, a correction must be made to the fatigue cycles' load ranges to analyze the data as if each cycle occurred about a fixed mean load.

This is known as the Goodman correction that can be considered using the following equation:

$$L_i^{RF} = L_i^R \left(\frac{L^{ult} - L^{MF}}{L^{ult} - L_i^M} \right) \tag{239}$$

Where L_i^R is the ith cycle's range about a load mean of L_i^M .

From a practical point of view, the lifetime damage of a wind turbine is estimated using a number of time-series data which covers a much shorter time period than the real design lifetime. To correctly estimate the total lifetime damage from these short input time-series, the time-series damage-cycle counts must be extrapolated over the whole design lifetime of the wind turbine. This can be done using an extrapolation factor for each single time-series. This extrapolation factor is given by:

$$f_j^{life} = \begin{cases} \dfrac{T_d . A . p_l^v}{T_l}, & V_{in} < V_{ave} \le V_{out} \\ \dfrac{T_d . p_l^v}{T_l}, & \text{Otherwise} \end{cases} \tag{240}$$

Where A is the availability factor, V_{ave} is the average wind speed, T_d is the design lifetime period, T_l is the total elapsed time for all power production time-series that have a mean wind speed falling in bin l, f_j^{life} is the extrapolation factor for the time-series j, and p_l^v is the probability of the wind speed falling into bin l. As can be seen from the equation above, the cycle-count extrapolation is affected by the wind distribution (through the probability of the

wind speeds) and by the turbine's availability factor, A. Therefore, the extrapolated cycle counts for one time-series over the design lifetime are given by:

$$n_{ji}{}^{life} = f_j{}^{life}.n_{ij} \qquad (241)$$

Where n_{ij} is the ith cycle count for time-series j. Using this, the lifetime damage that will be accumulated for all cycles and time-series is given by:

$$D_m{}^{life} = \sum_j \sum_i \frac{n_{ji}{}^{life}}{N_{ji}} \qquad (242)$$

In addition to calculating the damage over a design lifetime, MLife computes the time until failure. Since failure occurs when damage equals one, the time until failure, T^{fail}, is simply the ratio of the design lifetime over the accumulated damage:

$$T^{fail} = \frac{T_d}{D_m{}^{life}} \qquad (243)$$

The program computes also the lifetime DEL^{life} which includes the fatigue cycles from all time-series. In this case, a lifetime equivalent cycle count is determined using the lifetime count extrapolation factor, $f_j{}^{life}$, and the short-term equivalent count, $n^{life,eq}$, such that,

$$n^{life,eq} = \sum_j f_j{}^{life}.(f^{eq}.T_j) \qquad (244)$$

Where f^{eq} is the DEL frequency, and T_j is the elapsed time of time-series j. The term between brackets is the total equivalent fatigue counts for time-series j. In the case of an equivalent load about a fixed mean, the DEL^{life} can be computed using equation 245.

$$DEL^{life} = \left(\frac{\sum_j \sum_i \left(n_{ji}{}^{life}.\left(L_{ij}^{RF} \right)^m \right)}{n^{life,eq}} \right)^{\frac{1}{m}} \qquad (245)$$

Where L_{ij}^{RF} is the adjusted load ranges about a fixed-mean. Using six different time-series, generated with 10-minute (690 seconds) simulations per 1m/s wind speed bin from the cut-in wind speed to the cut-out wind speed, the results of the analysis of fatigue loads on the blade structure (in the flapwise and the edgewise directions) are given in table 68.

Lifetime period (seconds) : 6.31E+008			
Lifetime Damage			
n^{life}=2.32E+9	Flapwise	Edgewise	Centrifugal
b (1/m)=0.1			
L^{Ult} (kN)	2.31E+001	9.8E+000	4.95E+001
D_m	1.73E-006	1.38E-005	2.78E-001

Time Until Failure			
n^{life}=2.32E+9	Flapwise	Edgewise	Centrifugal
b (1/m)=0.1			
L^{Ult} (kN)	2.31E+001	9.8E+000	4.95E+001
T^{fail} (seconds)	**3,65E+014**	**4.56E+013**	**2.27E+009**

Table 68: Results of FAST simulation

As can be seen, the accumulated damage over the lifetime of the wind turbine is lower than unity. Therefore, with respect to the main blade directions (flapwise, edgewise, and Z-direction), the small wind turbine blades seem to be safe against fatigue. Results show also that SLM model overestimates the number of fatigue cycles as FAST code computed the fatigue damage with only 2.32E+9 cycles over the lifetime of the blades instead of 5.43E+9 cycles from SLM model.

9.8 Blade fatigue analysis using nCode DesignLife

To make sure of the damage ratios generated by FAST and Mlife codes, verification was carried out using nCode DesignLife composite. This tool combines the calculated stresses (from Finite Element Method) together with specific fatigue properties to generate fatigue hotspots and life damage ratios. Fatigue damage prediction is generally done in one direction; however, in the case of the blade wind turbine, the loads are expressed in multi-axial directions. In order to have accurate results, a method of multi-axial correction is adopted in nCode DesignLife (strain life). In this work, the fatigue analysis of the blade is conducted using the EN method (strain life). For material characterization, short composite fiber composite module was adopted. After choosing the module for fatigue analysis of the blade, the used material should be entered by creating a new material in the dataset of nCode short fiber composite Basquin curves design. Among the required mechanical characteristics are: ratio of test, volume fraction, fatigue cut-off, Standard error of Log N, ultimate tensile strength, fiber share, etc.

To conduct fatigue analysis, many steps should be performed. First, the blade geometry must be defined meshed. The loads and the fixations should be also created. These steps are conducted in the structural analysis of the blade. For material characterization, an orientation tensor file should be created. The file gives the orientation tensor for each part in the blade from the root to the tip. The tensor for the spar caps and the shear web are also defined in the file. The definition of the file is done based on the number of elements (mesh) of the blade.

In nCode DesignLife, there are four options to conduct fatigue analysis. These are constant amplitude, time step, time series and vibration. Time series gives the best results as it simulates approximately the real change of the loads applied on the blade in a period of time. Therefore, this option is adopted in this work. nCode DesignLife has the option to create the time series files (.s3t format) only by importing files with text format. In this paper, the variation of the loads as a function of time is generated in the range in which the wind turbine is operating (from the cut-in wind speed of 3 m/s to the cut-out wind speed of 15m/s). The fatigue damage was evaluated in the main directions: flapwise direction, edgewise direction, and centrifugal direction. Once the required parameters for the analysis were defined, the simulation of the fatigue damage can be done. Figures 9 shows the results of fatigue damage prediction in the flapwise direction.
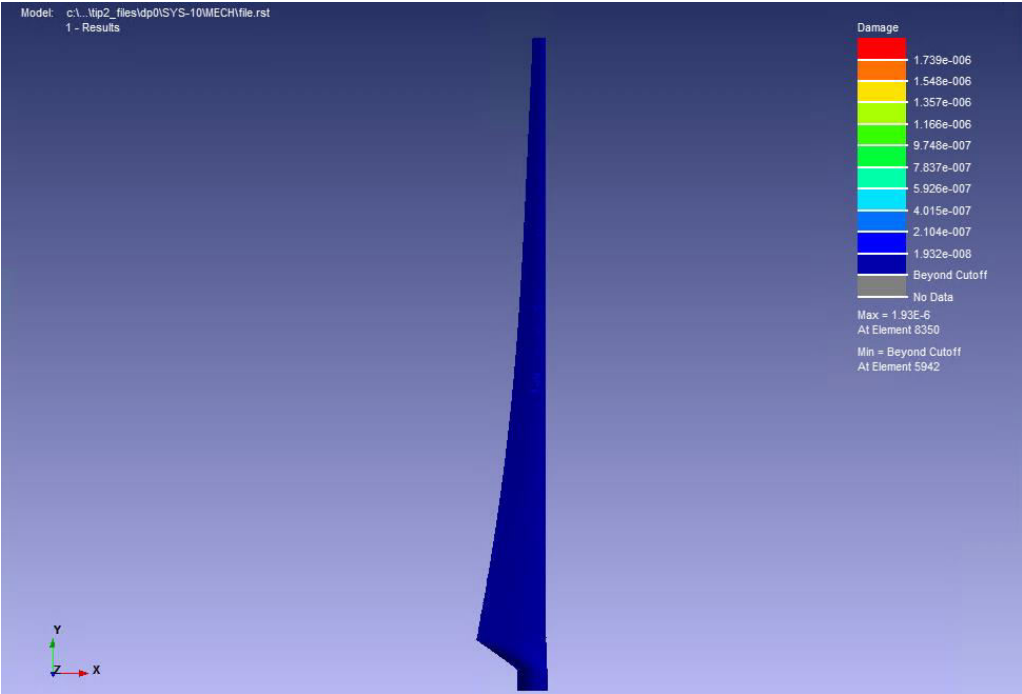
Figure 97: Fatigue damage in the flapwise direction

Table 69 summarizes the results using nCode DesignLife composite.

Load direction	Damage ratio (D_m)
Flapwise direction	1.73 E-06
Edgewise direction	1.38 E-05
Centrifugal direction	0.2747

Table 69: Results of fatigue analysis using nCode DesignLife module

As can be seen, nCode DesignLife give similar results to those found using FAST and Mlife codes. The fatigue damage is very small following the flapwise and edgewise direction. A damage factor of 0.27 was found in the centrifugal direction. This is not surprising given that

the cyclic loads in this direction are very high in comparison to the other loading directions. Therefore, the rotor blades are safe against fatigue during a design lifetime of 20 years.

9.9 Conclusion

The major loads on a wind turbine blade are mainly generated by wind and by gravity. Wind loads mainly induce both flap wise and edgewise bending. These loads have both a static and a dynamic component (variations in wind speed for example) that induce fatigue on the blade material. Gravity loads mainly induce edgewise bending, when the blade is horizontal. The rotation of the blades cause alternating edge-wise bending and thus fatigue of the material.

The loading regime to which small wind turbines are subject to complex and requiring special attention during any design process. For this reason, the final chapter of the present thesis was mainly devoted to the wind turbine loads assessment. In order to evaluate the functional response of the wind turbine to different applied loads, the structural integrity of the system was first analyzed using Simple Load Model (SLM). This model is recommended by the international standard of small wind turbines; IEC-64100-2-Design requirements for small wind turbines as a starting point in the design analysis. Results from SLM shows that the shaft passes all the load scenarios for normal and extreme load case. For the blade analysis, the results show that the blades passes extreme load scenarios and fails the fatigue analysis. To validate the results obtained using SLM, a full computational analysis of the blade strcture was conducted using FAST-Mlife codes and nCode Designlife composites. The obtained results reveal that the blade structure passes the fatigue analysis with a cumulative damage factor less than unity, and this along the all load directions.

CONCLUSION

In this thesis, a detailed design procedure of a small wind turbine with a rated power output of 11 kW was emphasized. The first section was devoted to the determination of the key design parameters upon which the design process will be based. As a first step in this design process, the electricity requirements of the users were evaluated; the daily electricity consumption (kWh/day) of a typical Moroccan household was determined. This particular information defines the equivalent power output of the turbine system that will be able to ensure a stable power supply for the overall household appliances (including pumping system for irrigation). The second step consists in defining the wind conditions at which the wind turbine will operate. Throughout this part, a study of site-specific wind conditions was conducted. The main purpose of this part is to define an appropriate wind turbine class. This latter defines the wind conditions to be considered during the whole design process (including the average wind speed, the design wind speed, the reference wind speed, and the survival wind speed).

The second section aimed to provide a full picture of the previous experiences in the small wind energy industry. An overview of technological trends in the design of small wind turbines was presented. This review section provided a comparative study of technologies that are commonly used by the small wind turbine manufacturers.

The third section of the design process was devoted to the small wind turbine rotor blade design. The blade aerodynamic shape with the chord length and the twist angle distribution, at a specific design tip speed ratio at which the blade has an optimum annual energy production, was determined. A direct procedure of design of the rotor blades was fully presented. Initially, the airfoil of the rotor blades was selected. Then, XFOIL program was used to determine the aerodynamic data of the used airfoils. The obtained results were compared to the results of wind tunnel aerodynamic tests. Afterwards, a practical selection method for determining the optimum blade design parameters was used. Finally, optimum blade geometry was defined using three different approaches (Optimum rotor theory, SWRDC code, and QBlade software). The aerodynamic performance of the turbine blades (Cp) was evaluated and the results showed that the used approaches are computationally efficient.

The fourth section of this report was concerned by the preliminary design and analysis of the most important nacelle components. A first tentative design of the nacelle cover, rotor hub, nose cone, main shaft, shaft bearings, coupling, breaking system, furling system, yaw bearing, and generator was conducted. This preliminary design was performed based on a set of design considerations. These include: aesthetics, aerodynamics, manufacturability of the components and structural considerations. It should be noted that this first design may be subject to further

modifications during the design refinement. In this same section, the wind turbine operation modes and the turbine control strategy were defined. A direct drive, fixed-pitch variable speed (FPVS) approach was selected. This operation mode fulfills the general project requirements, which are expressed in terms of cost-effectiveness, improved reliability, and low-maintenance. Regarding the turbine control strategy, a control strategy for the Generator-side converter with output maximization of a generator-based small-scale wind turbine was selected. This choice if justified by the fact that this option is simple, effective, and not expensive.

Once the nacelle design has been developed, the next step was to develop a first tentative design of the wind turbine tower. In the fifth section, the tower type was selected, and an octagonal cross-sectioned tapered tower was chosen. Additionally, the tower height, the top/base diameters, as well as the wall thickness of the different sections were determined. An optimum tower height was determined using an optimization approach that maximizes the average energy output per unit price. Finally, the resistance of the tower to both buckling and fatigue was evaluated.

The section number six was devoted to the determination of a typical geometry of the small wind turbine foundation. The main objective of this section was to determine appropriate foundation geometry by involving both site-specific wind conditions (vertical loading and total overturning moment) and the geotechnical characteristics of a typical agricultural soil. An optimum geometry of the foundation was adopted to maintain stability of the system over the lifetime of the wind turbine.

Small wind turbine noise assessment was also presented. In this section, noise power level of the wind turbine was calculated, and the sound pressure level at different distances from the turbine was determined. Noise assessment was performed using the category I prediction model which is a basic model that uses simple algebraic relations (based on the main wind turbine parameters) to predict the emitted noise from the wind turbine. This model is simple and fast, however it is by far not universal. As a consequence, more critical models (e.g. models belonging to the category III, which take into consideration the complex three dimensional and time-dependent distributions of the acoustic sources, should be used to accurately predict the noise level around the wind turbine system.

In order to ensure that the wind turbine system will operate safely, the various components of the wind turbine must be designed in a way that they can withstand the loads without damage. Loads applied to each element must be assessed by calculation or tests to determine if the integrity of the structure satisfies the security requirements. This was the subject of the last section of the present design procedure. The wind turbine loading was assessed on the basis

the simple Load Model (SLM). Using this model, the life cycle of a wind turbine was represented by a set of design situations covering all the most important external conditions which the wind turbine is supposed to face, and the turbine loading for each load case was determined. The loads calculated were then converted into equivalent stresses, and compared with the allowable stresses of the corresponding components. Then it was decided if the component will be safe against loading or not.

As the equations of the SLM model computes the stress in the blade root, a comparison of the maximum stress from ANSYS shows that SLM model gives good results the stress on the blade structure.

For fatigue damage prediction, SLM showed that the turbine blades fail the fatigue analysis during normal operation. The failure of the rotor blades to pass fatigue analysis using SLM is due mainly to three reasons: The first reason is related to the rough approximation used by SLM and which consists in using one single bin to compute the number of fatigue cycles, ni. This calculation method lead to an overestimation of the number of fatigue cycles with a difference of 3.1E+9 cycles compared to the results obtained from FAST-MLife code. The second reason concerns the forces and moments on the blade during normal operation (load case A). The associated stress level, that is used to calculate the fatigue damage factor, was determined based on the assumption that the wind speed during normal operation has a constant value of 10.5 m/s. The use of such a relatively high wind speed leads to an overestimate of the centrifugal loads and the bending moments on the blade during normal conditions. The third reason concerns the high safety factors that are imposed by IEC 61400-2 when full material characterization cannot be achieved, especially during early stages of the design process. This usually leads to heavy structure and affects the cost of the final blade design.

The present paper suggests a revision of both the design parameters (such as the design wind speed and the design torque for fatigue loads) and the partial safety factors for material characterization when the requirements of full characterization cannot be fulfilled. Finally, simple and reliable aeroelastic models are still needed to accurately compute the fatigue damage on the rotor blades during the design process of wind turbine systems.

An accurate fatigue simulation should involve a full-field flow that contains coherent turbulence structures and which reflect the real pattern of the wind. Cycle count over the lifetime of the wind turbine must be determined for individual time-series covering the whole operating range of the wind speeds (typically from the cut-in speed to the cut-out wind speed). To ensure that the rotor blades will be safe against fatigue, more accurate approach was used. This consists in simulating fatigue of the blade using both FAST-MLife codes and nCode

Designlife composite. FAST-MLife codes an aeroelastic simulator capable of predicting both the extreme and fatigue loads of two-and three-bladed horizontal-axis wind turbines. By using six different time-series, generated with 10-minute (690 seconds) simulations per 1 m/s wind speed bin from the cut-in wind speed to the cut-out wind speed, the fatigue simulations show that the accumulated damage over the lifetime of the turbine was below unity, therefore, the rotor blades will not fail under fatigue loads in normal operating conditions (lad case of power production).

PUBLICATIONS AND CONFERENCES

- Journal Paper: Structural design and analysis of a small wind turbine blade using Simple Load Model (SLM), FAST-MLife codes and ANSYS nCode DesignLife (**Wind Engineering**)

- Journal Paper: Improvement of the Aerodynamic Performance of a Small Wind Turbine Blade (**Wind Engineering**).

- Journal Paper: Efficiency of a small wind turbine using BEM and CFD (**IOP Conf. Series: Earth and Environmental Science**)

- Journal Paper: Optimum design of a small wind turbine blade for maximum power production (**IOP Conf. Series: Earth and Environmental Science**)

- Journal Paper: Potential assessment of hybrid PV-Wind systems for household applications in rural areas: Case study of Morocco (**E3S Web of Conferences**)

- Conference paper: Aerodynamic optimization of an airfoil for a horizontal wind turbine (ICOA2017: 3rd International Conference on Optimization and Applications,

- Conference paper: Assessment of wind energy potential using generic models (**IEEE Explore**)

- Participation to the international conference on renewable energy and energy efficiency "REEE-2019", Munich, Germany 19th to 22nd August 2019 (**oral communication**)

- Participation to the international conference of renewable energies and energy efficiency "International Conference on Renewable Energy and Energy Efficiency", FST Fez, November 8 & 9, 2017 (**oral communication**)

- Participation to the international conference "International Renewable and Sustainable Energy Conference (IRSEC'16)", Marrakech, November 14, 2016 - November 17, 2016 (**oral communication**),

- Participation to the summer school "International wind power summer school (SSWTT-03)", Aarhus, Denmark, 14th August 2016 - 26th August 2016 (**Summer school**)

- Participation to the summer school "International Young Scholars Forum (YSF)", Nicosia, Cyprus, June 08 - 14, 2015 (**Oral communication**)

- Participation to the First Meeting of Young Researchers in Engineering Sciences of the USMBA & 5th edition of the LSSC Doctoral Students Day, Fez, December 22, 2015 (**oral communication**),

- Participation to the Energy pole doctoral students Forum, Fès, December 05, 2015 (**Poster**)

REFERENCES

1. Manwell JF, McGowan JG, Rogers AL (2009) Wind energy explained: theory, design and application, 2nd edn. Wiley, Chichester

2. Su L, Janajreh I (2012) Development and application of an improved blade element momentum method model on horizontal axis wind turbines. International Journal of Energy and Environmental Engineering 3/1/30: 1-10

3. Schaffarczyk AP (2014) Understanding wind power technology: Theory, Deployment and Optimisation. Wiley, Chichester

4. Sessarego M, Wood D (2015) Multi-dimensional design of wind turbine blades. Renewables: Wind, Water, and Solar 2(9):2-11

5. Marten D, Wendler J (2013) QBlade Guidelines, v0.6 – software

6. Ying D, Ting X, Guoqiang Z, Hang L, De T (2013) Blade tip deflection calculations and safety analysis of wind turbine. In: Proceedings of renewable power generation conference (RPG), 2nd IET, Beijing, China

7. International Electrotechnical Commission (2011) Wind turbines-Part 2: requirements for small wind turbines

8. Gsänger S, Pitteloud JD (2015) Report summary: Small Wind World Report. World Wind Energy Association (WWEA), Bonn, Germany

9. El Moutez N, Bouhelal OM, Laouina A (2015) Synthesis report: Evaluation de l'efficacité énergétique des régions marocaines en termes de consommation d'électricité et choix d'indicateurs de performances. Research center on energy economics and law, Montpellier, France

10. Deutsche Gesellschaft für Technische Zusammenarbeit-GTZ (2011) Final report (updated version): Assessment of regional potential development of photovoltaic in regions of Meknes-Tafilalet, Oriental and Souss Massa Draa, Eschborn/Bonn, Germany

11. French global environment facility (FFEM) Decentralized rural electrification in Morocco. http://www.ffem.fr

12. Firth S, Lomas K, Wright A, Wall R (2008) Identifying trends in the use of domestic appliances from household electricity consumption measurements. Energy and Buildings 40:926–936

13. Murata A, Kondou Y, Hailin M, Weisheng Z (2008) Electricity demand in the Chinese urban household-sector. Applied Energy 85:1113–1125

14. Jung-Hyun Y, Kee Han K (2014) Development of methodology for estimating electricity use in residential sectors using national statistics survey data from South Korea. Energy and Buildings 75:402–409

15. Higher Planning Commission (2007) Synthesis report: Morocco's national survey of households living standards, Rabat, Morocco

16. Higher Planning Commission (2015) Synthesis report (first results): General census of population and housing, Rabat, Morocco

17. National telecommunications regulatory agency (2013) Synthesis report: Survey on access and usage of ICTs by households and individuals, Rabat, Morocco

18. Ministry of agriculture and fisheries (2005) Final report: National report on animal genetic resources, Rabat, Morocco

19. Attijariwafa Bank (2012) Le décollage économico-social du Maroc, une analyse sur les deux dernières décennies. In proceedings of the second edition of the economic conference of Attijariwafa bank, Casablanca, Morocco

20. National institute of agricultural research (2007) Second report on the state of the plant genetic resources for food and agriculture, Rabat, Morocco

21. Lahmouri A (1989) L'eau souterraine: une ressource vitale pour l'alimentation en eau potable du monde rural

22. Rakhi S, Shivanshu S, Sumit T (2020) Design optimization of solar PV water pumping system. Materials Today: Proceedings 21 (3): 1673-1679

23. Luc JP, Tarhouni J, Galvez R, Liman M, Sablayrolles C (2004) Performances des stations de pompages en irrigation : application aux forages de petits périmètres irrigués de la plaine de Kairouan (Tunisie) et impact des dysfonctionnements sur le prix de l'eau. In proceedings of the Seminar on modernization of irrigated agriculture, Rabat, Morocco

24. Dubois C (2009) Le guide de l'éolien, techniques et pratiques. Eyrolles, Paris

25. Katsigiannis YA, Stavrakakis GS, Pharconides C (2013) Effect of wind turbine classes on the electricity production of wind farms in Cyprus Island. In: Proceedings of the second International energy conference on power options for the eastern Mediterranean regions, Nicosia, Cyprus

26. Anurag C, Saini RP (2014) Statistical analysis of wind speed data using Weibull distribution parameters. In: Proceedings of the first international conference on non-conventional energy (ICONCE), Kalyani, India

27. Akdag SA, Bagiorgas HS, Mihalakakou G (2010) Use of two-component Weibull mixtures in the analysis of wind speed in the Eastern Mediterranean. Applied Energy 87:2566–2573

28. Ouammi A, Dagdougui H, Sacile R, Mimet A (2010) Monthly and seasonal assessment of wind energy characteristics at four monitored locations in Liguria region (Italy). Renewable and Sustainable Energy Reviews 14:1959–1968

29. Kavak Akpinar E, Akpinar S (2005) An assessment on seasonal analysis of wind energy characteristics and wind turbine characteristics. Energy Conversion and Management 46:1848–1867

30. Tar Karoly (2008) Some statistical characteristics of monthly average wind speed at various heights. Renewable and Sustainable Energy Reviews 12:1712–1724

31. Safari B, Gasore J (2010) A statistical investigation of wind characteristics and wind energy potential based on the Weibull and Rayleigh models in Rwanda. Renewable Energy 35:2874-2880

32. Weisser D (2003) A wind energy analysis of Grenada: an estimation using the 'Weibull' density function. Renewable Energy 28:1803–1812

33. Ramırez P, Carta JA (2005) Influence of the data sampling interval in the estimation of the parameters of the Weibull wind speed probability density distribution: a case study. Energy Conversion and Management 46:2419–2438

34. Dorvlo ASS (2002) Estimating wind speed distribution. Energy Conversion and Management 43: 2311–2318

35. Celeska M, Najdenkoski K, Stoilkov V, Buchkovska A, Kokolanski Z, Dimchev V (2015) Estimation of Weibull parameters from wind measurement data by comparison of statistical methods. In: Proceedings of the International Conference on Computer as a Tool (EUROCON), Salamanca, Spain

36. Acosta JL, Djokić SZ (2010) Assessment of Renewable Wind Resources in UK Urban Areas. In: Proceedings 15th IEEE Mediterranean Electrotechnical Conference, Valletta, Malta

37. Yeh TH, Wang Li (2008) A Study on generator capacity for wind turbines under various tower heights and rated wind speeds using Weibull distribution. IEEE Transactions on Energy Conversion 23: 592-602

38. Richardson FD, Mcnerney GM (2002) Wind energy systems. IEEE 81:378 - 389

39. Ofualagba GO, Ubeku EU (2008) Wind energy conversion system-wind turbine modeling. In: Proceedings of the power and energy society general meeting-conversion and delivery of electrical energy in the 21st century, Pittsburgh, USA

40. National Oceanic and Atmospheric Administration (NOAA), National climatic data center, http://www.ncdc.noaa.gov

41. Wood D (2011) Small wind turbines analysis, design, and application. Springer-Verlag, London

42. Tang X, Liu X, Sedaghat A, Shark LK (2009) Rotor design and analysis of stall-regulated horizontal axis wind turbine. In: Proceedings of the 44th International universities power engineering conference (UPEC), IEEE, Glasgow, Scotland

43. Liu X, Wang L, Tang X (2013) Optimized linearization of chord and twist angle profiles for fixed pitch fixed-speed wind turbine blades. Renewable Energy 57:111-119

44. Song Q (2012) Design, fabrication, and testing of a new small wind turbine blade, PhD thesis, University of Guelph, Ontario, Canada

45. Wind energy online reader, TU Delft, http://mstudioblackboard.tudelft.nl

46. Madani N (2011) Design of a permanent magnet synchronous generator for a vertical axis wind turbine. Master's thesis, (public version). Royal Institute of Technology, Stockholm, Sweden

47. Bang D, Polinder H, Shrestha G, Ferreira JA (2008) Review of generator systems for direct-drive wind turbines. In: Proceedings of the European Wind Energy Conference & Exhibition, Brussels Belgium

48. Bang DJ, Polinder H, Shrestha G, Ferreira JA (2008) Promising direct-drive generator system for large wind. In: Proceedings of the first seminar on Wind Power to the Grid, TU Delft, The Netherlands

49. Eriksson S, Bernhoff H, Leijon M (2008) Evaluation of different turbine concepts for wind power. Renewable and sustainable energy reviews 12:1419-1434

50. Polinder H, van der Pijl F, de Vilder GJ, Tavner P (2006) Comparison of direct-drive and geared generator concepts for wind turbines. IEEE 21:725-733

51. Ragheb A, Ragheb M (2010) Wind turbine gearbox technologies. In: Proceedings of the first international nuclear and renewable energy conference (INREC10), Amman, Jordan

52. McMillan D, Ault GW (2010) Techno-economic comparison of operational aspects for direct drive and gearbox-driven wind turbines. IEEE 25: 191-198

53. Singh RK, Rafiuddin MA, Zullah MA, Lee YH (2012) Design of a low Reynolds number airfoil for small horizontal axis wind turbines. Renewable Energy 42: 66-76

54. Wanga L, Tanga X, Liu X (2012) Optimized chord and twist angle distributions of wind turbine blade considering Reynolds number effects. In Proceedings of the international conference on wind energy: Materials, Engineering and Policies (WEMEP), Hyderabad Campus, India

55. Najafian Ashrafi Z , Ghaderi M, Sedaghat A (2015) Parametric study on off-design aerodynamic performance of a horizontal axis wind turbine blade and proposed pitch control. Energy Conversion and Management 93:349-356

56. Tabesh A, Iravani R (2006) Small-Signal Dynamic Model and Analysis of a Fixed-Speed Wind Farm—A Frequency Response Approach. IEEE Transactions on Power Delivery 21:778-787

57. Giguere P, Michael SS (1997) Low Reynolds number airfoils for small horizontal axis wind turbines. Wind Engineering 21:367-380

58. Miley SJ (1982) A catalog of low Reynolds number airfoil data for wind turbine applications. RFP-3387 UC-60, Texas A&M University, Texas, USA

59. Selig MS, Deters RW, Williamson GA (2011) Wind tunnel testing airfoils at low Reynolds numbers. In: Proceedings of the 49th AIAA Aerospace Sciences Meeting, Orlando, USA

60. Lutz TH, Würz W, Wagner S (2000) Numerical optimization and wind-tunnel testing of low Reynolds–numerical airfoils. In: Proceedings of conference on fixed, flapping and rotary wing vehicles at low Reynolds numbers, Notre Dame, Indiana, USA

61. Watanabe Y, Iwashita H, Ito M (2007) Shape optimum design of horizontal axis wind turbine in low Reynolds number range. In: Proceedings of the European wind energy conference, Milan, Italy

62. Tang X (2012) Aerodynamic design and analysis of small horizontal axis wind turbine blades, PhD thesis, University of Central Lancashire, Preston, United Kingdom

63. Tangier JL, Somers DM (1995) NREL airfoil families for HAWTs. NREL/TP-442-7109, Golden, CO, USA

64. Michael SS, McGranahan BD (2004) Wind tunnel aerodynamic tests of six airfoils for use on small wind turbines. Journal of Solar Energy Engineering 126: 986-1000

65. Michael SS, Guglielmo JJ, Broeren AP, Giguere P (1995) Summary of low-speed airfoil data. University of Illinois, USA

66. Giguere P, Michael SS (1998) New airfoils for small horizontal axis wind turbines. Journal of Solar Energy Engineering 120: 108-114

67. Worasinchai S (2012) Small wind turbine starting behaviour, PhD thesis, Durham University, England

68. Timmer WA, van Rooij RPJOM (2003) Summary of the delft university wind turbine dedicated airfoils. TU Delft, The Netherlands

69. Kale SA, Varma RN (2014) Aerodynamic design of a horizontal axis micro wind turbine blade using NACA 4412 profile. International Journal of Renewable Energy Research 4: 69-72

70. Wilson RE, Lissaman PBS, Walker SN (1976) Aerodynamic performance of wind turbines. Energy Research and Development Administration, Oregon State University,

71. DE Paor A.M (1982) Aerodynamic design of optimum wind turbines. Applied Energy 12:221-228

72. Yurdusev MA, Ata R, Çetin NS (2006) Assessment of optimum tip speed ratio of wind turbines using artificial neutral networks. Energy 31: 2153–2161

73. Wang L, Tang X, Liu X (2012) Blade design optimization for fixed-pitch fixed-speed wind turbines. ISRN Renewable Energy 2012: 1-8

74. Predescu M, Bejinariu A, Nedelcu A, Mitroi O, NAE C, Pricop MV, Crăciunescu A (2008) Wind tunnel assessment of small direct drive wind turbines with permanent magnets synchronous generators. In: Proceedings of the international conference on renewable energies and power quality (ICREPQ'08), Santander, Spain

75. Viterna LA, Corrigan RD (1981) Fixed pitch rotor performance of large horizontal axis wind turbines. In: Proceedings of DOE/NASA workshop on large horizontal axis wind turbine, Cleveland, OH, USA

76. Drela M (1989) XFOIL: an analysis and design system for low Reynolds number airfoils, Cambridge, Massachusetts, USA

77. Leloudas D (2006) Optimization of wind turbines with respect to noise, Master's Thesis, (public version). Technical University of Denmark- DTU, Denmark

78. Sessarego M (2013) Small wind-turbine rotor design code (SWRDC) user's guide, University of Calgary, Calgary, Alberta, Canada

79. Raghuwanshi MM, Singru PM, Kale U, Kakde OG (2005) Simulated binary crossover with lognormal distribution. Complexity International 12:1-10

80. Mishnaevsky LJ (2011) Composite materials in wind energy technology, Technical University of Denmark – DTU, Roskilde, Denmark

81. Supeni EE, Epaarachchi JA, Islam MM, Lau KT (2012) Design of smart structures for wind turbine blades. In: Proceedings of 2nd Malaysian postgraduate conference (MPC2012), Bond University, Gold Coast, Queensland, Australia

82. Zangenberg J, Brøndsted P, Koefoed M (2013) Design of a fibrous composite preform for wind turbine rotor blades. Materials and Design 56:635–641

83. Wind energy handbook, Wind turbine blade structural engineering, www.gurit.com

84. Bulent E, Aysegul A, Vardar A (2006) Using of composite material in wind turbine blades. Journal of Applied Science 6:2917-2921

85. Brøndsted P, Lilholt H, Lystrup A (2005) Composite materials for wind power turbine blades. Annual Review Materials Research 35:505–538

86. Mishnaevsky LJ (2012) Composite materials for wind energy applications: micromechanical modeling and future directions. Springer-Verlag 50:195-207

87. Samir A, Izhar UH (2012) Wind blade material optimization. Advances in mechanical engineering 2:48-57

88. Cripps D, Published courtesy of David Cripps, Gurit: Guide to composite www.netcomposites.com

89. Wind energy handbook, Blade manufacturing processes, www.gurit.com

90. Wind energy Handbook- 6- Blade Cost Analysis: Prepreg vs Infusion Material Technology, www.gurit.com

91. Hutchinson JR, Schubel PJ, Warrior NA (2011) A cost and performance comparison of LRTM and VI for the manufacture of large scale wind turbine blades. Renewable Energy 36:866-871

92. Skramstad JD (1999). Evaluation of hand lay-up and resin transfer molding in composite wind turbine blade manufacturing. Master's thesis, (public version). Montana State University-Bozeman, Montana, USA

93. Correia NC, Robitaille F, Long AC, Rudd CD, Sîmacek P and Advani SG (2005) Analysis of the vacuum infusion molding process: I. Analytical formulation. Composites: Part A 36 :1645–1656

94. Shah DU, Schubel PJ, Licence P, Clifford MJ (2012) Determining the minimum, critical and maximum fibre content for twisted yarn reinforced plant fibre composites. Composites Science and Technology 72:1909–1917

95. Mohd Yuhazri Y, Phongsakorn PT, Haeryip S (2010) A comparison process between vacuum infusion and hand lay-up method toward Kenaf/polyester composites. International Journal of Basic & Applied Sciences 10:54-57

96. Cosby Newsom M (2001) Reusable vacuum bagging device for producing composite parts. Bondline Products. http://www.bondlineproductscorp.com

97. Xu HHK, Ostertag CP, Braun LM (1994) Effects of fiber volume fraction on mechanical properties of SiC-fiber/Si_3N_4- matrix composites. Journal of the American ceramic society 77:1897–1900

98. Eker AA, Eker B (2013) General Assessment of Fiber-Reinforced Composites Selection in Wind Turbine Blades. Recent advances in composite materials for wind turbine blades. 61-79

99. Darshil USB (2013) Characterization and optimization of the mechanical performance of the plant fibre composites for structural applications, PhD thesis, university of Nottingham, United Kingdom

100. Kaw AK (2006) Mechanics of composite materials , Second Edn. CRC Press, Boca Raton

101. Seop Kim H, Hong SI, Sun-Jae Kim (2001) on the rule of mixture for predicting the mechanical properties of composites with homogeneously distributed soft and hard particles. Journal of Materials Processing Technology 112(1):109–113

102. Thorvaldsen T, Johnsen BB., Olsen T, Hansen FK (2015) Investigation of Theoretical Models for the Elastic Stiffness of Nanoparticle-Modified Polymer Composites. Journal of Nanomaterials 2015: 1-18

103. Sudheer M, Pradyoth KR, Somayaji S (2015) Analytical and Numerical Validation of Epoxy/Glass Structural Composites for Elastic Models. American Journal of Materials Science 2015, 5(3C): 162-168

104. Chamis CC (1984) Mechanics of Composite Materials: Past, Present, and Future. NASA Technical Memorandum 100793. Lewis Research Center, Cleveland, Ohio

105. Hart-Smith LJ (1992) The Ten-Percent Rule for preliminary sizing of fibrous composite structures. In: Proceedings of the 51st SAWE international conference, Hartford, Connnecticut, USA

106. Hart-Smith LJ (2002) Expanding the capabilities of the Ten-Percent rule for predicting the strength of fibre–polymer composites. Composites Science and Technology 62:1515–1544

107. Richardson D. The Fundamental Principles of Composite Material Stiffness Predictions. University of the West England, Bristol

108. Migneault B, Koubaa A, Erchiqui F, Chaala A, Englund K, Wolcott MP (2010) Application of micromechanical models to tensile properties of wood–plastic composites. Springer-Verlag 45: 521-532

109. Bourchak M, Harasani W (2013) Analytical and experimental investigation of tensile properties of cross-ply and angle-ply GFRP composite laminates. Science and Engineering of Composite Materials 22(3): 297‑301

110. Chandler HD, Campbell IMD, Stone MA (1995) An assessment of failure criteria fibre-reinforced composite laminates. International Journal of Fatigue 17: 513-518

111. Habalia SM, Saleh IA (1999) Local design, testing and manufacturing of small mixed airfoil wind turbine blades of glass fiber reinforced plastics Part I: Design of the blade and root. Energy Conversion & Management 41:249-280

112. Tangler JL (2000) The evolution of rotor and blade design. In: In Proceedings of the American Wind Energy Association WindPower. NREL/CP-500-28410, Golden, CO, USA

113. Ashworth Briggs AJE, Zhang ZY, Dhakal HN (2015) Study on T-bolt and pin-loaded bearing strengths and damage accumulation in E-glass/epoxy blade applications. Journal of Composite Materials 49(9):1047–1056

114. Schubel PJ, Crossley RJ (2012) Wind turbine blade design. Energies 5:3425-3449

115. Quinlan AR (2013). BroncoBlade: An open source wind turbine blade analysis tool. Master's thesis, (public version). Western Michigan University, USA

116. Sieradzan T, Vestergaard B (2014) On certification aspects of wind turbine blade load carrying structure. In: proceedings of Europe's premier wind energy event, Barcelona, Spain

117. Canales AG (2008) Evaluation of bondline thickness on wind turbine blade subcomponents, PhD thesis, TU Delft, The Netherlands

118. Madsen HA, Fuglsang P (1997) Numerical investigation of different tip shapes of wind turbine blades. Risø-R-891(EN), Roskilde, Denmark

119. Johansen J, Sørensen NN (2002) Numerical Investigation of Three Wind Turbine Blade Tips. Risø-R-1353(EN), Roskilde, Denmark

120. Burton T, Sharpe S, Jenkins N, Bossanyi E (2001) Wind energy handbook. Wiley, Chichester

121. He L, Qiu H, Fu X, Wu Z (2013) Camera-based portable system for wind turbine blade tip clearance measurement. In: proceedings of international conference on imaging systems and techniques (IST), IEEE, Beijing, China

122. Germanischer Lloyd Windernergie GmbH (2010) Guidelines for the certification of wind turbines; Hamburg

123. Tong W (2010) Wind power generation and wind turbine design. WIT Press, Southampton

124. Fu X, He L, Qiu H (2013) MEMS gyroscope sensors for wind turbine blade tip deflection measurement. In: Proceedings of international conference on instrumentation and measurement technology, IEEE, Minneapolis, MN, USA

125. Choi KS, Huh YH, Kwon IB, Yoon DJ (2012) A tip deflection calculation method for a wind turbine blade using temperature compensated FBG sensors. Smart materials and structures 21: 1-9

126. Tartibu LK, Kilfoil M, VAN DER Merwe AJ (2012) Vibration analysis of a variable length blade wind turbine. International Journal of Advances in Engineering & Technology 4: 630-639

127. Punmia BC, Kumar Jain A, Kumar Jain A (2001) Mechanics of Materials. Laxmi Publications Pvt Limited, New Delhi

128. Jonkman JM, Marshall L. Buhl Jr (2005) Technical report of National Renewable Energy Laboratory: FAST User's Guide, Colorado, USA

129. Gunjit SB (2005) Technical report of National Renewable Energy Laboratory: User's Guide to PreComp (Pre-Processor for Computing Composite Blade Properties), Colorado, USA

130. Gunjit SB (2005) Technical report of National Renewable Energy Laboratory: User's Guide to BModes (Software for Computing Rotating Beam Coupled Modes), Colorado, USA

131. Jonkman BJ, Kilcher L (2012) Technical report of National Renewable Energy Laboratory: TurbSim User's Guide: draft version 1.06.00, Colorado, USA

132. BVG Associates (2011) Offshore wind: Opportunities for the composites industry, United Kingdom

133. Gipe P (1995) Wind energy comes of age. Wiley & Sons, New York

134. Bulut EO et al (2013) HOLI 300. Design report, (public version). Fachhochschule Flensburg, Germany

135. Wanga F, Baia L, Fletcherb J, Whitefordc J, Cullen D (2008) Development of small domestic wind turbine with scoop and prediction of its annual power output. Renewable Energy 33:1637–1651

136. HAU E (2013) Wind turbines: fundamentals, technologies, application, economics. 3rd edn. Springer-Verlag Berlin Heidelberg

137. Shimada K, Ishihara T, Noda H (2006) Wind forces and peak wind pressure distributions on wind turbine nacelle. In: Proceedings of the 19th national symposium on wind engineering, Japan association for wind engineering, Japan

138. Ancona D, McVeigh J (2001) Wind turbine - materials and manufacturing fact sheet. Princeton Energy Resources International, LLC, USA

139. Courbois A (2013) Etude expérimentale du comportement dynamique d'une éolienne offshore flottante soumise à l'action conjuguée de la houle et du vent, PhD thesis, Central School of Nantes, France

140. Colorado School of Mines. Shaft design, Chapter 9. http://inside.mines.edu

141. Khurmi RS, Gupta JK (2005) A text book for machine design. Eurasia publishing house (PVT.) LTD. Ram Nagar, New Delhi

142. Schmid SR, Hamrock BJ, Jacobson Bo (2013) Fundamentals of machine elements, 3rd Edn. CRC Press, Boca Raton

143. Lasdon LS, Fox RL, Ratner MW (1974) Nonlinear optimisation using the generalized reduced gradient method. Revue française d'automatique, d'informatique et de recherche opérationnelle. 3: 73-103

144. DNV/Risø (2002) Guidelines for design of wind turbines, 2nd edn, Denmark

145. Moleejane CM et al (2014) Microstructural features and mechanical behaviour of unalloyed medium carbon steel (EN8 steel) after subsequent heat treatment. In: Proceedings of the world congress on engineering and computer science, San Francisco, USA

146. British stainless steel association. Tolerances to BS EN 10060 for hot rolled steel bars, www.bssa.org.uk

147. Mancuso J, Corcoran J (2003) What are the differences in high performance flexible couplings for turbomachinary. In proceeding of the thirty-second turbomachinary symposium, Texas, USA

148. Mancuso JR (1999) Couplings and Joints: Design, Selection & Application, 2nd edn. CRC Press, Boca Raton

149. American Gear Manufacturers Association (1996) AGMA 922-A96, load classification and service factors for flexible couplings, Washington, D.C, USA

150. OEP Couplings. The selection and specification of shaft couplings, www.oepcouplings.com

151. Schaeffler (2014) Bearing solutions and service for wind turbines. www.schaeffler.de

152. YAGI S (2004) Bearings for wind turbine. NTN technical review No.71

153. SKF, Double row tapered roller bearings. www.skf.com

154. NSK global website, Selection of bearing size. www.nsk.com

155. The timken company, pillow-block-2-bolt-base-bearing. www.cad.timken.com

156. Cao W, Xie Y, Tan Z (2012) Advances in Wind Power. Rupp Carriveau, Rijeka

157. Suzuki T, Okitsu H, Kawahito T (1982) Characteristics of a small wind-power system with DC generator. IEEE 129: 217-220

158. Simões MG, Chakraborty S, Wood R (2006) Induction generators for small wind energy systems. IEEE power electronics society newsletter

159. Tiwari AR, Shewale AJ, Gagangras AR, Lokhadna NM (2014) Comparison of various Wind Turbine Generators. Multidisciplinary journal of research in engineering and technology 1:129-135

160. Li H, Chen Z (2007) Overview of different wind generator systems and their comparisons. Renewable power generation 2: 123-138

161. Xu D, Luo Z (2009) A novel AC-DC converter for PMSG variable speed wind energy conversion systems. In: Proceedings of 6th international conference power electronics and motion control, IPEMC '09. IEEE, Wuhan, China

162. M. Hussein M et al (2013) Control of a stand-alone variable speed wind energy supply system. Applied sciences 3:437-456

163. Hsiao CH, Yeh SN, Hwang JC (2014) Design of high performance permanent-magnet synchronous wind generators. Department of electrical engineering. Energies 7:7105-7124

164. Predescu M, Crăciunescu A, Bejinariu A, Mitroi O, Nedelcu A (2007) Impact of the design method of permanent magnets synchronous generators for small direct drive wind turbines for battery operation. In: Proceedings of the international conference on renewable energies and power quality (ICREPQ'07), Seville, Spain

165. Bang DJ (2010) Design of transverse flux permanent magnet machines for large direct drive wind turbines. Master thesis, (public version). Pukyong National University, Korea

166. Aydin M, Huang S, Lipo TA (2004) Axial flux permanent magnet disc machines: A review. Research report, University of Wisconsin-Madison, Madison, USA

167. Ferreira AP, Costa AF (2010) Direct driven axial flux permanent magnet generator for small-scale wind power applications. In: Proceedings of the international conference on renewable energies and power quality (ICREPQ'11), Las Palmas de Gran Canaria, Spain

168. Olano A, Moreno V, Molina J, Zubia I (2008) Design and construction of an outer-rotor PM Synchronous Generator for small Wind Turbines; comparing real results with those of FE model. In: Proceedings of the international conference on electrical machines, Vilamoura, Portugal

169. Lampola P (2000) Directly driven, low-speed permanent-magnet generators for wind power applications, PhD thesis, Helsinki university of technology, Finland

170. Augustin AP, , Jurca F, Oprea C, Chirca M, Breban S, Radulescu MM (2013) Axial-flux vs. radial-flux permanent-magnet synchronous generators for micro-wind turbine application. In: Proceedings of 15th European conference on power electronics and applications (EPE), Lille, France

171. Chen Y, Pillay P, Khan A (2004) PM wind generator comparison of different topologies. In proceedings of industry applications conference, 39th IAS annual meeting, Rome, Italy

172. Erneo, solutions de motorisations électriques. Data Sheet PM Generator – Assembled version. www.erneo.fr

173. Cuesta AB et al (2013) Feasibility of a simple small wind turbine with variable speed regulation made of commercial components. Energies 6: 3373-3391

174. Narayana M, Putrus GA, Jovanovic M, P.S. Leung, McDonald S (2012) Generic maximum power point tracking controller for small scale wind turbines. Renewable Energy 44: 72-79

175. Valentini M, Ofeigsson T, Raducu A (2007) 9th Semester report of institute of energy technology (Aalborg University): Control of a variable speed variable pitch wind turbine with full scale power converter. Aalborg, Denmark

176. Muljadi E, Pierce k, Migliore P (1998) Control strategy for variable-speed, stall-regulated wind turbines. In: Proceedings of American controls conference. NREL/CP-500-24311. Golden, CO, USA

177. Grauers A (1994) Synchronous generator and frequency converter in wind turbine applications: system design and efficiency, Thesis for licentiate of engineering, Chalmers university of technology, Göteborg, Sweden

178. Broe AMD, Drouilhet S, Gevorgian V (1999) A peak power tracker for small wind turbines in battery charging applications. IEEE 14:1630 – 1635

179. Chinchilla M, Arnaltes S, Burgos JC (2006) Control of permanent-magnet generators applied to variable-speed wind-energy systems connected to the grid. IEEE 21:130 – 135

180. Miller A, Muljadi E, Zinger DS (1997) A variable speed wind turbine power control. IEEE 12: 181–186

181. Haque Md, Negnevitsky M, Muttaqi KM (2010) A novel control strategy for a variable-speed wind turbine with a permanent-magnet synchronous generator. IEEE 46: 331 – 339

182. Morimoto S, Nakayama H, Sanada M, Takeda Y (2005) Sensorless output maximization control for variable-speed wind generation system using IPMSG. IEEE 41:60 – 67

183. Chen J, Chen Jie, Gong C (2011) New overall power control strategy for variable-speed fixed-pitch wind turbines within the whole wind velocity range. IEEE 60:2652 – 2660

184. Mihet-POPA L, Boldea I (2005) Control strategies for large wind turbine applications. Journal of electrical engineering 2:1-8

185. EL-Shimy M (2013) Probable power production in optimally matched wind turbine generators. Sustainable energy technologies and assessments 2:55–66

186. Neammanee B, Sirisumrannukul S and Chatratana S (2010) Control Strategies for Variable-speed Fixed-pitch Wind Turbines, Wind Power, S M Muyeen (Ed.), ISBN: 978-953-7619-81-7, InTech, Available from:http://www.intechopen.com/books/wind-power/control-strategies-for-variable-speedfixed-pitch-wind-turbines

187. Schaffarczyk AP (2014) Introduction to wind turbine aerodynamics. Springer-Verlag Berlin, Heidelberg

188. Knight AM, Peters GE (2005) Simple wind energy controller for an expanded operating range. IEEE 20:459-466

189. Björk-Svensson J, Muñoz Pascual JO (2007) Torque control of a wind turbine using 6-phase synchronous generator and a dc/dc converter. Master's thesis, (public version). Chalmers University of Technology Göteborg, Sweden

190. Wall S, Jackson R (1993) Fast controller design for practical power-factor correction systems. In: Proceedings of the International conference on Industrial electronics, control, and instrumentation (IECON '93), Maui, Hawaii

191. Jiao S, Hunter G, Ramsden V, Patterson D (2001) Control system design for a 20 kW wind turbine generator with a boost converter and battery bank load. In: Proceedings of the IEEE 32nd Annual Conference on power electronics specialists (PESC), Vancouver, Canada

192. Muljadi E, Pierce K, Migliore P (2000) A conservative control strategy for variable-speed stall-regulated wind turbines. In: Proceedings of the 19th American society of mechanical engineers (ASME) wind energy symposium. NREL/CP-500-24791, Nevada, USA

193. Wright AD, Fingersh LJ (2008) Technical report of National Renewable Energy Laboratory: Advanced Control Design for Wind Turbines. Part I: Control Design, Implementation, and Initial Tests, Colorado, USA

194. Hur S, Leithead WE (2012) Collective control of a cluster of stall regulated wind turbines. In: Proceedings of the International Conference on Sustainable Power Generation and Supply (SUPERGEN 2012), Hangzhou, China

195. IHS Engineering 360, Electric Brakes Information. Permanent Magnet Brakes, www.globalspec.com

196. McMahon NM, Burton PR, Sharman DM (2015) On Electrodynamic Braking for Small Wind Turbines. WIND ENGINEERING 39 (5): 549–556

197. Chiras D, Sagrillo M, Woofenden L (2009) Power from the wind: achieving energy independence, 1st edn. New Society Publishers, Gabriola Island

198. Gipe P (2004) Wind power: renewable energy for home, farm, and business, 2nd edn. Chelsea Green Publishing, USA

199. Arifujjaman MD, Tariq Iqbal M, Quaicoe JE, Jahangir Khan M (2005) Modeling and control of a small wind turbine. In: Proceedings of Canadian conference on electrical and computer engineering, Saskatoon, Canada

200. Bu F, Huang W, Hu Y, Xu Y, Shi K, Wang Q (2009) Study and implementation of a control algorithm for wind turbine yaw control system. In: Proceedings of world non-grid-connected wind power and energy conference, Nanjing, China

201. Wan S, Cheng L, Sheng X (2015) Effects of yaw error on wind turbine running characteristics based on the equivalent wind. Energies 8:6286-6301

202. Bikdash M, Chen DA, Harb M (2000) A hybrid model of a small auto furling wind turbine. Journal of vibration and control 7:127-148

203. Audierne E, Elizondo J, Bergami L, Ibarra H, Probst O (2010) Analysis of the furling behavior of small wind turbines. Applied Energy 87:2278–2292

204. Bartmann D, Fink D (2009) Homebrew wind power: A hands-on guide to harnessing the wind. Buckville Publications LLC, Masonville

205. Polhamus EC (1966) A concept of the vortex lift of sharp edge delta wings based on the leading-edge-suction analogy. NASA TN D-3767, Washington DC, USA

206. Polhamus EC (1971) Predictions of vortex-lift characteristics by a Leading-Edge Suction Analogy. Journal of Aircraft 8:193-199

207. SKF company website. Slewing bearings. www.skf.com

208. International Organization for Standardization (1999) ISO 4014, 3rd edn: Hexagon head bolts, Product grades A and B. Genève, Swaziland

209. International Organization for Standardization (2009) ISO 898-1, 4th edn: Mechanical properties of fasteners made of carbon steel and alloy steel-Part 1: Bolts, screws and studs with specified property classes - Coarse thread and fine pitch thread. Genève, Swaziland

210. Windpower website (2003) Wind turbine towers. Retrieved January 2010 from Danish wind industry association. www.windpower.org

211. Sagrillo M (2005) Siting towers and heights for small wind turbines. Windletter 24 1-2

212. Lee J, Cho W, Lee KS (2014) Optimization of the hub height of a wind turbine. Journal of Industrial and Intelligent Information

213. Wood DH (2001) An improved determination of the tower height that maximizes the power output per unit cost of a small wind turbine. Wind Engineering 25:191-196

214. American Wind Energy Association (2002) Final report: ROADMAP, A 20-year industry plan for small wind turbine technology. National Wind Technology Center (NWTC), Boulder, USA

215. Sagrillo M (2009) Determining the minimum tower height for your site. Windletter 28 1-4

216. Arbaoui A, Asbik M (2010) Constraints based decision support for site-specific preliminary design of wind turbines. Energy and power engineering Journal 2:641-647

217. Wood, DH (2001) Determination of the optimum tower height for a small wind turbine. International Journal of Renewable Energy Engineering, 3:356-359

218. Canadian Wind Energy Association (2008) Purchasing guide: Small wind turbine purchasing guide, off-grid, residential, farm and small business applications. Ottawa, Canada

219. Tran AT (2014) Resistance of circular and polygonal steel towers for wind turbines, Licentiate thesis. Luleå University of Technology, Sweden

220. European standard for hot-rolled structural steel (2004) EN 10025-2:2004, Part 2-Technical delivery conditions for non-alloy structural steels.

221. Chen WF (1997) Handbook of Structural Engineering. CRC Press, Boca Raton

222. Chen WF, Lui EM (2005) Principles of Structural Design, 1st Edn. CRC Press, Boca Raton

223. Joung J, Kim Y, Baek k, Bang B (2015) Experimental and numerical study of wind loads for newly-proposed steel wind turbine towers. Journal of ocean and wind energy 2:153–159

224. Clifton-Smith MJ, Wood DH (2010) Optimization of self-supporting towers for small wind turbines. Wind Engineering 34:561–578

225. Australian Standard (1998) AS 4100-1998: Steel Structures. Standards Association of Australia, Sidney, Australia

226. Australian/New Zealand Standard (2011) AS-NZS 1170-2, 2nd edn: Structural design actions - Part 2: Wind actions. Standards New Zealand, Wellington

227. Kuhn M (1997) Soft or stiff, a fundamental question for designers of offshore wind energy converters. In: Proceedings of the European wind energy conference (EWEC'97), Dublin, Ireland

228. Karpat F (2013) A virtual tool for minimum cost designs of a wind turbine tower with ring stiffeners. Energies 6:3822-3840

229. Adhikari S, Bhattacharya S (2012) Dynamic analysis of wind turbine towers on flexible foundations. Shock and vibration 19:37-56

230. Rao SS (2004) Mechanical vibrations, 4th edn. Pearson Education, New Jersey

231. Bader Q, Kadum E (2014) Mean stress correction effects on the fatigue life behavior of steel alloys by using stress life approach theories. International Journal of Engineering and Technology 14:50-58

232. Pekka M (2008) Design of wind turbine foundation slabs. Master's thesis, (public version). Lulea University of Technology, Hamburg, Germany

233. SVENSSON H (2010) Design of foundations for wind turbines. Master's thesis, (public version). Lund University, Sweden

234. Stavridou N, Efthymiou E, Baniotopoulos CC (2015) Verification of anchoring in foundations of wind turbine towers. American Journal of Engineering and Applied Sciences 8: 717-729

235. MacGregor GJ, Wight JK (2011) Reinforced concrete: Mechanics and design, 6th edn. Pearson, New Jersey

236. Sørensen JD, Sørensen JN (2011) Wind energy systems: optimising design and construction for safe and reliable operation. Woodhead Publishing, Sawston Cambridge

237. Braja MD (2011) Principles of foundation engineering, 7th edn. Cengage learning, Boston

238. Nicholson JC (2011) Design of wind turbine tower and foundation systems: optimization approach. Master's thesis, (public version). University of Iowa, USA

239. Brown RW (2001) Practical Foundation Engineering Handbook. 2nd edn. New York: McGraw Hill

240. Liu Y, Zhan QS, Zhan YG (2015) Ultimate bearing capacity of strip footings on multi-layered clayey soils. Electronic journal of geotechnical engineering 20:4181-4188

241. Michalowski RL, You L (1998) Effective width rule in calculations of bearing capacity of shallow footings. Computers and Geotechnics 23:237-253

242. Rogers AL, Manwell JF, Wright S (2006) White paper: Wind turbine acoustic noise. Renewable Energy Research Laboratory, Massachusetts, USA

243. Guarnaccia C, Mastorakis NE, Quartieri J (2011) A mathematical approach for wind turbine noise propagation. In: Proceedings of the American conference on applied mathematics and the 5th WSEAS international conference on computer engineering and applications, Puerto Morelos, Mexico

244. Hubbard HH, Shepherd KP (1990) Wind turbine acoustics. NASA technical paper 3057, DOE/NASA/20320-77, Washington, D.C, USA

245. Tonin R (2012) Sources of wind turbine noise and sound propagation. Acoustics Australia 40:20-27

246. Wood DH (1997) Noise measurement and prediction for small wind turbines. In Proceedings of the 35th Annual Australian and New Zealand Solar Energy Society Conference, Canberra, Australia

247. Kłaczyński M, WSZOŁEK T (2013) Acoustic Study of REpower MM92 wind turbines during exploitation. Archives of Acoustics 39:3-10

248. Hessler GF, Hessler DM (2006) Baseline environmental sound levels for wind turbine projects. Sound and Vibration Journal 10-13

249. British Wind Energy Association (2008) Small wind turbine performance and safety standard. Renewable Energy House, London, United Kingdom

250. Koppen E, Fowler K (2015) International legislation for wind turbine noise. In: Proceedings of the 10th European congress and exposition on noise control engineering, Maastricht, The Netherlands

251. Haugen K M.B (2011) International review of policies and recommendations for wind turbine setbacks from residences: setbacks, noise, shadow flicker, and other concerns. Minnesota Department of Commerce, Minnesota, USA

252. Kamperman GW, James RR (2008) THE "how to" guide to siting wind turbines to prevent health risks from sound. Institute of noise control engineering (INCE), USA

253. International Electrotechnical Commission (2002) IEC 61400-11, wind turbine generator systems: Part 11: Acoustic noise measurement techniques, Genève, Switzerland

254. Tickell CE, Ellis JT, Bastasch M (2004) Wind turbine generator noise prediction-comparison of computer models. In: Proceedings of Annual conference of the Australian acoustical society, Gold Coast, Australia

255. Villar Alé JA, dos Santos CA, Astrada Chagas Filho JG, da Silva Simioni GC (2011) Aerodynamic loads and fatigue of small wind turbine blades: standards and testing procedures. In: Proceedings of Europe's premier wind energy event (EWEA 2011), Brussels, Belgium

256. Mandell JF, Samborsky D, Agastra P (2008) Composite materials fatigue issues in wind turbine blade construction, Montana State University, Bozeman, USA

257. Bach PW (1992) Final report of Netherlands energy research foundation (ECN): Fatigue properties of glass- and glass/carbon-polyester composites for wind turbines. ECN-C--92-072, The Netherlands

258. Mandell JF et al (1998) Fatigue of composite material beam elements representative of wind turbine blade substructure. NREL/SR-500-24379, Golden, CO, USA

259. Mandell JF, Reed RM, Samborsky D, Pan Q (1993) Fatigue performance of wind turbine blade composite materials. ASME wind energy 14:191-198

260. Mandell JF et al (1994) Fatigue of fiberglass generic materials and substructures. ASME wind energy 15:207-215

261. Paquette J, van Dam J, Hughes S, Johnson J (2008) Fatigue testing of 9 m carbon fiber wind turbine research blades. In: Proceedings of the 46th AIAA Aerospace Sciences Meeting and Exhibit, Nevada, USA

262. Mandell JF, Samborsky D, Cairns DS (2002) Final report of Montana state university: Fatigue of composite materials and substructures for wind turbine blades, Montana, USA

263. Sutherland HJ (1999) A Summary of the Fatigue Properties Wind Turbine Materials. SAND99-26135, Albuquerque, New Mexico

264. DOE/MSU (2010) Final report (Version 19.0): Composite materials fatigue database. Michigan state university, USA

265. International Electrotechnical Commission (2005) Wind turbines-Part 1: Design requirements

266. Rychlik I (1987) A new definition of the rainflow cycle counting method. International journal of fatigue 9:119-121

267. Sutherland HJ (1999) On the Fatigue Analysis of Wind Turbines. Sandia National Laboratories, Albuquerque, New Mexico

268. Marsh G, Wignall C, Thies PR, Barltrop N, Incecik A, Venugopal V, Johanning L (2016) Review and application of Rainflow residue processing techniques for accurate fatigue damage estimation. International Journal of Fatigue 82:757–765

269. Freebury G, Musial W (2000) Determining Equivalent Damage Loading for Full-Scale Wind Turbine Blade Fatigue Tests. In: Proceedings of the 19th American Society of Mechanical Engineers (ASME) Wind Energy Symposium, Reno, Nevada, USA

270. Madsen PH, Pierce K, Buhl M (1999) Predicting ultimate loads for wind turbine design. In: Proceedings of the American Institute of Aeronautics and Astronautics (AIAA/ASME) Wind Energy Symposium, Reno, Nevada, USA